WALL FRICTION AND LUBRICATION IN POWDER FLOWS

by

María Isabel Blázquez Martín

A dissertation submitted to the University of London for the degree of Doctor of Philosophy

Department of Chemical Engineering and Chemical Technology,
Imperial College of Science, Technology and Medicine,
London SW7 2BY

November 1990

TO MY PARENTS

" O could I flow like thee, ..."

Cooper's Hill, p 189
Sir John Denham, 1615-1669

PREFACE

This dissertation is a description of the work carried out in the Department of Chemical Engineering and Chemical Technology, Imperial College, University of London, between October 1986 and October 1990. Except where acknowledged, the material presented is the original work of the author and includes nothing which is the outcome of work done in collaboration, and no part of it has been submitted for a degree at any other university.

I would like to express my sincere gratitude to Dr. Brian J. Briscoe for his supervision, advice and support throughout the course of this work. I am also grateful to Dr. Paul D. Evans for his help and support. I would like to thank the members of the Particle Technology group for their friendship.

My thanks are also due to the members of the technical staff at the Department of Chemical Engineering, mainly the Departmental Workshop, Photography Services and Analytical Services for their help. The technical assistance in the use of the SEM provided by Mr. N. Taylor from the Department of Mechanical Engineering is also gratefully acknowledged.

I am also grateful to the Diputación Foral de Vizcaya, British Nuclear Fuels Ltd. and the Basque Government for the financial support provided.

Finally the support, encouragement and understanding of my family and T. K. Wee is very much appreciated.

M. Isabel Blázquez

November 1990

ABSTRACT

This Thesis considers the roles of interface friction in the mechanically induced densification process of ceramic powders. The oxide ceramic powders, alumina, zirconia and ferrite, have been coated with a range of organic materials, PVA (polyvinyl alcohol), PEG (polyethylene glycol), mixtures of both of them, and other commercially available binders. These materials are used to convey certain interfacial properties upon the powders. The interfacial rheological and thermal properties of the binder/ceramic systems have been analysed.

The emphasis has been placed upon the interfacial phenomena, mainly the frictional forces between the powders and the walls of their containers which affect the flow characteristics of these powders. The ways in which these forces act in free and constrained flow and their effects have been measured and interpreted using data obtained from a number of model experiments. The origins of these wall friction effects have been, to some extent, rationalised by adopting a simple modified friction model in conjunction with a simple contact mechanical model of the interface which takes into account the dependence of the coefficient of friction with the real area of contact or contact pressure. This model has also been used in conjunction with an established model due to Janssen-Walker to describe the stress transmission during uniaxial compaction and during green ejection. The density, mechanical properties and surface properties of the compacted bodies have been characterised by a number of techniques.

The study has shown that the wall friction is modified, and is indeed almost entirely controlled, by the presence of the organic coating on the surfaces of the particles or the walls. The important property of the coating is its interfacial rheology as defined by its interface shear stress. This is a function of the polymer, the contact pressure and the degree of plasticisation. These characteristics may be established using a variety of experiments involving model contacts.

CONTENTS

LIST OF FIGURES

CHAPTER 6

CHAPTER 7

CHAPTER 8

CHAPTER 9

LIST OF TABLES

CHAPTER 7

CHAPTER 8

CHAPTER 9

LIST OF PLATES

NOTATION

CHAPTER 2

$A_{s\text{-}w}$	Wall-solid area of contact in rotary kilns
D	Cylinder internal diameter
H	Powder heap or pile height
L	Loading degree of the cylinder
c	Powder pile circumference at its base
δ	Central angle of the sector occupied by the solid bed in a rotary kiln
θ	Angle of repose

CHAPTER 3

A_{app}	Apparent or geometric area of contact
A_r	Real area of contact
C	Cohesion
C_w	Adhesion
D	Elastic constant (equation 3.8)
E_1, E_2	Young's modulus of elasticity of the contacting bodies
E_p, E_s	Young's modulus of elasticity of the asperities and sphere
F	Frictional force (adhesion term)
F_{ad}	Adhesion term of the frictional force
F_{pl}	Ploughing term of the frictional force
F_f	Total friction force
H	Indentation hardness
N	Number of particle contacts
P	Contact pressure
P_o	Flow stress

P_r	Real contact pressure
R	Mutual radius of curvature of a contact (sphere radius)
R_p, R_s	Radii of the spherical asperities and of the sphere
T	Tensile strength
W	Normal load
W'	Logarithmic mean of the load range
a	Ratio α/c
b	Load index (Warren-Spring equation) (equation 3.25)
c	Constant (equation 3.10)
k	Friction factor (equation 3.5)
k'	Proportionality constant, load dependence of the area of contact (equation 3.6)
k"	Proportionality constant (equation 3.14)
m	Load index, load dependence of the area of contact (equation 3.6)
n	Load index, load dependence of the frictional force (equation 3.5)
z	Coefficient (equation 3.13)
α	Pressure coefficient
β	Fraction of the ploughing frictional work dissipated within the body
δA	Real area of contact of an individual contact
δF	Frictional force on an individual contact
μ	Coefficient of friction
μ_i	Coefficient of internal friction
μ_w	Coefficient of wall friction
υ_1, υ_2	Poisson's ratio of the contacting bodies
σ	Consolidation load
σ_w	Normal stress at the wall
τ	Shear strength

τ_{or}	Intrinsic shear strength
τ_r	Real interface shear strength
τ_w	Wall shear strength
ϕ	Total work done in deforming the body, per unit distance
φ_i	Angle of internal friction
φ_w	Angle of wall friction
ψ	Contact density

CHAPTER 4

C	Degree of volume reduction
C_t	Degree of volume reduction after tapping
D	Cylindrical die internal diameter
H	Height of powder or compact
H_o	Initial powder height in the die
K_w	Coefficient of pressure; ratio of horizontal to vertical stress at the wall
N	Tapping number
P, P_a	Applied normal stress or surcharge
P_e	Ejection pressure
P_t	Transmitted stress
P_y	Yield pressure
V	Actual powder or compact volume at a given applied pressure P
V_o	Volume of compact at zero pressure, initial apparent volume
V_r	Volume of compact over solid material volume ratio, V/V_s
V_s	Solid material volume (void-free or theoretical solid volume)

a	Kawakita constant
a_t	Kawakita tapping constant
a_1, a_2	Constant (Table 4.1)
b	Kawakita constant
b_t	Kawakita tapping constant
c	Compaction modulus

k	Constant (equation 4.10)
k'	Constant (equation 4.12)
k_1, k_2	Constants (Table 4.1)
m	Compressibility factor
n	Constant (Table 4.1)
Δ	Distribution factor
α	Pressure coefficient
β	Constant (Spencer equation) (equation 4.7)
δy	Elemental slice width
μ_e	Coefficient of friction during ejection
μ_w	Average coefficient of wall friction
ρ	Density
ρ_a	Apparent or bulk density of the compact
ρ_r	Ratio ρ_a/ρ_s
ρ_s	True density of solid material
ρ_y	Density at the point of yielding
σ_{xx}	Radial stress
$\sigma_{(xx)w}$	Radial stress at the wall
σ_{yy}	Effective vertical stress
$\sigma_{(yy)w}$	Vertical stress at the wall
σ'_{yy}	Mean vertical stress
τ_e	Interface shear strength during compact ejection
τ_e^*	Mean ejection interface shear strength
τ_o	Intrinsic shear strength
τ_w	Net shear strength at the wall

CHAPTER 5

C_t	Degree of volume reduction
D	Cylindrical die diameter
E	Young's modulus of elasticity
E_c	Fracture energy
E_c/M	Specific fracture energy
F_s	Sliding frictional force
H	Tensile strength of a single bond
H_s	Scratch hardness
H.R.	Hausner ratio
L	Compression load at failure
M	Mass of the specimen
M_c	Mass of the cylinder
M_t	Total mass of cylinder and powder
N	Tapping number
T	Temperature
T_f	Final temperature
T_i	Initial temperature
V	Powder volume
V_o	Initial apparent volume
Vo	Sphere unit volume
W	Normal applied load
a_t, b_t	Kawakita empirical constants for tapping
d	Diameter of a spherical particle or ball-shaped pellet
g	Acceleration due to gravity
k	Constant (equation 5.3)
m	Weibull's coefficient of uniformity
n	Index (equation 5.3)
r	Indentation average radius
r_w	Half scratch width
std dev	Standard deviation

t	Time
ε	Void fraction in the particle assembly
κ	Mean coordination number
ν	Poisson's ratio
ρ	Density
ρ_a	Apparent bulk density
ρ_t	Tap bulk density
σ_c	Compressive strength or breaking stress
σo	Strength of a sphere of unit volume Vo
σ_t	Mean tensile strength per unit section area
ω	Angle of inclination for the onset of rolling of the cylinder with powder
ω'	Angle the centre of gravity of the bed makes with the horizontal for the onset of rolling of the cylinder with powder
ω''	Angle of inclination for rolling of the empty cylinder

CHAPTER 6

A_{app}	Apparent area of contact
D	Cylinder internal diameter
H	Apparent bed height in the rolling cylinder
L	Cylinder length
L_1	Lower class boundary of modal class
M	Mode of a set of numbers
N	Sample size
R	Cylinder radius
S	Circular perimeter occupied by the powder in the cylinder
X_i	Class mark
c	Size of the modal class interval
cov	Coefficient of variation
f_i	Class frequency

s	Standard deviation
t	Student's t
v	Variance
w	Powder bed width inside the cylinder
Δ_1	Excess of modal frequency over frequency of the next lower class
Δ_2	Excess of modal frequency over frequency of the next higher class
$\bar{\alpha}$	Arithmetic mean of a given variable α
α_i	Each of the values of the variable α in a set of data
ϕ	Angle subtended by the bed inside the cylinder

CHAPTER 7

A_{app}	Apparent or geometric contact area powder-cylinder wall
A_r	Real area of contact
D	Elastic constant (equation 7.9)
E_1, E_2	Young's modulus of elasticity of the two contacting bodies
F	Interface wall friction force
F_f	Frictional force required to initiate motion in cylinder and contents
L	Cylinder length
M_c	Mass of the empty cylinder
M_t	Total mass of cylinder and contents
P	Contact pressure
P_a	Apparent contact pressure
P_o	Plastic yield pressure or flow stress
R	Cylinder radius
W	Applied normal load
W'	Logarithmic mean of the load range used

a	Ratio α/c
a'	Ratio α/c'
c	Constant (equations 7.8 and 7.9)
c'	Constant (equation 7.16)
c''	Ratio τ_o/P_o
c*	Constant c or c'
g	Acceleration due to gravity
k	Friction factor
n	Load index (equation 7.5)
r	Hemispherical compact radius
r'	Radius of spherical indenter
w	Powder bed width in the cylinder
α, α'	Pressure coefficient
α_a	Apparent pressure coefficient
μ	Coefficient of friction
μ_A	Coefficient of friction for uranium dioxide compact A
μ_B	Coefficient of friction for uranium dioxide compact B
υ_1, υ_2	Poisson's ratio of the two contacting solids
ρ	Specific density
τ	Shear strength
τ_a	Apparent interface shear strength
τ_o	Intrinsic shear strength
τ_{oa}, τ'_{oa}	Apparent intrinsic shear strength
ϕ	Angle subtended by the powder bed in the cylinder
ω	Angle the centre of gravity of the bed makes with the horizontal
ω'	Angle of inclination at which the cylinder with powder begins to roll down
ω''	Angle required to induce motion in the empty cylinder

CHAPTER 8

A_{app}	Apparent, geometric area of contact
A_r	Real, effective area of contact
C	Degree of volume reduction
D	Cylindrical die internal diameter
H	Powder or compact height
$(H/D)_o$	Initial height/die diameter ratio
K_w	Coefficient of pressure; ratio of horizontal to vertical stress at the wall
P	Pressure
P_a	Applied pressure
P_e	Ejection pressure
P_t	Transmitted pressure
P_y	Pressure at the point of yielding
V	Volume at any given pressure
V_o	Initial volume
a, b	Kawakita empirical constants
k	Proportionality constant (equation 8.13)
k'	Proportionality constant (equation 8.14)
m	Compressibility factor
Δ	Distribution factor; ratio between the vertical stress at the wall and the mean vertical stress
α	Pressure coefficient
ζ	Real to apparent area ratio
μ_e	Coefficient of friction during ejection
μ_w	Coefficient of wall friction
ρ	Density
ρ_y	Density at the point of yielding
σ_{xx}	Radial stress

$\sigma_{(xx)mean}$	Mean radial stress at the wall
τ	Interface shear strength
τ_o	Intrinsic shear strength
τ_w	Apparent wall shear strength
τ_{wr}	Real shear strength at the wall
ϕ	Internal angle of friction

CHAPTER 9

$(H/D)_o$	Initial height/die diameter ratio
K_w	Coefficient of pressure; ratio of horizontal to vertical stress at the wall
P_a	Applied pressure
P_t	Transmitted pressure
t	Resultant of the v forces
v	Resultant force of the reactions w and y
w	Inward component of the radial force
x	Outward component of the radial force
y	Downward component of the axial force
z	Upward component of the axial force

CHAPTER 10

K_w	Coefficient of pressure; ratio of horizontal to vertical stress at the wall
a	Kawakita empirical constant
b	Kawakita empirical constant
α	Pressure coefficient of the interface shear strength
τ_o	Intrinsic interface shear stength

CHAPTER 1

INTRODUCTION

This Thesis describes a study of the wall friction and lubrication effects which occur during the flow of ceramic powder materials. Wall friction is a dominant phenomenon at several stages of ceramic components manufacture. The levels of wall friction generated during material flows in ceramic processing and their variation with normal stress have been analysed. The action of a number of organic materials which have been used to coat the ceramic particles or the wall surface has also been considered and their contributions to the friction and lubrication effects have been evaluated. The wall shear stresses which are transmitted by a solid or by a powder which is confined during its flow are described by simple constitutive relationships and by an examination of the interface at a microscopic level. Some well established models of friction and a simple contact mechanical model of the interface are applied. This will be illustrated using a range of data obtained in model solid and powder flow experiments.

The remainder of this Introduction outlines some general aspects of ceramic processing and of the role played by the frictional forces. A brief description of the general outline of this Thesis is also included.

1.1 CERAMIC COMPONENT MANUFACTURE

Ceramic components have been routinely manufactured since prehistoric times using relatively crude equipment combined with empirically generated skills. The classical techniques have involved what is currently described as "wet" processing techniques. A ceramic powder is combined with water to produce a pliable dough which is then dried and finally fired to produce a dense product. The advent of

improved engineering and hence machines has allowed a relatively new technique to be developed where "dry" powders may be formed into a strong compact or "green" which may be successfully fired to produce a viable product. Today a large proportion of the ceramics manufactured in the world are produced by "dry" processes. The obvious principle economic benefit is that the dry route obviates the need to dewater or dry the preformed component. Alumina, ferrite and certain porcelains have been effectively produced by this means on a large scale for at least forty years. In recent times, wet routes have found favour in what might be described as the processing of "difficult" ceramic powders and ceramic products. This is currently the case for alumina fibres, high critical temperature superconductors and some high performance ceramic materials. Dry processing will always be preferred if it is viable and in the foreseeable future it is likely to be, in volume terms, the major processing route for ceramic component manufacture.

The dry processing route of a typical ceramic component involves numerous stages. Usually the basic powder is a multicomponent system; a ferrite powder comprises of six distinct components whilst an engineering alumina may contain only two. Good mixing of the ingredients is essential. The resulting powder must flow easily into a mould where it may be effectively formed into a green body by the application of pressure. The three operations; mixing, transport and compaction generally necessitate the introduction of a species or a number of species termed processing aids. When the green product is produced these entities are burnt out of the green during the initial firing procedure. An additional constraint is that these materials should not produce undesirable residues in the sintered product. The processing aids are seen to produce a variety of effects some of which are mutually conflicting in the production of an optimal product. A scheme of a current processing route and associated analytical procedures is shown in Figure 1. The figure includes the different aspects considered in this study.

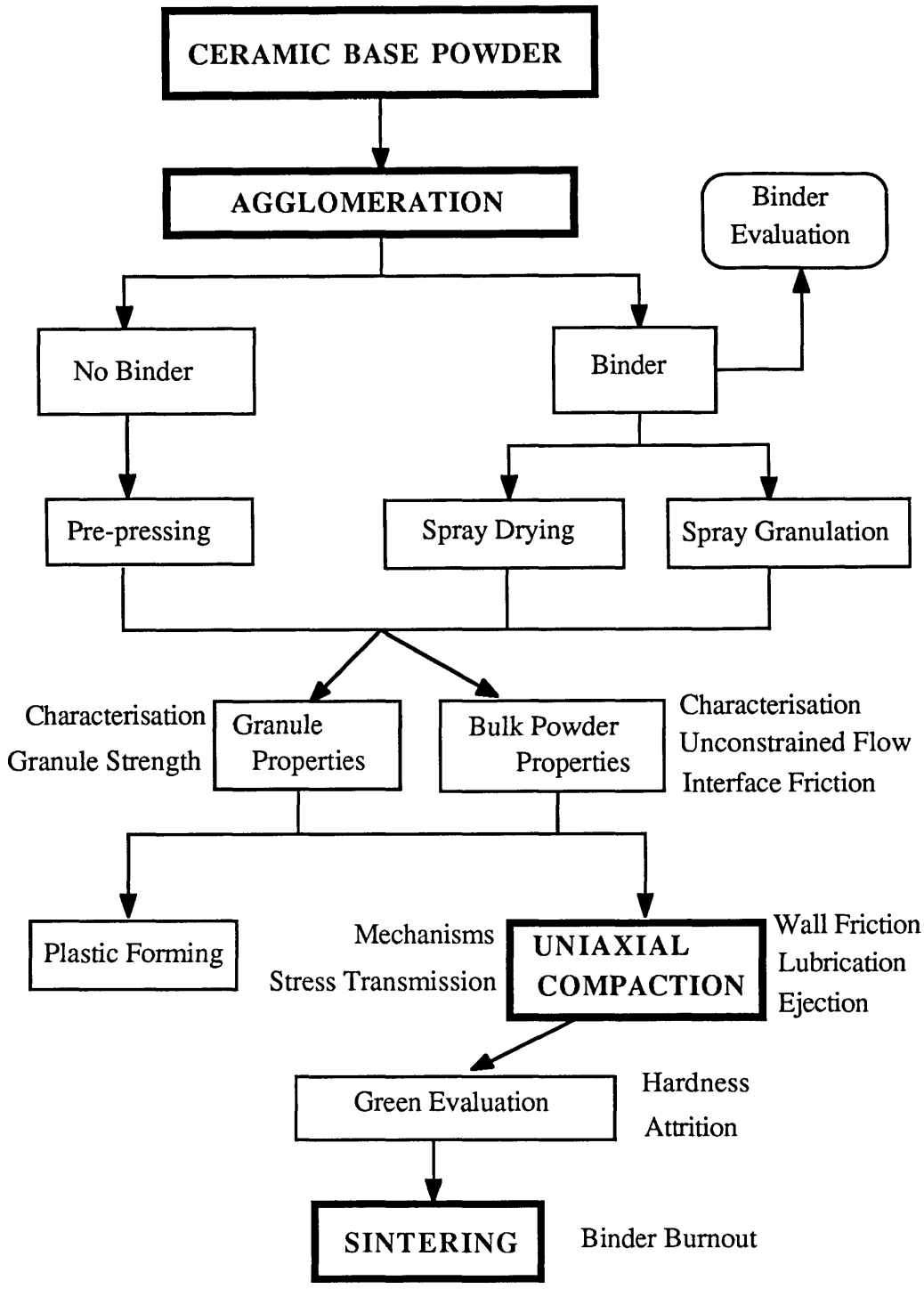

Figure 1.1 Diagram showing a general ceramic dry processing route and the main aspects considered in this study.

1.1.1 Friction Effects and Processing Aids

Friction plays a significant role in many aspects of the dry processing of ceramic materials. Particle-particle and particle-wall friction effects will control the way in which the particles interact amongst themselves and with their confining walls. The various elements in the densification process are controlled by solid-solid interactions and therefore an optimisation of these interactions will lead to the production of an optimum product. These interactions are primarily responsible for the flow characteristics of the powder and therefore for the efficiency in die filling prior to pressing. Additionally, these same interactions, although under different conditions, will control the particle-particle and particle-wall tractions and the particles mobility during pressing. These aspects will have a pronounced effect on the density distribution in the pressed piece and in the force fields generated during sintering and therefore in the quality and final shape of the sintered product. These frictional dissipation processes are thus of great relevance. A better understanding of their function and of the mechanisms involved and the evaluation of the magnitude of the forces involved will therefore contribute to the optimisation of ceramic component manufacture.

Generally, processing aids are introduced into these ceramic systems where appreciable solid-solid contact occurs in order to modify certain features of the interactions between the solid bodies. The types of processes which are modified are of two general kinds; the energies or forces required to move the solid bodies with respect to each other, and the types and extent of the effects produced as a consequence of this dissipation of energy.

1.2 GENERAL DESCRIPTION OF THE THESIS

This Thesis considers several aspects of the role of particle-wall friction in the dry processing of several ceramic powders. The oxide ceramic powders used, alumina, zirconia, ferrite and uranium dioxide, were mainly in an agglomerated state as this is one important requirement in the overall ceramic powder processing. These granulated powders have been treated with a range of organic materials which act as "processing

aids". The organic polymers used were PVA (polyvinyl alcohol) and PEG (polyethylene glycol), mixtures of both of them, and other commercially available binders. They convey certain properties upon the powder which ultimately control, in a large part, the quality of the sintered product. Their purpose is to bind the particles together and to "lubricate" the flow of the resulting granules during transport and compaction. The deposition of these organic coatings on the surface of the ceramic particles will modify the particle interactions. Their action and the contributions they make to the overall processability of these ceramics and the quality of the green product have been evaluated. The ceramic powders have been characterised and the main powder properties, including both the single particle and the bulk powder parameters, which will affect the subsequent dry processing of these materials have been described. Also, the thermal properties of the binders used to coat the ceramic particles and of the binder/ceramic systems were analysed.

The main objectives of this study are to investigate the influence of organic interface layers on the frictional effects during the preparation of green bodies. The practical aim is to establish means of reducing the potential damage created by the presence of these frictional forces and to find ways of quantifying the severity of the stresses likely to be produced. The interface wall friction effects developed during three stages of the ceramic powder processing; the die filling and unconstrained or free flow, the constrained flow or uniaxial compaction, and the green compact ejection have been investigated in some detail by using several model experiments. Also, their effects on the final green characteristics have been studied. Several simple models and theories available for describing the stresses produced in constrained and in unconstrained flow processes are used. An attempt to model these effects by examining the properties of individual particles and their interactions with their neighbours and confining walls will be presented. The variation of the coefficient of friction as a function of the contact situation existing at the interface and the magnitude of the contact stresses developed will be predicted.

1.2.1 Free Flow

Good bulk powder flow is required for dry ceramic processing. The free flow properties of the material are important during transport and to produce a uniform die filling prior to the pressing which leads to a more uniform pressing and homogeneous green compact. Interparticulate friction and the interactions of the bulk powder with the walls of the container during unconstrained flow characterise the flow behaviour of the material. The flowability of the different organic binder-ceramic systems was analysed and their frictional behaviour during unconstrained flow has also been evaluated by determining the situation at the wall-powder interface during unconstrained flow.

1.2.2 Constrained Flow

The main features relating to the uniaxial single-sided dry pressing of ceramic powders have been studied. The areas of pressure-volume relationships, the interface friction effects during pressing and green ejection, the stress transmission along the compact, and finally the characterisation of the resulting green compact are covered. The role played by the state of agglomeration of the starting materials, and the binders and lubricants are also analysed. Binders and lubricants provide pressed strength and facilitate pressing and ejection as well as minimising die abrasion by reducing the undesirable wall friction forces. Two established models, due to Janssen-Walker and to Spencer, have been used to describe the stress transmission data in conjunction with a simple modified friction model based upon the interfacial shear of the organic coating at the walls of the containers or dies.

This study has also investigated the effect of the stress transmission during die-pressing on the resulting density distribution in the compact. A new method based on the controlled attrition of the green has been introduced to evaluate the stress and density distributions inside the compact generated during compaction. These data were correlated with the friction characteristics of the powders, especially during compaction.

1.3 GENERAL OUTLINE OF THE THESIS

This Thesis is divided into several chapters. The Thesis begins with a general introduction of the areas studied and presented in this work. Chapters 2 to 4 present a literature review on three main aspects of ceramic processing; the powder bulk flow properties, the interface friction effects during unconstrained and constrained flow, and the uniaxial compaction of powders. Several models describing the interface friction of solids and the stress distribution during compaction are included. Chapter 5 describes the materials studied, their properties and characteristics, and it also describes the experimental methods adopted to evaluate the powders properties and friction characteristics. Chapters 6 to 9 present the experimental data and the analysis of these results on each of the three areas outlined above. Data on the flow properties, particle-wall friction, uniaxial compaction and compact characteristics are discussed. A brief conclusion is also included in each of these chapters. The final Chapter presents the general conclusions and discusses the overall role of solid-solid friction in the processing of ceramic powders.

In summary, this work has concentrated on the study of the effect of particle-wall friction on ceramic powder flow as a function of the magnitude of the applied normal load. The effects of the presence of a boundary lubricating layer have also been considered. The organic coatings will influence the interactions between the solid bodies. It is expected that the processing aids coating the ceramic material will markedly alter the rheology of the powder and its interaction with its containers. Therefore, a proper choice of processing aids to coat the ceramic particles will optimise the interface friction effects during powder processing. The effects produced by the coatings are illustrated for a number of situations in solids' flow. The interfacial wall friction generated during solid flow will be predicted from single particle frictional properties and a geometric description of the particle assembly adjacent to the wall.

CHAPTER 2

FREE FLOW

2.1 INTRODUCTION

This Chapter describes the flow properties of bulk powders and their effect on ceramic powder processing. The Chapter is divided in several parts including a general introduction and a literature review of previous work.

The flowability of a powder is a very important parameter in powder processing. This is specially so during the handling and the transport of the material prior to processing and during the filling of the die in the compaction stage. These processes involve unconstrained or free flow. Powder handling is an important aspect of powder processing and it affects subsequent fabrication steps such as forming, sintering, and development of the microstructure (Carson, 1988). The flow properties of the material will affect the characteristics of the manufactured component.

The flowability of the different organic binder-ceramic systems and of the uranium dioxide powders was analysed in order to characterise these materials as free or cohesive powders and their frictional behaviour during unconstrained flow has also been evaluated. The measurement of the frictional force, the evaluation of the static friction coefficient, and the determination of the situation at the wall-powder interface during unconstrained flow have also been considered. The experimental data corresponding to the flow properties are presented in Chapter 6. Chapter 3 reviews the friction properties including the wall-solid friction during unconstrained flow. The friction data generated are presented in Chapter 7.

2.2 LITERATURE REVIEW

This review on powder flow is restricted mainly to a description of some of the techniques available for the measurement of the flow properties of a powder. These include the determination of the angle of repose of the powder, the use of the shear cell, the implementation of the rolling cylinder experiment, and the measurement of the Hausner ratio. The main powder characteristics that affect the flow are also reviewed. In this study the main interest is the effect on the material flow properties of the state of agglomeration of the powder and of the type of binder system used. The particle size and size distribution, the particle shape and the interparticle friction characteristics also play an important role in the flowability of the material.

2.2.1 Powder Characteristics Affecting Flow

According to their flow behaviour, powders may be divided into two broad types (Harnby, 1987). Cohesive powders; these powders lack a general mobility and the particles also lack individual mobility. They are held within a structure by adhesive bonds and in order to liberate and relocate individual particles these bonds have to be repeatedly broken. Free flowing powders; they have both a general and an individual mobility. This is a desirable process property for many industrial operations and the trend in many process industries is towards the production of free flowing powders. Ceramic powders may exhibit a range of flow problems depending on the flow properties of the material and the processing equipment used. The most common problems encountered are; no flow, erratic flow, flooding and segregation (Carson, 1988). Frequently fine particles are agglomerated in order to give a free flowing product and to assist the agglomeration process some type of binder or bonding agent is added to the powder. These two important aspects are considered in the following sections.

2.2.1.1 Agglomerates

Powder flow is affected by the state of agglomeration of the particles in the material. A powder flows freely when the inertial forces exceed the attractive forces between the particles. The attractive interparticle force is inversely proportional to the particle diameter. In dry fine powders the attractive interparticle Van der Waals forces present are very large compared with the inertial forces. Hence, fine powders exhibit poor flow. One of the effects of agglomeration, a size enlargement process, is the reduction of the interparticle attractive forces and the increase of the inertial forces. This enhances the flow of the material. In general, agglomerates are free flowing materials presenting better flow characteristics than the base powders.

To characterise an agglomerate it is necessary to determine how the particles are bound together. That is, the nature of the adhesive forces and also how the particles are arranged within the agglomerate. Its microstructure and packing density are thus important. In addition, the size, size distribution and shape of the agglomerate are also of consequence (Halloran, 1984). These properties will influence not only the flow but also the material behaviour in all the stages of ceramic processing.

The benefits obtained from the agglomeration of a powder are that the agglomerates withstand transportation and handling and they have good flow properties. Agglomerates flow easily and flow control is facilitated. This is of interest during the compaction process as agglomeration leads to a greater uniformity in die filling and so reduces stress and density variations during compaction which is necessary in order to obtain a dense, homogeneous compact. This will subsequently affect the grain growth rates during sintering (Capes, 1980; Sherrington and Oliver, 1981; Adams *et al.*, 1987b).

2.2.1.2 Processing Aids: Binders

Binders and lubricants play a major role in the several steps of the fabrication route. Binders are used to convey certain properties upon the powder which improve the

processing of the material and ultimately control the quality of the final sintered product. Usually, the binder is added during the agglomeration stage, as one of the binder functions is to promote the agglomeration of the powder particles. They hold particles together to produce high agglomerate strength and free-flowing units. The behaviour of the agglomerates formed depends on the type, quantity, and properties of these binders. Binders affect the interparticle and particle-wall friction properties which in turn affects the bulk powder flow properties. As it has been mentioned in the previous Section, good flow is desirable during compaction to obtain a tough and homogeneous green.

In the present study, the particle interactions have been modified by deliberate deposition of a range of organic coatings onto the surfaces of the particles. These additives, or processing aids, have been applied to produce the agglomerates. The influence of these organic interface layers on the bulk powder flow properties has been investigated. These additives affect the flow and compaction behaviour of the agglomerated ceramic powders. The basic requirements for the powder, with respect to the flow, as introduced by the processing aids are several and include the reduction of cohesion and the improvement of the free flow properties, and the creation of durable agglomerates to maintain these flow characteristics.

In summary, the binder and agglomerate requirements, with respect to the flow properties, are to produce particles tough enough to transport and also a free-flowing material to obtain a uniform die filling in the pressing process.

2.2.1.3 Other Factors Affecting Powder Flow

2.2.1.3.1 Material-Wall Interface

In all flow channels, storage containers and regions of mechanical interaction between the equipment and the material in transit, the apparent deformation characteristics of the bulk material are influenced by the interface between the equipment parts and the loose solids (Bates, 1977). This is a major effect and its study

is central to this Thesis. Further is said about this subject in later sections.

2.2.1.3.2 Material Physical Properties

The flow properties of a solid are naturally dependent on the physical characteristics of the material (Johanson, 1971/72; Carson, 1988; Perry and Chilton, 1973). Particle size is one of the most common factors which affect the flowability of a given material. In general, it may be assumed that the larger the particle size and the more "free" the material is from "fines", the more easily the material will flow. The influence of particle size on the flow behaviour has been described in Section 2.2.1.1. Moisture content is a major variable. As the surface moisture content increases the powder flows less easily. Most materials may safely absorb moisture up to a certain point; further addition of moisture may cause significant flow problems. Moisture addition or removal may make a free flowing powder become cohesive or vice-versa. Small changes in moisture content may produce incremental changes in bulk powder flow. The flow is affected by the temperature or by variations in temperature. High temperatures may cause serious flow problems in some materials which contain soluble or low melting point components. These materials become "sticky" at high temperatures. Chemical composition also affects the flow if a chemical reaction occurs. Age appears to improve flowability of certain materials. This is probably due to particle surface oxidation, more even moisture distribution, and the rounding of particle corners caused by handling. The consolidating pressure exerted in a powder influences its flow. The time under consolidation, if the powder compacts, causes flow to become more difficult. Several authors have outlined the factors affecting powder flow; Orr, 1966; Johanson, 1971/72; Sherrington and Oliver, 1981; Carson, 1988. The bulk density, the permeability, the surface roughness, the interparticle contact area and the interparticle cohesive forces are some of the other factors that may influence the flow of powders.

2.2.2 Granular Flow Regimes

Two idealised flow regimes may be distinguished for cohesionless granular materials. In the case of slow flow it is governed by interparticle friction and under

rapid flow conditions particle collisions dominate. Boundary conditions are of great importance; at a rigid wall, depending on its roughness sliding may be assumed (Schweiwiller and Hutter, 1983). Schweiwiller and Hutter, 1983 applied a continuum model to describe the rapid flow of granular materials under gravity driven flow down a chute. They also presented a review on the gravity flow of cohesionless materials. Shahinpoor and Ahmadi, 1983 developed a kinetic theory for the rapid flow of rough inelastic spherical particles. By a "rapid flow", it is meant a flow that is primarily maintained by exchange of momenta between the colliding particles. This theory demonstrated the effect of intergranular friction and grain inelasticity on the nature of the flow regimes. When in rapid motion the material creates a field of random fluctuations on all pertinent variables such as velocity, bulk density, and interparticle dispersive and frictional forces. Kanatani, 1983 has reviewed various viewpoints of the theoretical approach in the mechanics of granular materials. First, he examined the macroscopic plasticity approach. Next, he considered a microscopic approach considering an assembly of rigid spherical particles. Finally, he reviewed the use of entropy in the description of the random packing state.

2.2.3 Measurement of Flow Properties

A number of techniques have been developed to try to determine the flow properties of solids. A summary of the most common methods used to study powder flow are presented in this Section.

2.2.3.1 Hausner Ratio

The powder bulk density is an indirect indicator of the flow characteristics of a powder. The Hausner ratio is defined as the tap density over the apparent bulk density. Harnby, 1987 used the powder bulk density as an indirect indicator of the flow characteristics of powders, characterising the bulk powder flow using the Hausner ratio. According to their Hausner ratio values he classifies powders as aerating types (Hausner ratio value less than 1.2) and cohesive types (value greater than 1.4). Grey and Beddow, 1969 compared values of Hausner ratios, flow times and angles of

repose for three types of dry copper powder. They found that there was a relationship between the Hausner ratio and the flow rate and between the Hausner ratio and the angles of repose. In particular, the Hausner ratio corresponded more closely to the dynamic angle of repose than it did to the static angles of repose.

A detailed review of the significance and use of the Hausner ratio and its definition are included in Chapter 5.

2.2.3.2 Characteristic Angles of a Powder

The ability of a bulk powder to flow, to be fluidised and to transmit forces, is reflected in the values of its several characteristic flow angles.These include the angle of repose, the angle of slide, the angle of rupture, the angle of internal friction, the effective angle of internal friction, and the angle of wall friction (Orr, 1966; Carson, 1988). Most of these parameters may be measured using a direct shear cell tester. The significance of these various angles is reviewed below.

Angle of Repose: One of the characteristic angles of a powder is the angle of repose. It is defined as the angle at which a material will rest on a pile (Perry and Chilton, 1973). Flow on an inclined plane exists only when the inclination angle exceeds the angle of repose (Kanatani, 1983). There are various experimental methods for the measurement of the angle of repose of a powder. These include fixed height or free standing cone, fixed base cone, tilting table and rotating cylinder drum (Motamedi, 1985; Sherrington and Oliver, 1981). The simplest apparatus for evaluating this angle consists of a conical hopper with a small opening at its apex mounted above a horizontal surface. The hopper is filled with the material and is opened at the bottom, then a heap or pile forms underneath. The angle of repose θ is calculated by

$$\tan \theta = \frac{2 \pi H}{c} \qquad (2.1)$$

where H is the pile height and c is the pile circumference at its base. Particle shape, particle specific gravity, average particle diameter and moisture content influence the angle of repose (Orr, 1966). Deming and Mehring, 1929 determined the angle of repose by pouring a convenient quantity of the material into a heap upon a level surface and measuring the angle between the sloping side of the pile and its base at several points and averaging the results. The angle of repose is not a definitive quantity, the size of the heap or pile can be a significant factor in the value of the angle of repose (Orr, 1966). Perry and Chilton, 1973 classified bulk solids according to their flowability on the basis of the value of the angle of repose. Materials with angle of repose up to 30 deg are very free flowing; materials with angle of repose 30 to 45 deg are considered free flowing and materials with angle of repose 45 deg and above are classified as "sluggish".

Angle of slide: The angle of slide is defined as the maximum angle with the horizontal at which a powder can retain its position on a plate. It is more readily measured by spreading a thin layer of the material over a horizontal plate and then raising one edge of the plate until the powder rolls or slides off. The angle of slide increases as granule diameter decreases (Orr, 1966).

Angle of rupture: The angle of rupture is the angle with the horizontal formed when a bulk powder slides under the force of gravity against a stationary solid (Orr, 1966).

Angle of internal friction: Another physical property of powders is the angle of friction between particles. The angle of internal friction is an important parameter for characterising the mechanical behaviour of bulk solids. Beddow, 1983 found a correlation between the angle of internal friction and the morphic terms. Orr, 1966 has discussed the different methods for measuring the angle of internal friction. The methods include shear measurements, the angle with the horizontal assumed by the solids discharging from a container, and the difficulty of the movement of a bed of powder in a vertical tube. The effective angle of internal friction is measured indirectly by the shear test and has significance during steady flow of the solid.

Angle of wall friction: The value of the angle of friction on a wall surface is measured directly by the shear test, its tangent is defined as the shear force necessary to maintain motion of the bulk solid on a wall surface over the load applied perpendicular to the wall. In certain cases it can vary with apparent normal pressure.

The values of all these angles are interrelated. The angle of internal friction represents a dynamic equilibrium between individual grains moving in contact against bulk solids; the angle of rupture is the result of bulk solids moving against stationary bulk solids; while the angle of repose reflects a static equilibrium between uncontained solids and the surrounding fluid medium. The angle of slide depends on the frictional force between particles and the inclined surface; it is a function of the surface composition as well as the particle characteristics (Orr, 1966).

2.2.3.3 Mass Flow Through an Orifice

The measurement of the rate at which a powder flows through an orifice gives an idea of the flowability of the powder. This technique has been used by Prior and Sharma, 1987 to study the flow properties of several ferrite agglomerates. The flow of particulate materials through an orifice has been the subject of many studies. Beddow, 1983 found that a good correlation is obtained between this parameter and the morphic terms which describe the shape of the particles. Deming and Mehring, 1929 determined the mass flow, i.e. the time for a given mass to flow through an orifice by allowing a weighed mass of the material, sufficient in quantity to be timed accurately to flow through a funnel by the action of gravity. The axis of the funnel was kept vertical.

2.2.3.4 Shear Test

The pioneering work of Jenike, published in 1961 (Perry and Chilton, 1973), changed radically the area of bin storage of bulk materials. Prior to Jenike storage-bin design was empirical. Jenike identified the criteria that affect material flow in storage vessels describing the stress situation when a particulate material is constrained to flow under the influence of gravity through a converging hopper. He established and

numerically solved the differential equations defining bulk flow. He also developed an experimental technique to measure the actual stress-strain behaviour of a material using a shear tester. The procedure is based on the conditions at which a given material just fails within itself causing incipient flow to occur (see Section 3.2.5.1). A flow function curve which describes the material's ability to flow is determined. This allows the design of bulk storage vessels so that the material will flow (Sherrington and Oliver, 1981). Schwedes and Schulze, 1990 have presented a survey of the numerous types of shear testers available for the measurement of the flow properties of bulk solids. The work of Jenike has been extended and it has led to the study of stress distributions when a powder in a die is compacted (see Chapter 4).

2.2.3.5 Inclined Plane Experiment

Briscoe *et al.*, 1983 designed a model experimental technique to study the interfacial sliding friction during pipe flow. The experiment senses the angle of inclination required to initiate motion in a cylinder, partially filled with the powder, down an inclined plane. The basis of the experimental system is the application of a gravity-induced potential energy gradient to generate continuous interfacial sliding. This same experimental technique has been used in this work to study the flow and wall friction properties of several ceramic powders under unconstrained flow.

The behaviour of the powder confined in a horizontal cylinder is similar to the situation in rotary kilns. In a kiln flow a particle in a bed of the material remains stationary with respect to the kiln wall until it reaches a position close to the surface of the bed. Then it cascades down along the bed surface in a direction such that it progresses a short distance axially through the kiln and finally comes to rest. This cycle is repeated over and over again for each particle (Orr, 1966). The motion of particles in a rotating cylinder is determined by the diameter and speed of rotation of the cylinder and by the quantity of material introduced and its physical characteristics, such as its specific gravity, the shape and size of particles, and its moisture content (Oyama, 1980). In the case of a material flowing down an inclined plane or between parallel inclined walls, the angle of inclination of the confining structure must be greater than

both the angles of internal friction of the material and the angle of sliding friction of the material with the structure walls (Orr, 1966).

Cross, 1978 classified the transverse motion of solids moving through rotary kilns into two main categories although three types of motion have been observed experimentally; rolling and slumping may be considered as different aspects of the same type of motion. These categories are characterised by whether or not the frictional forces exerted by the material on the kiln wall are extensive enough for the material to maintain its position (relative to the wall) until its angle of repose is exceeded. These two modes of transverse motion are the rolling/slumping mode where the frictional forces exerted by the material on the side of the kiln wall are extensive enough to maintain its position until the material's angle of repose is exceeded. When this happens, the material at the wall rolls down and mixes in with the bulk. This may either happen in a continuous (rolling) or a discrete fashion; in the latter case it is called slumping. The second mode is the sliding mode where the frictional forces are not large enough for the material to remain in contact with the wall until the angle of repose is reached. Thus, the characteristic wall sliding occurs. Cross derived an equation that defines the degree of filling required to ensure that the material moves in the rolling/slumping mode, as a function of its angle of repose and coefficient of friction with the wall. The flow regimes associated with the transverse motion of particles in rotating cylinders are functions of the total normal load and the bed velocity. Briscoe *et al.*, 1983 observed the motion of solids in a rotating cylinder, at low angular velocities, sliding occurred in the case of small bed loads and cascading was evident at higher bed loads. A smooth transition zone between both regimes was defined. They developed a quantitative method to identify both regimes and a theory that predicted the transition between the sliding and slumping modes.

Figure 2.1 shows the modes of motion of material in a drum at various speeds or as a function of the degree of filling (after Sherrington and Oliver, 1981). At low rotational speeds, material slides about in the bottom of the drum with very little relative motion between particles. As the drum speed is increased the material begins to roll and, at half the critical speed cascading occurs. The speed ranges over which the

various regimes occur are not well defined and are in any case a function of the nature of the solids and their moisture content (Sherrington and Oliver, 1981).

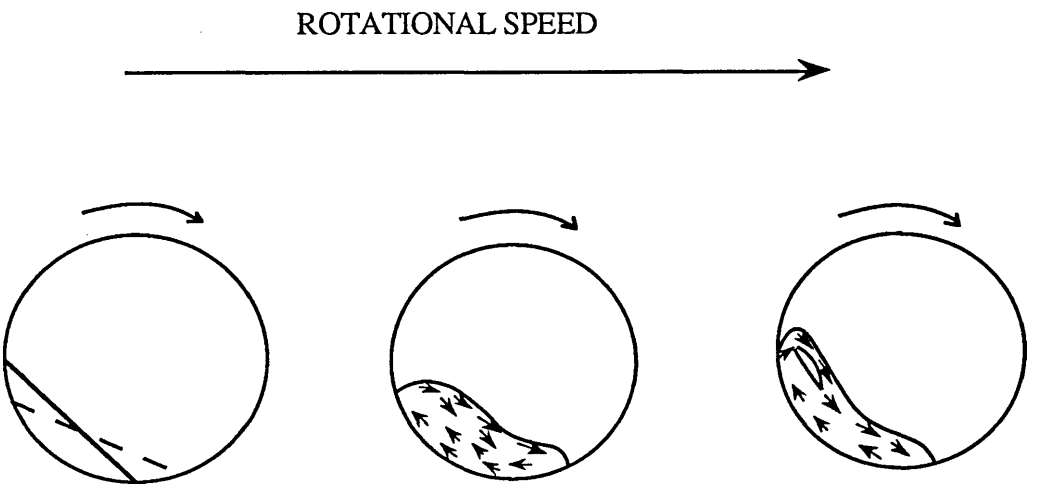

Figure 2.1 Typical modes of motion of material in a rolling drum as a function of the rotational speed (after Sherrington and Oliver, 1981).

Ruiz de Gordoa *et al.*, 1986 studied the interrelation between the properties of the solids and the dynamic behaviour of rotary cylinders. They found a simple logarithmic correlation relating the central angle of the sector occupied by the solid in rotary cylinders to the central angle without rotation (see Figure 2.2) for alumina, calcium hydroxide, limestone and dolomite. The results are useful to describe the influence of the operation variables on the gas-solid and wall-solid areas. They calculated the wall-solid area of contact, $A_{s\text{-}w}$, through the expression

$$A_{s\text{-}w} = \frac{\delta \pi D L}{360} \qquad (2.2)$$

where δ is the central angle of the sector occupied by the solid bed with rotation, D is the cylinder diameter, and L is the loading degree.

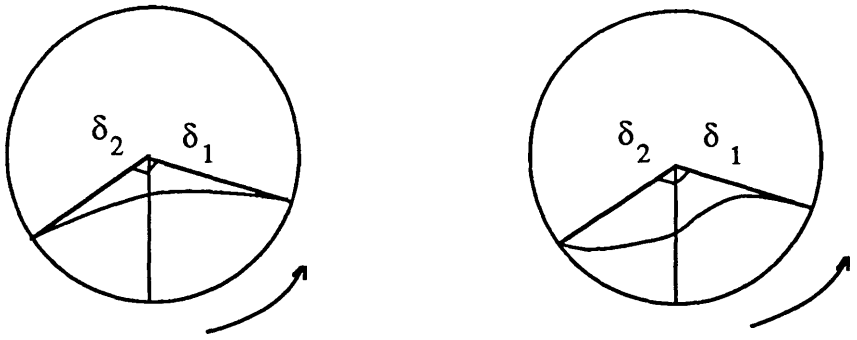

Figure 2.2 Schematic representation of the measurement of the central angle of the sector occupied by a solid in rotating cylinders (after Ruiz de Gordoa *et al.*, 1986).

2.2.4 Friction

The friction effects occurring during the processing of ceramic materials have been studied in this work. Both interparticle and particle-wall friction are important. They affect the flow properties. These friction effects and their relationship to the flow properties and also the compaction and ejection stages will be considered in some detail in Chapter 3.

CHAPTER 3

INTERFACE FRICTION

3.1 INTRODUCTION

In this study the frictional effects at several distinct stages during the processing of dry ceramic materials have been analysed. The study concentrates on three areas in the production of ceramic green bodies which are the die filling and unconstrained powder flow, the compaction or constrained flow and finally the green ejection. In this Chapter a general literature review on interface friction and, in particular, on wall-powder friction is included. Several models used to describe the situation at the wall-powder interface are presented. The experimental results on the wall friction during unconstrained flow and during the dry pressing of the ceramic materials are presented and analysed in Chapters 7 and 8 respectively.

3.2 LITERATURE REVIEW

3.2.1 General Laws of Friction: An Historical Review

If two bodies are placed in contact under a normal load W, a finite force is required to initiate or maintain sliding; this is the force of friction F_f, for static or dynamic conditions. The static frictional force is the force required to initiate relative motion and the dynamic frictional force is the force required to maintain this motion. The magnitude of the dynamic frictional force is equal to the work done per unit sliding distance.

The scientific study of the dynamics of motion and of friction phenomena started with the work done 370 years ago by Galileo with his discovery of the "principle of

inertia". Next, Newton formulated the basic laws of classical mechanics. Amontons in 1699 and Coulomb in 1785 formulated the two basic first order laws of friction (Dowson, 1979):

- The frictional force is directly proportional to the normal load; $F_f = \mu W$ where μ is the coefficient of friction and can be expressed as the tangent of the frictional angle.
- The frictional force is independent of the apparent area of contact.

The first law had been found by Leonardo da Vinci by the middle of the fifteenth century. These laws are of limited validity and do not generally apply to powders (Brostow, 1979). The friction of powder-wall contacts is usually directly proportional to the apparent area of contact and the coefficient of friction is usually dependent on the normal load or apparent contact pressure and hence not a constant. In the 1920's Hardy and Tomlinson put forward the "adhesion theory" of friction. Desagulier in 1724 had suggested that adhesional forces might be involved in friction. This theory requires that the frictional force is proportional to the area of contact which is in disagreement with numerous experimental results. These discrepancies were clarified in about 1940 by Bowden and Tabor with their adhesion theory of friction. They noted a great difference between the apparent geometrical area of contact and the real area of contact. They introduced the dual nature of friction; both deformation and adhesion processes are involved in friction (Czichos, 1978).

In the next sections some models of the interface friction of solid materials in contact with plane surfaces are presented. Two main approaches, the particulate and the continuum models, are considered.

3.2.2 The Two Term Model of Friction

The sliding of two bodies involves two main energy dissipation processes. Adhesive junction rupture which occurs at the regions of real contact and ploughing or deformation of one surface by the asperities on the other, harder surface. These two factors are considered largely to be non-interacting, and hence may be studied quite

independently. The adhesive or interface friction originates at the interface and is scaled by the real contact area, the deformation friction arises from subsurface energy losses and is scaled by the apparent or geometric contact area (Tabor, 1975).

The total frictional force, F_f, is obtained by adding the adhesion, F_{ad}, and the ploughing or deformation, F_{pl}, terms considering there is negligible interaction between these two processes (Tabor, 1975)

$$F_f = F_{ad} + F_{pl} \tag{3.1}$$

These ideas originated from the study of the friction of coherent, homogeneous solid bodies. However, they may be applied to the interface friction of powders or particle arrays sliding over smooth and rigid walls (Briscoe *et al.*, 1985).

3.2.2.1 Ploughing or Deformation Mode

If a hard asperity ploughs its way through the surface of a softer material, the friction or ploughing force is expressed as

$$F_{pl} = \phi \beta \tag{3.2}$$

where F_{pl} is the work done per unit sliding distance. The parameter ϕ is the total work done in deforming the body, per unit distance; β is the fraction of this work which is dissipated within the body. The magnitude of ϕ is directly related to the apparent area of contact and β is related to the viscoelastic or plastic character of the solid. Ploughing friction is caused by inelastic deformation in the bulk. This component of friction arises from energy losses within a large volume of material adjacent to the contact; a volume of similar dimensions to the contacting asperities. The magnitude and the nature of this dissipation process are dependent on the response of the material to deformation, the strain rate, the temperature, and the geometry of the sliding contact. When the rigid counterface is smooth the ploughing term may be neglected. One accepted method for

measuring the energy dissipated in this component of friction and for elucidating the friction mechanisms involved is to perform a scratch hardness analysis of the material (Carter, 1988; Briscoe and Evans, 1988).

3.2.2.2 The Adhesion or Interface Mode of Friction

The present knowledge of friction derives mainly from experiments on metals. The Bowden-Tabor adhesion theory was first derived for metallic contacts and boundary lubrication (Bowden and Tabor, 1954). When two clean and ductile bodies are brought together the interaction of surface attractive forces creates a set of discrete, adhesive junctions between the sliding surfaces and frictional work is required for their rupture. This component of friction arises during the sliding of these bodies which involves shearing and failure of these adhesive junctions and the formation of new ones. The energy dissipation process occurs at the interface, at the contact points, and corresponds to a continuous mechanism of interfacial shear work (Briscoe *et al.*, 1987; Adams *et al.*, 1987a). The adhesion mechanism involves an interaction of surface forces and bulk deformation. The true contact area is given by the total area of these junctions which is significantly less than the apparent contact area. The adhesional theory of friction states that the friction force between two sliding solids is given by:

$$F = \tau_r A_r \tag{3.3}$$

where τ_r is the real interface shear strength, it is the work done per unit contact area per unit sliding distance, and A_r is the real contact area which is assumed to be independent of the frictional force. The parameters τ_r and A_r, and hence F are functions of the normal load. Both parameters are sensitive to the contact conditions, particularly the contact pressure, the load and the temperature. Generally, at constant temperature and sliding velocity, it is found empirically that the contact pressure dependence of τ is given by

$$\tau_r = \tau_{or} + \alpha P_r \tag{3.4}$$

τ_{or} and α are characteristic interfacial rheological parameters independent of pressure for a given interface (Amuzu *et al.*, 1977). τ_{or} is some intrinsic shear strength and α is the pressure coefficient. The real contact pressure, P_r is defined as the normal load over the real area of contact.

The traditional approach of the study of friction states that the frictional force is a function of the applied normal load. This load dependence of the frictional force may be described by the empirical power law expression:

$$F = k\, W^n \tag{3.5}$$

where k, the friction factor, and n, the load index, are constants. The value of the load index n depends on the type of contact and takes values in the range 2/3 to unity. n is a function of the surface topography, the load and the state of the interface deformation; and it is also a function of the variation of the area of contact with load.

The two approaches represented by equations 3.3 and 3.5 are considered in the following sections.

First, it is necessary to consider model single point contacts. Several different situations will be distinguished regarding the type of contact (elastic or plastic) and the surface topography (smooth or rough). All these cases are considered in the following sections. When two surfaces are placed in contact the contact occurs only where the asperities on one surface touch the other. The true area is that area over which the atoms in one surface are within the repulsive fields of those on the other and it is generally very much smaller than the apparent area. This is due to the presence of surface irregularities (Tabor, 1975). The real area of contact is sensitive to the normal load, the contact topography, and the deformation characteristics of the solids. As the normal load increases the real area increases. The size of the existing contact points will increase and perhaps new points of contact will be formed. Generally, the real area of contact cannot be measured directly but it is calculated from contact mechanisms providing several assumptions are adopted. In general the variation of the real area of

contact with the load is given by

$$A_r = k' W^m \tag{3.6}$$

where k' is a constant and m is a load index whose value depends on the contact conditions and some materials properties of the contacting solids. A number of classical analytical models, based on contact mechanics, of predicting A_r or its variation with the normal load will be presented. These models are combined with the adhesion model of friction to predict the variation of the frictional force with the normal load on the body (Briscoe *et al.*, 1985).

3.2.2.2.1 Elastic Contact

For elastically deforming contacts two cases arise depending upon whether the contact comprises of either a single asperity or several asperities. First the single asperity situation, represented by a single elastic, smooth sphere is presented.

3.2.2.2.1.1 Single Asperity Model; Hertz

In the first instance an elastic contact of a smooth sphere on a smooth flat plane is assumed. For smooth elastic surfaces $A_r \propto W^m$ (m=2/3) and the real contact area is computed from the Hertz theory of elasticity (Briscoe *et al.*, 1985; 1987) by

$$A_r = \pi (D\, W\, R)^{2/3} \tag{3.7}$$

where W is the normal load applied on the individual particle contact, R is the mutual radius of curvature of the contact; in this case the sphere radius, and D is a mutual elastic constant defined by

$$D = \frac{3}{4}\left(\frac{1-\upsilon_1^2}{E_1} + \frac{1-\upsilon_2^2}{E_2} \right) \tag{3.8}$$

where E_1 and E_2, and υ_1 and υ_2 are the modulus of elasticity and the Poisson's ratio of the two contact solids respectively.

Combining equations 3.3, 3.4 and 3.7, the friction force is given by:

$$F = \tau_o \pi (D W R)^{2/3} + \alpha W \tag{3.9}$$

which has the general form

$$F = c W^{2/3} + \alpha W \tag{3.10}$$

where $c = \tau_o \pi (D R)^{2/3}$

Therefore, according to equation 3.9 the load dependence of the friction force has the form expressed in equation 3.5; $F = k W^n$ where the value of n is a function of the ratio α/c=a (Briscoe *et al.*, 1985). It has been shown (Adams *et al.*, 1987a) that by transposing equation 3.9 into the powder law form (equation 3.5) the value of n is given explicitly by

$$n = \left(\frac{2 + 3 a W'^{1/3}}{3 + 3 a W'^{1/3}} \right) \tag{3.11}$$

and

$$k = \frac{c + \alpha W'^{1/3}}{W'^{z}} \tag{3.12}$$

where W' is the logarithmic mean of the load range used and z is

$$z = \frac{a W'^{1/3}}{3\left(1 + a W'^{1/3}\right)} \tag{3.13}$$

The load index depends on the relative load coefficients in equation 3.10 and may vary between 2/3 and 1 even for an Hertzian contact. For large values of a or at high loads (W'>>1) n tends to 1. Whilst for small values n tends to 2/3. Smooth contacts yield small values of a, and n is ca. 2/3.

3.2.2.2.1.2 Multiple Asperity Contact; Archard

It has been shown that the area of contact for a single sphere or asperity under a load W is given by the Hertz solution, equation 3.7. If the contact is not a point, as it is the case for rough solids, the evaluation of the real area of contact is less certain. These multiple asperity contacts (non-Hertzian) were usefully analysed by Archard, 1957. He deduced a series of equations for the area of contact when a body has layers of asperities on its surface.

In general, a typical contact produced between rough surfaces will comprise multiple asperities some of which will deform elastically and others plastically. The plastic deformation case is presented in Section 3.2.2.2.1. For elastically deforming asperities there are two distinct types of behaviour for a contact with a flat body depending on the distribution of asperity heights and the change in asperity interactions during loading (Archard, 1957; Briscoe *et al.*, 1987). These two distinct bounds which govern the contact mechanics of rough surfaces, as pointed out by Archard, are:

- All the asperities are of the same height and the number of asperity contacts remains constant with increasing load so that an increase in load increases the elastic deformation of each contact; then the area of real contact is proportional to $W^{2/3}$ and n=2/3. This is an uncommon situation in practice.

- There is a normal distribution of asperity heights; and the number of asperity contacts increases with load so that the average area of each deformed asperity remains constant and increasing the load increases the number of regions of contact. Non-contacting asperities come into contact with increasing load and provide a load bearing capacity which reduces the load on the contacting asperities. Then, the real area of contact is directly proportional to the load.

An intermediate case is the case where all the asperities are of the same height but all of them are on the curve surface of a larger sphere. In this case, for an array of elastic spheres of radius R_p on a larger sphere of radius R_s, also deforming elastically, the real area of contact is

$$A_r = k'' \frac{1}{E_p^{2/3}} \frac{1}{E_s^{2/9}} R_p^{2/3} R_s^{2/9} \psi^{1/3} W^{8/9} = k' W^{8/9} \qquad (3.14)$$

where ψ is the contact density, E_p and E_s are the modulus of elasticity of the asperities and the sphere and k" is a proportionality constant. n is predicted as 8/9. This is the so-called Archard precursor (Briscoe *et al.*, 1987).

Archard concluded that in any real situation where elastic deformation occurs, the area of contact will be proportional to W^m where m lies between 2/3 and unity. A multiple asperity model (surface covered with asperities which are covered with smaller asperities) involving purely elastic deformation tends to give an area almost linearly proportional to the load.

3.2.2.2.2 Plastic Contact

For a plastically deforming contact, i.e. at high normal loads exceeding the flow stress of the material, the mean asperity contact pressure remains constant and is of the order of the flow stress of the asperities of the softer body, P_o, which is comparable to its indentation hardness, H, then

$$A_r = \frac{W}{P_o} \tag{3.15}$$

The area is thus proportional to the load, and from equations 3.3 and 3.4 the frictional force is expressed as:

$$F = \left(\frac{\tau_o}{P_o} + \alpha \right) W \tag{3.16}$$

and then the load index, n in equation 3.5, is unity. Therefore the frictional force is directly proportional to the applied normal load.

These ideas explaining the interfacial friction of solids may be applied to the interface friction of powders or particle arrays (Briscoe *et al.*, 1985) and to studies on the friction of polymers (Briscoe, 1980). Amuzu *et al.*, 1976 presented data to confirm the validity of the adhesion model of friction for several polymers. They measured the shear strength and friction of a number of polymers. Their results confirmed that the shear strength of the contact is related to the contact pressure by equation 3.4 and that the energy generated during sliding of bulk polymers is dissipated within a narrow region close to the interface. Briscoe and Smith, 1980 reviewed the magnitude of, and the factors which influence the frictional losses of organic solids in sliding contacts. The main interest was the variation of the interfacial shear strength with the nature of the organic layer and the contact variables.

3.2.2.2.3 Discrete Particle-Wall Interactions in Assemblies

The friction models described in the previous sections have referred to continuous bodies in contact. These models may be applied to powder systems. The difference is that the particles are autonomous unlike asperities. To describe the interface an analogy may be established between the deformation of rough solids against planes and the sliding of particle arrays against planes, since the rough surfaces may be considered as an array of hemispheres (which themselves may be rough) known as asperities (Adams

et al., 1987a).

For particle assemblies or arrays, the total friction force wall-particle array may be expressed as the sum of the individual friction contributions ($F = \sum \delta F$):

$$F = \tau \sum \delta A \tag{3.17}$$

where there are N discrete particle contacts of area δA. Several assumptions must be made to model the contact conditions for assemblies. The particles are close packed elastic spheres. The particles have autonomy in the vertical direction but not in the friction plane. The resulting total normal stress at the wall is then shared by the contacts and it is assumed that each wall contact supports the same fraction of the load; i.e, the load is evenly distributed between the discrete contact points (Briscoe and Evans, 1988). The number of contact points is assumed to scale with the apparent or geometric contact area of the particle bed, A_{app} (Briscoe *et al.*, 1984). For elastically deforming contacts assemblies of smooth spherical particles may be represented by the case of a constant number of asperity contacts so that the friction is a function of the normal load, $2/3<n<1$. For rough spheres the analogy to the Archard case of a variable number of contacts means that n=1. With increasing roughness the friction becomes less dependent on the gross contact area and closer to a linear dependence on the load. These cases are for elastic deformation of the interface. If plastically deforming contacts are considered then, the situation described in Section 3.2.2.2.2 is applicable; i.e., the real area of contact is proportional to the normal load.

3.2.2.2.4 Load Dependence of the Coefficient of Friction

From equation 3.5 the coefficient of friction can be expressed as a function of the load:

$$\mu (W) = \frac{F}{W} = k\, W^{n-1} \qquad (3.18)$$

When n = 1 the coefficient of friction is independent of the load, and when n < 1 the coefficient of friction decreases with the load (Adams *et al.*, 1987a). Considering the pressure dependence of the friction force and for an elastic deformation of the interface (equation 3.10) it may be seen that the coefficient of friction decreases with the load according to

$$\mu = (c\, W^{-1/3}) + \alpha \qquad (3.19)$$

and consequently the coefficient of friction is a function of the normal load and the radius of the particle. For a rough surface the coefficient of friction is independent of the load, m=n=1, and it decreases with increasing roughness due to the reduction in the real area of contact (Briscoe, 1990).

The coefficient of friction may also be expressed as a function of the contact pressure (Amuzu *et al.*, 1976)

$$\mu = \left(\frac{\tau_o}{P} + \alpha \right) \qquad (3.20)$$

this expression predicts that for elastic deformation of the interface, the coefficient of friction decreases with the contact pressure until some asymptotic value is reached. High contact pressures induce plastic deformation of the interface and the mean contact pressure P, is constant and of the order of the flow stress or hardness of the interface. Under these conditions, for a plastically deforming contact, equation 3.20 may be written as

$$\mu = \left(\frac{\tau_o}{P_o} + \alpha \right) \tag{3.21}$$

the coefficient of friction is independent of the load but is a function of the hardness of the softer solid. For most cases $\tau_o/P_o << \alpha$, and hence the friction coefficient is largely controlled by the magnitude of α. Amuzu *et al.*, 1976 showed for several polymers sliding using three different configurations that an increase in the contact pressure results in a decrease in the coefficient of friction.

3.2.2.2.5 Summary: Load Dependence of the Friction Force and Load Index

The frictional force is a function of the applied normal load. In general, the frictional force is found to vary with the applied normal load according to the expression;

$$F = k\, W^n$$

The parameter k is equal to the coefficient of wall friction, $\mu_w = F / W$, only when n is equal to 1. The value of n will be mainly governed by the variation of the real area of contact with the normal load. In general the real area of contact is proportional to W^m where m ranges from 2/3 to unity,

$$A_r = k'\, W^m$$

and incorporating the adhesion model of friction,

$$F = \tau_o\, k'\, W^n + \alpha\, W \tag{3.22}$$

so that m≤n≤1. The value of m and hence n depends on the surface topography at the contact, the magnitude of the applied normal load and the state of the interface deformation. It has been found that n can take any value from 2/3 to 1 depending on the elasticity and smoothness of the contact. A value of 2/3 for n represents a totally smooth, elastic contact, but values greater than this indicate a rougher surface and/or plastic deformation. Figure 3.1 represents in a schematic way the different situations at the interface.

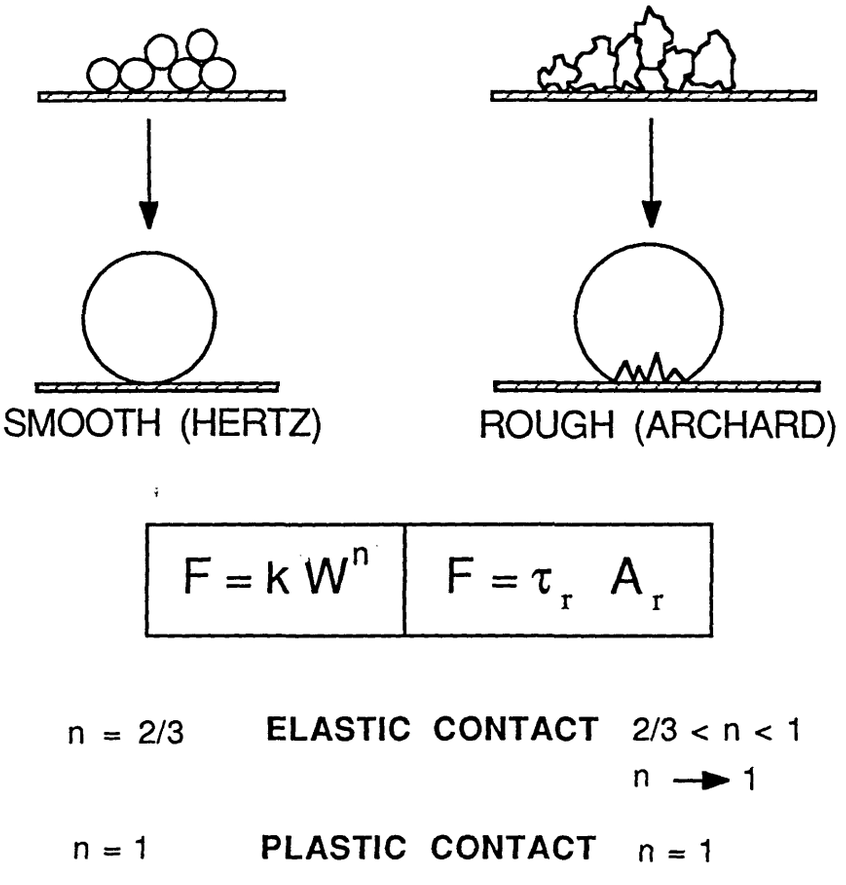

Figure 3.1 Schematic representation of the situation at the wall interface for different types of contacts.

Some means of predicting the coefficient of friction and its variation with load, from the knowledge of a number of mechanical and interfacial rheological properties,

the contact geometry, and the surface topography have been discussed. The main mathematical expressions describing the friction behaviour for the different types of contact have been summarised in this Chapter. One may be referred to a wide literature, e.g. Briscoe, 1987 who reviews the use of established contact mechanics as a means of modelling particle wall interactions. Adams *et al.*, 1987a and Tüzün *et al.*, 1988 provide more detailed explanations.

3.2.3 Continuum Approach

The propagation of stresses in powders is often described by considering that the material behaves as a continuum. The assembly of particles is ascribed an effective yield stress and the system is then amenable to analysis using continuum mechanical or rheological notions. An example is the method of characteristics of the slip line field theory (Nedderman, 1982). Discrete particle interaction approaches are comparatively rare (Briscoe, 1987). The frictional behaviour of powders in all engineering applications is described by two independent parameters; the coefficients of internal and wall friction. Two types of materials are described; cohesive and cohesionless materials.

3.2.3.1 Interparticle Friction

The coefficient of internal friction in powders determines the stress distribution within a bed of powder undergoing strain (Tüzün, 1987).

3.2.3.1.1 Cohesionless Materials

This term refers to those granular materials whose intrinsic shear strength under zero consolidation load ($\sigma = 0$) is negligible. The lack of cohesion in granular materials suggests that the magnitude of interparticle forces is negligible (Coulomb-type materials). For these materials the internal yield locus is given by

$$\tau = \sigma \tan\varphi_i \tag{3.23}$$

where τ is the shear stress, σ is the consolidation load, and φ_i the angle of internal friction. These materials have a coefficient of internal friction independent of its bulk density and hence of the magnitude of the interstitial voidage of the material bed (Tüzün, 1987).

3.2.3.1.2 Cohesive Materials

Their intrinsic shear strength under zero consolidation load is large. Using the Coulomb criterion the yield locus at incipient failure may be expressed as

$$\tau = (\tan \varphi_i)\, \sigma + C \tag{3.24}$$

C is termed cohesion.

Experimental measurements sometimes indicate significant curvature of the yield locus and the data may be fitted using the Warren-Spring equation

$$\left(\frac{\tau}{C}\right)^{b} = \frac{(\sigma + T)}{T} \tag{3.25}$$

where T is the tensile strength of the material. Experiments have shown that the load index b varies between 1 and 2.

3.2.3.2 Wall Friction

The coefficient of wall friction of powders describes the magnitude of the stresses between the material bed and the walls of its container (Tüzün, 1987). The wall friction of particulate materials is a critical factor in a number of engineering operations and in the design of process machinery. A number of approaches to determine the wall stress distribution should be mentioned; Coulomb's method of wedges; the differential slice technique and the method of characteristics (Fernando, 1987).

Movement of a bulk material with relation to a boundary wall involves surface friction. The angle of friction of the contact surface represents the relationship between the normal pressure and the frictional resistance to motion. Fine or wet materials can exert additional forces of a tensile or cohesive nature and a significant difference between initial failure and sustained slip may be observed (Bates, 1977).

3.2.3.2.1 Cohesionless Materials

The wall friction behaviour of the Coulomb-type materials (cohesionless) is characterised by the lack of adhesive forces between the particles and the wall surface, this is known as non-stick behaviour; the wall yield locus can be described by;

$$\tau_w = \sigma_w \tan \varphi_w \tag{3.26}$$

where τ_w is the wall shear stress, σ_w is the normal stress at the wall, and φ_w is the angle of wall friction. The angle of wall friction is often assumed to be independent of the magnitude of the normal stress acting on the wall and also of the bed voidage adjacent to the wall. In some cases there is indication of a dependence of the wall friction angle on the normal load on the wall.

3.2.3.2.2 Cohesive Materials

In this case the adhesion forces between the wall and the material bed must be taken into account

$$\tau_w = (\tan \varphi_w)\, \sigma_w + C_w \tag{3.27}$$

the term C_w is the adhesion. Some experimental measurements indicate that the wall friction angle is a function of the normal stress acting on the wall and this equation fails to explain this. A dynamic friction criterion becomes necessary and the individual particle properties will have to be considered (contact mechanical approach) (Briscoe,

1984; Tüzün, 1987) (see Section 3.2.4).

3.2.4 Continuum vs. Particulate Approach

Tüzün, 1987 explained that the conventional continuum mechanics approach is not capable of explaining fully the frictional behaviour of Coulomb materials during sustained flow in bulk solids containers. He attributes these deficiencies to the effect of some particle properties on the frictional behaviour of the material and suggests the investigation of single particle friction characteristics as a means of providing the necessary predictive relationships. Adams *et al.*, 1987a explained the wall friction behaviour of cohesionless materials in smooth silo walls by a contact mechanical model which considers the particles properties. This analysis couples the continuum model of the bulk stress state with the contact mechanical features at the particle bed-wall interface. A dynamic friction criteria becomes necessary and the individual particle properties have to be considered using a contact mechanical approach. The contact mechanical approach aims to arrive at the frictional behaviour from a consideration of the contact frictional behaviour of the individual particles making up the bulk (Briscoe *et al.*, 1973; Briscoe, 1984).

3.2.5 Friction Measurements

The values of the internal and wall friction coefficients are in general determined empirically; there have been only a limited number of attempts to predict them analytically. There are many parameters that may affect wall friction such as particle size and shape, particle size distribution, moisture content, wall surface properties, surface roughness, and lubrication. This requires explicit definitions of the functional relationships between the friction coefficients and particle properties and/or some assembly characteristics such as internal voidage, compressibility and cohesive strength (Tüzün, 1987).

Various methods for measuring the coefficient of friction have been used (Motamedi, 1985). The internal angle of friction may be approximated by the angle of

repose of the material when the cohesive strength of the material is believed to be negligible. Two ways have been used to determine the angle of repose; materials are either discharged from a flat-bottomed container or are allowed to form a heap on a horizontal surface (Tüzün, 1987). Chapter 2 reviewed the characteristics angles of a material and their measurement.

The angle of wall friction may be determined by accommodating a layer of the bulk material on an inclined surface and measuring the angle of inclination of the surface at the point of initiation of particle sliding (Tüzün, 1987). A direct determination of the wall friction in silos is the simultaneous measurement of the normal and shear loads at their walls using twin-axis load cells. Tüzün *et al.*, 1988 described an alternative approach. They compared the measured stresses at the wall of a silo with predictions derived from single particle friction properties and a geometric description of the particle assembly adjacent to the wall. "Quasi-static" measurement is possible using either annular or Jenike-type shear cells and determining the wall yield locus.

3.2.5.1 Shear Cell

The internal and wall coefficients of friction of powder materials may be measured indirectly in a number of ways. The most common method to determine directly the effective angle of internal friction of a powder and the angle of friction between a powder and a surface is the use of a "shear cell", where a normal force is applied to the upper part of the cell and the shear force required to maintain movement amongst the particles of the material or between the material and the surface is determined under various normal loads. From these measurements the material or the wall yield locus is obtained,

$$\tau = f(\sigma) \tag{3.28}$$

where τ is the shear stress parallel to the plane and σ is the compressive stress normal to the plane. The slope of the material or wall yield locus determines the coefficient of internal or wall friction respectively and the angle of friction may be calculated (Tüzün, 1987):

$$\tan \varphi = \text{shear force/normal force} \tag{3.29}$$

$$\mu_i = \tan \varphi_i \tag{3.30}$$

$$\mu_w = \tan \varphi_w \tag{3.31}$$

where φ_i is the angle of internal friction, and φ_w is the angle of wall friction.

Van den Bergh and Scarlett, 1987 used a Jenike shear cell to determine the coefficient of wall friction and the internal friction coefficient of sand and stainless steel (polished and rough surface) as a function of the ratio of the particle diameter to the wall roughness. They concluded that the wall friction coefficient will increase due to breakage of the particles in the bulk of the material when subjected to high normal loads and strain, tending towards a maximum value. The original wall friction changes to powder-powder friction due to the creation of fines and dust particles smaller than the wall roughness grooves.

3.2.6 Friction During Unconstrained Flow

Briscoe *et al.*, 1985 have developed an experimental technique for measuring the interfacial wall friction during powder flow. They studied the influence of particle surface topography on the interfacial friction using two types of particles differing in their surface topography (smooth and rough surfaces). Briscoe *et al.*, 1984 have studied the frictional characteristics of an interface generated by an array of particles in contact with a smooth body and they explained the experimental results according to the multiple asperity nature of the individual particle contacts. Briscoe *et al.*, 1983 have evaluated the static and dynamic coefficients of sliding friction for wet and dry systems for application in hydraulic conveying, simulating pipeline flow using a rotating glass cylinder partially filled with sand.

3.2.7 Friction During Die Pressing and Green Ejection

During compaction, a surcharge is applied at the die wall and the pressure compacts and densifies the powder. The wall friction opposes the applied pressure and it influences the development of the stresses and strains within the compact. These processes naturally lead to significant density gradients within the compact. This is undesirable mainly as it creates a variation in sintering rates and as a result internal stresses are developed during the sintering phase. A low friction coefficient at the walls, μ_w, will minimise these variations in the density distribution. During compaction lubricants and binders may reduce interparticle frictional forces and improve compact strength. The principal role of the lubricant is in reducing die wall friction. The effect of lubrication is to facilitate the uniform transmission of forces reducing the pressure gradients, effectively increasing the pressure near the bottom of the compact and reducing compaction density variations (Reed and Runk, 1976). Internal lubricants are added to the material feed not only to improve its flow properties (flow into the mould or die and rearrangement during compaction) but also to assist in the release of the final agglomerate from the mould or die, effectively reducing the ejection pressures (Capes, 1980).

3.3 SUMMARY

In this Chapter two main approaches to describe the interface frictional behaviour between two solids in contact have been presented. The particulate approach originates from the adhesion model of friction which describes the interface friction of a solid in contact with a smooth wall as a function of the real area of contact. The magnitude of the real area of contact is a function of the type of contact (elastic or plastic deforming contact) and the surface topography. The expressions describing the frictional force for these different types of contacts have been described. The continuum approach model describes the propagation of stresses in powders considering that the material behaves as a continuum. It describes the yield locus at the point of incipient failure.

These models will be applied to the study of the wall friction of ceramic powders submitted to a range of applied loads. The interactions between the walls and the powders will be rationalised by applying these models, modified according to the particular conditions present at a given interface. They provide the basic ground to predict the magnitude of the friction force and to explain the observed frictional behaviour.

CHAPTER 4

COMPACTION

4.1 INTRODUCTION

The forming step in ceramic processing is reviewed in this Chapter. There are a great variety of forming methods, that can be classified as:

- compaction; dry, wet and isostatic pressing
- plastic forming; extrusion, injection moulding

The present Thesis is concerned with the dry pressing of powders where the powder, confined in a die, is compacted by the application of an external force to obtain a strong, dense piece called the "green". In this Chapter the main features related to the uniaxial single-sided dry pressing of ceramic powders will be presented. Some of the areas of interest, such as the state of agglomeration of the starting materials, the use of binders as processing aids, and the characteristics of the resulting compact will be covered also in other chapters.

4.2 LITERATURE REVIEW

This Review deals with the main areas of interest in the study of the complex process of powder compaction. A general review covering the importance of the state of the powder, the stages and corresponding mechanisms involved in compaction, the transmission of the applied pressure along the compact and the friction forces involved is presented in this Chapter.

4.2.1 Uniaxial Compaction: Introduction

Dry pressing is a relative inexpensive method especially suitable when a large number of simple shapes are required. It is used extensively for refractories, tiles, special electrical and magnetic ceramics, nuclear-fuel pellets and a variety of other products (Kingery *et al.*, 1976). During compaction, powders are densified by the application of an external force in a confined space. The attainment of a dense product depends on the effective utilisation and transmission of the applied external force and on the physical properties of the particulate material. Usually, it is necessary to use some additives as binders or bonding agents and lubricants to give the necessary strength and to reduce the interparticle and particle-wall friction. Another requirement is to convert the powders into an agglomerated state which conveys certain useful characteristics to the material regarding mainly its flow properties. Particle size and size distribution and the packing arrangement within the powder have also an important effect on the compaction of powders (Capes, 1980; Hersey and Rees, 1970). The influence of such factors as agglomerate size, binder and type of lubrication on the compaction of some powders has been studied and will be described in Chapter 8.

The resulting green compacts should have the necessary strength or toughness to suffer minimal damage while being ejected from the die and during their handling prior to sintering. The shrinkage of the green on sintering must also be considered (Waye, 1967; Orr, 1966). The characterisation of the green compact is described in Chapter 9.

4.2.2 Agglomeration

Powder agglomeration plays its most crucial role during forming operations. The compaction behaviour of a fine powder is largely determined by the state of agglomeration. Fine powders are agglomerated to achieve the flow response required for die pressing. The agglomerates will determine the initial packing configuration which influences the particle rearrangement during compaction. As a result, the green microstructure and subsequent sintering are strongly dependent upon the nature of the agglomerates. The compaction also depends upon the strength or hardness of the

agglomerates which are deformed or crushed during the pressing operation. Powders with hard aggregates usually have poor compaction behaviour since the aggregates are difficult to crush or deform. In practice it is normal to avoid a severely aggregated powder and choose a relatively aggregate-free powder which would be agglomerated by for example spray-drying (Halloran, 1984).

4.2.3 Binders and Lubricants

The compaction behaviour of a granulated powder is strongly dependent not only upon the characteristics of the agglomerates but also upon the properties of the binder that bonds the granules together.

Binders and lubricants are employed to facilitate the compaction process by varying the interparticle and particle-wall friction. The lubricant should have low shear strength over a wide range of pressure conditions. They may be classified as internal; where they are added to the particulate feed to improve its flow properties and to assist in the release of the final compact from the die. Alternatively the additives may be regarded as external and here they are used to reduce the friction and the wear at the mould surface and are applied directly to the walls.

Adsorbed binders and lubricants can reduce interparticle frictional forces and improve compact strength. The mechanical interlocking of particles and short range attractions between molecular groups of absorbed polymer binders contribute to the strength. Empirical evidence suggests that minor additions of admixed lubricant first increases the density a few percent, but a relative maximum is quickly attained above which no further improvement is realised. The principal role of the lubricant is in reducing undesirable high die wall frictions during compaction. The effect is to facilitate the uniform transmission of forces, reducing the pressure gradients by effectively increasing the pressure near the bottom of the compact and as a result reducing compact density variations. The ideal binder, or combination of additives, will improve flowability, reduce abrasion, improve bonding strength, increase internal lubrication, and aid external or die wall lubrication. Such an ideal binder system should also burn

off the compact during the initial stages of the sintering cycle without deleterious effects (Reed and Runk, 1976).

4.2.4 Compaction Mechanisms

Generally, in the compaction of powders three steps are distinguished; the filling of the die where the flow properties of the material play a significant role (see Chapter 3); the compression, involving the rearrangement and deformation of particles and the ejection of the piece from the mould (Reed and Runk, 1976).

Cooper and Eaton, 1962 have divided the process of compression or void reduction into two stages. The first one is the filling of holes of the same order of size as the original particles; this occurs by the process of particles sliding past one another, often accompanied by elastic deformation. The second process concerns the filling of voids that are substantially smaller than the original particles; these can be filled only by plastic flow or by particle fragmentation.

Van der Zwan and Siskens, 1982 made a distinction between the compaction of granulated powders and the densification among the primary particles themselves extending to four the number of stages in the compaction process. Lukasiewicz and Reed, 1978 have also inferred the existence of three stages making as well a distinction between porous and non-porous agglomerates.

4.2.5 Friction: Transmission of Pressure

When a powder, confined in a die, is compacted the pressure is not transmitted uniformly through the particle assembly but it conforms to a stress pattern imposed by the die-wall restraint. Frictional effects at the die wall and between the particles extract some of the energy. Interparticle friction will be dominant at an early particle rearrangement stage of densification and die wall friction will be dominant in the remainder of the compaction process (MacLeod and Marshall, 1977). These frictional effects lead to variations in stresses and thereby densities in both the radial and the axial

directions. The shear force between the die wall and the particle material is of the most significance (Capes, 1980; Isherwood, 1987; Orr, 1966).

4.2.5.1 Models of Pressure Transmission During Compaction

The present work analyses the compaction behaviour of several ceramic materials dealing mainly with the non-homogeneous stress transmission during dry pressing and the influence of the interfacial frictional properties on this process. There are two main approaches to estimate the variations of the mean axial and radial pressures on the die wall. One of them, proposed by Janssen in 1895 (Nedderman, 1982), assumes that the particulate is continuous and the other, suggested by Spencer *et al.* in 1950, takes some account of the particulate nature of the material. The compaction of a powder constrained in a cylindrical geometry has been described by Janssen. The model predicts the wall stresses during the compaction by considering the forces acting on an elemental slice of the material. Figure 4.1 illustrates the classical Janssen slice for an element of material.

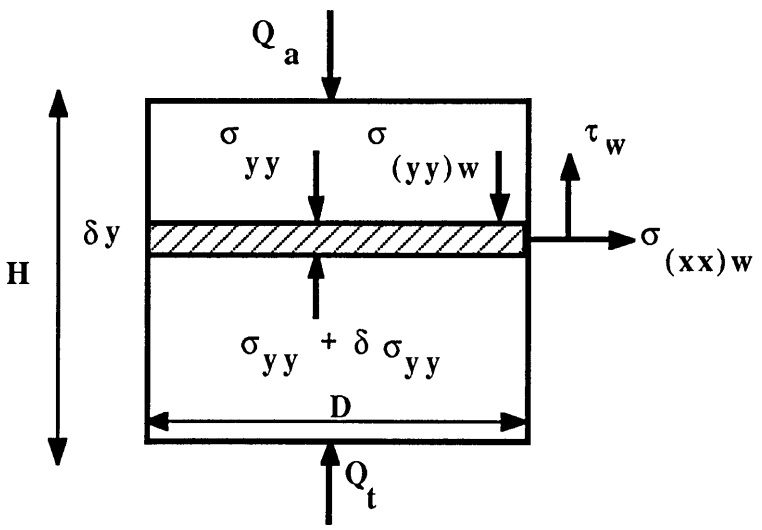

Figure 4.1 Stress transmission during compaction, balance of forces.

Considering a force balance on the elemental slice through the compact, and neglecting the weight of material, gives:

$$\frac{1}{4}\pi D^2 \delta\sigma_{yy} = -\tau_w \pi D \delta y \tag{4.1}$$

where D is the cylinder diameter; τ_w is the nett shear stress at the wall and σ_{yy} is the effective vertical stress. One of the original assumptions of the Janssen analysis was that the vertical stress σ_{yy} was only a function of the y direction. Walker, 1966 allowed for the variation of σ_{yy} with x by defining the vertical stress at the wall $\sigma_{(yy)w}$ and the mean vertical stress σ'_{yy}, these quantities were related by the distribution factor:

$$\Delta = \frac{\sigma_{(yy)w}}{\sigma'_{yy}} \tag{4.2}$$

In the original Janssen analysis:

$$\tau_w = \mu_w \sigma_{(xx)w} \tag{4.3}$$

where μ_w is an average coefficient of wall friction and $\sigma_{(xx)w}$ is the radial stress at the wall and

$$\sigma_{(xx)w} = K_w \sigma_{(yy)w} \tag{4.4}$$

The limits of the coefficient K_w correspond to the Rankine active and passive stress states (Sundaram and Cowin, 1985). Equation 4.1 becomes:

$$\frac{1}{4}\pi D^2 \delta\sigma'_{yy} = -\mu_w K_w \Delta \sigma'_{yy} \pi D \delta y \tag{4.5}$$

which on integration produces;

$$P_t = P_a \exp\left(- 4 \mu_w K_w \Delta \frac{H}{D} \right) \tag{4.6}$$

where H is the present height of the compacted cylinder, P_a is the surcharge or applied compaction pressure and P_t is the transmitted stress (Briscoe *et al.*, 1987).

An alternative analysis has been suggested by Spencer *et al.* in 1950. They considered that the total force acting in the system is the sum of the forces acting on the individual particles. They based their theory on a particulate model for the wall at least. The total friction force acting at the discrete particle-wall contact points is proportional to the number of particles contacting the wall and they assumed that the total number of wall contacts is constant during the compaction. According to this assumption it was found that the ratio of transmitted to applied pressure is constant during the consolidation process and can be expressed as:

$$\text{Ln} \frac{P_t}{P_a} = - 4 \beta \mu_w \frac{H_o}{D} \tag{4.7}$$

where μ_w is the die wall-particle friction coefficient, H_o is the initial powder height, D is the die diameter and β is a constant. This is nominally the same expression as the one obtained from the Janssen analysis except that the current height is replaced by the original height.

4.2.5.2 Stress Distribution

As a result of the non-homogeneous transmission of forces during compaction an irregular stress pattern develops in the compacted body. Several studies have confirmed that major stress and density fluctuations commonly occur during die compaction. Train, 1957 showed that the density distributions within a compact are a result of the

stress distributions occurring during pressing. There are several methods to determine the pressure gradient and density distributions during compaction; these methods are presented in detail in Chapter 9 where this area of stress and density distributions originating in the compact as a result of the transmission of forces during the pressing process is reviewed.

4.2.6 Pressure-Volume Relationships

Several mathematical relationships which attempt to describe the variation of the compaction pressure with the density, porosity or compaction volume have been published. These pressure-density curves have been widely used to interpret the microscopic origins of the consolidation of materials. Messing *et al.*, 1982 have reviewed the use of pressure-density curves for the characterisation of ceramic powder compaction processes. Van der Zwan and Siskens, 1982 discussed the mathematical relationships proposed by several authors to describe the compaction processes. The studies mentioned include those due to Balshin, Smith and Bouchner who have proposed relationships between the pressure and the density of the pressed sample; Konopicky and Heckel, 1961 who have reported data on the interdependence of the pressure and the porosity; Cooper and Eaton, 1962; Leroy and Ledocq; Kawakita and Lüdde, 1970/71; and Bockstiegel who have found relationships between the pressure and the relative volume compaction. Only a few authors (Cooper and Eaton, and Kawakita) have considered the existence of a limiting maximum in the densification. These latter equations give an acceptable fit for almost the whole pressure range whereas most of the other equations are only suitable for generating a fit of experimental data in a relatively small pressure range. There does not however appear to be a generally acceptable equation to represent all situations. A selection of some of the many equations that have been suggested in the literature to represent the compaction of powders in cylindrical die cavities is given in Table 4.1 (after Capes, 1980). Where P is the applied compacting pressure; V is the volume of the compact at P; V_o is the volume of the compact at zero pressure; V_s is the solid material volume (void-free); V_r is V/V_s; ρ_a is the apparent or bulk density of the compact; ρ_s is the true

density of the solid material; $\rho_r=\rho_a/\rho_s$; and a, m, b, a_1, a_2, k_1, k_2 are constants.

TABLE 4.1 Equations Representing the Compaction of Powders.

AUTHOR	EMPIRICAL EQUATION
Huffine Stewart	$\log P = m V_r + b$
Spencer, Gilmore and Wiley Heckel	$\log 1 / (1-\rho_r) = m P + b$
Cooper and Eaton	$(V_o-V) / (V_o-V_s) = a_1 \exp(-k_1/P) + a_2 \exp(-k_2/P)$
Jones	$\log P = m \log \rho_a + b$
Kawakita	$(V_o-V) / V_o = ab\ P / (1 + bP)$

The Kawakita expression for the observed relationship between pressure and volume has the general form

$$C = \frac{V_o - V}{V_o} = a\,b\,\frac{P}{(1 + bP)} \tag{4.8}$$

which may be expressed as

$$\frac{P}{C} = \frac{1}{a\,b} + \frac{P}{a} \tag{4.9}$$

where C is the degree of volume reduction; V_o is the initial apparent volume; V is the

powder volume under the applied pressure, P; and a and b constants characteristic of the powder. In the case of a "tapping" compaction we may replace the pressure by the tapping number N,

$$\frac{N}{C_t} = \frac{1}{a_t b_t} + \frac{N}{a_t} \tag{4.10}$$

The constant a is equal to the initial porosity and the constant b is considered to be related to the resisting forces in the case of piston compression. The constant b_t is considered to be related to the cohesive forces of powder particles (Kawakita and Lüdde, 1970/71).

Experimentally, it is observed that the logarithm of the pressure plotted against the volume yields a substantially straight line. Thus, the compaction of powders over various ranges of pressure is often described by simple exponential expressions. Among the most widely used is:

$$\text{Log } P = - c \frac{V}{V_t} + k \tag{4.11}$$

where V is the actual compact volume; V_t is the void-free or theoretical solid volume; and c and k are constants. The term c, the absolute slope of log P plotted against V/V_t, has been designated a compaction modulus and shown to be a constant up to intermediate pressures. It varies with such factors as particle size and shape (Orr, 1966). The compaction of agglomerated powders is often described by this type of expression.

4.2.6.1 Pressure-Density Curves for Agglomerated Powders

Bruch in 1967 (Messing *et al.*, 1982) was the first to use compaction curves to interpret the consolidation of ceramic powders and he has demonstrated that if the green density is plotted as a function of the logarithm of the compacting pressure for a

powder, that two straight line segments are observed. The break in the curve was interpreted as the onset of the granule breakdown. The general deformation behaviour of granulated powders may be described as follows. At very low pressure, very little compaction occurs until a "yield pressure" is reached at which time the granules begin to deform or crush and thereby fill in the intergranular void space. At a somewhat higher pressures, this deformation process is nearly complete and upon further compaction, the density, ρ, and pressure, P, are frequently approximately related by the empirical expression

$$\rho - \rho_y = m \ln \frac{P}{P_y} \tag{4.12}$$

where P_y and ρ_y are the pressure and density at the point of yielding, and m is an empirical constant called the compressibility factor. This expression is similar to equation 4.11. The density at yielding, ρ_y, is the compact density at which the granules begin to deform and is close to, and correlates with, the tap density of the granulated powder. It depends upon the packing efficiency of the granules and upon the volume fraction solids within the granule. The empirical constant, m, appears to correlate with the yield pressure, P_y, increasing roughly linearly with P_y. The yield pressure is related to the strength of the binder system and is proportional to the binder content. It is particularly sensitive to the mechanical properties of the binder itself (Halloran, 1984; Frey and Halloran, 1984).

The breakpoint observed in the logarithmic representation of the pressure versus the green density is a measure of the compressive strength of the agglomerates in the powder. The lack of breakpoints indicates the absence of agglomerates that have strengths in the pressure range measured; the powder may contain agglomerates that are too strong to be broken down in the pressure range measured (Niesz *et al.*, 1978).

Similarly, Lukasiewicz and Reed (1977 and 1978) and also, Harvey and Johnson, 1980 have used pressure-density curves to evaluate the deformation of spray-dried

powders. Lukasiewicz and Reed (1977 and 1978) have investigated the compaction behaviour of agglomerated and "bulky" powders. In the case of "bulky" powders they observed an initial rapid rise of the density vs. the logarithm of the pressure curve followed by a second linear portion with a lower slope. In the case of the agglomerated powders the compaction takes place in two stages. No significant densification occurs until a yield pressure is exceeded. At pressures higher than the yield pressure the agglomerates deform plastically. Thus, pressure-density curves are commonly used to characterise ceramic powder compaction by making it possible to interpret the mechanistic nature of the compaction process. These curves are specially useful for the study of powders that have been granulated (Messing *et al.*, 1982).

Ciftcioglu *et al.*, 1986 have reported no breakpoints in the compaction curve of agglomerated powders. This may arise from a wide agglomerate strength distribution so that the agglomerates break over a broad range of applied pressure.

Youshaw and Halloran, 1982 have compared the compaction behaviour of two Mn-Zn ferrite powders differing in volume fraction and composition of a polyvinyl alcohol-gum arabic binder. They observed that compaction is affected by the pressing rate, temperature and moisture content. A compaction model, analogous to that used to describe ductile metal powders, was suggested.

4.2.6.2 Summary

The literature provides a great number of expressions that attempt to represent the compaction process; as it has been explained these equations are of an empirical character. Due to the use in this work of mainly agglomerated powders, the general expression represented by equation 4.12 will be applied to the analysis of the data to represent the densification of the powders. Also the Kawakita equation, equation 4.10, will be used due to its applicability to the densification of powders by tapping.

4.2.7 Ejection

The last step in the pressing process is the ejection of the compact out of the die. On ejecting of the pieces residual elastic strains are relieved and the dimensions of the compact may increase as much as 0.5%. Since the compact is relatively weak in tension, relatively small stresses may cause damage or fracture of the compact on ejection (Reed and Runk, 1976). When a lubricant has been introduced the die wall friction is reduced both during pressing and during ejection, effectively reducing the ejection pressures.

Leopold and Nelson, 1965 examined the variation of the ejection pressure with compact mass and lubrication conditions. In the absence of lubricant they found that the ejection pressure was directly proportional to the area of contact between the material and the die wall. They also observed that die wall lubrication was much more effective in reducing the ejection pressure than internal lubrication.

MacLeod and Marshall, 1977 recorded the maximum pressure required for the ejection of a compact from the die. The value of the ejection pressure varied directly with die wall frictional forces and was dependent on the compact aspect ratio, the lubrication conditions and to a lesser extent on the compaction pressure. For constant compaction conditions it was observed that the ejection pressure, P_e, was related to the compact height to diameter ratio according to the expression:

$$\ln P_e = k\frac{H}{D} \tag{4.13}$$

where D is the diameter and H is the height of the compact.

Briscoe and Evans, 1988 have studied the frictional forces during the process of ejecting the compact from the die. The ejection pressure, P_e, required to push a green compact out of the die is controlled by the ejection interface shear strength, τ_e, whose

value is governed by the wall area and the radial stress, σ_{xx}, normal to the die wall. For a constant compaction pressure the ejection pressure is given by;

$$P_e = 4\,\tau_e^*\,\frac{H}{D} \tag{4.14}$$

where H and D are the compact height and diameter respectively; and τ_e^* is some mean interface shear strength over the whole surface. The interfacial shear strength may be expressed as (Briscoe and Smith, 1980):

$$\tau_e^* = \tau_o + \alpha\,\sigma_{xx} = \mu_e\,\sigma_{xx} \tag{4.15}$$

where σ_{xx} is some mean radial stress in the compact. Using the Janssen-Walker analysis to estimate the radial pressure during ejection they were able to calculate the coefficient of friction during the ejection of the compact.

CHAPTER 5

MATERIALS AND EXPERIMENTAL TECHNIQUES

5.1 INTRODUCTION

This Chapter will describe the properties of the ceramic materials used in this study. These powders have been characterised and the main powder properties which will affect the subsequent dry processing of these materials are described. These properties include the particle and agglomerate size and size distribution; the particle and agglomerate shape and shape distribution; the microstructure; the bulk density; the agglomerate strength; and the water adsorption. Also, the thermal properties of the binders used to coat the ceramic particles and of the binder/ceramic systems are reported.

A second area included in this Chapter describes the experimental techniques used in this work to analyse the flow properties, the characterisation of the interface friction, the compaction process and finally the properties of the resulting compacts.

5.2 AGGLOMERATE PROPERTIES

The characterisation of the agglomeration process and the resulting agglomerates properties are two important areas in ceramic research. The current interest in the agglomeration is explained by emphasising that the powders used in this study were mainly in an agglomerated state as this is one important requirement in the overall ceramic powder processing as it has been explained in Chapter 2, Section 2.2.1.1.

Size enlargement involves any process in which small particles are formed into larger entities. Capes, 1980 has reviewed the different size enlargement methods available. Agglomeration is a special case of size enlargement which is reviewed in detail in this Section. Lange, 1984 defined an agglomerate as a multiple particle packing unit produced by either attractive (Van der Waals) interparticle forces or partial sintering during calcination. Agglomerates can be classified according to the nature of the adhesion mechanism, as either hard (partially sintered or cemented groups of particles which can be broken apart by attrition) or soft (groups held together by Van der Waals forces and easily broken apart with surfactants) (Lange, 1984). The attractive forces which hold particles together are a function of the physical characteristics of the individual particles and the nature of the process by which the particles interact. Rumpf, 1962 classified the attractive forces causing primary particles to stick together into solid bridges, liquid bridges, attraction between the solid particles, such as intermolecular Van der Waals attractive forces and electrostatic forces, and mechanical interlocking.

Some important properties of the granulated materials have been determined and are presented in Section 5.4.

5.3 MATERIALS

Several different ceramic oxide materials have been used in this work. They include ferrite, uranium dioxide, alumina, and zirconia. The particular characteristics of each of these materials will be described in some detail in the following Sections.

The alumina and zirconia starting powders were spray granulated and coated with selected organic materials, containing nominally 1% of the organic binder. The organic polymers used were PVA (polyvinyl alcohol) and PEG (polyethylene glycol) and mixtures of both of them. The received ferrite powders, which had been spray-dried, contained a range of binders consisting of polyvinyl alcohol (PVA), polyethylene glycol (PEG) and other commercially available binders.

In the case of the uranium dioxide powders, due to their special use as nuclear fuel elements, no binder was added because of the strict requirements concerning the purity of the final product. Any residue resulting from the calcination of the binder during the sintering step is not acceptable. These powders, received in non-agglomerated form, were granulated using a pre-pressing technique.

With the exception of the uranium dioxide, the prepared powders were dried in an air oven at 95 °C for 48 hrs. and stored over silica gel in desiccators prior to further processing. The uranium dioxide powders were dried and stored over phosphorus pentoxide and these powders were not dried using an oven to avoid the surface oxidation to higher oxides that occurs even at relatively low temperatures.

5.3.1 Ferrite

The ferrite material used in this work was based upon a commercial Mn-Zn ferrite which had been granulated with a range of organic materials acting as binders and lubricants. The polycrystalline manganese-zinc ferrite ($MnZnFe_2O_4$) was supplied by Mullard Magnetic Components Ltd. at Southport; the basic composition was 71.5% Fe_2O_3, 17% MnO and 11.5% ZnO. The ferrite powders were granulated in a granulation pan and after pre-sintering at temperatures between 800-1300 °C had a true density, measured by water displacement, of 4.9 g/cm^3. The resulting granules were wet milled to an average grain size of 115 μm and this product was mixed with the corresponding binder which was incorporated by spraying a 10%w/w aqueous solution, obtaining a ca. 1%w/w binder content. Finally, the wet ground ferrite was spray dried and the resulting apparent density was ca. 0.53 g/cm^3 (data provided by the supplier). Table 5.1 summarises the binder systems investigated.

5.3.2 Uranium Dioxide

This material was supplied by British Nuclear Fuels Ltd. and consisted of two different batches. The "as-received" materials were in unagglomerated form and had no binder added to them. The mean values of some physical properties were: 0.14% water

TABLE 5.1 Type of Binders for the Different Ferrite Materials.

POWDER CODE NAME	BINDER MATERIAL	BINDER TYPE
IC0	Factory Binder	----
IC1	PVA	72000
IC2	PVA	14000
IC3	75% PVA	14000
	25% PEG	400
IC4	75% PVA	72000
	25% PEG	400
IC5	50% PVA	72000
	50% PEG	400
IC6	50%PVA	14000
	50% PEG	400
IC7	50% PVA	14000
	50% PEG	4000
IC8	50% PVA	72000
	50% PEG	4000
IC9	75% PVA	72000
	25% PEG	4000
IC10	75% PVA	14000
	25% PEG	4000
IC11	Primal	----
IC12	Gohsenol	----
IC13	Optapix	PA F 35
IC14	50% Optapix	PA F 35
	50% Glydol	----
IC15	Optapix	PS 13
IC16	50% Optapix	PS 13
	50% Glydol	----

content, 2.7 m^2/g surface area, 0.71 g/cm^3 bulk density and 1.67 g/cm^3 tap density with a resulting value of Hausner ratio of 2.35 (data provided by the supplier). The two UO_2 powders were agglomerated prior to pressing by tabletting followed by a partial mechanical breaking down of the tablets in a sieve. Both the "as-received" and agglomerated materials have been studied.

5.3.3 Alumina and Zirconia

The alumina powder was supplied by BA Chemicals Ltd. (Alcan), it consisted of a very fine, unagglomerated powder. The zirconia powder, a MgO partially stabilised zirconia, with a nominal size of less than 5 μm and a medium size of 1.0 μm was supplied by Unitec Ceramics Ltd. They were treated in the same way. The powders were spray granulated using a conical rotary mixer (Pascall Lab-mixer II) and a binder consisting of PVA, PEG or a 50/50 mixture of PVA/PEG. The organic phase was added as an aqueous solution to coat the powder particles to obtain a binder concentration of ca. 1%w/w.

5.3.4 Binders and Lubricants

Mainly two organic compounds have been used as binders; Polyvinyl alcohol (PVA) and Polyethylene glycol (PEG) each at two molecular weights. The stoichiometric formulae are shown in Table 5.2. The lubricant used in most cases has been zinc stearate, supplied by BNFL. Calcium stearate, supplied by BDH Chemicals Ltd., Laboratory Reagent, has also been used as a lubricant in some cases. Polyethylene glycol 400 and 4000 and Polyvinyl alcohol 14000 and 72000 were supplied by BDH Chemicals Ltd., Laboratory Reagent; Polyethylene glycol 400 was in solution (1.12 g/cm^3 at 20 °C).

TABLE 5.2 Formulae of the Binders.

NAME	ABBREVIATION	FORMULA
Polyvinyl alcohol	PVA	$-(CH_2CHOH)-_n$
Polyethylene glycol	PEG	$HO(CH_2CH_2O)_nCH_2CH_2OH$

The main characteristics conveyed by these binders and their intrinsic properties may be summarised as follows:

PVA, Polyvinyl Alcohol

- high green strength
- hard, brittle greens
- needs lubricant, high wall friction
- "good" with almost any ceramic
- must be dissolved in water

The main problems caused by this binder are the poor release from the die and the brittleness of the greens.

PEG, Polyethylene Glycol

- self lubricating
- high green density
- medium green strength
- rapid burn-out

This binder is often mixed with PVA. The main benefit of using a mixture is that PVA increases the green strength and PEG reduces the brittleness of the PVA product. The major drawback of PEG is the high burn-out rate which causes problems in sintering. Table 5.3 summarises the properties of these binders in various applications.

TABLE 5.3 Binders Properties and Characteristics.

Name	Typical Ceramics	Typical Amount	Fabrication Techniques	Pressures Used	Burnout Range
PVA	Clays		Slip Cast	7 MPa	
	Al_2O_3	0.1-2%	Extrusion	70 MPa	250-400°C
	ZrO_2		Dry Press	5-100MPa	
	$MgAl_2O_4$				
PEG	All Oxides	1.0-3.0%	Dry Press	15-100MPa	250-350°C
Lubricant					
Stearate	All	0.1-1.5%	Dry Press	All	275-500°C

5.4 PROPERTIES AND CHARACTERISATION

This Section deals with the characterisation of the bulk and the agglomerated powders. A literature review of the different experimental techniques available to determine the properties of powders is included. The experimental techniques used to determine these properties and the data obtained are also presented in this Section.

5.4.1 Properties Studied

As it has been explained in the previous sections, the characteristics of the final sintered ceramic body depend to a high degree on the characteristics of the ceramic powders which will affect the behaviour of the powder during the different stages of the manufacturing process. Some important properties and characteristics of the ceramic powders, including both the single particle and the bulk particle parameters, are; the chemical composition, the particle shape, size and size distribution, the agglomerate

size, shape and size distribution, the particle and agglomerate hardness, the surface area, the surface free energy, the bulk density and the porosity, the flow characteristics (powder rheology), the cohesion and adhesion, the granule and bulk material strength characteristics, and the moisture content or hygroscopicity (Kim, 1976; Sherrington and Oliver, 1981).

During the agglomeration process a binder is usually added to the powder system to facilitate the creation of adhesive bonds or interparticle adhesion forces. The important role of the binder system, not only during the agglomeration but also during the whole ceramic fabrication process, will be considered in detail in Section 5.5.

5.4.1.1 Powder Morphology

The term powder morphology refers mainly to the size, and shape parameters. They are related to other physical and chemical properties of the material. For instance, particle size determines the effective surface area which affects the reactivity. The angle of internal friction and the flow characteristics through an orifice correlate with the morphological terms. Particle shape is important in determining the bulk powder properties such as the bulk density (Kim, 1976; Veale, 1972; Beddow, 1983). Particle size and shape may define how a powder will flow, pack, react and yield the microstructure of the finished compact ceramic body (Katz, 1976).

The morphology of particulates is related to their mode of production. Holt, 1981 has reviewed the literature on the shape of particles produced by comminution. It has been observed that in the crushing and grinding of rocks the particle shapes depended on the particle size. Both the character of the material (properties) and the type of mill or reduction machine used had a marked effect on the shape of the resultant product. Also, the processing steps affect the morphology of the particle in addition to the original process of formation.

Many techniques for determining the characteristics of powders have been described but there is no universally accepted classification of the analytical methods. A

general classification of the different techniques available to determine the size of powders was given by Perry and Chilton, 1973. Goldman and Lewis, 1984 have provided a review of the theory and statistical methods used in particle size analysis. Meloy *et al.*, 1986 presented a critical review on particle shape analysis and separation techniques, dividing them into two distinct categories; image analysis techniques and behavioural techniques. The techniques more often employed to characterise the shape of a particle are microscopy (electron microscopy, SEM, TEM), particle image analysis systems, and X-ray line broadening (Beddow, 1983; Veale, 1972; McClung and Johnson, 1988; Kim, 1976). The size of a mixture of particles in a powder may be defined in terms of a particle-size distribution. Particle-size distribution is a function giving the proportionate amount of each size of individual particles in the powder (Perry and Chilton, 1973). A comprehensive morphological analysis produces a set of morphic descriptors consisting of the equivalent radius which is a measure of the size of the particle and a series of shape terms which are unique for a given particle (Beddow, 1983).

5.4.1.2 Water Adsorption

The amount of water adsorbed on the ceramic particles affects their behaviour, especially the friction and compaction characteristics. Water can act as a plasticiser lowering the glass transition temperature of the binder and the particle strength which affects the processing of the material, mainly in their compaction, and the binder burnout properties (DiMilia and Reed, 1983).

The effect of the moisture content has been studied in this work in relation to certain properties of the materials, such as the Hausner ratio, the flow properties, the interface friction and the compaction response.

5.4.1.3 Bulk Density and Hausner Ratio

Hausner, 1967 showed that the density of a loose mass of metallic powder reflects the friction conditions between the powder particles. He distinguished between the

initial apparent bulk density and the tap density of the powder. The apparent density of a given material depends on a variety of powder characteristics which affect, to a large extent, the friction conditions between the powder particles. High friction between the particles results in a low apparent density. The tap density also depends to a certain extent on the powder characteristics. During tapping however, the powder particles jump and loose contact with each other and during this frictionless moment the particles rearrange and improve the packing conditions. Hausner used the ratio tap/apparent density to define the material packing characteristics. This ratio, called Hausner ratio, reflects to some extent the friction conditions between the particles in a mass of powder and is therefore an important characteristic of the powder. It is an indication of the structural collapse induced when the powder is submitted to incremental forces and indicates the structural resistance to mechanical stresses or cohesivity of the powder (Berrin *et al.*, 1972; Harnby, 1987).

There are two basic methods to determine the relative bulk density of a powder. The bulk or apparent density, which is a measure of the ratio of powder weight to volume before any compaction by tapping, is determined by allowing the dispersed powder to settle under free fall in a container. The tap or packed density, which is the powder density after the material has been compacted by a given tapping or vibrating action, is determined by tapping or vibrating the aerated sample. Ultimately a condition is reached when no further densification is possible without particle deformation. The bulk density at this point is termed the "tap" density and is a unique property of the powder (Katz, 1976). The Hausner ratio is of use in gaining a basic understanding of the initial stages of powder compaction. Harnby, 1987 characterised the bulk powder flow using the Hausner ratio. Grey and Beddow (1968/69) compared the Hausner ratio values of several copper powders with the flow times and the angles of repose. They concluded that in the case of dry powders there is a relationship between the three properties. The reciprocal value, i.e., the ratio of poured density over tapped density has been used by MacLeod, 1983 to characterise the surface properties and frictional behaviour of monosize ceramic granules. For smooth spheres the ratio then has a value close to unity and any departure from surface smoothness or sphericity results in a decrease in its value. Both, the apparent and the tap density are influenced by the size and the shape

distribution of the particles. Values of tap/apparent density have been shown to increase with the increasing irregularity of the powder grain shape (Kim, 1976).

5.4.1.4 Mechanical Properties

The strength or toughness of the agglomerates is a very important parameter. For good free flow, high agglomerate strength is needed as the agglomerates must be tough enough to transport without attrition. In compaction, a weaker agglomerate strength is preferred to facilitate the breakdown of the agglomerates to be shaped. A compromise is necessary. Binders and lubricants contribute significantly to agglomerate strength, binders through particle-particle bonding and lubricants through the reduction of particle-particle friction to allow lower void fraction and closer particle contact (Capes, 1980). The mean tensile strength of a granule is related to the particle structure and the properties of the binding medium (Sherrington and Oliver, 1981).

It has been reported that hard agglomerates should be eliminated or controlled in size as they produce a nonuniform particle rearrangement hence limiting the efficiency of the sintering process (Lange, 1984).

5.4.1.4.1 Theoretical Review and Size Effects

The pioneering work in this field was undertaken by Rumpf, 1962. He developed a model to estimate the mean tensile strength of an agglomerate based on the statistical evaluation of the active bonds within a monosized, randomly distributed assembly of spherical particles, which yields the following equation:

$$\sigma_t = \frac{9}{8} \frac{(1-\varepsilon)}{\pi d^2} \kappa H \qquad (5.1)$$

where σ_t is the mean tensile strength per unit section area, ε is the void fraction in the assembly, d is the diameter of the spherical particles, κ is the mean coordination number and H is the tensile strength of a single bond. According to this equation the

main variables affecting the strength of an agglomerate, other than the bonding mechanism, are the void ratio and the size of the particles from which it is composed. The value of the particle-particle bond strength, H, cannot be accurately calculated from first principles for all of the many interparticle adhesive mechanisms. Only for the weaker bonding mechanisms and in the simplest of cases for the strong classes of bonding is a credible theoretical treatment possible. In practice a wide spectrum of compressive strengths are encountered. The major variable determining these values is the particle-particle bonding mechanism; an increase in strength is found as the bonding changes from the adhesion of submicron powders through capillary liquid bonding to the various forms of solid bridging mechanisms (Capes, 1980).

Rumpf, 1962 also measured experimentally the compression strength of ball-shaped pellets. Experimentally, it is easier to measure the compression strength than the tensile strength. Invariably, the determination of the fracture force is inaccurate, for often, from a small primary crack, the pellets crumble and the total fracture cannot be obtained. The compression strength, σ_c was calculated from the formula:

$$\sigma_c = \frac{4\,L}{\pi\,d^2} \tag{5.2}$$

where L is the compression force at failure and d is the diameter of the ball-shaped pellet. In the present study this expression has been used to calculate the crushing strength of individual agglomerates from the experimentally determined compression force values.

When comparing compressive strength values of spherical agglomerates of different sizes the individual loads at failure, L, are normalised by the square of the pellet diameter, d, equation 5.2. This assumes that a uniform radial distribution of bonds exist within the agglomerates in the generalised relationship between load at failure and agglomerate diameter,

$$L = k\, d^{n} \qquad (5.3)$$

when n has a value of 2, the binding forces are considered to be exerted uniformly over the whole cross-section. On the other hand, when most of the binding forces are concentrated as a surface crust, the binding cross-section would be directly related to the pellet circumference and n has a value close to one. A simple geometric model has been proposed by Capes, 1971/72 to show how the exponent n might assume values ranging between 1 and 2 for bonding situations intermediate between the two extremes of "surface-hardened" and uniformly-bonded agglomerates.

A second important theoretical study has been contributed by Yashima *et al.*, 1987. They approached the problem of a sphere being compressed from the viewpoint of fracture mechanics considering the fracture mechanism theory proposed by Griffith. These authors have investigated theoretically the relationships between the specific fracture energy and the compressive strength of spherical particles, obtaining a new equation for the change in fracture energy with size

$$\frac{E_c}{M} = 0.897\,(6)^{\frac{5}{3}m}\,\rho^{-1}\,\pi^{\frac{2m-5}{3m}}\left(\frac{(1-\upsilon^{2})}{E}\right)^{2/3}\left(\sigma o Vo^{1/m}\right)^{5/3} d^{-5/m} \qquad (5.4)$$

where E_c/M is the specific fracture energy; E_c is the fracture energy and M is the mass of the specimen; m is the Weibull's coefficient of uniformity, ρ is the density, υ is the Poisson ratio, E is the Young's modulus, σo is the strength of a sphere of unit volume Vo, and d is the sphere diameter. They arrived to this expression by considering the theories of Hertz, 1881 (as summarised by Timoshenko and Goodier, 1951) to predict the load-deformation curve of a system composed of an elastic sphere placed between two parallel stiff platens. The expression for tensile or compressive strength given by Hiramatsu (Yashima *et al.*, 1987) from the stress analysis concerning the compression under point loading of spherical specimens, and by considering that the difference between the ideal fracture stress and those actually observed experimentally can be

explained by the presence of Griffith cracks in the material. Strength is a structure-sensitive property. It depends on the minute flaws, called Griffith cracks present in the material, and it depends on the specimen's volume. The fracture is caused by the stress concentration around these cracks and then the strength of the specimen is determined by the weakest crack within it.

Capes, 1980 has attempted to explain the mode of failure of a spherical pellet. Figure 5.1 shows a schematic representation of an agglomerate at fracture.

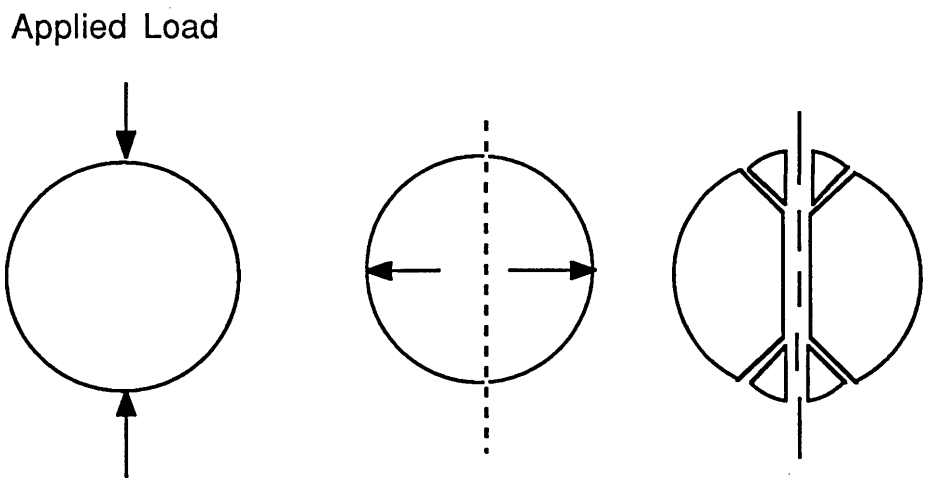

Figure 5.1 Schematic representation of a brittle agglomerate at fracture under a normal load (after Sherrington and Oliver, 1981).

During compression flat areas are produced at the poles where the load is applied. High local stresses acting on the interparticle bonds cause the particles to shear apart and to be driven into adjoining voids. Small, dense wedgelike elements are thus formed in the regions adjacent to the pole surfaces and at failure the agglomerate splits in tension into two hemispherical sections along a circumferential crack joining the two poles of loading. This is the familiar "double-cone" failure mechanism. In translating the

compressive load into a tensile strength through the formation of the double cone compacted areas, internal friction effects between the moving particles must be overcome in addition to the tensile rupturing of the bonds in the crack plane. It follows that the compressive load at failure should be greater than the corresponding tensile values. Orr, 1966 stated that because of the internal friction present in compression tests, a linear relationship between σ_t and σ_c is not expected but, as both strengths become greater, σ_t/σ_c should approach unity more closely. This agrees with Rumpf's results.

5.4.1.4.2 Experimental Techniques

The common strength testing methods can be divided in two categories. Methods which provide information on the fundamental nature of the bonding; this is done by the direct measurements of tensile strength and indirectly by a means of a number of compression, bending and indentation tests which allow the tensile strength to be calculated because the mode of failure is well understood as for example the diametral compression tests (Capes, 1980). The second group includes compression, impact, abrasion, attrition, and dissolution tests.

It is usual to examine the strength of granules by deforming them individually using a variety of methods, the most common being a crushing or compressive test. Compressive strength is widely used as an index of agglomerate quality. The compressive strength test consists of crushing the agglomerate between flat parallel plates and registering the load at failure. The platen is moved at a constant rate. When a granule is subjected to a compressive load acting vertically downwards, depending on the rate of deformation at the contacting surface, the granule will eventually fail either under tension or under compression. Precise instruments are available to follow the total load-deformation process, allowing quantitative analysis of the maximum load at failure, the modulus of the granular material (i.e. the stress/strain ratio), the deformation until complete failure and the total work done or energy required to break down the particle (Sherrington and Oliver, 1981). Varying the method of load application leads to variations in crushing strength values. To obtain reproducible and

accurate results, the rate of loading and the method of load application must be strictly controlled. Cahn and Karpinski, 1968 have shown that the fracture load for plastic agglomerates (wet iron pellets) is highly dependent on the rate of loading. After drying, these same pellets become much more brittle and a lesser sensitivity to deformation rate of the compressive strength was observed. Two modes of operation are possible in applying a load to an agglomerate: CDRT, constant deformation rate testing where the platens are moved at a constant rate and CLRT, constant loading rate testing where the compressive force on the agglomerate is increased at a constant rate. Cahn and Karpinski, 1968 have compared these two modes of operation.

5.4.2 Experimental Techniques and Data

Conventional techniques were used to measure the physical and mechanical properties of the materials. The experimental measurements performed and the data values obtained for the materials properties studied are presented in this Section.

5.4.2.1 Size and Shape Analysis and Microstructure

The size, size distribution and shape of the materials used in this work have been analysed. There are a great number of sizing techniques, the selection of the most appropriate one for a particular case must be based on what type of information one is interested in obtaining and on the intrinsic characteristics of the sample being dealt with. In this work several ceramic powders presenting very different characteristics have been used. The main difference being the state of the powder, fine cohesive material in some cases and agglomerated powders in others. This meant that the range of particle sizes was very wide and no one sizing technique was appropriate for, or applicable to, all of the materials. This is the reason why different sizing techniques have been employed to take into account the intrinsic state and properties of the materials. From the great number of sizing measurement techniques three methods were selected and applied to the samples to determine their size distribution and in some cases, whenever it was feasible, their shape as well.

Pospech and Schneider, 1989 showed that there are noteworthy systematic differences between granulometric information from two independent methods. They showed that image analysis of photomicrographs gives systematically larger powder particles sizes and broader particles size distributions than does sedimentation. Goldman and Lewis, 1984 have described the statistical methods available to analyse the particle size distribution data. They also provided methods for the comparison of data obtained from two different measuring devices. The present study has not attempted to correlate the data from the different particle sizing methods used as the aim was to select a convenient method to determine the particle size of the different powders used in this study.

5.4.2.1.1 Experimental Techniques

5.4.2.1.1.1 Microscopic Methods

Two different microscopic techniques were used, an optical travelling microscope with a micrometer was used to determine the dimensions of the irregular uranium dioxide granules prior to their being tested for their strength characteristics. An automatic image analyser was used to determine the size of the ferrite spherical granules for the same purpose. This latter technique was also used to determine the particle size distribution of the uranium dioxide and ferrite powders and their shape factors.

In the optical microscope method the longest dimension and the maximum width perpendicular to the length are measured. This provides a measure of the particle size by combining both quantities and by dividing them one obtains a measure of the particle aspect ratio (Meloy, 1984).

The automatic particle image analysis system used was an Optomax V Image Analyser supplied by AMS (Analytical Measuring System) and consists of a camera connected to a computer via an AD converter with an accompanying monitor display. The output data was transmitted to a larger computer for further processing. The original particles themselves may be viewed, or if the particles are of intermediate size

an optical microscope (Olympus BH-2) was used to present the particle image to the camera. The optical information was converted into an electrical signal via the TV camera. The features of an image were then detected by signal modulation, i.e., by a measurement of the grey level of the image using a signal discriminator (Beddow, 1983; Meloy, 1984; Davies, 1984). The results may be presented in a variety of ways; as a single size measurement or as a particle-size distribution. This equipment also provides the measurement of the particle shape in terms of a shape factor whose value indicates the closeness to sphericity of the particle, this parameter takes the value of unity in the case of a sphere.

5.4.2.1.1.2 Sieving

The technique of sieving was used with two purposes. First, as a technique for the separation of particles on the basis of their different sizes which groups them into several size portions of more uniform sizes. This allowed the study of the influence of particle size in the compaction of powders. The particle size distribution of the powders may also be obtained. Sizing by sieves or screens is a complex process by which particles are allowed to pass through a series of screens, each with a decreasing screen opening. The likelihood of the particle passing through the screen is a function primarily of its width and secondarily of its height; its length has little effect on whether it will pass or not (Meloy, 1984).

Standard sieves with standard size openings were used for the sieve analysis. The test sieves certified to British Standard BS 410 were manufactured by Endecotts and supplied by Pascall Engineering Ltd. (UK). The sieves apertures were 1000, 850, 600, 425, 300, 212, 106 and 53 μm. The testing sieve shaker was manufactured by Pascall Engineering Ltd. (UK) and was a mechanical shaker imparting to the sieves both a circular and a tapping motion. The experimental procedure was as follows. A weighed amount of powder was poured into the top sieve, 1.0 mm aperture, and the shaker was operated for about 8 minutes. After this time the powder retained on each of the sieves and the amount of fines which had passed through all the sieves was collected and weighed.

5.4.2.1.2 Data

5.4.2.1.2.1 Uranium Dioxide

The "as-received" uranium dioxide material was extremely fine and highly agglomerated. Two techniques were applied to the sizing of this material; laser diffraction and image analysis. Prior to its processing the uranium dioxide was agglomerated and the sizing of the resulting agglomerates was performed using image analysis. The sieving technique was employed to classify the agglomerates into different sizing groups.

5.4.2.1.2.1.1 "As-Received" Uranium Dioxide

In the case of the "as-received" material, two different entities were distinguished; large and highly agglomerated species and small hard agglomerates. The image analysis technique was employed to determine their size and shape. The sizing results are presented in Table 5.4. A problem encountered with this system was the separation of both types of structures in order to be able to measure them independently. Figure 5.2a shows the frequency size distribution for the two types of UO_2 materials.

TABLE 5.4 Particle Size and Shape Analysis Results for the "As-Received" Uranium Dioxide Powders.

MATERIAL	MEAN DIAMETER (μm)	STD. DEV.	FORM FACTOR	STD.DEV.
UO_2 A	4.47	3.38	0.53	0.07
UO_2 B	6.42	5.25	0.52	0.11

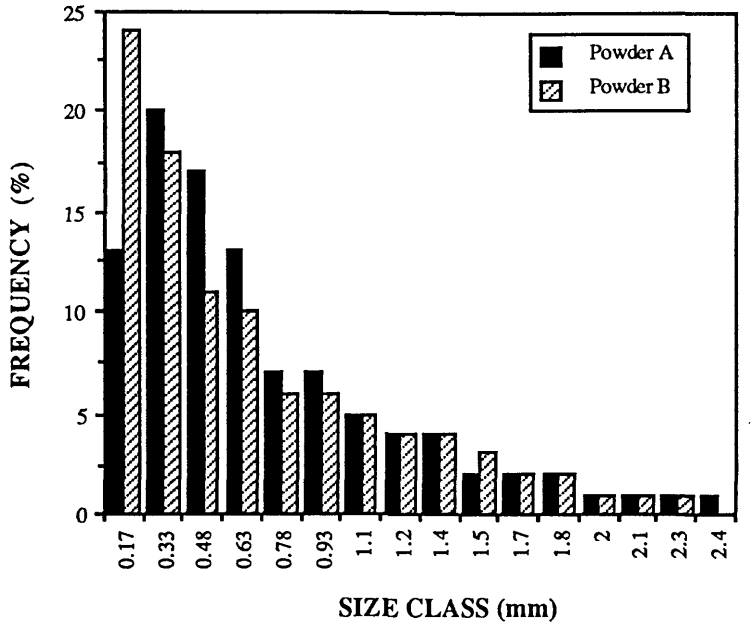

Figure 5.2a Histogram of the frequency size distribution for the "as-received" uranium dioxide materials. Data obtained using the image analysis technique.

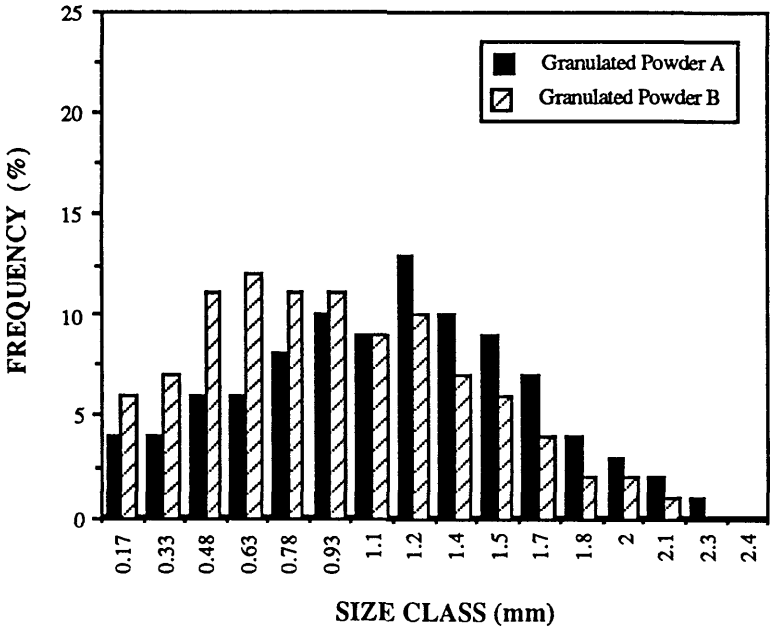

Figure 5.2b Histogram representing the frequency size distribution of the granulated uranium dioxide powders. Data obtained using the image analysis technique.

The data in Table 5.4 correspond to the analysis of the small, hard agglomerates in the powder. There were also observed some large, soft agglomerates which were analysed separately giving a mean diameter of 755 μm for powder A and 711 μm for powder B.

The results shown in Table 5.4 and Figure 5.1a indicate no difference between both systems. The mean sphere diameters are quite similar and the form factor is the same in both cases.

5.4.2.1.2.1.2 Uranium Dioxide Agglomerates

The granules were produced by pre-pressing the "as-received" powders under an applied pressure of 9.64, 96.37 and 160.62 MPa. The resulting compacts were broken through a 1.40 mm sieve and the resulting granules were denominated as 9, 96 or 160 according to the pressure used in their preparation.

TABLE 5.5 Particle Size and Shape Analysis Results for the Uranium Dioxide Granules.

MATERIAL	MEAN DIAMETER (μm)	STD. DEV.	FORM FACTOR	STD. DEV.
A_9	548	5.19	0.63	0.12
A_{96}	1171	5.62	0.80	0.10
A_{160}	987	7.24	0.67	0.13
B_9	557	5.51	0.63	0.12
B_{96}	950	5.12	0.79	0.08
B_{160}	1063	7.49	0.70	0.14

The size distribution and the shape of the agglomerated systems were analysed using the Optomax V Image Analyser. This technique is specially appropriate for the case of a granulated powder size distribution and where one is interested in characterising one individual granule size prior to carrying out the single granule crushing experiment, see Section 5.4.2.4. In the case of the agglomerates no problems were encountered and this technique was successfully used to determine both their size and shape. An average of 1000 granules were scanned to determine the size distribution of the bulk agglomerated powder. The results obtained are shown in Table 5.5. Figure 5.2b shows the size frequency distribution for the agglomerates in comparison to the distribution corresponding to the "as-received" materials. In most cases a log-normal frequency size distribution was obtained and in the case of the form factor distribution a Gaussian normal shape distribution was obtained.

5.4.2.1.2.2 Ferrite

The agglomerated ferrite particles had a large enough particle size to be handled individually. This allowed a quick and more accurate measurement of their size using the image analysis technique. The shape of the agglomerates was also determined. In order to select a certain size range, sieving was performed and at the same time the particle size distribution was obtained. Figure 5.3 shows the size distribution obtained by the sieving technique for two ferrite systems; in the case of IC2, which contains the binder PVA 14,000, a narrower distribution was obtained.

All the ferrites showed a similar size distribution and shape factors reflecting the same production procedure. A wide range of sizes (in the hundred of microns range) was present in the bulk material with an average size of ca. 450 μm and an average shape factor of 0.88 (std. dev.=0.065) which means these granules are quite spherical.

It can be concluded that the method of sieving is preferred to determine the size distribution due to the sampling problem in the case of the image analysis technique whilst this latter method has a greater sensitivity to characterise the size of individual granules.

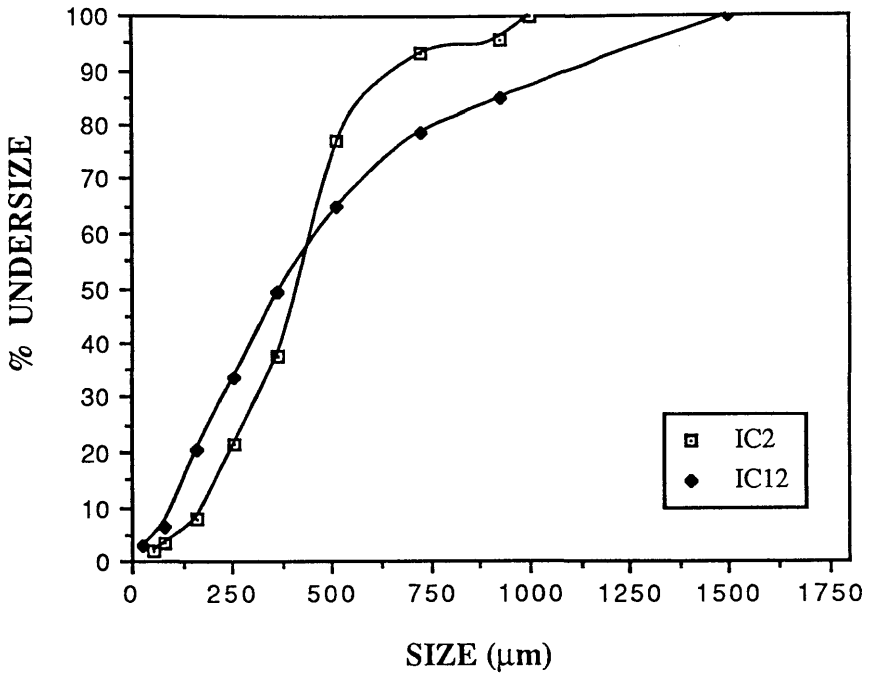

Figure 5.3 Size distribution curves for the Ferrite/PVA (IC2) and Ferrite/Gohsenol (IC12) systems. Data obtained by the sieving technique.

5.4.2.1.2.3 Alumina and Zirconia

The commercial "as-received" powders, of very fine character were agglomerated using a spray agglomeration technique and the resulting granules were sieved and classified according to their resulting size. Different fractions were subsequently used, mainly the 212-425 μm and 425-600 μm size ranges. The mean sizes of the alumina- and zirconia-binder systems were ca. 260 μm in the case of aluminas and 256 μm for the zirconias.

5.4.2.1.3 Microstructure: SEM

Scanning electron microscopy was used to study the physical characteristics of the materials mainly their shape, size and microstructure in a qualitative manner. A JSM-T200 scanning microscope (Joel, Ltd.) was used.

Due to the nonconductivity of these powders a thin coating of conductive material was applied over their surfaces prior to the microscopic examination to avoid charging of the surface of the specimen when it was exposed to the electron beam. An electrical connection was made between the film and the specimen stage so that the charge was dissipated. The powder surfaces were initially vacuum coated with a very thin layer of gold, so as not to obscure the specimen surface, using a S150 A (Edwards) sputter coater. Gold is especially useful as a coating material because it is easily evaporated, has a reasonably small granularity and has a high secondary electrons emission coefficient, thus giving a high signal-to-noise ratio in the image (Wischnitzer, 1981; Lo, 1976). Silver conductive paint was used to fix the powder to the specimen stub. The powders were examined under the following conditions; 20 mm working distance and 25 kV accelerating voltage.

Photomicrographs corresponding to the UO_2 systems, both "as-received" and in agglomerated form, and to the ferrite granules are shown in Plates 5.1 and 5.2. In the case of the "as-received" UO_2 powders, Plate 5.1a, the degree of aggregation and surface roughness are observed. The uranium dioxide granules, Plate 5.1b, are very angular in contrast to the ferrite granules, Plate 5.2, which are almost perfectly spherical. Their sphericity was determined using image analysis as it has been explained in Section 5.4.2.1.2.2. This is a reflection of the type of technique that was used to agglomerate the powders; spray drying produced spherical granules as is the case for the ferrite, whilst the angular shape observed for the uranium dioxide granules is produced by the breakage of pre-pressed compacts to form agglomerates.

It may be seen from the SEM photomicrographs corresponding to the powder uranium dioxide A_{96}, Plate 5.1b, that there is strong evidence of the formation of liquid bridges between the granules. This effect was not observed in the case of the powder uranium dioxide B_{96}. The water in powder A may act as a lubricant at low contact pressures during the compaction producing lower local stress concentrations and a more uniform compaction. It may also facilitate the lubricant distribution. These effects will make themselves evident in Chapters 8 and 9 which describe the compaction and the density distributions in these compacts.

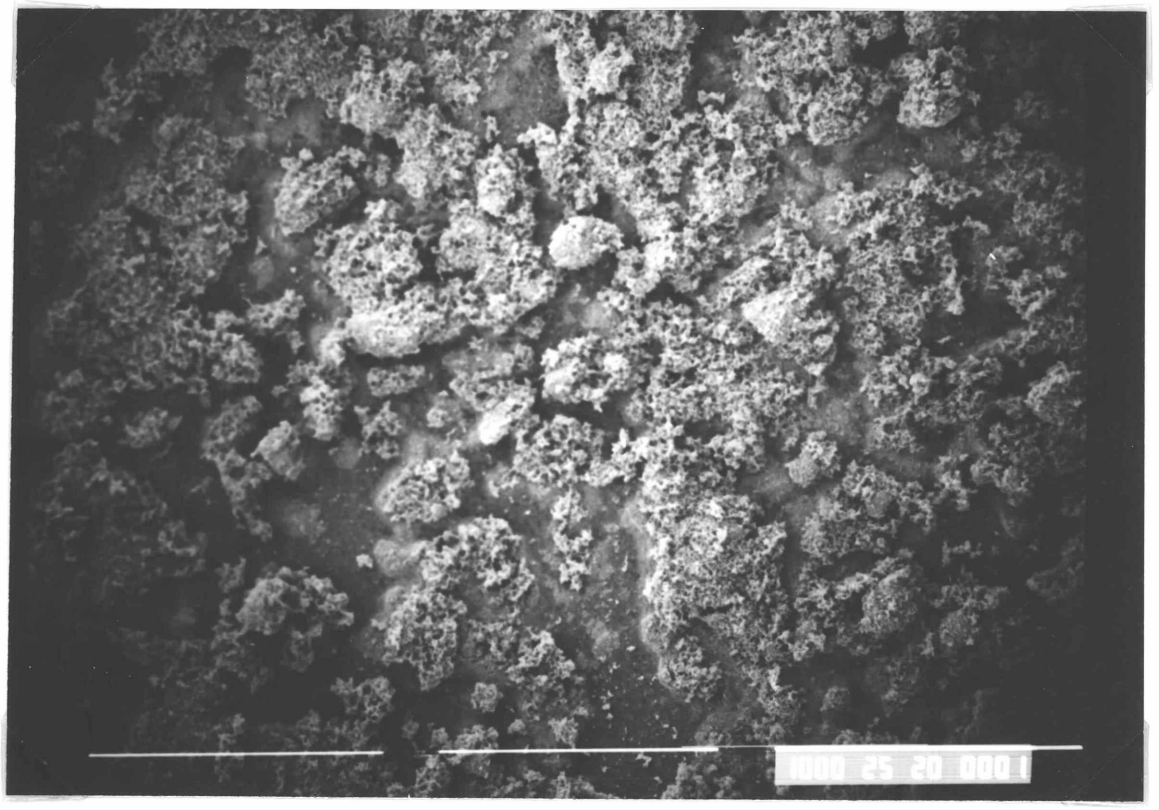

Plate 5.1a Uranium dioxide "as-received" powder A, x35.

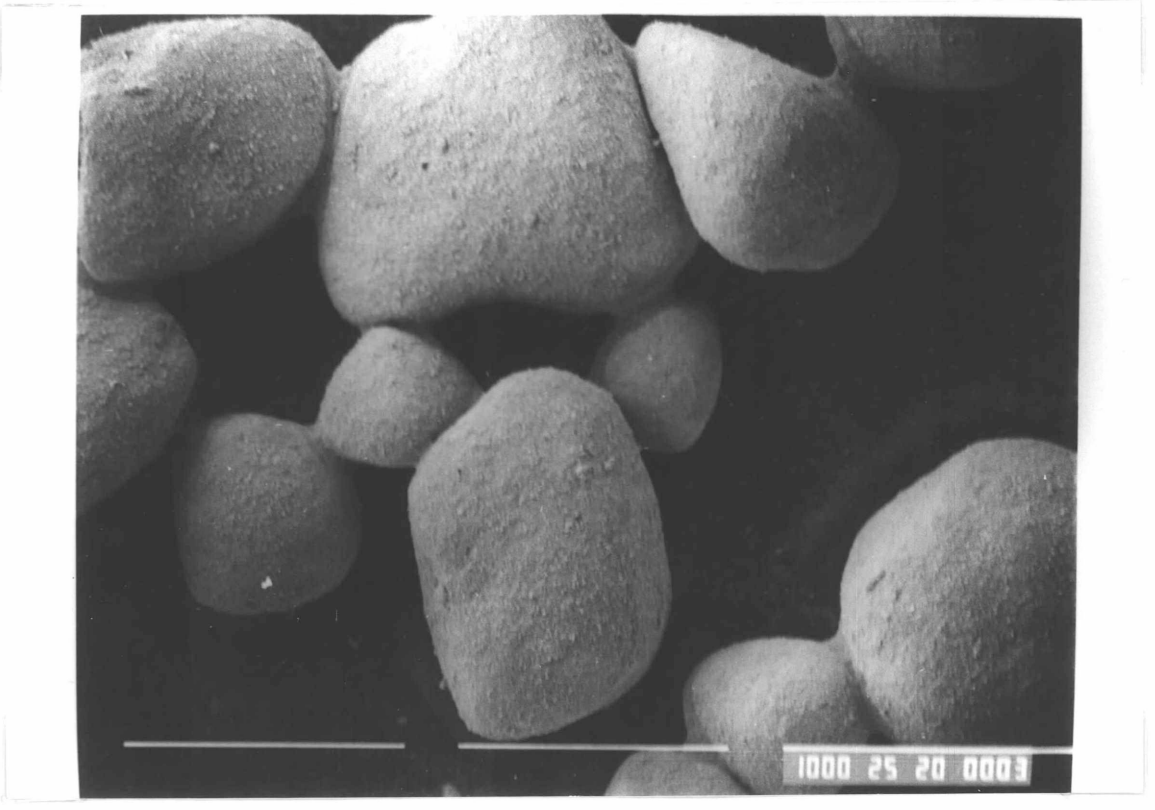

Plate 5.1b Uranium dioxide granulated material, A_{96}, x35

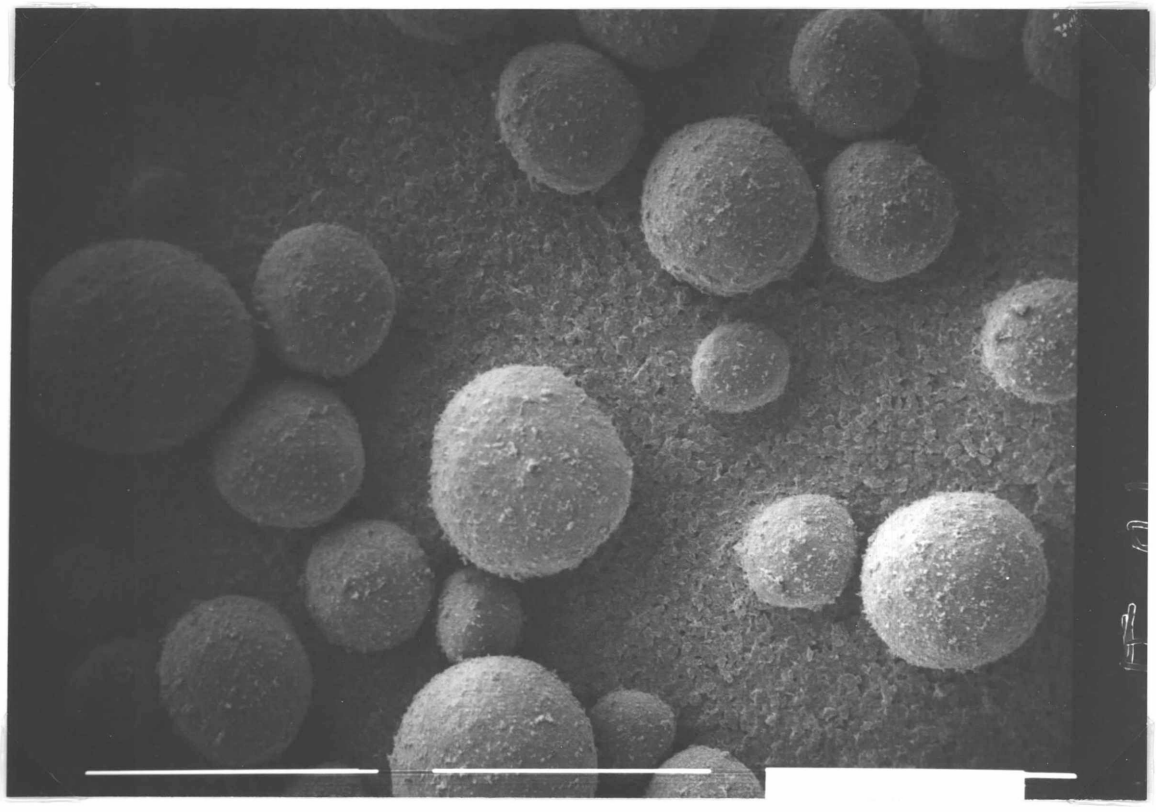

Plate 5.2 Ferrite/PVA 14,000 granules (IC2) x35.

5.4.2.2 Moisture Content and Water Adsorption

Prior to compaction the powders were dried by keeping them in an oven at 95 °C for 48 hours and then storing them over silica gel in a desiccator until used or storing them for at least one week over phosphorous pentoxide. This latter method was used in the case of uranium dioxide due to its oxidation at low temperature. The moisture content and water adsorbed were determined gravimetrically. Table 5.6 presents the results from these two types of measurements. The amount of water present in the materials is quite low in all the cases studied, as is the water adsorption taking place at the different relative humidities.

TABLE 5.6 Moisture Content and Water Adsorption.

MATERIAL	MOISTURE CONTENT (%wt)	WATER ADSORBED (%wt) 66% rh	81% rh	94% rh
Uranium Dioxide				
A	0.10	0.015	0.040	0.166
B	0.10	0.015	0.032	0.157
A_{96}	0.08	0.058	0.114	0.199
B_{96}	0.05	0.034	0.107	0.195
$A_{96\text{-}L}$	0.09	0.000	0.066	0.000
$B_{96\text{-}L}$	0.09	0.000	0.056	0.000
Ferrite				
PVA 14,000; IC2	0.41	----	----	----
Gohsenol; IC12	0.22	----	----	----

5.4.2.3 Hausner Ratio

The Hausner ratio, H.R., is defined as the ratio of the tap (ρ_t) to the apparent bulk density (ρ_a) of a powder

$$H.R. = \frac{\rho_t}{\rho_a} \tag{5.5}$$

The experimental technique used to determine the apparent and tap bulk densities of the powders consisted of weighing a fixed amount of powder (0.050 kg) which was poured into a closed funnel, the bottom side was opened by pulling apart a metallic cap end and allowing the powder to flow through the funnel into a measuring cylinder. The

initial height of the powder in the cylinder was measured and from its value the apparent bulk density was determined. The powder in the measuring cylinder was tapped until the height remained constant. Usually, after about 100 taps no further densification was observed. The final constant height of the powder bed, after tapping, was noted and from it the tap bulk density of the powder was determined. The Hausner ratio was calculated from these measurements and the resulting data for several systems under different conditions regarding the state of the powder, binder system and humidity, are shown in Table 5.7. The values for the case of the ferrite granules ranged between 1.11 and 1.38.

The influence of the moisture content on the tap density behaviour was also investigated. A measuring cylinder with a stopper was used to avoid the sample coming into contact with the ambient atmosphere during the experiment. The samples were previously conditioned by storing them in desiccators under atmospheres of 80% relative humidity or over water (saturated conditions). It may be seen in Table 5.7 that the influence of the water adsorption in the density and Hausner ratio values is often significant.

In the case of the uranium dioxide, the interface properties of sample A appear to be much more sensitive to atmospheric humidity than sample B. The loose bulk densities of sample B are all rather similar as are the Hausner ratio's. With sample A, the loose bulk density of the "as-received" powder is significantly lower than either of the treated samples and the Hausner ratio is higher. Also, the greatest difference between A and B is with the "as-received" powder. With sample A, drying the powder with P_2O_5 reduces the interface friction and improves the bulk flow. Similarly, with the powder stored at high humidity, the moisture adsorbed appears to act as an interface lubricant. The intermediate levels of moisture present in the "as-received" sample would seem to give the powder a cohesive nature (cf. the rotating cylinder experiments). These effects may also be evident to a lesser extent in sample B.

TABLE 5.7 Hausner Ratio Values.

Material	Apparent Density (g/cm^3)	Tap Density (g/cm^3)	H.R.	Kawakita a_t	Kawakita b_t	Sample Conditions
Uranium Dioxide						
A	0.91	1.44	1.58	---	---	---
	0.99	1.42	1.42	---	---	dry
	1.02	1.40	1.37	---	---	80% rh
B	0.98	1.50	1.53	---	---	---
	0.95	1.36	1.43	---	---	dry
	0.96	1.36	1.42	---	---	80% rh
A_{96}	2.80	3.10	1.11	---	---	---
B_{96}	2.74	3.07	1.12	---	---	---
Ferrite						
PVA 72,000; IC1	1.34	1.58	1.18	---	---	<200μm
	1.37	1.56	1.14	---	---	200-300 μm
	1.37	1.50	1.09	0.09	0.12	300-500 μm, dry
	1.35	1.55	1.15	---	---	300-500 μm, saturated
PVA 14,000; IC2	1.32	1.45	1.10	0.10	0.13	300-500 μm, dry
1:1 PVA/PEG; IC8	1.31	1.75	1.34	---	---	300-500 μm, dry
	1.18	1.77	1.50	0.26	0.13	300-500 μm, saturated
Alumina						
"as-received"	1.07	1.33	1.24	0.20	0.33	<100 μm, dry
Zirconia						
"as-received"	0.81	1.65	2.04	0.54	0.14	<200 μm, dry
PVA, granulated	1.32	1.89	1.13	0.12	0.10	<200 μm, dry

Also in Table 5.7 the effect of size on the Hausner ratio values may be observed for a Ferrite/PVA 72,000 system. The three size fractions have very similar initial loose densities but the finer size consolidates to a higher degree resulting in higher Hausner values. No great effect of moisture content on the Hausner ratio was observed for the ferrites.

A more complete set of experiments was carried out in which the tapping of the container was done in a controlled way, allowing it to free fall from a fixed, small height, ca. 2 mm, onto the bench and the powder bed height as a function of the number of taps was recorded in order to study the density variations with the number of taps; that is with the degree of compaction. In this case a more complete analysis involving the whole tapping process was carried out by applying the Kawakita equation (Kawakita and Lüdde, 1970/71) of the compaction of powders to this process which can be compared with the initial stages of powder die compaction

$$\frac{N}{C_t} = \frac{1}{a_t b_t} + \frac{N}{a_t} \tag{5.6}$$

where N is the number of taps or tapping number; C_t is the degree of volume reduction and is defined by $(V_o\text{-}V)/V_o$ where V_o is the initial apparent volume and V is the powder volume under applied tapping; a_t and b_t are empirical constants. The linear relationship between N/C_t and N allows the constants a_t and b_t to be evaluated graphically. The constant a_t is equal to the initial porosity and $1/b_t$ is considered to be related to the cohesive forces between the powder particles or their ease of compression. In general Kawakita and Lüdde, 1970/71 did not find a clear relationship between the constants a_t and b_t and the physical properties of the powders.

A typical experimental curve resulting from this type of experiment is shown in Figure 5.4. It may be seen how the reduction in sample volume is very rapid at the beginning of the tapping process, followed by a decrease in rate of volume reduction and finally a steady-state is reached where no further densification occurs. The results reflect the initial state of the sample regarding the porosity and the level of friction

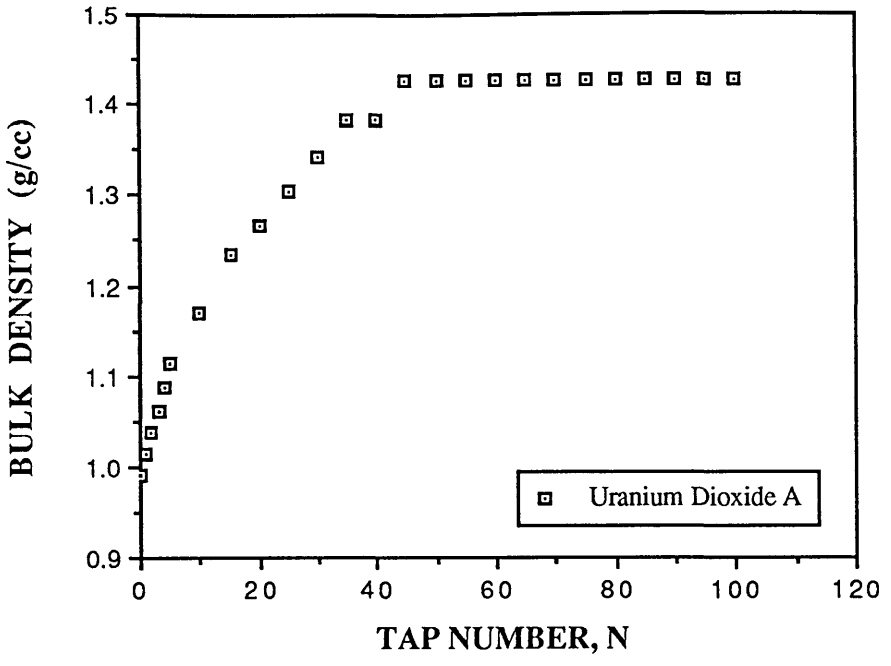

Figure 5.4 Powder bulk density plotted as a function of the number of taps for the case of the "as-received" uranium dioxide powder A.

between the particles in the powder bed. The experimental parameters a_t and b_t in the Kawakita equation corresponding to the diverse materials studied are shown in Table 5.7. These experimental results were plotted according to equation 5.6 (Figure 5.5).

This same analysis due to Kawakita will be used to analyse the compaction behaviour during the actual pressing of the sample. An additional type of information obtained from this experiment concerns the flow characteristics of the material which are related to the interparticle friction and cohesion or adhesion between the particles. This aspect will be treated in more detail in the chapter dealing with the flow properties (Chapter 6).

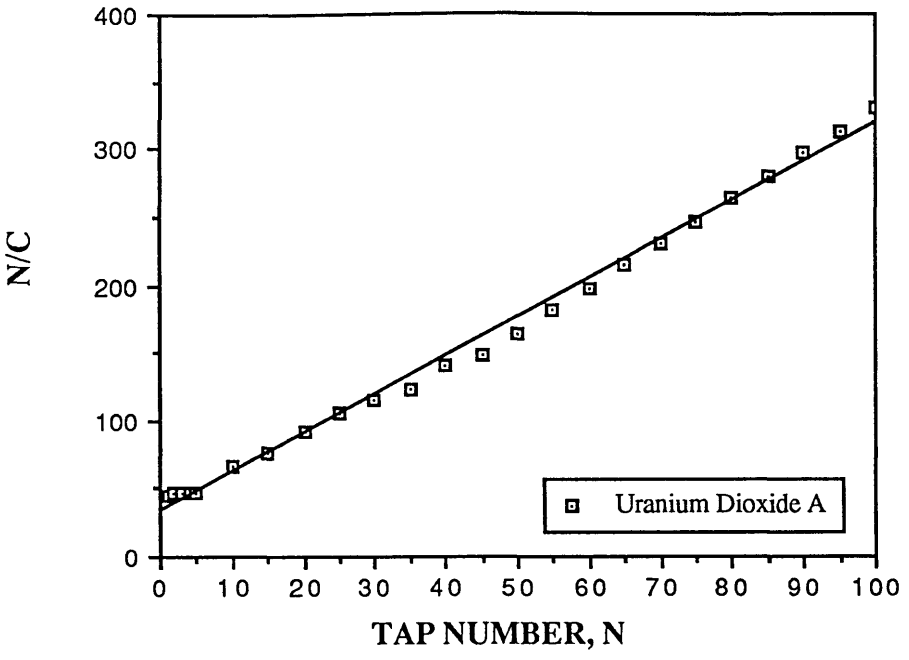

Figure 5.5 Tap density results plotted according to the Kawakita equation for the "as-received" uranium dioxide powder A. The number of taps over the degree of volume reduction is plotted as a function of the tap number.

5.4.2.4 Mechanical Properties: Single Granule Crushing

The different granules have been tested for their compressive strength which is widely used as an index of agglomerate quality. The granules of uranium dioxide A_{96} and B_{96}, and several ferrite, alumina and zirconia systems with a variety of binders were individually crushed between two flat platens and the breaking strength was calculated. The equipment consisted of a spring steel beam driven in the vertical direction by a 5 r.p.m. motor and micrometer. Strain gauges attached to the beam registered its displacement. The gauges were connected to a Wheatstone carrier wave frequency bridge (Philips, PR9307) and a chart recorder to record the net displacement. The applied force was obtained by calibrating the strain gauges using known weights. A constant deformation rate of 4×10^{-5} m/sec was applied.

The calibration curve is shown in Figure 5.6; a calibration factor of 0.067 N/cm was obtained after a least squares fitting. The granule area was calculated from the particle dimensions measured using a travelling microscope to determine the longest dimension in the case of the irregular uranium dioxide granules and using the image analysis technique to determine the sphere equivalent diameter in the case of the ferrite spherical granules. Due to the observed dependence of the fracture load on the granule dimensions a sample of ca. 30 to 50 granules was examined in each case. The breaking stress σ_c, was calculated by using equation 5.2.

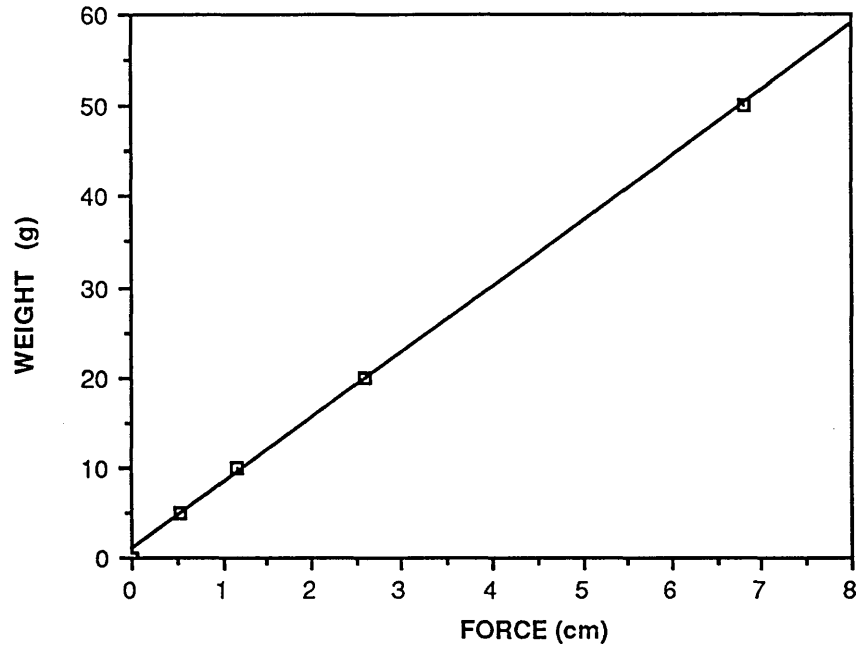

Figure 5.6 Calibration curve corresponding to the single granule crushing experiment showing the linear relationship between the applied weight and the resulting displacement observed.

The whole crushing event in the case of the ferrite was followed optically using an eye-piece and in most of the cases a fracture in tension was evident. The granules broke through fracture and fragmentation rather than ductile yielding. All the granules exhibited a brittle behaviour, i.e., they failed in a sudden catastrophic way. The applied load increases linearly up to the breaking point when it falls suddenly to zero indicating that fracture of the granule has occurred.

Figure 5.7 shows a typical distribution of results for a Ferrite/Gohsenol system; it may be observed that there is great scatter in the data. This is due to the fact that the strength is a statistically distributed parameter. It depends on the size, density and the existence of flaws or microcracks in the granule, and these characteristics will vary from one specimen to another. In the case of the uranium dioxide material, these granules were very irregular in shape and therefore accurate particle size measurement was difficult. Also, the diameter is a function of the direction of measurement. The longest dimension was the parameter chosen to characterise their size. This may affect the values of strength calculated and contribute to the scattering of data observed.

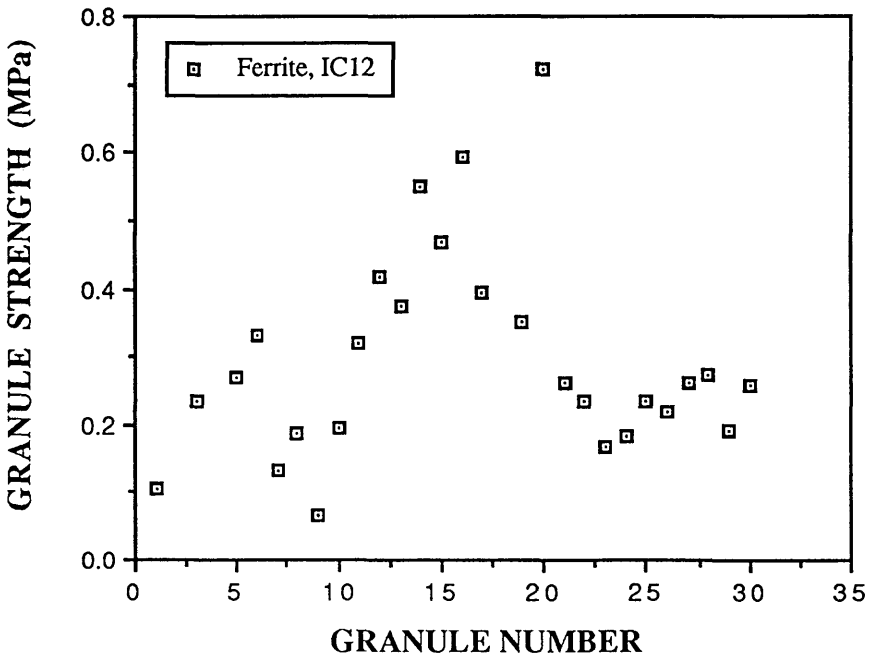

Figure 5.7 Granule strength values obtained after testing 30 Ferrite/Gohsenol granules using the single granule crushing technique.

Several mathematical relationships have been proposed to correlate the crushing strength results with material parameters (see Section 5.4.1.4.1). The present interest is centred on the value of the granule strength itself and because of this a simple statistical analysis of the data was carried out. The results are shown in Table 5.8 together with the significant statistical parameters.

TABLE 5.8 Granule Compressive Strength Results.

Material	Average Compressive Strength (MPa)	[std. dev.]	Mean Size (μm)	Sample Conditions
Uranium Dioxide				
A	0.52	[0.15]	1570	----
B	0.48	[0.21]	1480	----
Ferrite				
PVA 14,000; IC2	1.64	[0.79]	300-800	dry
PVA 72,000; IC1	2.17	[1.25]	300-800	dry
	2.05	[0.89]	300-800	saturated
3:1 PVA/PEG; IC3	1.17	[0.59]	300-800	dry
1:1 PVA/PEG; IC8	1.03	[0.62]	300-800	dry
	0.79	[0.54]	300-800	saturated
Gohsenol; IC12	2.77	[1.55]	>1000	----
Alumina				
PVA 14,000	1.20	[0.42]	300-400	dry
PEG 400	0.44	[0.24]	300-400	dry
Zirconia				
PVA 14,000	0.80	[0.30]	300-400	dry
PEG 400	0.19	[0.12]	300-400	dry

It will be shown that these values may be correlated with some other particle parameters and the behaviour of the powder during compaction. The compressive strength is influenced by the water content. The effect of water adsorption in reducing the granule strength may be seen in Table 5.8 where the values of the mean compressive strength in the case of dry granules (the granules were dried in an oven to nominally 0% rh and stored over silica gel in desiccators prior to testing) and granules kept under humid conditions (stored over water for about four days, with a resulting water adsorption of ca. 1% w/w) are shown. This is caused by the plasticising effect of the water, a similar effect is produced by the use of PEG and the resulting reduction in granule strength as PEG is substituted for PVA may be observed in Table 5.8.

5.5 BINDERS AND BINDER BURNOUT

This Section covers the final step in the processing of the ceramic powders, the sintering stage, and most specifically the burnout behaviour of the several organic binders used to modify the characteristics of the ceramic powders. In order to obtain a first insight into the behaviour of the different organic systems used, their behaviour as the temperature increases was analysed using thermogravimetric analysis. There are two important aspects to be considered in relation to the binder burnout; the temperature or temperature range at which the binder burns out and the rate at which this process takes place. These two aspects have been studied and the results are presented in this Section. First a literature review on this area of the ceramic processing is presented. There is an extensive literature coverage of this area involving mainly the characterisation and the selection of binders for different binder-ceramic material systems.

5.5.1 Why Use Binders?

Ceramic processing requires in most cases the use of certain processing aids, mainly binders and lubricants, to improve the efficiency of several steps in the manufacture of ceramic parts. These additives will improve some important properties and characteristics of the material contributing in this way to the overall formability and

increasing the level and uniformity of the final green and sintered density of the ceramic part. The selection and application of binders is one of the most critical factors in the dry pressing process (Reed and Runk, 1976). It is not only necessary to select a binder to provide specific qualities desired in each phase of the operations (granulation, storage, transportation, pressing, burnout and firing); it is also necessary to assure that they will not be detrimental to any specific phase of the operation (Hoffman, 1972; Fisher and Potter, 1955).

During the sintering it is necessary to eliminate these additives from the green and to avoid any deleterious effects that may arise during this stage. The ceramic compact is generally heated at temperatures up to 800 °C to remove the residual binders and lubricants and at temperatures up to 2000 °C to remove the residual porosity to obtain a dense homogeneous product (MacLeod, 1983).

Thus, the role of the organic polymers used as additives in many ceramic processing operations is temporary, as the polymer must be pyrolysed completely prior to the sintering of the ceramic. It should disintegrate completely on firing, preferably at low temperature without interfering with pore removal or degrading the physical properties of the ceramic for example by reacting with desirable components of the ceramic body or by volatilising at such a great rate as to create thermal stresses in the body producing cracks. It should have non-toxic characteristics not leaving behind noncombustible residues. Scheiffele and Sacks, 1988 have reported the effect of several processing variables on the degradation behaviour of PVB, poly(vinyl butyral), resins showing that binder burnout was accomplished more efficiently by using a heating schedule in which the heating rate was varied with temperature. Finally, the material must be efficient at low concentration so that the burn-out is more easily accomplished (Hoffman, 1972; Shih *et al.*, 1988).

5.5.2 Thermogravimetric Analysis

Thermogravimetric analysis (TGA) has been used to study the thermal response of several binder/ceramic powders mixtures as a function of the temperature. This

technique determines the change in sample mass as a function of the temperature and /or time. The resulting mass-change versus temperature profile provides a range of information concerning the thermal stability of the system.

In 1969 Levine described the advantages of TGA to determine quantitatively the amount of binder and lubricant present in ceramic materials. He determined the amounts of the dibutyl ester of phthalic acid (DBP) and polyvinyl alcohol (PVA) in alumina. Harvey and Johnson, 1980 have investigated the relative effects of two binder systems, polyvinyl alcohol and polyamine sulfone, on the microstructure, density and strength of pressed, spray-dried ferrite powders and the burnout behaviour of the binders. The burnout of the binder from the pressed compacts was studied using thermogravimetry. Shih *et al.*, 1988 have investigated the pyrolysis behaviour of poly(vinyl butyral) binders, PVB, using a variety of techniques, including thermal gravimetric analysis, differential thermal analysis, Fourier transform infrared spectroscopy, and gas chromatography.

In this study thermogravimetric analysis has been used to study the binder burnout characteristics of the several ceramic powders-organic binder systems. Both the thermogravimetric curves and the derivative thermogravimetric curves were analysed.

5.5.2.1 Derivative Thermogravimetry (DTG)

During the TG analysis the mass of the sample, M, was continuously monitored as a function of temperature or time; M = f (T or t). Derivative thermogravimetry follows the rate of weight change of the sample with respect to time or temperature; the derivative of the mass-change with respect to time or temperature is recorded as a function of time or temperature:

$$dM/dt = f(T \text{ or } t)$$
$$dM/dT = f(T \text{ or } t)$$

The advantages of representing the thermal process by a DTG curve are that this curve allows the rapid determination of the temperature at which the rate of mass-change is at a maximum and in the DTG curves subtle mass changes are emphasised. It shows a better resolution thus allowing the separation of overlapping reactions occurring at similar temperature which appear as one continuous mass loss in the TGA curve (Daniels, 1973; Wendlandt, 1986)

5.5.2.2 Thermogravimetric Curves

The information one can obtain from the TG curve includesthe temperature intervals of thermal stability, and regions of formation and existence of intermediates and the end-product.
Much of the information obtained from the TG curve is of a subjective nature (Blazek, 1973).

Thermogravimetry may also be used to study the kinetics of a chemical reaction and determine basic kinetic constants such as the rate constant, activation energy, order of the reaction, and frequency factor.

5.5.3 Experimental Technique

The equipment used to carry out the thermogravimetric analysis consisted of a TGS-1 Thermobalance (Perkin-Elmer) coupled with a DSC-2 Differential Scanning Calorimeter (Perkin-Elmer) a chart recorder and a Sartorius Balance 2024 HP, ± 0.01 mg. The experimental technique adopted to obtain the corresponding thermogravimetric curves was as follows: a small amount of powder, ca. 8-15 mg, was poured into the thermobalance basket and weighed. The basket was suspended by a thin glass filament in a microfurnace and attached to the force balance. The temperature was controlled by the Differential Scanning Calorimeter unit. A fixed maximum temperature (600 °C) and a minimum temperature (25 °C) were used. The heating rate was kept constant at 10 or 20 °C/min. for the case of samples containing only a binder. The ambient was purged

with air in the case of the ferrite samples and a flow of nitrogen was used in the other cases.

The apparatus was calibrated for weight loss by determining the output values corresponding to known weights. Also the temperature output signal was calibrated. The microfurnace of the thermobalance enables a 'Curie-point' temperature calibration to be performed. Standard ferromagnetic samples are place on the pan, and a magnetic field is applied. These substances affect the balance beam by their magnetic force, and this force is recorded as a function of the temperature. Every substance loses its ferromagnetic properties at a defined temperature (the Curie temperature) and this is manifested on the weight-change curve as an apparent weight loss. As each sample reaches its particular Curie-point it ceases to exert a magnetic force and an apparent weight-loss is recorded. Using several ferromagnetic materials a multi-point temperature calibration curve may be obtained under the normal operation conditions of the balance (Daniels, 1973; Blazek, 1973). The temperature recorded on the TG graph does not correspond exactly with the actual temperature sensed by the sample due to some magnetisation taking place so that the temperature does not increase linearly with time. The corresponding graph for the real temperature values was recorded and from this graph the corrected temperature readings were made; the difference between the real and measured values was found to be as high as 15 °C in some cases.

The corresponding mass change curve as a function of temperature was recorded on a continuous strip chart and the temperature was evaluated on the basis of a known temperature programme.

5.5.4 Data

Thermogravimetry has been applied to compare the relative thermal stability of the different polymeric systems used as binders; the effect of these additives on the thermal stability, and the moisture and additive contents were studied. From the TGA curves two different analysis have been carried out. The weight loss of the materials as a

Typical TGA and DTG curves corresponding to the system PEG are presented in Figure 5.8. The rate of binder burn-out was obtained by numerically differentiating the data from the TG curve (weight loss vs. temperature).

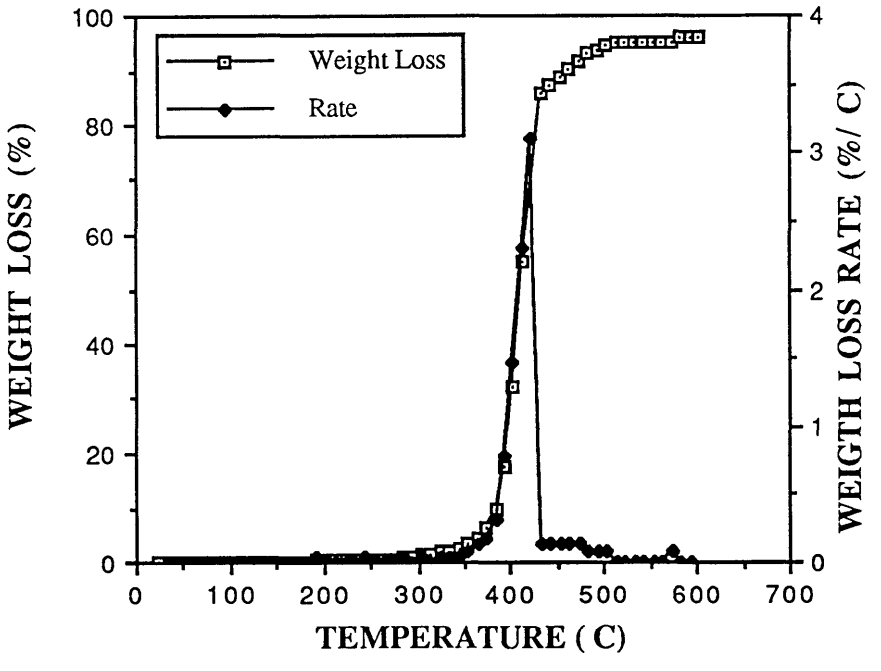

Figure 5.8 Thermogravimetric curves representing the weight loss and the rate of weight loss as a function of the temperature for the system PEG. Heating rate 20 °C/min., nitrogen flow.

The complex information that may be obtained from these two types of representation can be summarised in several points: (a) The determination of the region of thermal stability. (b) The value of the so-called decomposition temperature, which depends on the experimental conditions and it does not represent the true temperature of the decomposition reaction. Rather it is the lowest temperature at which the beginning of the change in the sample weight is observed with a particular apparatus. Due to this

problem Doyle, 1961 introduced the term "integral procedural decomposition temperature" (ipdt) to enable comparisons between polymers to be made. He defined the integral procedural decomposition temperature as a means of taking into account the entire shape of the normalised TG curve, with respect to both residual mass and temperature. The value of the ipdt has a practical meaning as a half-volatilisation temperature (Blazek, 1973; Wendlandt, 1986). For each single-stage in the mass-loss curve two temperatures may be selected as characteristic of any single-stage nonisothermal reaction: T_i; the initial temperature or procedural decomposition temperature (pdt), which is the temperature at which the cumulative mass-change reaches a magnitude that the thermobalance can detect, and T_f; the final temperature, which is the temperature at which the cumulative mass-change first reaches its maximum value, corresponding to complete reaction. The difference T_f-T_i is called the reaction interval (Wendlandt, 1986).

Also, the maximum rate of binder burnout and temperature at which the maximum rate occurs may be determined from the maximum peak in the DTG curve which corresponds to an inflexion point in the TG curve where mass is being lost the more rapidly.

A summary of the data obtained for the ferrite/binder systems studied are shown in Table 5.9, as the weight loss that has taken place at 700 °C. This temperature has been chosen because it was the minimum temperature tested at which all the binders were burnt out. The weight loss from the factory powder, IC0, was 0.6% and from all the experimental powders 1.2-1.5%. This compares with nominal binder contents of 0.6% and 1.0% respectively. The temperature at which the binder begins to burn out was not the same for all the powders. The experimental binders begun to burn-out at 200-300°C and were completely burnt out at 500 °C. Whereas, the behaviour of the factory binder in IC0 is quite different to the rest of the powders, the burn-out starts at a much higher temperature, 540 °C, a temperature at which in all the other cases the binder has burnt out completely. This powder exhibits the minimum weight loss and the minimum burnout rate. At 40 °C some irregularities were noted due to the moisture content of the

samples, but from 80 °C onwards the systems behaved consistently. The systems were allowed to equilibrate at 80 °C to allow all the moisture to evaporate prior to protracted heating at high temperatures. The temperature at which the binder burns out and the rate of weight loss with respect to temperature were calculated for all the systems. In the case of the ferrite/binder systems the derivative curve contains a multiplicity of maxima and minima, suggesting more than one decomposition reaction is occurring. These results are shown in Table 5.9.

TABLE 5.9 Summary of the TGA Results for the Ferrite/Binders.

Binder System	Weight Loss at 700 °C (%wt)	Temp. Range (°C)	Max.Rate and Temperature (%wt/°C)	(°C)
IC0	0.59	540-700	0.0056	660
IC1	1.30	193-413	0.0088	273
IC2	1.30	120-340	0.0095	180
IC3	1.50	140-400	0.0100	180
IC4	1.40	164-304	0.0191	264
IC5	1.60	161-361	0.0111	261
IC6	1.20	220-400	0.0095	260
IC7	----	200-400	----	----
IC8	1.30	120-460	0.0093	180
IC9	1.50	125-305	0.0111	185
IC10	1.50	137-297	0.0099	177
IC11	1.50	185-385	0.0216	365
IC12	1.40	120-320	0.0069	160
IC13	0.98	140-550	0.0035	160
IC14	0.87	136-476	0.0046	316
IC15	1.50	100-380	0.0115	300
IC16	1.40	137-357	0.0096	217

According to the Thermogravimetric Analysis results, Table 5.9, binders can be qualitatively classified as "good" or "bad" according to their performance with temperature, taking into account the temperature at which the binder burns out, and the rate at which this process occurs. A slow gradual burn out rate is preferred to minimise cracking in the body during sintering. The best binders are IC13, IC14, IC0 and IC12 and the worst ones, that is the ones with a higher binder burnout rate are IC11, IC4, IC15, IC9 and IC5.

A comparison of the powders with a variable content of PVA/PEG indicates that no general trend can be established. The maximum burn out rate is ca. 0.01 %wt/°C at about 200 °C which compares with a maximum rate of 0.006 %wt/°C at 600 °C for the factory binder. Of the other commercial binders tested, Optapix PAF 35, Optapix PAF 35/Glydol and Gohsenol, which correspond to powders IC13, IC14 and IC12, had "good" burn-out properties (< 0.007 %wt/°C) and Primal (IC11) was particularly poor, with the highest burn-out rate of all the binders tested (> 0.02 %wt/°C). Sintering trials would be required in conjunction with these data to examine whether the green bodies were capable of sustaining the high binder burn-out rate at the highest (1%) binder content.

Table 5.10 shows the results obtained from the thermogravimetric analysis of the alumina and zirconia samples. Also, the values corresponding to samples of the binders; PVA, PEG and a mixture of PVA/PEG are shown in Table 5.10.

In all the cases the temperature of maximum burnout rate is higher for the PEG system. The ipdt was determined for these two systems applying the method described by Doyle, 1961. A value of 304 °C for PEG and 404 °C for PVA was obtained. When the PEG is mixed with PVA the resulting effect is a reduction in the temperature range at which decomposition is taking place and in the temperature where maximum weight loss rate occurs. The mixture, PVA/PEG is appropriate as far as the binder burn out characteristics are concerned.

TABLE 5.10 Summary of the TGA Results for the Alumina, Zirconia and Binder Systems.

Binder System	Total Weight Loss (%wt)	Temp. Range (°C)	Max.Rate and Temperature (%wt/°C)	(°C)
Alumina/PVA	1.16	180-600	0.0076	321
Alumina/PEG	1.75	180-580	0.0084	460
Alumina/PVA-PEG	1.95	120-520	0.0115	321
Zirconia/PVA	1.44	130-570	0.011	270
Zirconia/PEG	1.25	120-520	0.010	380
PVA 72,000	100	110-496	0.881	325
PEG 400	96	195-500	3.093	422

We may summarise this Section on binder properties and binder burnout characteristics by remembering that the choice of organic materials will be, in practice, limited by their degradation characteristics in the green during their thermally induced removal. The sintering behaviour is a function of the green properties, such as porosity and dimensions, the firing cycle and the intrinsic degradation kinetics of the organic. A limited study of the burn-out behaviour of the binder systems from agglomerated ceramic powders has been carried out by thermogravimetric analysis. A slow, gradual burn-out is preferred with minimal or zero carbon residues to prevent cracking of the green during firing and to maximise product toughness. Ultimately, if an additive system proves to have a "poor" burn-out behaviour it is naturally unsuitable for adoption as a viable processing aid. Slow or gradual burn-out rate is required to avoid cracking of the green during the initial stages of firing. Minimum or zero carbon residue is required to maximise product toughness. Burn-out rate depends on the degradation kinetics of the organic, the physical operating parameters, eg. heating cycle, firing atmosphere and gas flow rate, the green density and porosity, and the green size.

5.6 EXPERIMENTAL TECHNIQUES

The second part of this Chapter will describe the different experimental techniques used to study the flow, friction and compaction of the ceramic systems.

5.6.1 Unconstrained Flow and Interface Friction of Loose Packed Powders Beds

5.6.1.1 Rotating Cylinder

The flow properties and the interface friction of the different powders have been studied to classify these materials in relation to their flowability and to measure the mean interface friction of each powder and its variation with the bed load or the apparent contact pressure. To determine these two properties of the powders the inclined plane experiment has been used. The basis of this experiment is that a cylinder partially filled with powder will begin to roll down an inclined plane at some critical angle of inclination.

The dynamics of the experiment are shown in Figure 5.9. The apparatus consists of a board (length=1.22 m and width=0.40 m) whose inclination could be varied using an adjustable screw mechanism fixed to one end of the board and connected to a 10 rpm electric motor. The rate of inclination of the board was constant and slow enough (1 degree in two minutes) to accurately determine the angle at the point of onset of motion. The angle of inclination was measured using an inclinometer (Higher & Watts) to an accuracy of 1 minute. The procedure was as follows: the dry empty cylinder and end caps were weighed. The cylinder was loaded with the desired amount of powder (from 0.010 to 0.160 kg) and placed near the top end of the board. The inclination of the board was increased gradually until the point of onset of motion when the cylinder begins to roll down the plane and the angle of inclination of the board was recorded. The cylinder used was made of borosilicate glass and has an internal diameter of 0.075 m, a length of 0.152 m and a weight of 0.405 kg with perspex end pieces. A second cylinder differing in its dimensions was used to analyse the influence of the cylinder

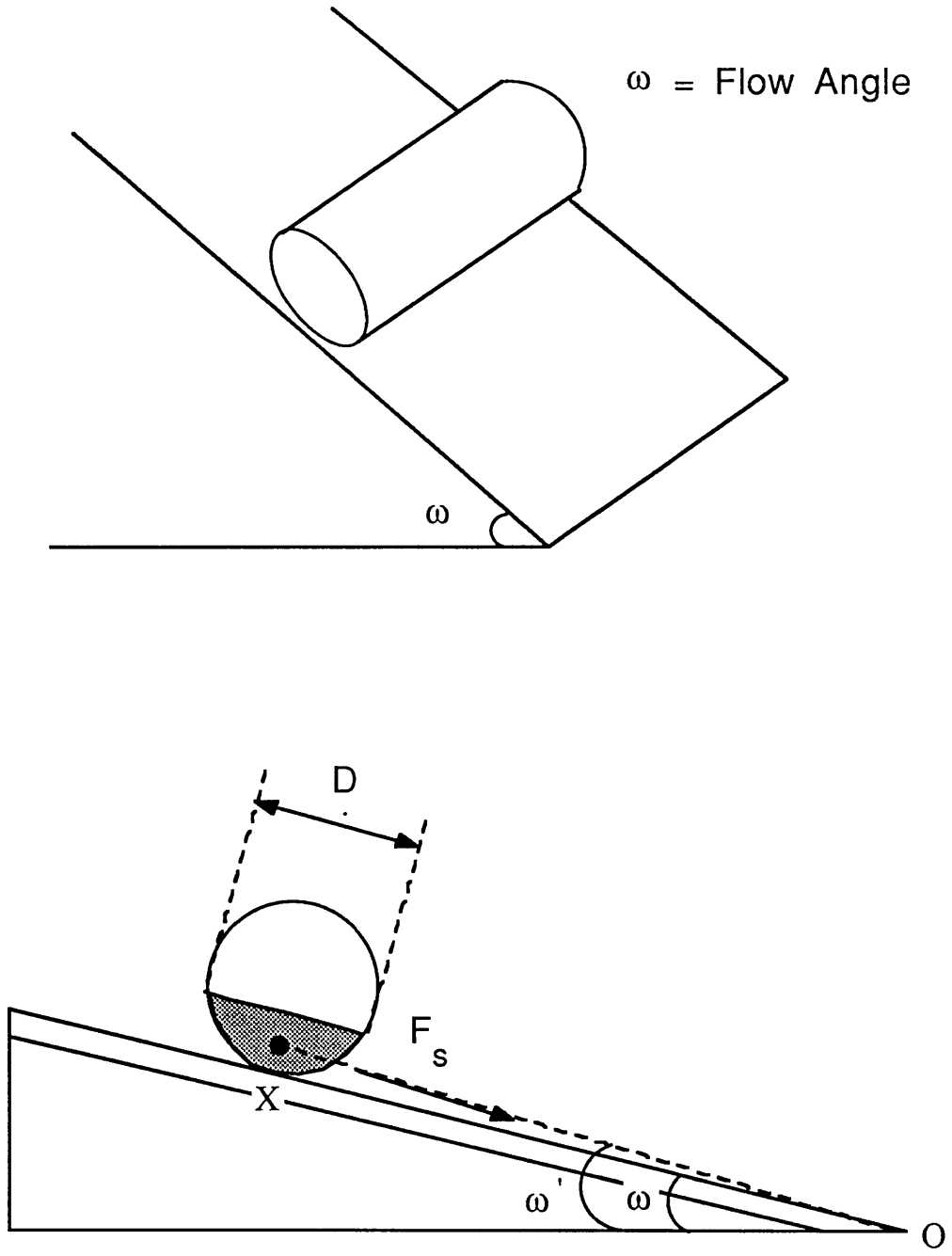

$$F_s = M_t \, g \sin \omega' - M_c \, g \sin \omega''$$

Figure 5.9 Schematic illustration of the dynamics of the rolling cylinder

dimensions on the critical angle for the onset of motion. This second cylinder has an internal diameter of 0.046 m, a length of 0.152 m and a weight of 0.263 kg.

The experiment primarily senses the particle-wall friction in the loose powder bed. It is possible to relate the critical sliding frictional force F_s, required to initiate motion, to the forces acting on the cylinder and contents;

$$F_s = M_t\, g \sin \omega - M_c\, g \sin \omega'' \qquad (5.7)$$

where M_t is the total mass of the cylinder and powder, M_c is the mass of the cylinder, g is the acceleration due to gravity, ω is the angle of inclination for the onset of rolling of the cylinder with powder, ω'' is the angle of inclination for rolling of the empty cylinder. The second term in equation 5.7 is the rolling friction of the empty cylinder. F_s is a measure of the net static frictional force that exists between the cylinder wall and the particles in contact with it.

At low packing volumes this experimental technique mainly senses the interface wall friction of loose packed powder beds. The mean interface friction of each powder was measured using this experimental technique and its variation with the bed load or the apparent contact pressure was examined. This same experimental arrangement was also used to study the internal flow properties of the powders. The method adopted was rather indirect and involves studying the variation of the inclination angle required to induce the rolling of the cylinder for relatively large contained masses of powder. Each experimental run was repeated a number of times to study the variability in the critical angle.

5.6.1.2 Flow Rate

The flow characteristics of the ceramic/binder powders was also analysed using a standard test; the flow rate. A known volume of powder, 20 cm^3, was poured in a glass tube of 0.20 m diameter and allowed to flow down freely through a nozzle of

diameter 0.01 m. The time for the powder to completely flow out of the tube was measured and the corresponding volumetric flow rate was determined.

5.6.2 Sliding Friction of Hemispherical Compacts

The compacts were prepared from the agglomerates in a hemispherical die, 0.0125m diameter, at a pressure of 200 MPa. The apparatus was an Eldredge machine (Bowden and Tabor, 1964) shown schematically in Figure 5.10. The apparatus essentially consisted of a balanced arm at one end of which the specimen was glued to a slider which was in turn supported by spring steel beams within the arm. The beams were deflected by the frictional force which was monitored continuously by strain gauges.

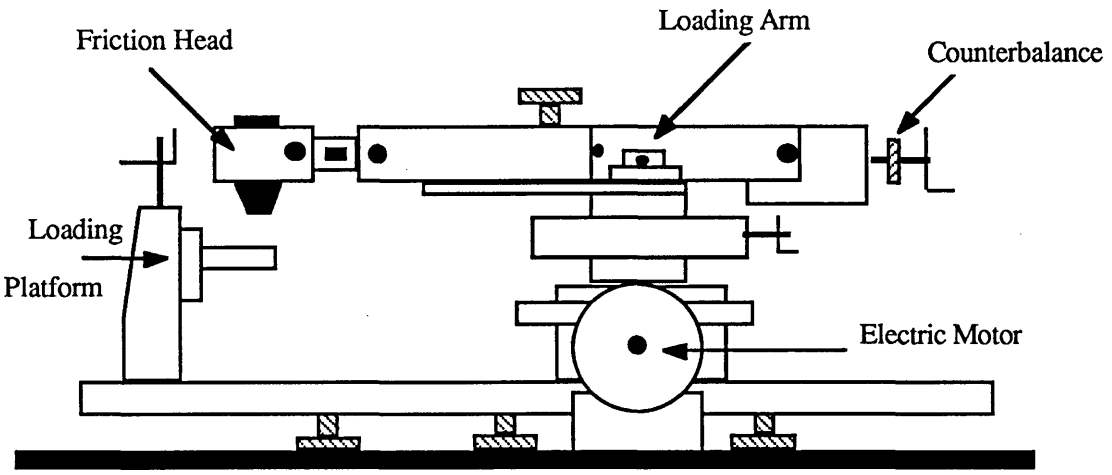

Figure 5.10 Schematic representation of the Eldredge machine.

The specimen was loaded with dead weights in the range 0.005 to 0.100 kg to contact a polished float glass slide. The compact was traversed repeatedly over the glass slide covering a distance of ca. 0.010 m per cycle. The resulting frictional force as a function of the load was calculated.

5.6.3 Interface Friction of Compacts

The surface friction of the compacts was measured by sliding ($2x10^{-4}$ m/s) a polished steel sphere (0.00635 m diameter) over the flat top surface under a range of normal loads between 0.5 N and 20 N. The apparatus has been described in the previous Section; in this case the slider held the indentor and the specimen was mounted on the loading platform. The surface friction of the cylindrical compacts was measured and from the width of the resulting scratch on the compact surface the value of the scratch hardness may be evaluated, as it will be explained in Section 5.6.5.1.

5.6.4 Compaction

The pressing behaviour of the different powders has been evaluated using single sided die compaction. The different specimens have been one-sided uniaxially dry pressed in cylindrical hardened steel dies with steel punches using an Instron machine. Three dies of different sizes were used with internal diameters of 0.0163, 0.019 and 0.022 m; the die was filled with a known amount of powder, the initial powder bed height inside the die was measured using a micrometer (Vernier± 0.02 mm) and a load varying from 0.22 to 44.4 kN was applied to compact the powders. The compaction pressure ranged from 0.8 to 157 MPa. After compaction the samples were ejected and characterised by measurement of their dimensions (Vernier micrometer, ± 0.02 mm) and weight, from which the green density of the resulting compacts was calculated.

The compaction experiments were carried out under lubricated and unlubricated conditions. In the former case for all but uranium dioxide the lubricant, zinc stearate, was applied directly and evenly onto the die wall and punches. In the case of the uranium dioxide materials the granulated powders were admixed with 0.2%wt zinc stearate (supplied by BNFL) using a laboratory mixer (Pascall, Lab-mixer II).

In addition, studies have been undertaken which measured in a continuous manner the applied and transmitted stresses developed during the compaction process as a function of the punch displacement. For this a known amount of powder was placed in

a 0.0163 or 0.022 m diameter cylindrical steel die and the height of the powder in the die was determined. The material was pressed using an Instron testing machine at a constant crosshead speed of 0.00336 m/min. or 0.015 m/min., and the applied and transmitted stresses were recorded using two pressure transducers attached to the upper moving punch and to the lower stationary punch. The signals from the pressure transducers were sent first to an amplifier and then via a A/D converter to a computer and the data recorded and plotted as applied and transmitted force versus punch displacement. The test temperature was kept constant at ambient. The ejection force required to eject the compact from the die was also measured continuously in the same way. A schematic representation of the experiment is shown in Figure 5.11.

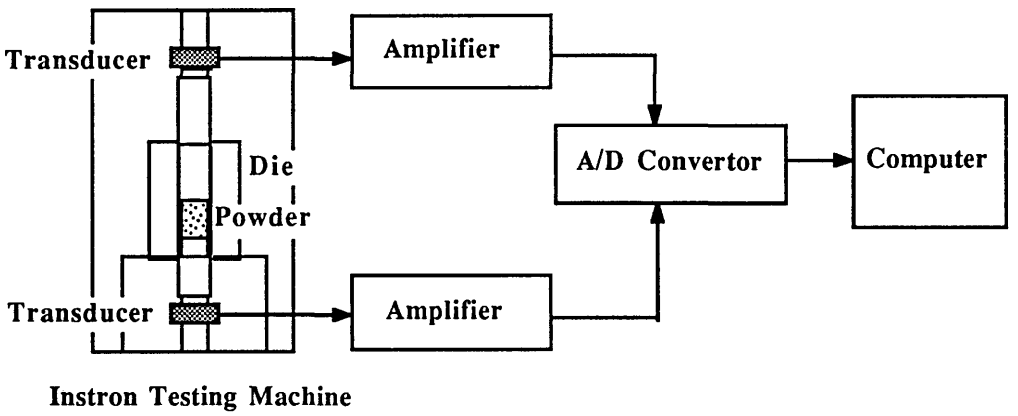

Figure 5.11 Schematic representation of the powder compaction experimental set-up.

Several experiments were carried out using different materials and conditions. The main experimental variables considered were: the type of material, the particle size, the type of binder and the lubricant used, if any, and the mode of application, the initial powder bed height/die diameter ratio and the maximum applied pressure.

5.6.5 Green Characterisation

After compaction and ejection out of the die, the resulting compacts were characterised firstly by calculating their green density from the measurement of their dimensions (Vernier micrometer, ± 0.02 mm) and weight. Some of the compacts were subjected to a further analysis which included the measurement of the hardness profiles along the compact and the study of the wear or attrition resistance of the compacts. The latter studies presented an insight into the strength and homogeneity of the resulting compacts and into the stress distributions in the compacts.

5.6.5.1 Hardness

Two types of hardness measurements have been carried out; indentation microhardness and scratch hardness. The machine used to carry out the scratch hardness experiments on the green compacts was an Eldredge machine (see Section 5.6.2). The slider hold a 120° cone indentor and a fixed load of 0.1 kg was applied to it. The indentor was traversed across the compact surfaces. The resulting scratch width, $2r_w$, was estimated at different points along the compact using a travelling microscope. The normal applied load, W, divided by the apparent contact area, $(\pi\ r_w^2)\ /\ 2$, was taken as a measure of the scratch hardness of the compact, H_s;

$$H_s\,(kg/mm^2) = \frac{2\,W}{\pi\,r_w^2} \qquad (5.8)$$

The projected contact area was taken as half the possible contact area because of the extensive plastic deformation which occurs with these compacted ceramic materials.

For the case of the indentation hardness measurements the hardness profiles of the compacts were obtained across the top and bottom surfaces and along the side as a function of the radius or height using a microhardness machine consisting of a mobile arm through which the load was applied to the specimen. A normal load of 0.100 kg.

was applied for 20 s. to the surface of the compact using a conical indentor with an angle of 120°. A travelling microscope was used to measure the indentation diameter to an accuracy of 0.01 mm. The normal hardness was taken as the applied load divided by the projected area of the indentation at the surface in the surface plane. If r is the average radius of the impression then the projected area is given by πr^2 hence the hardness is computed using equation 5.8.

5.6.5.2 Attrition of Compacts

The attrition of the green compacts has been studied to provide a measure of the density distributions and hence the stress transmission during compaction. The compact was placed in a bed of abrasive material (coarse grade sand, 850 μm, laboratory reagent, BDH Chemicals Ltd.) which was rotated in an hexagonal cone mixer (Pascall, Lab-mixer II) at a fixed speed for a certain period of time after which the changes in mass, dimensions and shape were measured and recorded.

CHAPTER 6

FLOW PROPERTIES DATA

6.1 INTRODUCTION

The flow behaviour of some bulk ceramic materials has been analysed. The importance of classifying the powders with respect to their flow properties has been highlighted in previous chapters (see Chapter 2). It has already been mentioned there, that the flow characteristics of the material influence the ceramic processing and the resulting green quality. The powders have been evaluated to assess some of the critical processing variables in the area of unconstrained or free flow. The action of various organic films, as a means of modifying the flow properties of several ferrite powders, has been investigated. These films markedly alter the rheology of the powder and its interaction with its containers. Some properties of the bulk material and the particles interactions with their neighbours, and with the confining walls, have been examined. The flow experimental results, the analysis of these data and some general conclusions are included in this Chapter.

6.2 EXPERIMENTAL TECHNIQUE: ROTATING CYLINDER

The experimental technique used to determine the flowability under unconstrained flow of the powders was the inclined plane or rotating cylinder experiment described in Chapter 5. The basis of this experiment is that a cylinder, partially filled with the powder, will begin to roll down an inclined plane at some critical angle of inclination. The cylinder was loaded with the desired amount of powder (from 0.010 to 0.160 kg) and placed near the top end of the board. The inclination of the board was then increased gradually until the point of onset of motion, when the cylinder begins to roll

down the plane, and the angle of inclination of the board was recorded. The dynamics of the experiment were shown in Figure 5.9. Before starting the experiment the cylinder laden with the powder was shaken in order to obtain a homogeneous bed.

The angle of inclination that causes the cylinder to roll was determined as a function of the applied normal load (powder mass). The powder apparent bed height and the surface contact area between the powder and the cylinder wall were also determined for each load. For each set of experimental conditions, the experiment was repeated a certain number of times in order to study the variability in this critical angle. A second objective of this experiment is to study the wall-powder friction. Thus, the experimental data obtained were also used to study the interface friction of loose powder beds. The analysis of these data will be presented in Chapter 7.

6.3 EXPERIMENTAL RESULTS: ROTATING CYLINDER

The unconstrained flow properties of the uranium dioxide powders, and the several ferrite/binder systems have been examined in some detail. Before presenting the experimental results for these ceramic powders the situation in the powder bed during the motion of the cylinder is described. The influence of the interface powder-wall and the effect of the cylinder dimensions are also considered.

6.3.1 Flow Regimes

The flow regimes associated with the transverse motion of a bed of particles in a rotating cylinder are functions of the total normal load and the bed velocity. At low angular velocities two modes of transverse motion exist; the "sliding" mode and the "slumping" or "cascade" mode (see Figure 2.1). The mode of flow may also be classified as continuous motion or stick-slip. In this experiment it was observed that at small bed loads sliding at the powder-cylinder interface occurs. The mass of material in the cylinder slides down the cylinder as a relatively immobile body. It was observed that the bed remains essentially static, and there is no apparent interparticle motion at the onset of motion. The whole bed moves in stick-slip action in the case of low bed loads

where no cascading occurs. At higher fill levels the powder cascades and the experiment senses a different powder property, mainly the interparticle interactions. A interrelation between the load or bed height and the mechanism of bed movement has been observed and reported by Motamedi, 1985.

6.3.2 Rolling of the Empty Cylinders

First, the angle of inclination at which the empty cylinder begins to roll was determined. It was necessary to determine the rolling angle for the empty cylinder to take into account the friction between the cylinder and the board. The inclined plane experimental results for the two different cylinders used in these experiments are shown in Table 6.1.

TABLE 6.1 Summary of the Inclined Plane Experiment Results for the Empty Cylinders.

Cylinder Internal Diameter, (m)	Cylinder Length (m)	Cylinder Mass (kg)	Mean Sliding Angle* (°)	Variance of Sliding Angle
0.075	0.152	0.405	1.28	0.110
0.046	0.152	0.263	1.05	0.079

* average value after five determinations

6.3.3 Effect of Cylinder Size

In most cases a 0.075 m internal diameter cylinder was used. The effect of the cylinder size on the flow angle has been examined using two different size cylinders for the powder ferrite IC0 (factory binder).

TABLE 6.2 Summary of the Inclined Plane Experiment Results for the Ferrite-Factory Binder, IC0, as a Function of the Amount of Powder and Cylinder Size.

Powder Load (N)	0.075 m Diameter Cylinder		0.046 m Diameter Cylinder	
	Mean Flow Angle* (°)	H/D**	Mean Flow Angle* (°)	H/D**
0.098	1.95	0.027	2.38	0.043
0.196	2.33	0.040	-----	-----
0.294	3.29	0.053	3.67	0.109
0.392	3.40	0.058	-----	-----
0.490	3.68	0.067	4.89	0.130
0.687	4.70	0.093	6.11	0.174
0.883	-----	-----	6.97	0.196
0.981	-----	-----	8.55	0.217
1.226	6.50	0.16	-----	-----
1.471	7.26	0.17	-----	-----

* average value after ten to twelve determinations
** H/D is the ratio apparent bed height to cylinder diameter ratio

These data are presented graphically in Figures 6.1a and b where the average sliding angle is plotted as function of both the powder load and the normalised apparent bed height respectively.

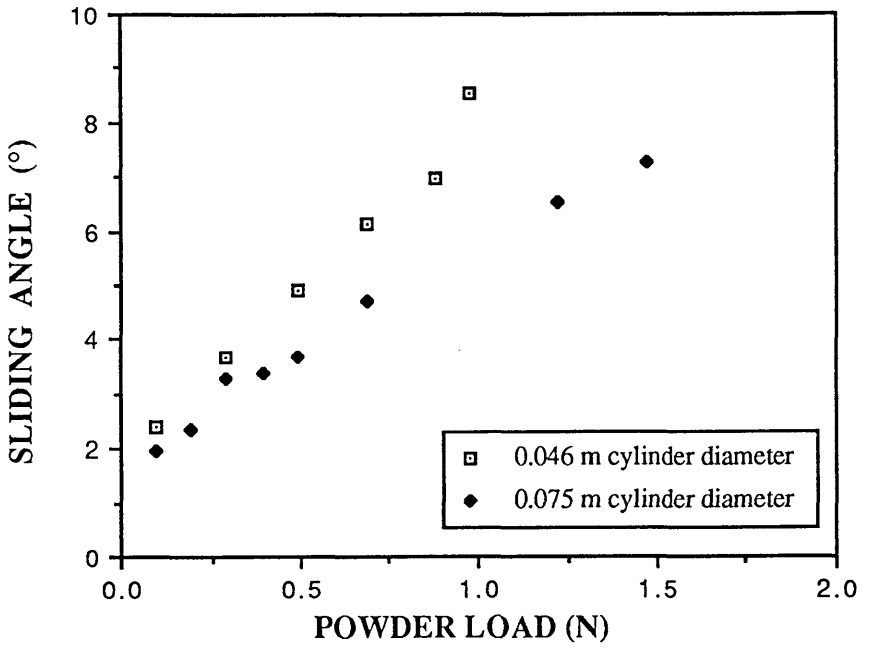

Figure 6.1a Variation of the sliding angle as a function of the powder bed normal load for the Ferrite/Factory Binder system and two different size cylinders.

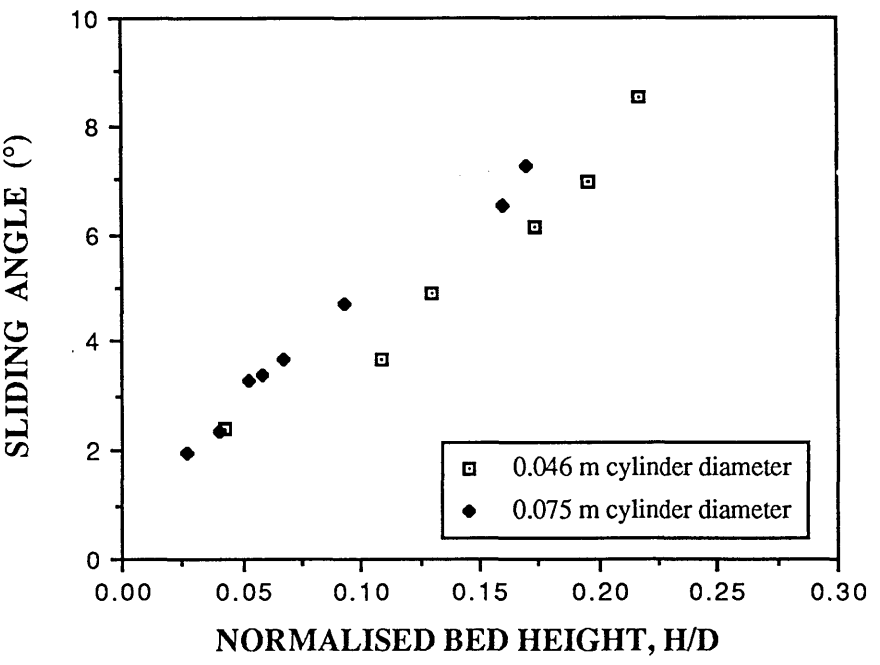

Figure 6.1b Variation of the sliding angle as a function of the normalised powder bed height for the Ferrite/Factory Binder system and two different size cylinders.

6.3.4 Apparent Area of Contact

The powder bed load is one of the variables of interest in this experiment. As it has been explained in the previous Section the type of motion observed depends on the powder fill level. The evident effect of the variation in the amount of powder is the change in the area of contact powder bed-cylinder wall. The area of contact is an important variable to consider when the friction force wall-powder bed is studied. The effect of the area of contact on the friction properties is examined in Chapter 7. In this Section the measurement of the area of contact is presented.

The area of contact between the powder and the wall was determined from geometric considerations from the measurement of the dimensions of the powder bed in the cylinder as represented in Figure 6.2.

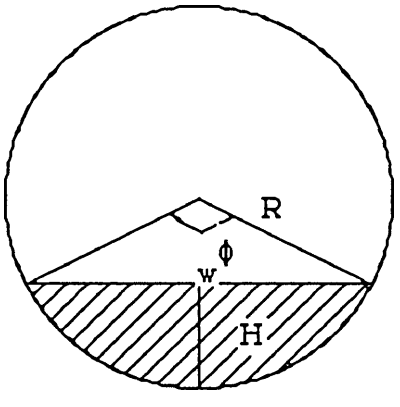

Angle; $w = 2R \sin(\phi/2)$

Perimeter; $S = R\,\phi$

Contact Area; $A_{app} = R\,\phi\,L$

Figure 6.2 Schematic diagram showing how to determine the area of contact powder-cylinder wall as a function of the powder bed width, w, or height, H, in the rolling cylinder.

The apparent area of contact is given by the expression:

$$A_{app} = 2 \arcsin \left(\frac{w}{2R}\right) R L \qquad (6.1)$$

where w is the powder bed width inside the cylinder, R is the cylinder radius and L is the cylinder length.

Table 6.3 shows the corresponding values of the ratio bed height/cylinder diameter for the various powder loads used; for the cases of the ferrite, the "as-received" uranium dioxide and the uranium dioxide granulated powders.

TABLE 6.3 Variation of the Normalised Bed Height as a Function of the Amount of Powder for Several Ceramic Powders.

Powder Mass (kg)	Normalised Apparent Bed Height, H/D		
	Ferrite Systems	UO_2 "As-Received"	UO_2 Granulated
0.010	0.027	0.027	0.013
0.020	0.040	-----	-----
0.030	0.053	0.067	0.040
0.040	0.058	-----	-----
0.050	0.067	0.107	0.053
0.070	0.093	0.133	0.067
0.090	-----	0.160	0.080
0.110	-----	0.187	0.093
0.125	0.160	-----	-----
0.130	-----	0.213	0.107
0.150	0.170	0.227	0.120
0.160	-----	0.253	0.127

6.3.5 Ceramic Systems Experimental Results: Flow Angle

The variable measured in all the cases is the sliding angle at which the cylinder rolls down the inclined plane or flow angle. In some cases it was observed that after an initial movement of the cylinder, which occurred at an intermediate angle, the cylinder stopped and then it would move again as the inclination angle was further increased. The angle considered is that which produces a continuous, accelerated motion of the system.

6.3.5.1 Ferrite Systems

The flow of the different ferrite/binder systems has been analysed. The effect of several variables on the flow angle was studied. These include the type of binder, the normal load and the cylinder size. This latter effect has been presented in Section 6.3.3.

6.3.5.1.1 Flow Angle as a Function of Binder System

The action of various organic films as a means of modifying the flow properties of several ferrite powders has been investigated. The inclined plane experimental results are shown in Table 6.4 for each ferrite-binder system. Tables 6.4 and 6.5 show the mean flow angle and the variance of the flow angle. The data were obtained for a 0.075 m diameter cylinder laden with a powder mass of 0.030 kg.

6.3.5.1.2 Flow Angle as a Function of the Normal Load

The variation of the mean sliding angle with respect to the applied normal load is presented in Figure 6.3 for the systems IC3 (75% PVA 14000-25% PEG 400) and IC12 (Gohsenol). The data for the case of the Ferrite/Factory Binder system was presented in Figure 6.1a. The results of the average sliding angle as a function of the powder mass for some of the ferrite systems examined are presented in Table 6.5.

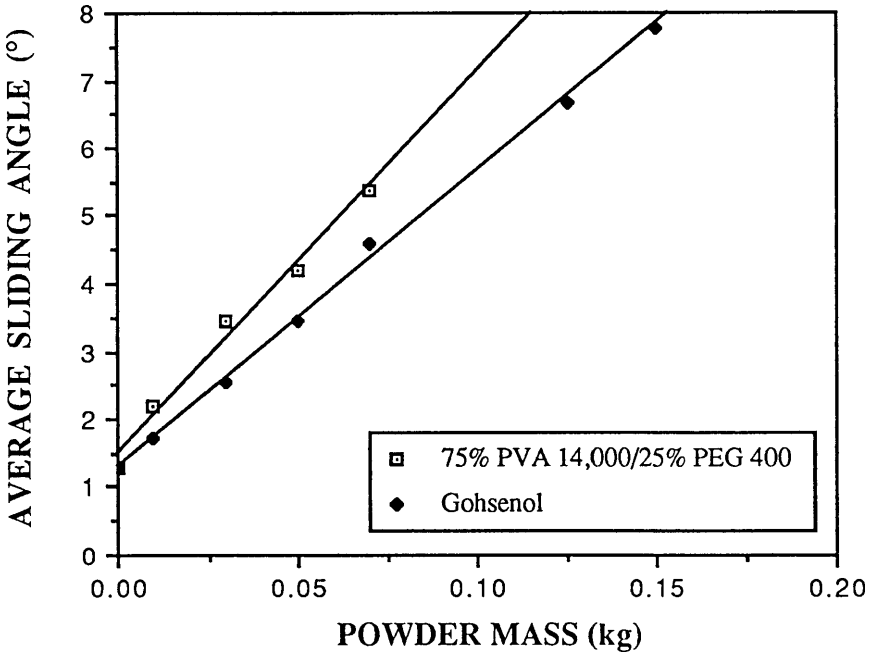

Figure 6.3 Variation of the average sliding angle as a function of the powder mass for two ferrite/binder systems.

6.3.5.1.3 Flow Angle Variability

Figure 6.4 shows some characteristic results of the variability of the flow angle for some ferrite systems. The data presented correspond to the results obtained after repeating the experiment under exactly the same conditions up to twelve times. The example corresponds to the sliding angle of two ferrite/binder systems; Ferrite/75% PVA 14000-25% PEG 400 and Ferrite/PVA 14000 at several normal applied loads.

TABLE 6.4 Summary of the Inclined Plane Experiment Results for the Different Ferrite-Binder Systems at a Constant Powder Load of 0.29N (0.030 kg Powder Mass).

SYSTEM	AVERAGE FLOW ANGLE (°)
IC0	3.29
IC1	3.08
IC2	3.19
IC3	3.46
IC4	3.45
IC5	2.93
IC6	3.10
IC7	3.13
IC8	3.41
IC9	3.74
IC10	3.26
IC11	2.91
IC12	2.56
IC13	2.57
IC14	2.52
IC15	2.86
IC16	2.80

*mean value after ten to twelve determinations

TABLE 6.5 Average Sliding Angle for Several Ferrite Powder Masses.

SYSTEM	POWDER MASS (kg)	AVERAGE SLIDING ANGLE* (°)
IC0**	0.010	2.38
	0.030	3.65
	0.050	4.89
	0.070	6.11
	0.090	6.99
IC0	0.010	1.97
	0.020	2.27
	0.030	3.27
	0.040	3.41
	0.050	3.67
	0.070	4.69
	0.125	6.50
	0.150	7.28
IC2	0.010	2.52
	0.030	3.18
	0.050	4.07
	0.060	4.39
	0.070	4.72
	0.125	5.62
	0.150	7.25
IC3	0.010	2.18
	0.030	3.44
	0.050	4.19
	0.070	5.36

* average value after ten to twelve determinations

** data corresponds to the 0.046m diameter cylinder

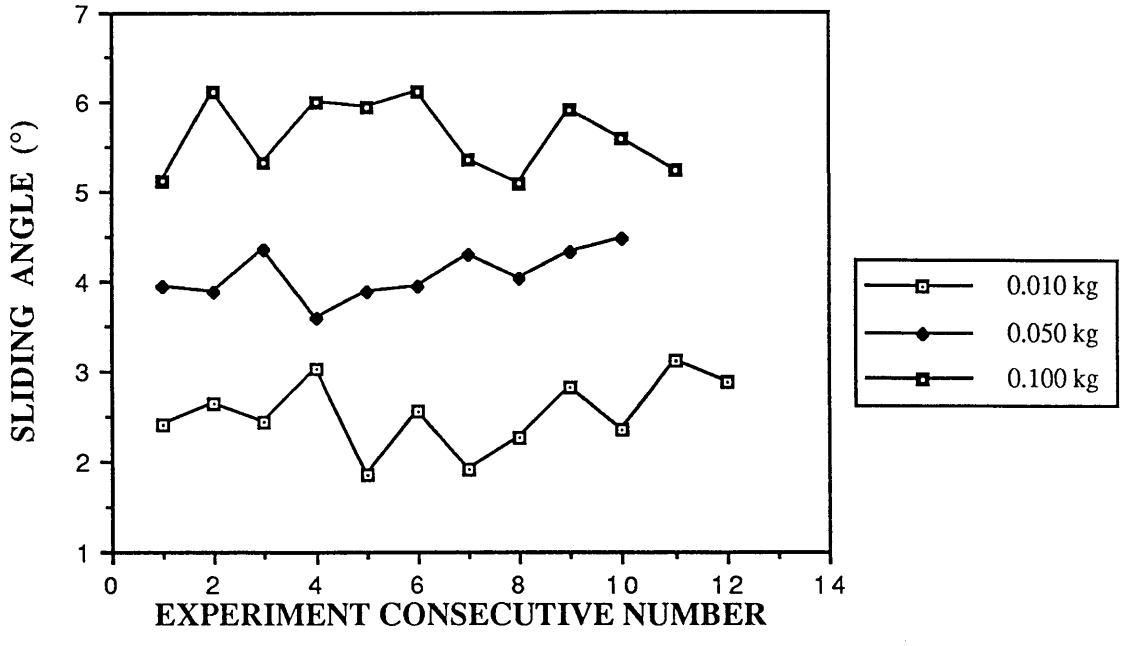

Figure 6.4a Sliding angle values for the system Ferrite/PVA 14000, the experiment is repeated a number of consecutive times for several powder weights.

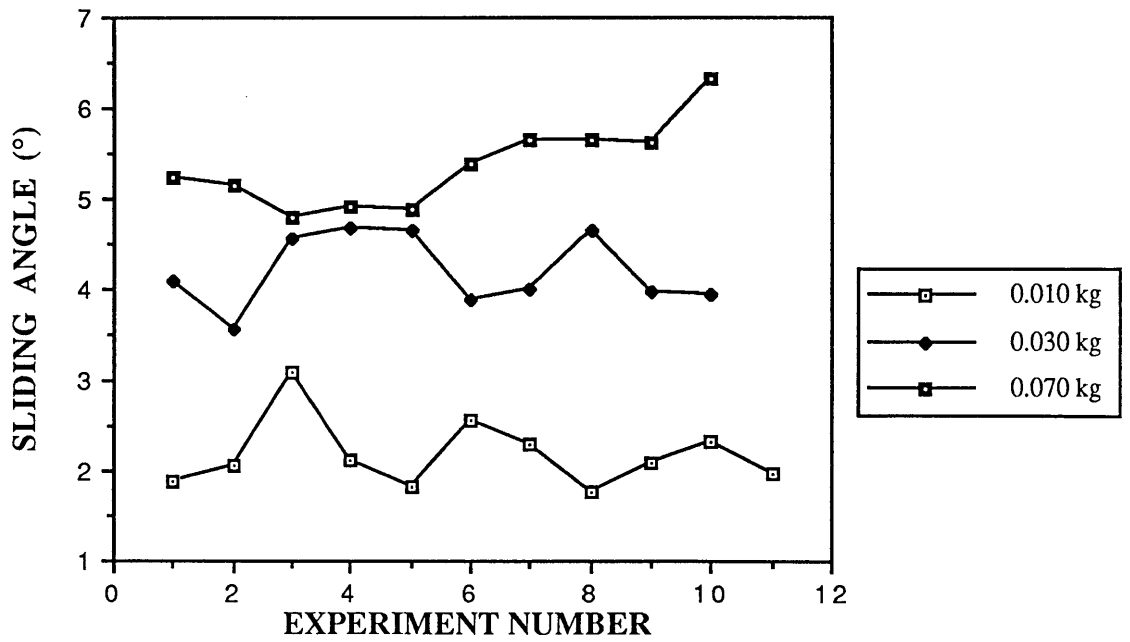

Figure 6.4b Sliding angle values for the system Ferrite/75% PVA 14000-25% PEG 400 as a given set of experiments is repeated for different weights.

6.3.5.2 Uranium Dioxide

6.3.5.2.1. A, B and A_{96}, B_{96}

The unconstrained flow properties of the two supplied uranium dioxide powders were also examined; the designations are A and B. These powders were compression granulated and comminuted. The unconstrained flow of the resulting granulated powders A_{96} and B_{96} were also evaluated following the same procedure.

In the case of the "as-received" materials, the powders have a high degree of cohesion making it difficult to obtain an homogeneous bed; lumps or agglomerates are easily formed. The results for the sliding angle of the powder bed in the rotating cylinder for the UO_2 materials are presented in Table 6.6 for a range of powder loads.

TABLE 6.6 Summary of the Inclined Plane Experiment Results for the Uranium Dioxide Systems as a Function of the Load.

POWDER LOAD (N)	AVERAGE FLOW ANGLE* (°)			
	"AS-RECEIVED"		GRANULATED	
	A	B	A_{96}	B_{96}
0.098	1.77	1.57	1.33	1.29
0.294	2.68	2.81	2.59	2.52
0.490	3.62	3.78	4.08	3.84
0.687	4.72	5.16	5.18	4.97
0.883	5.88	6.45	6.20	6.08
1.079	7.15	7.18	6.98	7.40
1.275	8.60	8.50	7.03	7.33
1.471	9.09	9.13	8.75	8.69
1.570	9.47	9.57	9.13	8.88

* average value after fifteen determinations

6.3.5.2.2 Moisture Effect

The effect of the moisture content on the unconstrained flow has also been analysed. The granulated powders were kept under controlled humidity conditions in two desiccators containing respectively P_2O_5 to dry them and saturated NH_4Cl solution (80% relative humidity). These powders are labelled dry and wet respectively. The treated granules were examined for one powder mass (0.050 kg). The experimental sliding angles obtained for the case of this intermediate load of 0.49 N in a 0.075 m internal diameter cylinder are shown in Table 6.7.

TABLE 6.7 Summary of the Inclined Plane Experiment Results for the Uranium Dioxide Systems as a Function of the Moisture Content for a Powder Mass of 0.050 kg.

MATERIAL	AVERAGE FLOW ANGLE* (°)
A_{96} dry	3.50
A_{96} wet	3.86
A_{96} non-treated	4.13
B_{96} dry	3.76
B_{96} wet	3.89
B_{96} non-treated	3.77

* average value after fifteen determinations

6.4 ANALYSIS OF THE EXPERIMENTAL RESULTS

Two main analyses are possible. From the variation of the sliding angle with the applied load, the mean wall friction may be analysed. From the repeatability of the

experimentally obtained angle of slide for a given set of experimental conditions the bulk flow characteristics may be assessed. In this Section only those aspects relating to the bulk flowability of the materials are considered.

6.4.1 Area of Contact

Due to the fact that the bulk apparent density of the different ferrite-binder systems is quite similar; ca. 1.37 g/cm^3; the calculated area of contact is nearly independent of the type of binder considered and it is only a function of the cylinder dimensions and the mass of the powder as may be observed in Table 6.2. Also, the apparent area of contact or normalised bed height is a strong function of the type of powder, mainly its bulk density, as may be deduced from the different values obtained for the case of granulated and "as-received" uranium dioxide powders; Table 6.3.

6.4.2 Empty Cylinders

It may be seen in Table 6.2 that the rolling (sliding) angle for the ferrite IC0 (factory binder) is a function of the applied load for both cylinders. The effect of varying the cylinder size is a change in the apparent area of contact wall-powder for the same powder load; i.e. the number of contact points changes. This has an effect on the observed sliding angle. The smaller cylinder presents a higher angle of slide for a given powder load as it is shown in Figure 6.1a. At a given load the powder in the smaller cylinder presents a higher height/diameter ratio, this produces a higher angle of slide. Figure 6.1b presents the variation of the angle of slide with the normalised bed height. Figure 6.5 presents the sine of the sliding angle as a function of the applied load normalised by the load of the empty cylinder. The difference observed previously in the results for the two cylinder sizes disappears. So the results from different size cylinder may be compared if the apparent normalised bed height and the normalised load are considered. Figure 6.6 presents the same experimental results in a slightly different way; the variation of the sliding angle normalised by the sliding angle corresponding to the empty cylinder as a function of the the apparent normalised bed height shows a similar behaviour for both cylinder sizes.

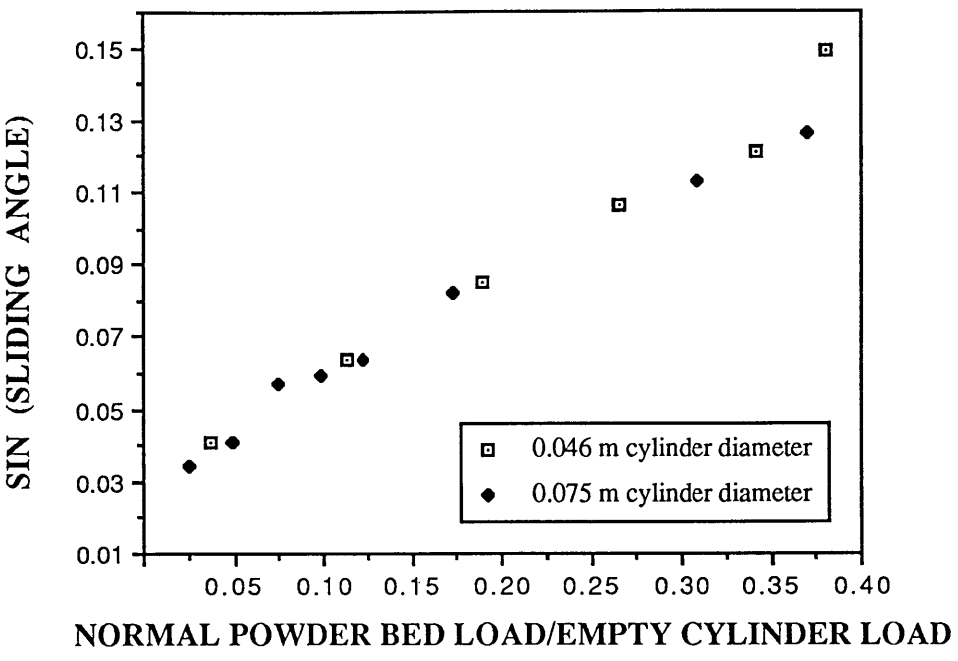

Figure 6.5 Variation of the sine of the sliding angle as a function of the normalised powder load. Ferrite/Factory Binder system and two different cylinders.

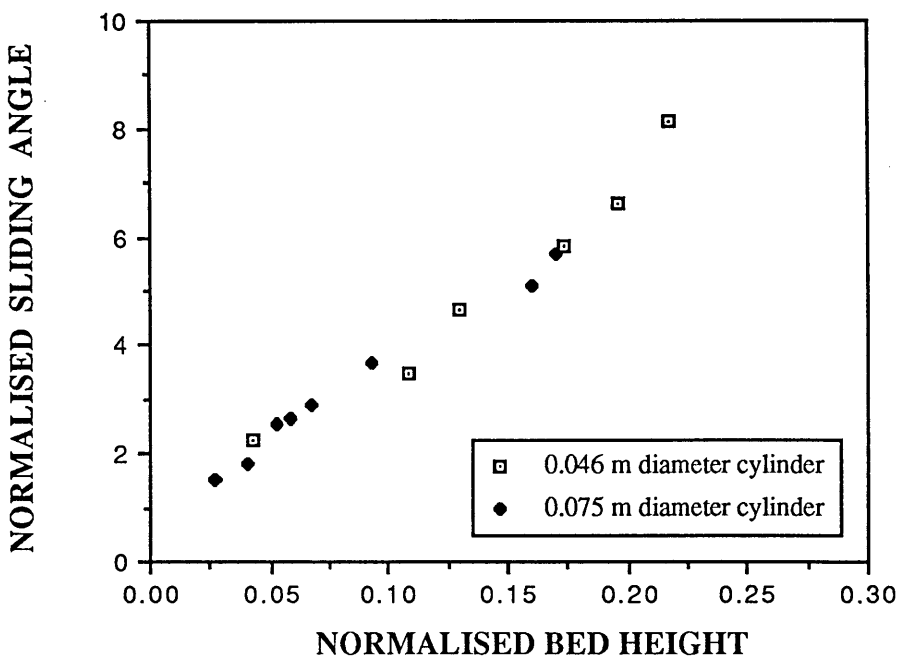

Figure 6.6 Variation of the normalised sliding angle with the normalised bed height for the Ferrite/Factory Binder system and two different size cylinders.

6.4.3 Flow Angle and Variation of the Flow Angle

The flow angle will be shown to be a function of the binder system, which affects the wall friction, so it affects the flow of the material against the container wall. But the sliding angle value is not an actual measure of the whole of the flow situation. This is better revealed by considering the variation of the sliding angle. This approach takes into account the homogeneity of the bed, i.e. the flow of the bulk system. The criteria introduced in this study to characterise the powders with respect to their flow characteristics $\underset{\alpha_{re}}{\wedge}$ based on the statistical analysis of the variation in the sliding angle.

Before discussing the analysis of the experimental data a brief general introduction to the statistical analysis is presented.

6.4.3.1 Statistical Considerations

As a means of studying the scatter of the sliding angle data for the different powders in the inclined plane experiment, a statistical approach was used. The different statistical parameters used to analyse the data are defined (Spiegel, 1972);

Measure of the central tendency:

- arithmetic mean or mean; the arithmetic mean of a set of numbers, α_i is defined as

$$\bar{\alpha} = \frac{\sum_{i=1}^{N} \alpha_i}{N} \qquad (6.6)$$

- arithmetic mean computed from grouped data; when data are presented in a frequency distribution, the mean is

$$\bar{\alpha} = \frac{\sum_{i=1}^{N} f_i X_i}{\sum_{i=1}^{N} f_i} \qquad (6.7)$$

where X_i is the class mark and f_i is the corresponding class frequency

- mode; the mode of a set of numbers is that value which occurs with the greatest frequency. From a frequency distribution or histogram the mode can be obtained from the formula

$$M = L_1 + \left(\frac{\Delta_1}{(\Delta_1 + \Delta_2)}\right) c \qquad (6.8)$$

where L_1 is the lower class boundary of modal class, Δ_1 is the excess of modal frequency over frequency of next lower class, Δ_2 is the excess of modal frequency over frequency of next higher class, and c is the size of the modal class interval.

Measure of dispersion:

The degree to which numerical data tend to spread about an average value is called the variation or dispersion of the data. Various measures of dispersion are available, the most common being:

- interval or range; it is the difference between the largest and smallest values in the set.

- standard deviation; it is a measure of the variability and in a sense it may be thought of as an average deviation from the mean. It is defined by

$$s = \sqrt{\frac{\sum_{i=1}^{N}(\alpha_i - \bar{\alpha})^2}{N}} \tag{6.9}$$

- variance; the variance of a set of data is defined as the square of the standard deviation

$$v = s^2 \tag{6.10}$$

- coefficient of variation; it is a measure of the relative dispersion of the data and is given by the standard deviation expressed as a percentage of the mean;

$$cov = \frac{100\ s}{\bar{\alpha}} \tag{6.11}$$

Small sampling theory; Student's t distribution

- confidence intervals; the population mean may be estimated within specified limits of confidence. For a given degree of confidence, the limits within which the true value of the mean lies are given by,

$$\bar{\alpha} \pm \frac{t\ s}{\sqrt{N-1}} \tag{6.12}$$

where t is the Student's t, and N is the sample size

- skewness; it is the degree of symmetry, or departure from symmetry, of a distribution. It may be expressed as

$$\text{skewness} = \frac{(\bar{\alpha} - \text{mode})}{s} \tag{6.13}$$

Graphically the obtained experimental values may be presented as a histogram which represents the frequency with which the sliding angle values occur. This type of representation has certain useful characteristics; the shape of the histogram may show if the process is producing a symmetrical, normally shaped distribution. Signs of abnormality, such as asymmetry, truncation, or bimodality may indicate the presence of filtered or mixed data. The width of the histogram shows the variability or spread of the data. The location of the centre of the histogram indicates where the process is centred and provides the value of the average output.

6.4.4 Ferrite

In this Section the analysis of the experimental results corresponding to the various ferrite/binder systems studied are presented. The analysis may be divided into two main areas. One deals with the actual values of the sliding angle and the second area refers to the variability or dispersion in the measured angles.

6.4.4.1 Flow Angle

From the data corresponding to the inclined plane experiment for the ferrite systems several features may be noted. First, the situation where a fixed cylinder size and a fixed amount of powder (0.030 kg) were used, i.e. the only experimental variable is the type of binder, is considered. It may be seen in Table 6.4 from the different angles at which the cylinder begins to roll down that this angle depends on the type of binder material. The flow angle is a function of the applied normal load and binder system as it may be seen in Figure 6.3 for some selected binder systems. As it has been mentioned previously, there is no marked effect of the bed height as the apparent contact area bed-cylinder wall is similar for all the different binder systems studied at any given load.

The value of the sliding angle is an indication of the frictional force at the interface powder/wall. An increase in the surface friction of the powder would result in poor flow behaviour. The increase of the angle of slide means a worse flow situation. A

better method to describe the flow of the bulk material is by analysing the dispersion of the sliding angle measurements.

6.4.4.2 Variance of Flow Angle

Plotting the corresponding histograms shows in a clear way the frequency distribution of the sliding angles. The magnitude of the angle range and the type of angle frequency distribution depends upon the binder system. The variance for each set of experiments was calculated and its value indicates the repeatability of the results. Some representative histograms for selected ceramic-binder systems are shown in Figures 6.7, for a cylinder of 0.075 m internal diameter and for 0.030 kg mass of powder. The differences are very marked. The histogram gives a clear idea of the flow performance of the powders. For a narrow distribution of the sliding angle, that is, a good repeatability of the data, it may be concluded that the powder has good internal flow properties. On the other hand when there is a large scattering of the data, that is, the angle distribution is broad, it may be concluded that that is a cohesive, non free-flow powder. The basic argument is that the distribution of angles arises from heterogeneities in the internal stress in the powders induced during the filling operation. The filling procedure will produce a range of stress conditions and fluctuations and the better the internal flow the less marked will be these fluctuations on the observed friction. An example of each of these two main types of behaviour is shown: the first one, ferrite IC12 (Gohsenol), Figure 6.7a indicates a good free flow powder, as the angle size distribution is narrow and the distribution is of a normal type. The mean is also the most probable value. In Figure 6.7b an example of a poor flowing powder is shown, ferrite IC11 (Primal). Here there is a wide and irregular angle distribution. It will be noted that a variety of frequency distributions are obtained; normal, bimodal, exponential. To describe the behaviour of these samples more accurately, these results were analysed statistically. The variance of all the binder systems are shown in Table 6.8. Table 6.8 also shows the mean flow angle and the variance of the flow angle for all the powders and the corresponding statistical parameters for some selected cases of ferrite systems. The confidence limits are calculated for a 95% degree of confidence, i.e. 0.05 probability level.

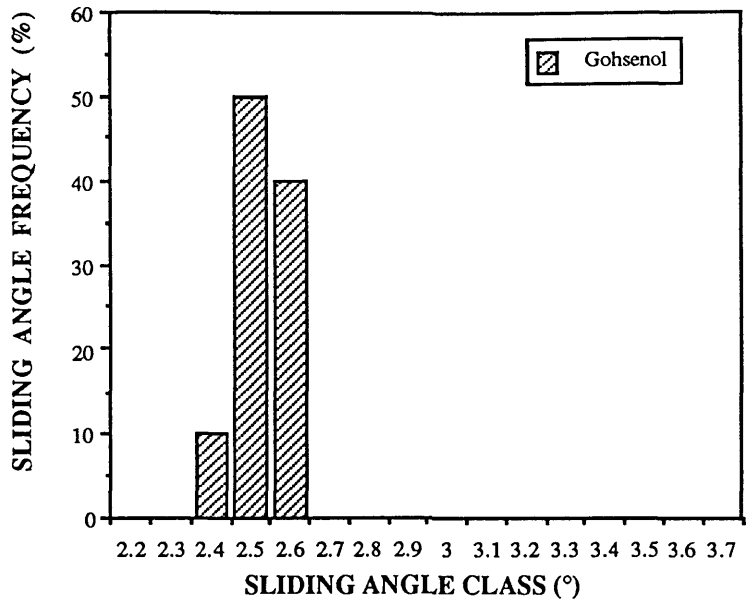

Figure 6.7a Sliding angle histogram for the system Ferrite/Gohsenol for a powder mass of 0.030 kg.

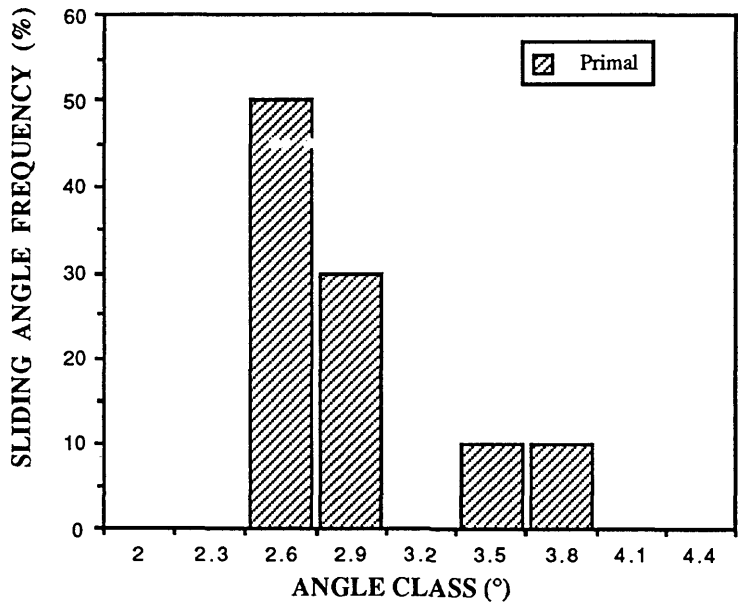

Figure 6.7b Sliding angle frequency distribution for the system Ferrite/Primal for a powder mass of 0.030 kg.

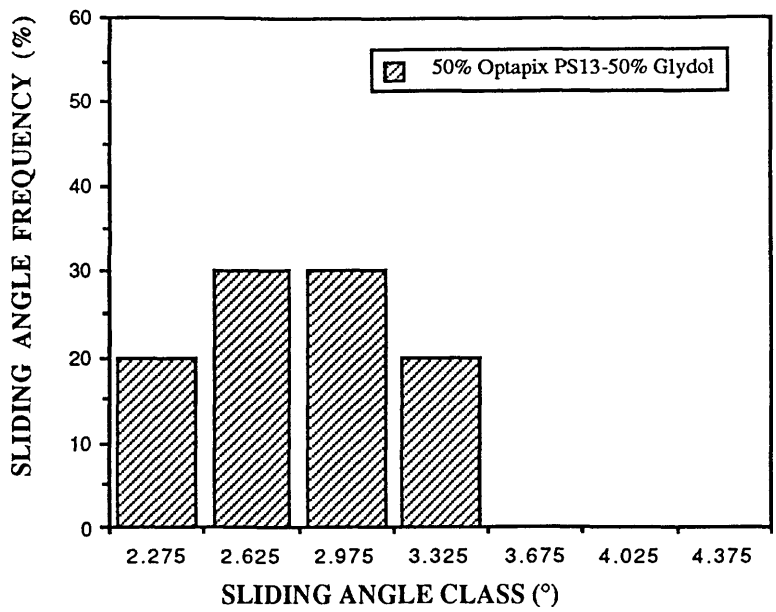

Figure 6.7c Sliding angle frequency distribution for the system Ferrite/50% Optapix PS13-50% Glydol for a powder mass of 0.030 kg.

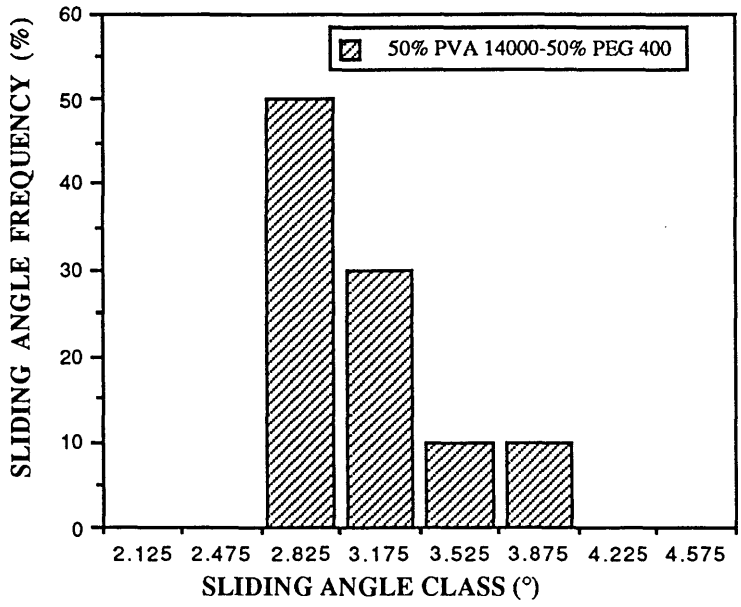

Figure 6.7d Sliding angle frequency distribution for the system Ferrite/50% PVA 14000-50% PEG 400 for a powder mass of 0.030 kg.

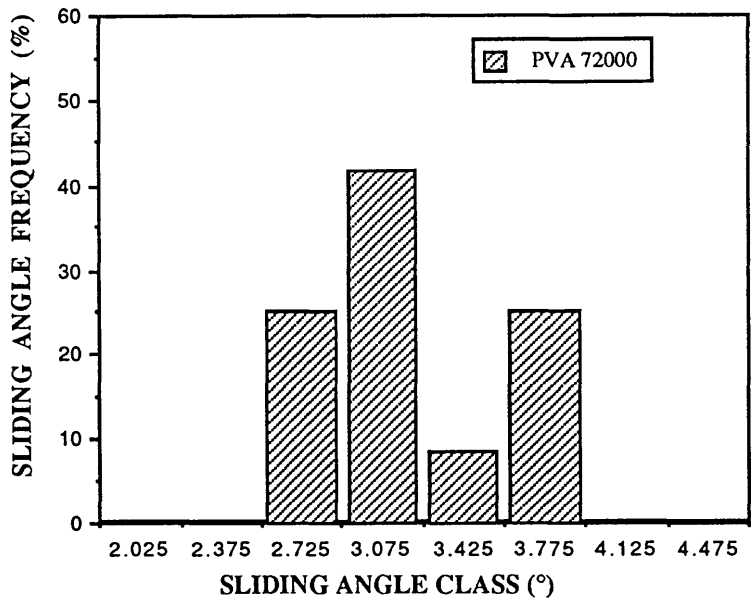

Figure 6.7e Sliding angle frequency distribution for the system Ferrite/ PVA 72000 for a powder mass of 0.030 kg.

TABLE 6.8 Descriptive Statistics for Ferrite Flow Angles for 0.030 kg Powder Mass.

System	Mean Angle (°)	Range (°)	Variance	Coefficient of Variation	95% Confidence Limit ±
IC0	3.29	2.98-3.53	0.022	4.51	0.18
IC1	3.08	2.62-3.90	0.119	11.20	0.22
IC2	3.19	2.40-3.88	0.167	12.81	0.34
IC3	3.46	2.98-4.48	0.174	12.06	0.30
IC4	3.45	2.92-3.93	0.094	8.89	0.20
IC5	2.93	2.60-3.13	0.036	6.48	0.13
IC6	3.10	2.73-3.98	0.118	11.08	0.24
IC7	3.13	2.63-3.47	0.106	10.40	0.23
IC8	3.41	2.87-4.00	0.149	11.32	0.26
IC9	3.74	2.83-4.37	0.264	13.74	0.17
IC10	3.26	2.97-3.88	0.104	3.19	0.23
IC11	2.91	2.48-3.88	0.162	13.83	0.29
IC12	2.56	2.37-2.63	0.005	2.76	0.05
IC13	2.57	2.20-2.77	0.027	6.39	0.12
IC14	2.52	2.23-2.77	0.028	6.64	0.12
IC15	2.86	2.57-3.45	0.056	8.27	0.17
IC16	2.80	2.18-3.45	0.129	12.83	0.25
IC0*	3.67	3.42-3.87	0.022	4.04	0.10

It is commonly observed with powders in continuously rotating cylinders undergoing stick-slip motion that the static forces are not a unique quantity; they show a pronounced variance. The static values are also it seems stochasticaly controlled.

6.4.4.3 Classification

From the value of the coefficient of variation, the systems have been classified as "good" or "bad", or "intermediate", in relation to their flowability. If the binders are

divided in three groups according to their flow angle value, a correlation amongst similar binder systems may be established. Table 6.9 shows the three groups into which binders have been divided depending on the possession of a low, medium or high sliding angle. In all cases the angle for a 0.075 m diameter cylinder loaded with 0.030 kg of powder has been used for comparison. In general it is observed that the powders with Optapix and/or Glydol have the smallest sliding angles (between 2.51-2.86). The materials with the system 50% PVA/50% PEG as a binder correspond to the middle zone with angle values between 2.93-3.13. Finally the materials with the greatest content of PVA exhibit the largest angles (3.19-3.46). The flow angle decreases as PEG is substituted for PVA.

TABLE 6.9 Classification of the Ferrite-Binder Systems According to Their Sliding Angle Values.

FLOW ANGLE RANGE (°)	FERRITE SYSTEMS		FLOWABILITY
2.51-2.56	IC14		
	IC12		"good"
	IC13		
2.78-3.27	IC16	IC15	
	IC11	IC5	
	IC6	IC7	"medium"
	IC1	IC2	
	IC10	IC0	
3.40-3.63	IC8		
	IC3		"bad"
	IC9		
	IC4		

The same analysis may be carried out by scaling the efficiency of the binder systems according to their sliding angle variance or coefficient of variation. This is shown in Table 6.10. The powder with a lowest coefficient of variation; that is, whose angle results show best repeatability, is IC12 (Gohsenol) and the one with a higher variance is IC3 (75% PVA/25% PEG). When grouping the different molecular weight PVA and PVA/PEG systems one sees all types of behaviour. From examining the different PVA systems compared with the PVA/PEG systems to establish which provides, in general, a lower sliding angle coefficient of variation no general conclusion can be drawn. Comparing both types of scaling no precise relationship is apparent. In some cases however a powder with a small sliding angle correspond with a small coefficient of variation as well. For example, in the case of IC12 (Gohsenol), and IC13, IC14 and IC15 (binder system Optapix and Glydol), but in the cases of IC11 and IC16 a small flow angle does not correspond with a small coefficient of variation.

TABLE 6.10 Classification of the Ferrite-Binder Systems According to Their Sliding Angle Coefficient of Variation Values.

Flow Angle Coefficient of Variation Range	Ferrite Systems		Flowability
2.76-4.51	IC12	IC5	
	IC10	IC14	"good"
	IC0	IC15	
	IC13		
10.40-13.83	IC4	IC3	
	IC7	IC2	
	IC6	IC16	"bad"
	IC1	IC9	
	IC8	IC11	

The different binder systems may be classified according to their flow angle coefficient of variation as shown in Table 6.10. From this comparison it may be concluded that the best free-flowing powder is IC12 which contains Gohsenol as the binder and the worst one is IC11 which contains Primal as binder.

6.4.5 Uranium Dioxide Powders

6.4.5.1 Flow Angle

In the case of the uranium dioxide materials the flow angle depends on the normal load, the type of material A or B, and the state of agglomeration of the material.

6.4.5.1.1 "As-Received" Materials; A and B

In general, for a given powder, it is observed that the tendency for cohesion increases the angle of repose. An increase in the friction at the powder-wall interface would result in poor flow behaviour. According to this criterion, powder A presents better flow characteristics giving a lower sliding angle than powder B, which is more cohesive. The results are presented in Table 6.6.

6.4.5.1.2 "As-Received" vs. Granulated Material

The different flowability characteristics of the "as-received" and granulated materials are evident from Figure 6.8 which represents the average sliding angle as a function of the applied normal load for these materials. The apparent area of contact is affected in a great measure by the state of agglomeration of the powder; see Figure 6.9 where the average sliding angle is plotted as a function of the apparent normalised bed height. The "as-received" powders present a higher bed height; i.e. a higher area of contact, than the granulated materials for any given load due to their lower bulk density. The materials A and B have an apparent bulk density of 0.91 and 0.98 g/cm^3 respectively and for the granulated powders A_{96} and B_{96} the values 2.80 and 2.74 g/cm^3 are obtained respectively. So, in general the sliding angle for the "as-received"

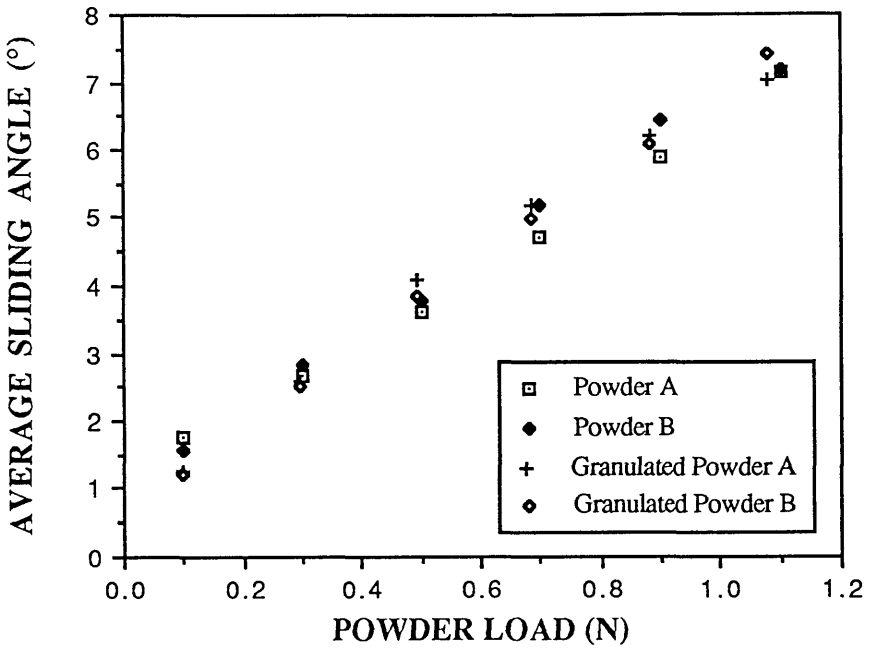

Figure 6.8 Variation of the average sliding angle as a function of the powder load for the two types of 'as-received" and granulated uranium dioxide powders.

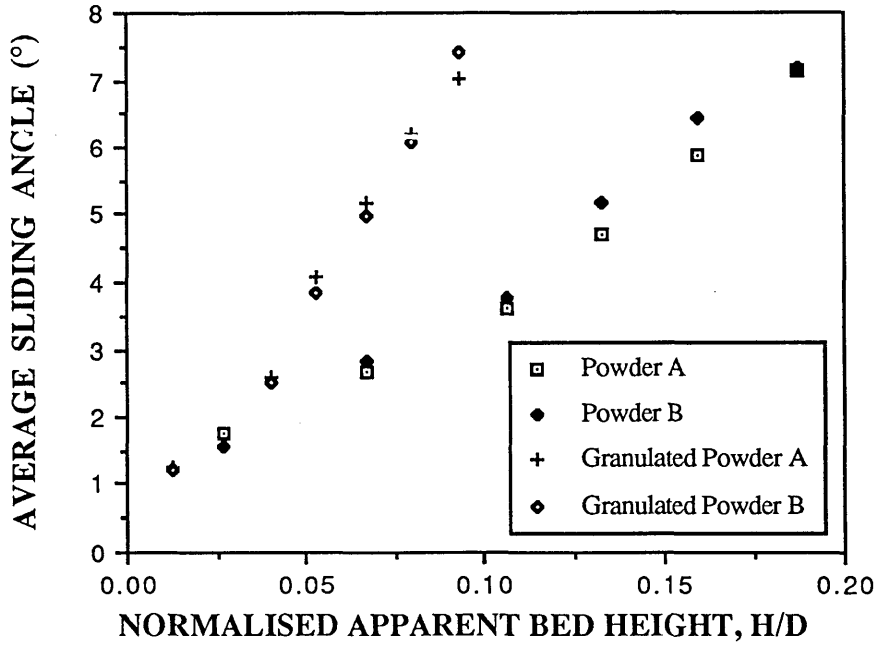

Figure 6.9 The average sliding angle is plotted as a function of the normalised apparent bed height for the uranium dioxide materials.

powders is higher than for the granules as may be seen in Table 6.6 and Figure 6.8.

6.4.5.1.3 Humidity Effects on Granules

The treated granules, kept under controlled humidity conditions and labelled "wet" and "dry" were also examined for one powder load (0.050 kg powder mass).The effect of the moisture content on the flow angle is shown in Table 6.7, where the values of the mean sliding angle for the powders stored under different humidity conditions are presented. For the case of the granulated powder B_{96}, the sliding angle is higher in the case of the wet conditions; the water adsorbed enhances the cohesion among the granules and/or the adhesion of the materials to the container walls. There is no significant change in the flow properties after drying the material. For the case of the granulated material A_{96}, in general it has a lower flow angle than the corresponding B_{96} powder, except for the non-treated granules where A_{96} has an unusually high angle. In this case the effect of water content in the flow properties of the granules is more marked than for the case of the type B_{96} granules. The differences in the values of the flow angle for the different materials and conditions are, in general, not very significant.

6.4.5.2 Variation of the Flow Angle

The experimental sliding angle results obtained for the "as-received" and granulated powders at different loads have been treated using a statistical approach. In Figures 6.10 and 6.11 the corresponding histograms of the sliding angle frequency distribution for the powders A and B and for the lubricated, granulated materials $A_{96\text{-}L}$ and $B_{96\text{-}L}$ are shown. Table 6.11 presents the most significant statistical parameters including the variance and the coefficient of variation for some selected cases of uranium dioxide systems. The confidence limits are calculated for a 95% degree of confidence, i.e. 0.05 probability level.

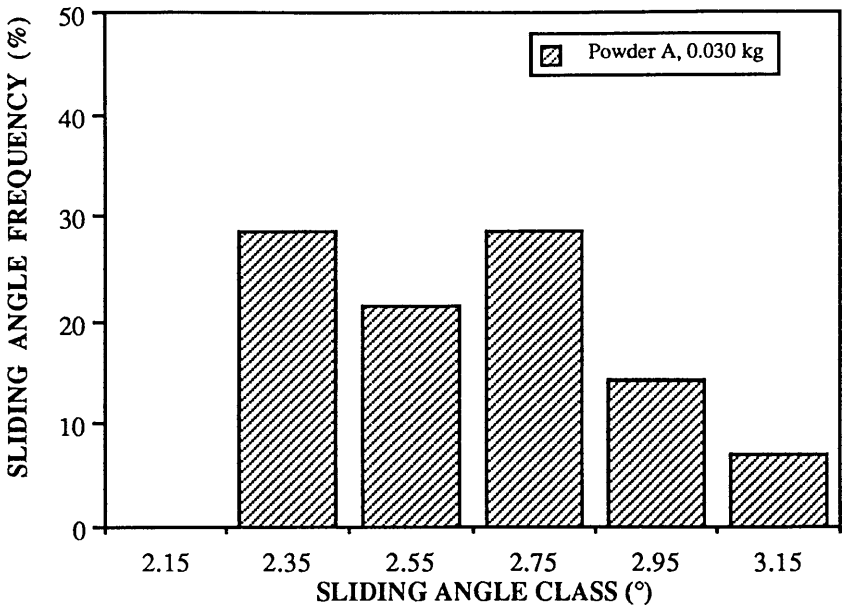

Figure 6.10a Sliding angle frequency histogram for the UO_2 "as-received" powder A at a powder mass of 0.030 kg.

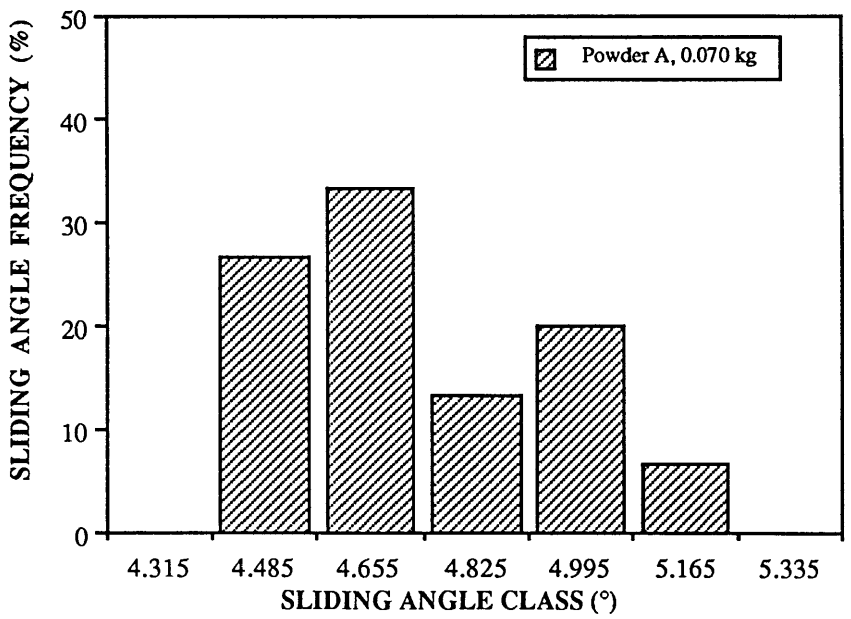

Figure 6.10b Sliding angle frequency histogram for the UO_2 "as-received" powder A at a powder mass of 0.070 kg.

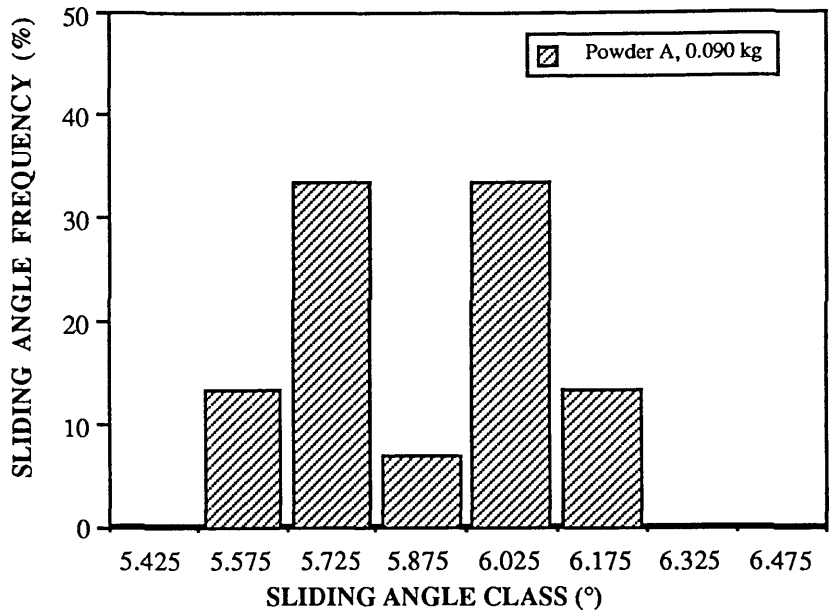

Figure 6.10c Sliding angle frequency histogram for the UO_2 "as-received" powder A at a powder mass of 0.090 kg.

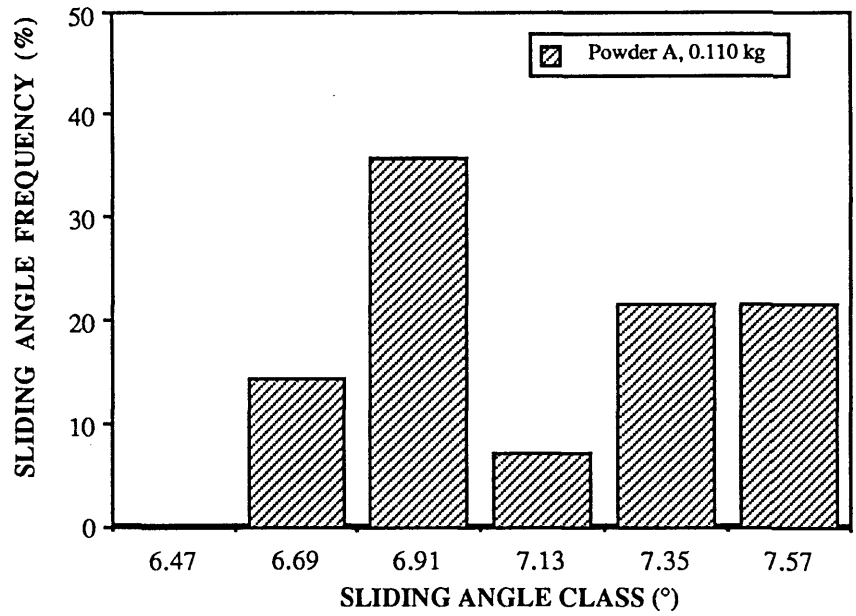

Figure 6.10d Sliding angle frequency histogram for the UO_2 "as-received" powder A at a powder mass of 0.110 kg.

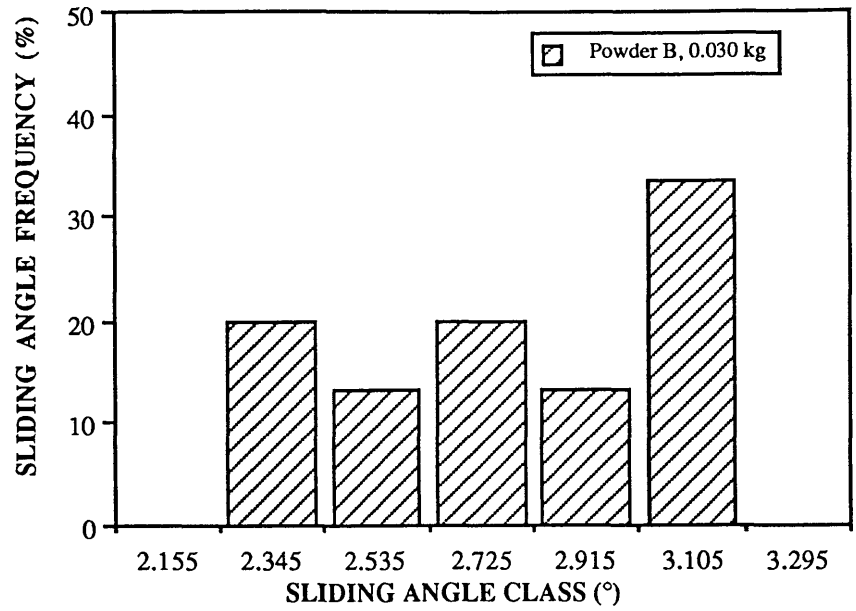

Figure 6.10e Sliding angle frequency histogram for the UO_2 "as-received" powder B at a powder mass of 0.030 kg.

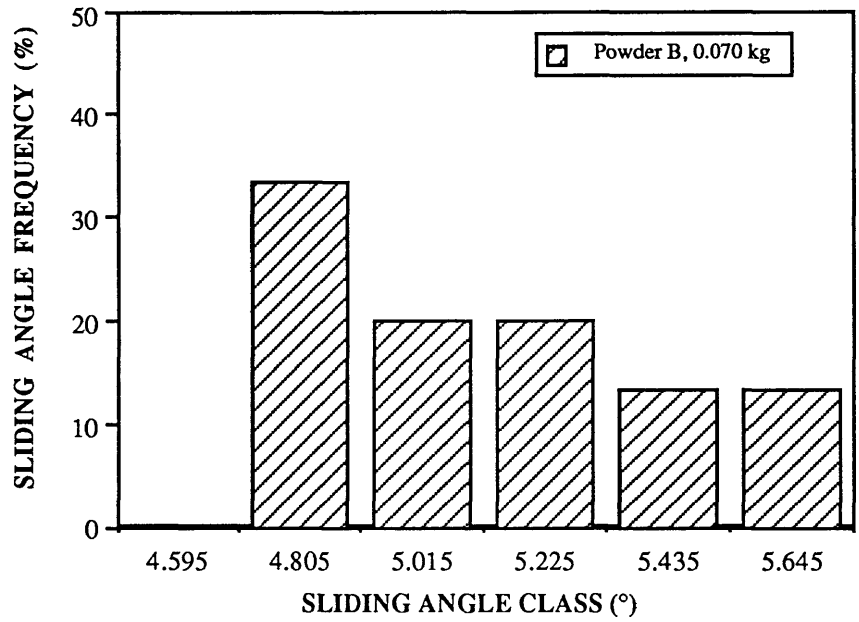

Figure 6.10f Sliding angle frequency histogram for the UO_2 "as-received" powder B at a powder mass of 0.070 kg.

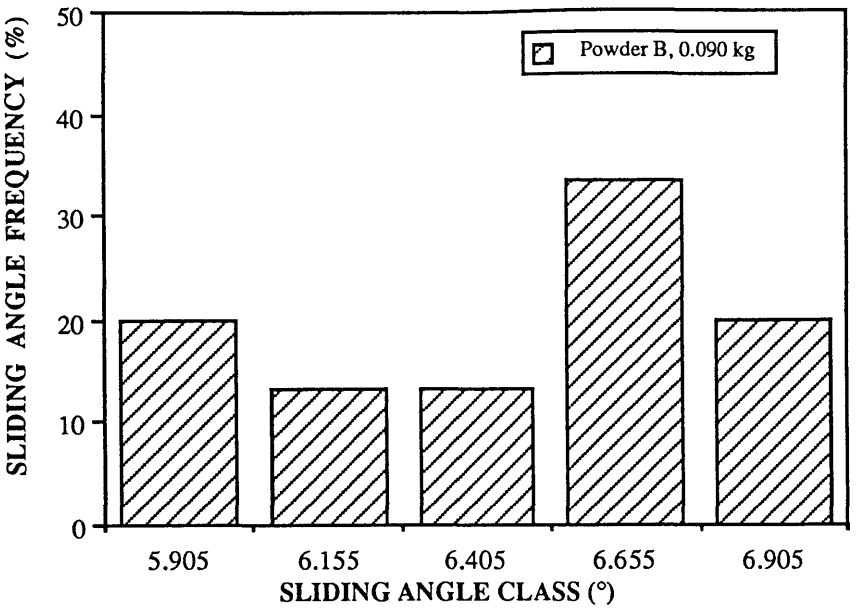

Figure 6.10g Sliding angle frequency histogram for the UO_2 "as-received" powder B at a powder mass of 0.090 kg.

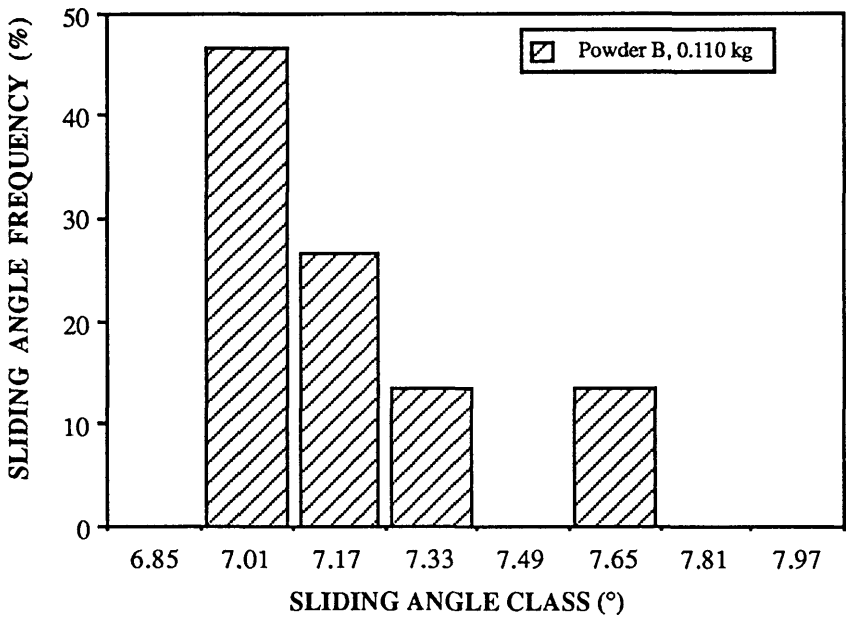

Figure 6.10h Sliding angle frequency histogram for the UO_2 "as-received" powder B at a powder mass of 0.110 kg.

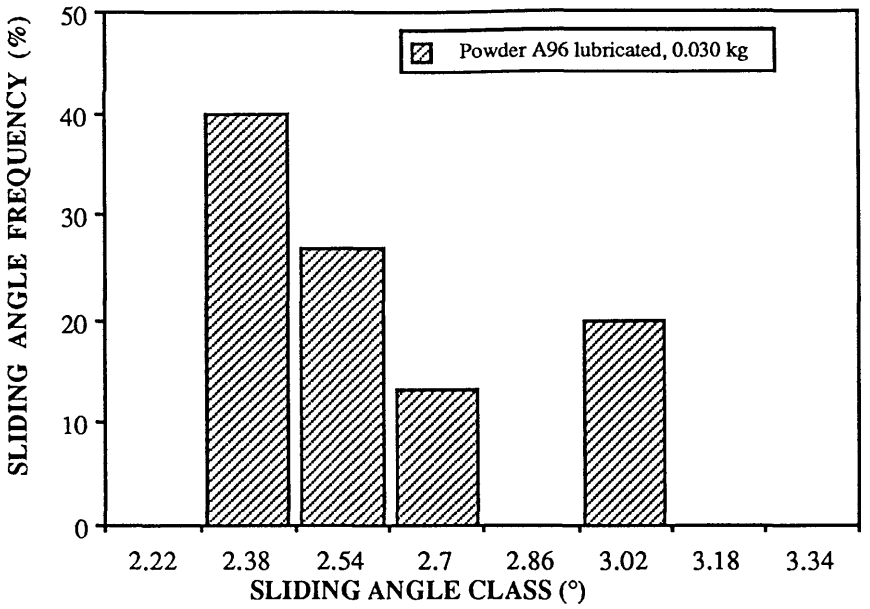

Figure 6.11a Sliding angle frequency distribution for the agglomerated and lubricated UO_2, $A_{96\text{-}L}$ at a powder mass of 0.030 kg.

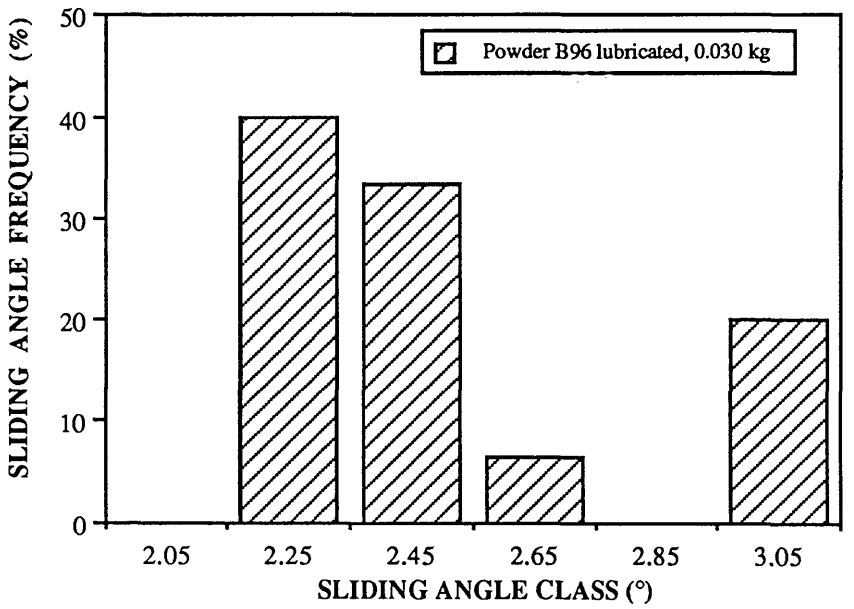

Figure 6.11b Sliding angle frequency distribution for the agglomerated and lubricated UO_2, $B_{96\text{-}L}$ at a powder mass of 0.030 kg.

TABLE 6.11 Descriptive Statistics for Uranium Dioxide Flow Angles for Several Powder Masses.

System	Amount (kg)	Mean Angle (°)	Range (°)	Variance	Coef.Variation	Conf Limit 95% (±)	Skewness
A	0.010	1.77	1.28-2.30	0.11	18.74	0.17	0.1
A	0.030	2.68	2.27-3.24	0.076	10.29	0.15	0.2
A	0.050	3.62	3.25-3.92	0.037	5.31	0.10	0.1
A	0.070	4.72	4.40-5.23	0.061	5.23	0.13	0.4
A	0.090	5.88	5.50-6.25	0.047	3.69	0.11	0.0
A	0.110	7.15	6.58-7.68	0.102	4.47	0.17	-0.1
B	0.010	1.57	1.22-2.02	0.037	12.25	0.10	0.3
B	0.030	2.81	2.28-3.20	0.086	10.44	0.16	-0.2
B	0.050	3.78	3.43-4.27	0.059	6.42	0.13	0.5
B	0.070	5.16	4.73-5.75	0.100	6.13	0.17	0.5
B	0.090	6.45	5.78-7.03	0.155	6.10	0.21	-0.2
B	0.110	7.18	6.93-7.72	0.053	3.21	0.12	1.3

6.4.5.2.1 Non-Granulated Materials

According to the histograms of the sliding angle frequency for both powders, Figures 6.10a to 6.10h, in most of the cases the type of distribution is not a normal distribution. In some of the cases a kind of bimodal distribution is observed (A 0.030 kg, A 0.090 kg) and in the cases of B 0.070 kg and B 0.110 kg an exponential distribution is obtained. It has proved difficult to effectively compare the shapes of the histograms to determine any difference between the powders. No general trend is observed as to the type of sliding angle distribution is concerned; neither if the distribution at different loads for a powder is considered nor if both powders are compared at a given load. The data are very similar for A and B but there is evidence of different distributions. In general, it can be said that powder A is a less cohesive

material than powder B. In order to compare both powder distributions the variance was calculated for each case and the values obtained are plotted against the load for both "as-received" powders in Figure 6.12. From this Figure it is observed that except for the lower and higher loads, powder A exhibits a lower variance. The variation of the variance within a powder does not show any general trend.

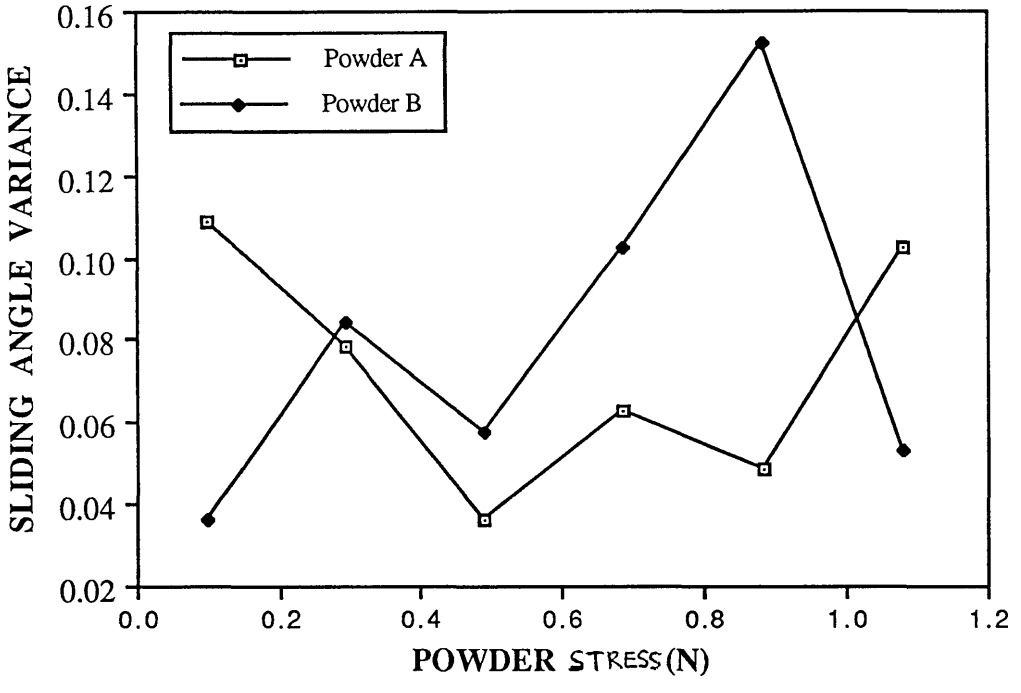

Figure 6.12 Sliding angle variance plotted as a function of the powder load for the two uranium dioxide "as-received" materials.

6.4.5.2.2 Granulated Materials

The sliding angle distributions for the case of the granulated materials are similar and like those of the base powders. It seems that the granular materials from the two sources are even more similar at a given load than the basic powders. There is quite a similar pattern for both types of granules, Figures 6.11a and b. From this it is observed that the base powders are virtually identical, but they are different to the granulated powders; particularly at low pressures, there is some evidence here of cohesion. The granulated powders are similar as well.

6.4.5.2.2.1 Moisture Content

The histograms corresponding to the sliding angle for the wet and dry granules are shown in Figure 6.13. If these results are compared with the data for the same amount of powder (0.050 kg) of non-treated granules and "as-received" powders the following features are apparent. In both cases, for the wet granules, the average sliding angle is higher. This is what one might expect as a stronger adhesion between the powders and between the powder and the wall occurs. The non-treated B granules present a behaviour in between the wet and the dry ones. The non-treated A granules exhibit a much higher value of the sliding angle than for the case of dry and wet granules. Table 6.12 shows the results of this experiment for the three types of granules: dry, non-treated and wet.

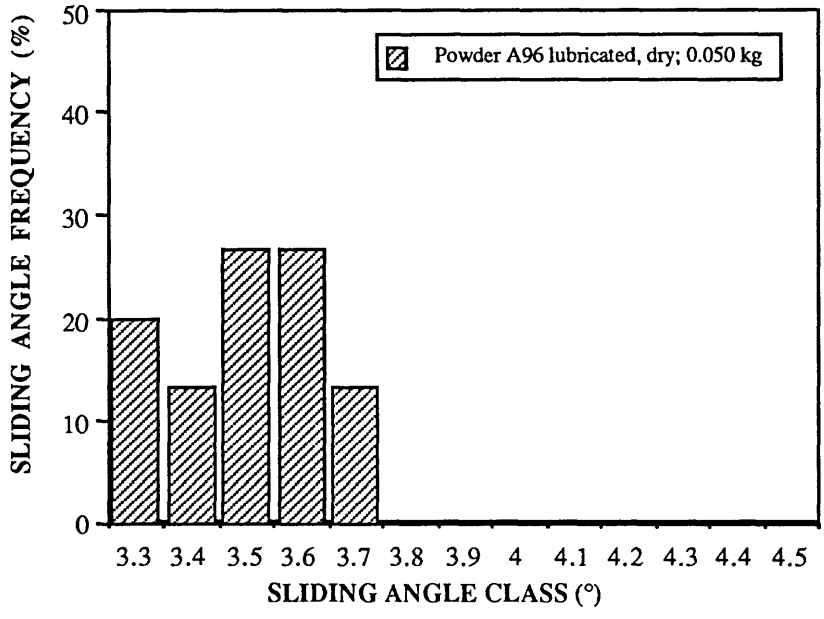

Figure 6.13a Sliding angle frequency distribution for the granulated and lubricated UO_2 powder $A_{96\text{-}L}$, dry at a powder mass of 0.050 kg.

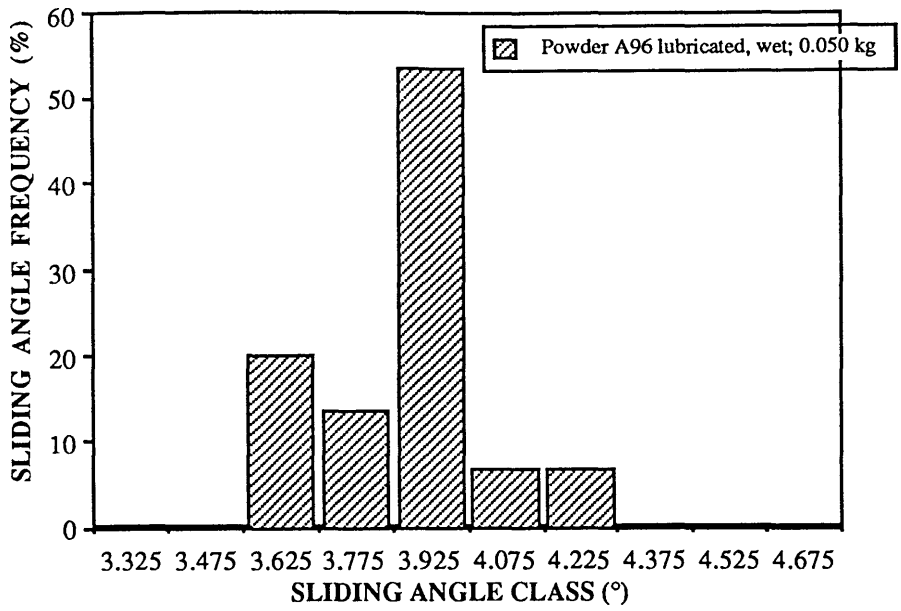

Figure 6.13b Sliding angle frequency distribution for the granulated and lubricated UO_2 powder $A_{96\text{-}L}$, wet at a powder mass of 0.050 kg.

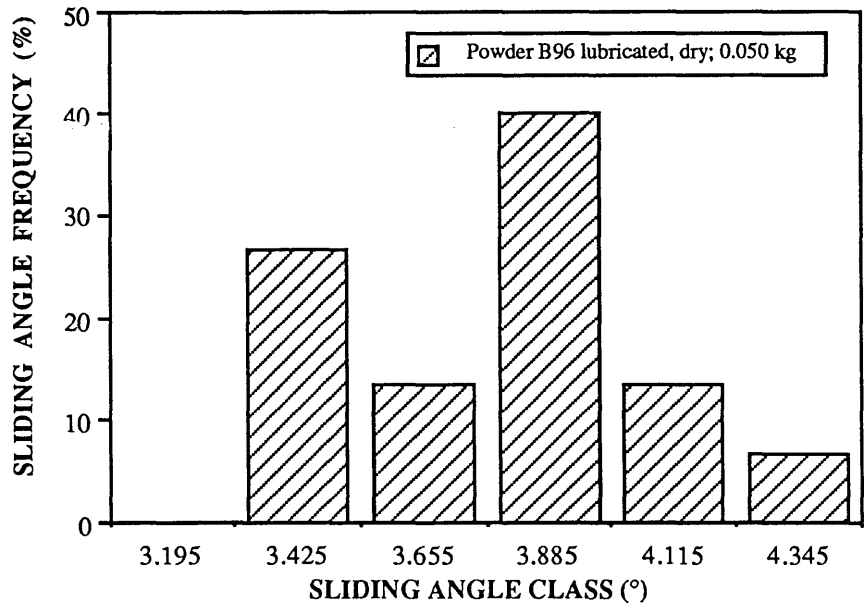

Figure 6.13c Sliding angle frequency distribution for the granulated and lubricated UO_2 powder $B_{96\text{-}L}$, wet at a powder mass of 0.050 kg.

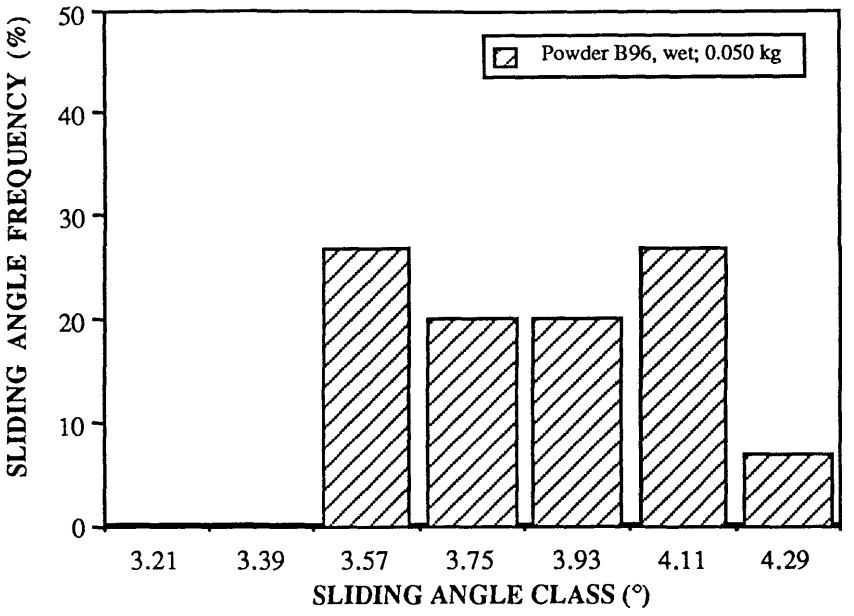

Figure 6.13d Sliding angle frequency distribution for the granulated and lubricated UO_2 powder $B_{96\text{-}L}$, wet at a powder mass of 0.050 kg.

TABLE 6.12 Statistical Parameters for the Granulated Materials at 0.050 kg.

System	Mean Angle (°)	Range (°)	Variance	Coef.Variation	95% Conf Limit ±	Skewness
A_{96} dry	3.50	3.27-3.73	0.018	3.80	0.071	-0.10
A_{96} normal	4.13	3.62-4.67	0.120	8.58	0.190	0.30
A_{96} wet	3.86	3.55-4.28	0.034	4.66	0.096	0.18
B_{96} dry	3.76	3.32-4.45	0.095	8.24	0.160	0.38
B_{96} normal	3.77	3.33-4.30	0.051	5.73	0.120	0.00
B_{96} wet	3.89	3.48-4.37	0.067	6.68	0.140	0.15

It seems that for the case of A_{96} the better transport conditions are obtained for the dry granules. In the case of B_{96} though, the normal condition has a value of the sliding angle and statistical parameters values in between the wet and dry conditions. Considering the wet and dry granules a lower sliding angle does not correspond with the lower statistical values. That is, a low friction does not correspond with a better free flow condition.

6.4.5.2.3 Summary

It may be concluded on the basis of these evaluations that the two "as-received" powders are remarkably similar in their free flow properties. There is no evidence of major differences in free flow for any of the different cases studied. The only differences observed correspond to the state of the powder (granulated or "as-received") not to the type of powder (A or B).

6.5 VALIDITY OF THE ROLLING CYLINDER METHOD

In order to check the suitability of deducing the flow properties from the variation of the sliding angle two test experiments were carried out. First, the inclined plane experiment was done under the same experimental conditions using a free flow model material, coarse sand. Secondly, two standard flowability tests, the Hausner Ratio and the flow rate, were also used to study the flowability of some of the materials. These results are compared with the values of the flow angle and sliding angle variation obtained from the inclined plane experiment introduced in this study.

6.5.1 Sand

Sand was selected as a model of a free flow material. The results for the inclined cylinder experiment for the case of a coarse grain sand at an intermediate powder mass of 0.030 kg are shown in Table 6.13, and graphically in Figure 6.14 which represents the angle frequency distribution histogram. It may be seen from these data that the angle frequency distribution for sand is a normal distribution. The angle range is narrow and

it presents a low variance. These results are those expected from a free flow material.

TABLE 6.13 Descriptive Statistics for Sand Flow Angles for 0.030 kg Powder Mass.

Mean Angle (°)	Range (°)	Variance	Coef. of Variation	95% Confidence Limit ±
2.48	2.23-2.67	0.019	5.56	0.11

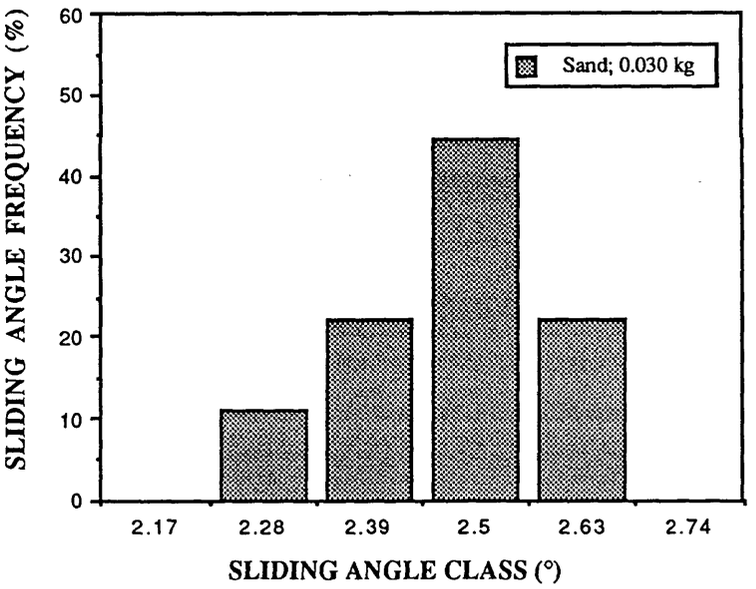

Figure 6.14 Histogram representing the sliding angle frequency for a coarse sand material at a powder mass of 0.030 kg.

6.5.2 Other Means of Determining the Flow of Bulk Powders

6.5.2.1 Flow Rate

The flow of the different ferrite/binder powders was also analysed using a standard test; the flow rate. The time for a known volume of powder to flow down freely through a nozzle of diameter 0.01 m was measured and the corresponding volumetric flow rate was determined. Some powders flowed smoothly while others did not flow at all even upon tapping. Table 6.14 includes the flow rate results for all the ferrite/binder systems. According to these experimental results, powders may be classified by their relative volumetric flow rate. These ferrite powders have been classified by their relative volumetric flow rate into two groups. The ferrite systems IC2, 12, 1, 13, 14, 7, 5, 3, and 0 seem to posses "good" flow properties. The materials IC6, 8, 9, 10, 11, 15, and 16 were classified as possessing "poor" flow properties. If these results are compared with the classification based on the sliding angle or sliding angle variance it may be seen that in general the powders with a low flow rate correspond to the powders with a high flow angle variance, i.e. presenting poor flow properties. But some of the powders with a good flow rate have a high flow angle variance. The "as-received" uranium dioxide powders did not flow at all. There is a general close agreement between both types of classifications in the cases of powders having poor flow properties and for the powders presenting the best flow properties.

6.5.2.2 Hausner Ratio

Chapter 5 reviewed the materials characterisation procedures. One of the parameters studied is the Hausner ratio. This parameter is an indication of the flow properties of bulk powders. The Hausner ratio was determined for all the powders, noting the height of the powder under free fall and after tapping the samples. The results obtained from the determination of the Hausner ratio for the different systems are shown in Table 6.14. The general results were presented in Chapter 5. In this Chapter a summary of the most important findings is presented.

TABLE 6.14 Flow Results from Several Different Experimental Techniques.

System	Average Flow Angle (°)	Variance	Flow Rate (cm^3/sec)	Hausner Ratio
IC0	3.29	0.022	3.4	1.11
IC1	3.08	0.119	4.7	1.14
IC2	3.19	0.167	5.7	1.11
IC3	3.46	0.174	3.5	1.15
IC4	3.45	0.094	----	1.16
IC5	2.93	0.036	3.8	1.19
IC6	2.97	0.031	NIL	1.18
IC7	3.13	0.106	4.0	1.18
IC8	3.41	0.149	NIL	1.24
IC9	3.74	0.264	NIL	1.25
IC10	3.26	0.104	NIL	1.14
IC11	2.91	0.162	NIL	1.12
IC12	2.56	0.005	5.0	1.12
IC13	2.57	0.027	4.3	1.17
IC14	2.52	0.028	4.1	1.38
IC15	2.86	0.056	NIL	1.17
IC16	2.80	0.134	NIL	1.17

For the Hausner ratio measurements no clear distinction can be made among the powders. It may be seen in Table 6.14 that the ratio tapped/aerated density for the different systems is very similar. All the materials are in the same narrow range (1.10-1.18). No clear distinction may be drawn from these experiments and hence the Hausner ratio is not a particularly discriminating tool to determine the flowability of these ferrites. All the powders have a ratio less than 1.20 which indicates that they will behave as aeratable or free-flow powders. Clearly however they have very different flow characteristics. The Hausner ratio does not discriminate between these powders.

6.5.3 Correlation

Table 6.14 shows the results obtained regarding the flow properties of the ferrite materials from three different experimental techniques. Several features are observed. There is a correlation in the case of powders presenting "bad" flow properties between the flow rate and flow angle values. There is a better correlation between the Hausner ratio or flow angle and the variance of the sliding angle than if one considers the angle of slide itself as a measurement of flow.

These results indicate the validity of using the inclined plane experiment to study the flowability of bulk materials.

6.6 CONCLUSIONS

In this Chapter the flow properties of several ceramic systems have been considered. From this analysis several conclusions may be drawn:

- The bulk powder flow studies have been shown to be able to distinguish between free-flowing and poor flowing powders in the case of several ferrite/binder systems and some uranium dioxide materials.

- The different ferrite/binder systems may be classified according to their flow angle variance and flow angle value. A narrow distribution of the sliding angle values indicates a free-flowing powder. Gohsenol on this basis is the binder that confers the best free-flowing properties to the ferrite material. On the other hand the powder IC13, which contains Primal as a binder, is the system with the worst flowing characteristics.

- The ferrite/binder systems were ranked using flow properties as criteria. The "worst" and the "best" binder systems were identified.

- The flow angle value for the ferrite systems decreases as PEG is substituted for PVA. The systems PVA/PEG behaves in a way such that increasing the amount of PEG

reduces the friction force.

- There is no clear evidence of different flow characteristics for the two types of uranium dioxide powders studied, A and B. There are significant differences in the flow properties between the "as-received" and granulated materials.

- The Hausner ratio does not discriminate between the different powders so it is not an useful tool to determine the "flowability" of these ferrites.

- There is a correlation between the flow properties as measured by the inclined plane experiment and the flow rate.

CHAPTER 7

MODEL FRICTION DATA AND ANALYSIS

7.1 INTRODUCTION

This study has investigated the interface friction and the deformation characteristics of the organic species and of the agglomerated ceramic powders in free flow and at high contact stresses. An attempt to model these effects by examining the properties of the individual particles and their interactions with their neighbours and confining walls is presented in this Chapter. The main factors considered are the type of binder system coating the ceramic particles and the magnitude of the applied normal load or contact pressure developed at the interface. Several model experiments have been used to study the particle-wall friction effects under a wide range of applied normal loads. In this Chapter experimental data for two model experiments, which simulate the powder-wall conditions existing in free flow and during green ejection, are described and analysed. One simulation involves the measurement of the wall friction of loose packed powder beds and the other the sliding friction of green compacts. These data have been interpreted using the adhesion model of friction. In the configurations covered in this work (smooth and rigid walls) it is reasonable to assume that adhesive forces account for all the frictional work and the actual work done arises from the shearing the junctions formed at the discrete contact points. The data corresponding to the friction forces developed during pressing and compact ejection are considered in Chapter 8.

7.2 EXPERIMENTAL RESULTS

7.2.1 Friction Effects During Unconstrained Flow

The model experiment, the rolling cylinder on an inclined plane, used to study the situation at the bulk powder-wall interface during the unconstrained flow of powders has been described in detail in Chapter 5 (see Section 5.6.1 and Figure 5.9). The experiment senses the angle at which a cylinder filled with the material begins to roll down an inclined plane. It is possible to correlate this angle of inclination of the plane with the static interfacial sliding friction force generated between the solid particles and the cylinder wall. Generally, it was observed that once motion commences, the cylinder rapidly accelerates down the plane since the interfacial frictional work is a decreasing function of the angular velocity of the rolling tube. The bed dilates and the friction decreases once flow commences. It is possible to relate the critical frictional force, F_f, required to initiate motion, to the forces acting on the cylinder and its contents and then to compute the frictional force between the powder bed and cylinder wall. Hence:

$$F_f = M_t \, g \sin \omega' \tag{7.1}$$

where M_t is the total mass of the cylinder and contents, g is the gravitational acceleration and ω' is the angle of inclination at which the cylinder begins to roll down. The correct angle to use should be the angle the centre of gravity of the bed makes with the horizontal, ω. However, provided the distance DO (see Figure 5.9) is large (>1m), which was always the case here, the angle ω' is independent of DO. Therefore, for practical purposes it is assumed that $\omega' = \omega$. The resistive force arises from two sources, the frictional force between the cylinder and the plane, which remains constant as the load is increased, and the frictional forces resisting motion within the cylinder. The former was determined by obtaining the angle ω'' required to induce motion in the empty cylinder of the same net mass. The corresponding frictional force could then be calculated and subtracted from equation 7.1 yielding:

$$F = M_t\, g \sin \omega - M_c\, g \sin \omega'' \qquad (7.2)$$

where M_c is the mass of the empty cylinder. F is then a measure of the net static frictional force that exists between the cylinder wall and the particles in contact with it.

The apparent area of contact between the powder and the cylinder wall was calculated from the measurement of the powder bed width or height in the cylinder at the different powder loads. The total contact area, A_{app}, is calculated from equation 7.3;

$$A_{app} = R\phi L \qquad (7.3)$$

where R is the cylinder radius, ϕ is the angle subtended by the bed, and L is the cylinder length. The angle ϕ is determined from the measurement of the powder bed width, w, from equation 7.4.

$$w = 2\, R \sin\left(\frac{\phi}{2}\right) \qquad (7.4)$$

From the measurement of the angle at which the cylinder begins to roll down the plane the mean interface friction of several powders has been determined and its variation with the bed load or the apparent contact pressure has been examined. The results for some of the ferrite, alumina, and zirconia-binder systems and for the uranium dioxide "as-received" and granulated materials are presented in the following sections.

7.2.1.1 Ferrite/Binder Systems

The inclined plane experimental results are shown in Table 7.1 for each of the ferrite-binder systems studied. The data presented were obtained for a 0.075 m diameter cylinder laden with 0.030 kg of powder. The friction force was calculated using equation 7.2.

TABLE 7.1 Interfacial Friction Results for Ferrite-Binder Systems at a Constant Load of 0.29 N: Inclined Plane Experiment.

MATERIAL	MEAN FLOW ANGLE* (°)	FRICTIONAL FORCE (N)
IC0	3.29	0.156
IC1	3.08	0.140
IC2	3.19	0.149
IC3	3.46	0.169
IC4	3.45	0.168
IC5	2.93	0.129
IC6	3.10	0.142
IC7	3.13	0.144
IC8	3.41	0.165
IC9	3.74	0.189
IC10	3.26	0.154
IC11	2.91	0.128
IC12	2.56	0.102
IC13	2.57	0.102
IC14	2.52	0.099
IC15	2.86	0.124
IC16	2.80	0.120

*mean value after ten to twelve determinations

In a second group of experiments the variation in the frictional force between the ferrite and the cylinder wall was evaluated as a function of the powder load. For these experiments several different binder systems were selected; ferrite IC0 (factory binder), IC1 (PVA 72000), IC2 (PVA 14000), IC3 (75% PVA 14000/25% PEG 400), IC5 (50% PVA 72000/50% PEG 400), IC8 (50% PVA 72000/50% PEG 4000), IC9 (75% PVA 72000/25% PEG 4000) and IC12 (Gohsenol). The results from some of these experiments and the computed frictional force for a given load and ferrite/binder system are shown in Table 7.2. The values of the apparent area of contact are also included.

TABLE 7.2 Results from the Inclined Plane Experiment for Several Ferrite-Binder Systems as a Function of the Applied Normal Load.

Binder	Load (N)	Area of Contact m^2	Flow Angle* (°)	Friction Force (N)
Factory	0.098	0.0038	1.97	0.051
	0.196	0.0046	2.27	0.076
	0.294	0.0053	3.27	0.155
	0.392	0.0056	3.41	0.170
	0.490	0.0059	3.67	0.196
	0.687	0.0071	4.69	0.292
	1.226	0.0094	6.50	0.500
	1.471	0.0096	7.28	0.600
PVA 14000	0.098	0.0038	2.52	0.090
	0.294	0.0053	3.18	0.148
	0.490	0.0066	4.07	0.227
	0.589	0.0071	4.39	0.260
	0.687	0.0076	4.72	0.294
	1.226	0.0094	5.62	0.420
	1.471	0.0102	7.25	0.597
75% PVA 1400	0.098	----	2.18	0.066
25% PEG 400	0.294	----	3.44	0.167
	0.490	----	4.19	0.237
	0.687	----	5.36	0.346
75% PVA 72000	0.294	0.0053	3.63	0.181
25% PEG 4000	0.981	0.0085	5.36	0.373
	1.226	0.0094	6.69	0.517
	1.471	0.0098	8.77	0.740

* average value after ten to twelve determinations

7.2.1.2 Uranium Dioxide

The inclined plane experiment was used to study the frictional behaviour under unconstrained flow of the different uranium dioxide materials; "as-received" and granulated A and B powders. From the mean sliding angle value the frictional force as a function of the applied load has been calculated according to equation 7.2. The results are presented in Table 7.3 for both the "as-received" A and B materials and for the granulated powders A_{96} and B_{96}.

7.2.1.3 Alumina and Zirconia

The wall friction in loose powder beds of several dry alumina and zirconia agglomerated powders, 200-300 μm sieve fraction, containing PVA 14000 or PEG 400 binders was examined. Also, the original unagglomerated alumina and zirconia powders were tested in the same way. In these cases a glass cylinder 0.140 m in length and 0.050 m in diameter was used. Table 7.4 presents some of the experimental results obtained for these powders for a range of powder loads or fill levels.

7.2.2 Interface Friction of Green Compacts

7.2.2.1 Sliding Friction of Hemispherical Compacts

Hemispherical shaped compacts were prepared as a means of modelling compact-wall tractions. The lubricated uranium dioxide granules were compacted in a 0.0125 m diameter die at 125 MPa into a hemispherical shape. Alumina and zirconia compacts were prepared from the agglomerates at a pressure of 200 MPa. These compact specimens were slid under a range of loads (0.0490 to 0.981 N), against smooth glass counterfaces. A simple friction force measuring device was used to study the friction of these hemispherical compacts as a function of the applied normal load for a fixed imposed sliding velocity of ca. 0.5×10^{-3} m/s. The frictional force was measured as a function of the applied normal load. These results are presented in Table 7.5 for the uranium dioxide compacts A and B.

TABLE 7.3 Results from the Inclined Plane Experiment for the Uranium Dioxide Materials as a Function of the Applied Normal Load.

Powder Load (N)	Area of Contact /10^{-4} m^2				Average Flow Angle* (°)				Friction Force (N)			
	A	B	A_{96}	B_{96}	A	B	A_{96}	B_{96}	A	B	A_{96}	B_{96}
0.098	39	31	20	21	1.77	1.57	-----	-----	0.037	0.022	-----	-----
0.294	52	57	39	37	2.68	2.81	2.59	2.52	0.111	0.120	0.104	0.099
0.490	66	68	45	45	3.62	3.78	4.08	3.84	0.193	0.205	0.228	0.210
0.687	82	83	47	50	4.72	5.16	5.18	4.97	0.294	0.330	0.332	0.315
0.883	89	85	59	54	5.88	6.45	6.20	6.08	0.409	0.457	0.436	0.426
1.079	99	94	60	60	7.15	7.18	6.98	7.40	0.540	0.542	0.525	0.561
1.275	101	99	62	64	8.60	8.50	7.03	7.33	0.696	0.687	0.553	0.581
1.471	111	103	66	66	9.09	9.13	8.75	8.69	0.770	0.774	0.738	0.733
1.570	112	108	74	71	9.47	9.57	9.13	8.88	0.822	0.832	0.790	0.766

* average value after fifteen determinations

TABLE 7.4 Results from the Inclined Plane Experiment for Several Alumina, and Zirconia-Binder Systems as a Function of the Applied Normal Load or Powder Fill Level.

Material	Load (N)	Height/Diameter Ratio	Frictional Force (N)
Alumina			
	0.07	0.037	0.03
	0.17	0.088	0.06
	0.36	0.192	0.15
	0.46	0.220	0.18
	0.68	0.238	0.24
Alumina/PVA 14000			
	0.07	0.062	0.05
	0.14	0.100	0.07
	0.23	0.140	0.11
	0.33	0.190	0.15
Zirconia			
	0.29	0.050	0.14
	0.59	0.090	0.32
	0.88	0.130	0.45
	1.18	0.220	0.69

TABLE 7.5 Results from the Sliding of Uranium Dioxide Hemispherical Compacts Against a Glass Counterface.

APPLIED NORMAL LOAD (N)	FRICTION FORCE (N)	
	A	B
0.049	0.022	0.019
0.098	0.035	0.034
0.196	0.084	0.068
0.491	0.190	0.170
0.981	0.370	0.370

7.2.2.2 Sliding Friction of a Rigid Body Against a Compact Surface

In a similar experimental configuration compact-wall tractions were modelled by sliding a polished steel sphere, 0.0635 m diameter, at a constant sliding velocity of 2.0×10^{-4} m/s over the top surface of cylindrical ferrite compacts. These compacts were pressed to 130 MPa in a 0.0163 m diameter cylindrical die. The surface friction force of the compacts was measured under a range of applied normal loads between 0.490 and 9.81 N. These results are presented in Table 7.6 for the case of the system Ferrite/75%PVA 72000-25%PEG 4000.

TABLE 7.6 Results from the Sliding of a Steel Sphere Against a Ferrite/75%PVA-25%PEG Compact Surface.

APPLIED NORMAL LOAD (N)	FRICTION FORCE (N)
0.49	0.09
0.98	0.21
1.96	0.42
3.92	0.86
5.89	1.25
9.81	1.94

7.3 ANALYSIS OF RESULTS

7.3.1 Friction Effects in Loose Packed Powder Beds

Two types of data were generated from the measurement of the force required to initiate flow in the rotating cylinder. Wall friction data and data which provide an indication of the magnitude of the internal friction. The wall friction data were evaluated from the mean force values and the results were modelled using an established friction model. The internal friction may be estimated from the variation of the force required to initiate motion under a given set of experimental conditions. This variation was interpreted as a measure of the heterogeneities of the internal stress distribution and hence the magnitude of the internal particle-particle friction. Higher internal frictions were presumed to provide a greater range of angles required to initiate flow.

7.3.1.1 Powder Bed-Wall Friction

At the relatively low fill levels adopted in the rolling cylinder experiment the powder bed did not cascade but slid at the wall. There was no apparent interparticle

motion within the powder mass and all of the restraining force seemed to arise from the sliding work dissipated at the particle-wall interface.

7.3.1.1.1 Load Dependence of the Friction Force

The friction force, F, calculated from the value of the angle of inclination at which the cylinder begins to roll down the plane according to equation 7.2, was determined as a function of the mean applied normal load. Typical data for the variation of the mean friction force, F, with the applied normal load, W, of several ferrite particles are shown in Figure 7.1. It may be seen that there is a logarithmic relationship between the friction force and the normal load and that all the powders do not fall on the same curve. The line, within experimental error, goes through the origin. This indicates that the autoadhesion component of the friction is negligible. The powders are thus non-cohesive at the wall in the range of detection available in these experiments. There is also no transition zone, only sliding is observed in the load range used as the load was not high enough to observe the transition to the cascading zone. The data corresponding to the uranium dioxide powders are plotted in the same way in Figure 7.2. From this representation it is observed that the frictional force is very similar for the two powders A and B. The resulting frictional force for the granules is similar to that of the "as-received" powders for any given load. The main difference observed between the "as-received" and the granulated materials is the magnitude of the apparent area of contact of the bed. The effect of the area of contact on the frictional characteristics of these powders is dealt with in Section 7.3.1.1.2.

In the cases studied it has been appropriate to assume that adhesion accounts for all the frictional work and accordingly apply the adhesion model of friction to interpret the experimental results. The data, as shown in Figures 7.1 and 7.2, are well described by;

$$F = k W^n \qquad (7.5)$$

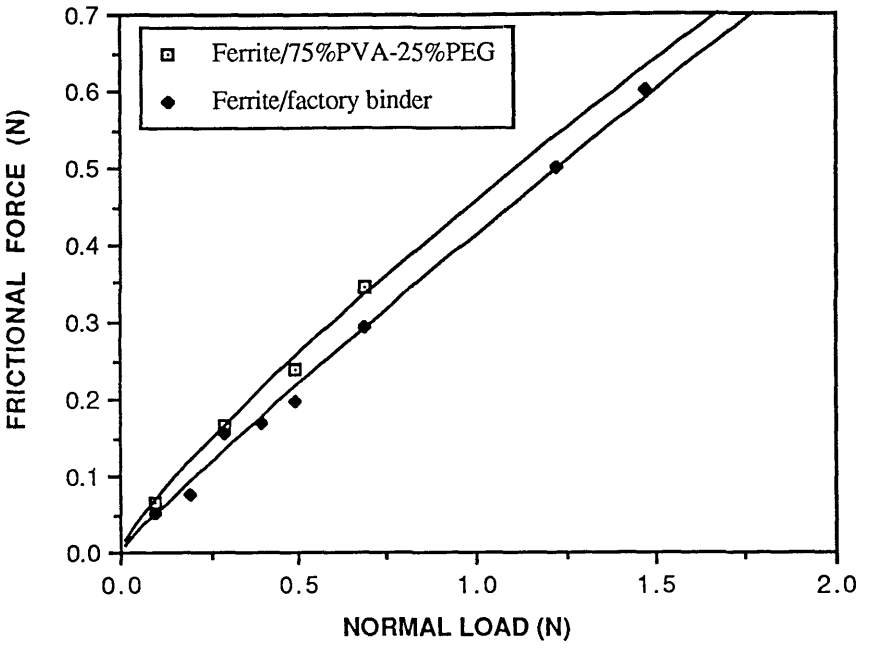

Figure 7.1a Variation of the wall frictional force during unconstrained flow with the applied normal load for two ferrite powders; IC3 and IC0. Data from the sliding of the powder beds in the rolling cylinder.

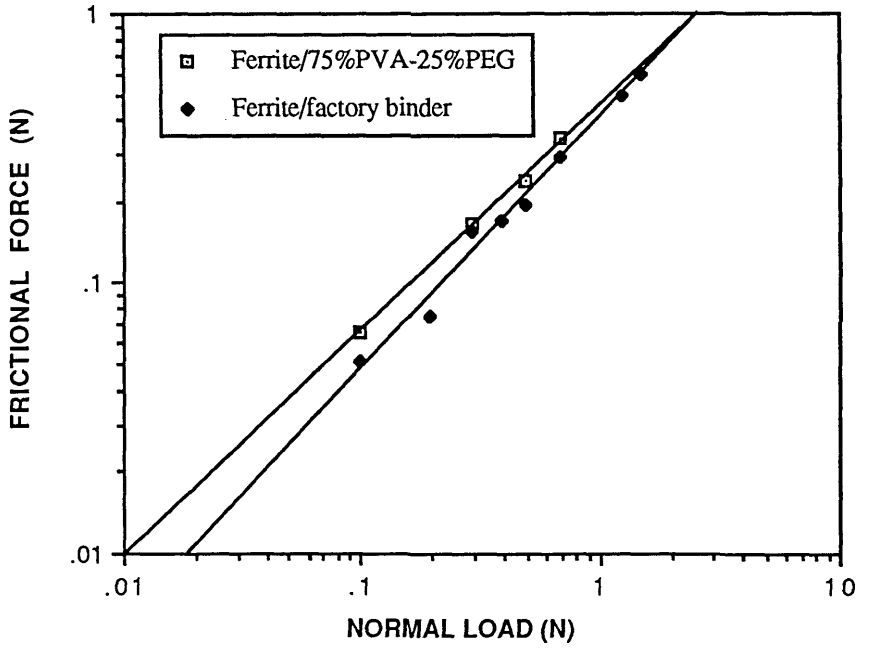

Figure 7.1b Logarithmic relationship between the wall frictional force and the applied normal load for the systems IC3 and IC0.

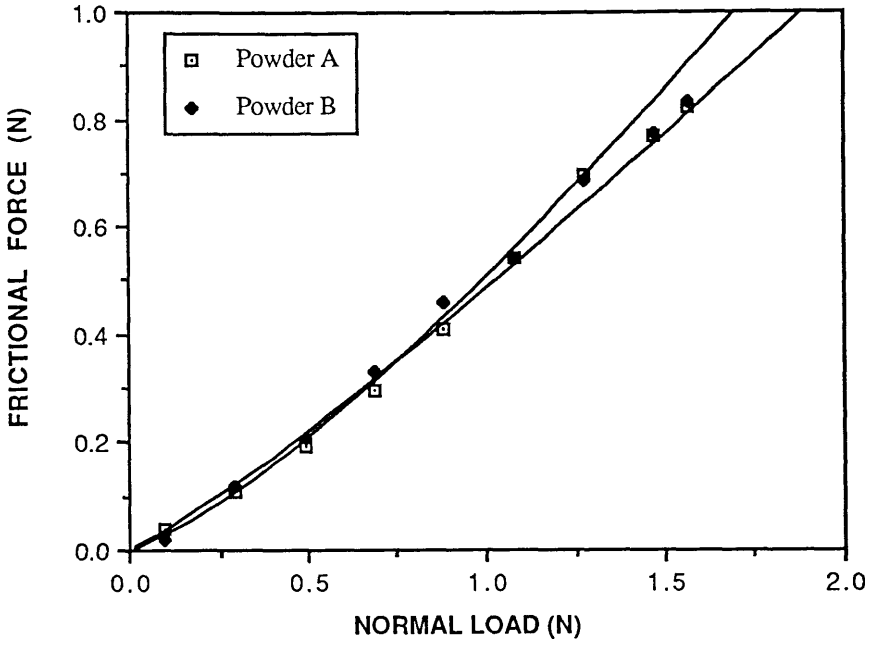

Figure 7.2a Variation of the wall frictional force during unconstrained flow as a function of the applied normal load for the two "as-received" UO_2 powders sliding in the rolling cylinder.

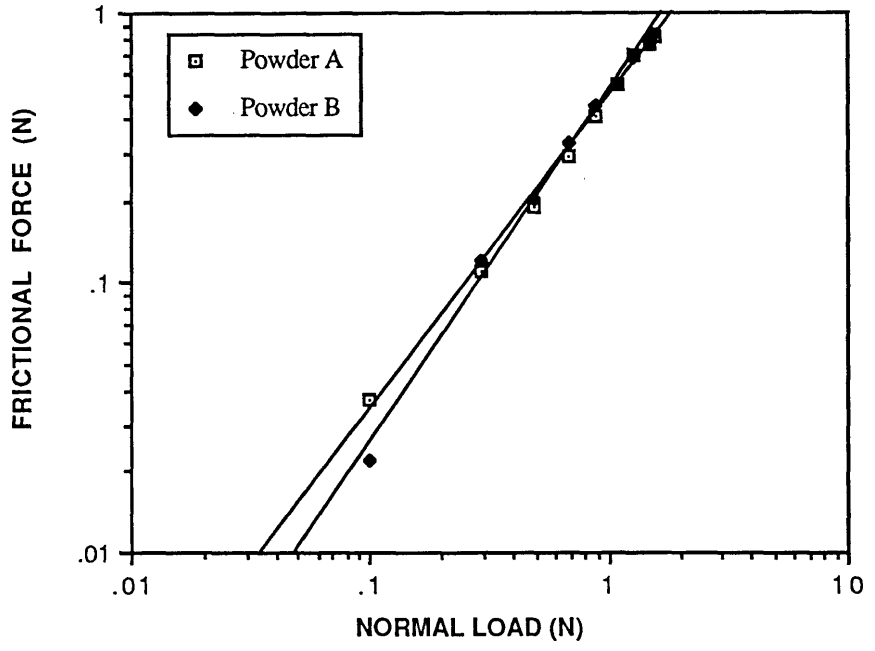

Figure 7.2b Logarithmic relationship between the frictional force and the applied normal load for the two "as-received" uranium dioxide powders.

where F is the computed wall friction force, W is the powder load, k is the friction factor and n is the load index. The significance of these two constants will be discussed later. The experimental values of k and n obtained from the logarithmic plots of the friction force against load are tabulated in Table 7.7.

7.3.1.1.2 Effect of the Apparent Area of Contact

The computed wall friction force, F, is an average value describing the character of the whole contact. It is assumed that the applied load is evenly distributed between the discrete particle contacts. As the load is increased, the pressure profile across the powder bed changes and alters the load per particle contact. The friction force and the total powder load have been normalised by the directly measured geometric contact area of the bed. The resulting computed average apparent interface shear strength, τ_a, is plotted as a function of the average apparent contact pressure, P_a, for some ferrite systems in Figure 7.3. Figures 7.4a and b show the variation of the mean interface apparent shear strength as a function of the average apparent contact pressure for the "as-received" and agglomerated uranium dioxide powders respectively. In general, these typical data for the apparent pressure dependence of the apparent shear strength are well described by;

$$\tau_a = \tau_{oa} + \alpha_a P_a \qquad (7.6)$$

where τ_{oa} and α_a are constants; τ_{oa} is the intrinsic apparent shear strength and α_a is the apparent pressure coefficient. The values of τ_{oa} and α_a obtained for several ceramic/binder systems from the type of plots presented in Figures 7.3 and 7.4, are also shown in Table 7.7.

From these data it is observed that the experimentally obtained values for the parameter α_a, the pressure coefficient, seem to be a function of the binder system. It presents the lowest values, in the range 0.25-0.29, for the alumina, zirconia and ferrite

TABLE 7.7 Interface Friction Parameters for Bulk Powders During Unconstrained Flow (Rolling Cylinder).

Ceramic	Binder	Experimental Values				Predicted
		k	n	τ_{oa} (Pa)	α_a	n
Ferrite	PVA 14000	0.39	0.71	14.8	0.27	0.79
Ferrite	PVA 72000	0.52	0.80	17.0	0.25	-----
Ferrite	Factory binder	0.41	0.93	3.3	0.38	-----
Ferrite	Gohsenol	0.39	0.84	4.6	0.39	-----
Ferrite	75%PVA 14000					
	25%PEG 400	0.45	0.83	-----	-----	-----
Ferrite	75%PVA 72000					
	25%PEG 4000	0.46	0.80	8.5	0.39	-----
Ferrite	50%PVA 72000					
	50%PEG 400	0.48	0.85	4.7	0.37	-----
Ferrite	50%PVA 72000					
	50%PEG 4000	0.68	0.91	----	-----	-----
Alumina		0.44	1.00	2.9	0.32	-----
Alumina	PVA 14000	0.42	0.80	1.7	0.25	0.84
Alumina	PEG 400	0.38	0.85	4.7	0.27	0.75
Zirconia		0.52	0.99	3.7	0.44	-----
Zirconia	PVA 14000	----	0.88	1.3	0.29	0.89
Zirconia	PEG 400	----	0.90	0.3	0.28	0.91
PVA 14000	----------	0.19	0.76	2.7	0.32	0.78
				τ'_{oa} (Pa)	α'_a	
UO_2 A	no binder	0.49	1.14	7.39	0.017	-----
UO_2 B	no binder	0.50	1.29	6.75	0.018	-----
UO_2 A_{96}	no binder	0.47	1.15	17.81	0.0085	-----
UO_2 B_{96}	no binder	0.47	1.20	16.12	0.0090	-----

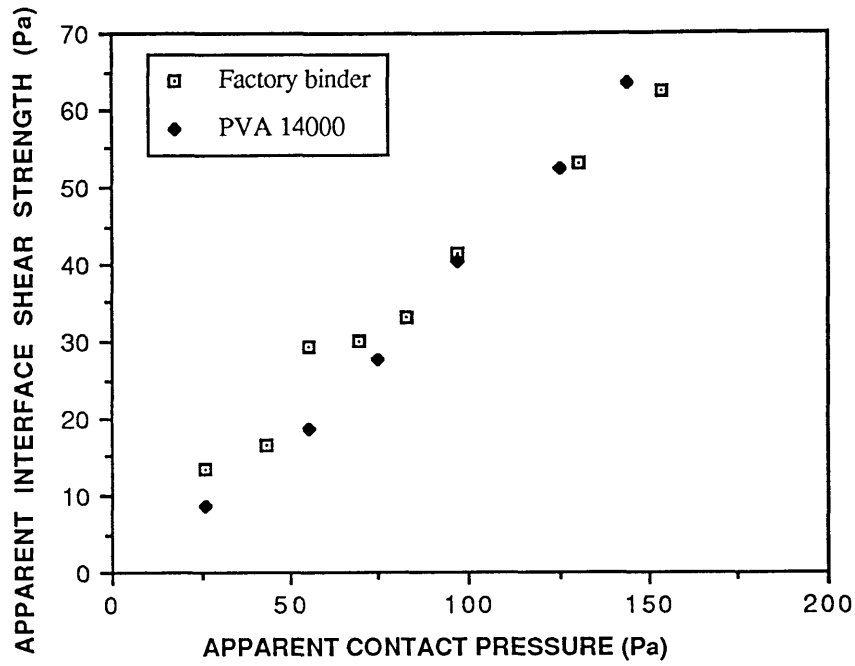

Figure 7.3 Variation of the apparent shear strength with the apparent contact pressure for two different ferrite systems. Rolling cylinder experiment.

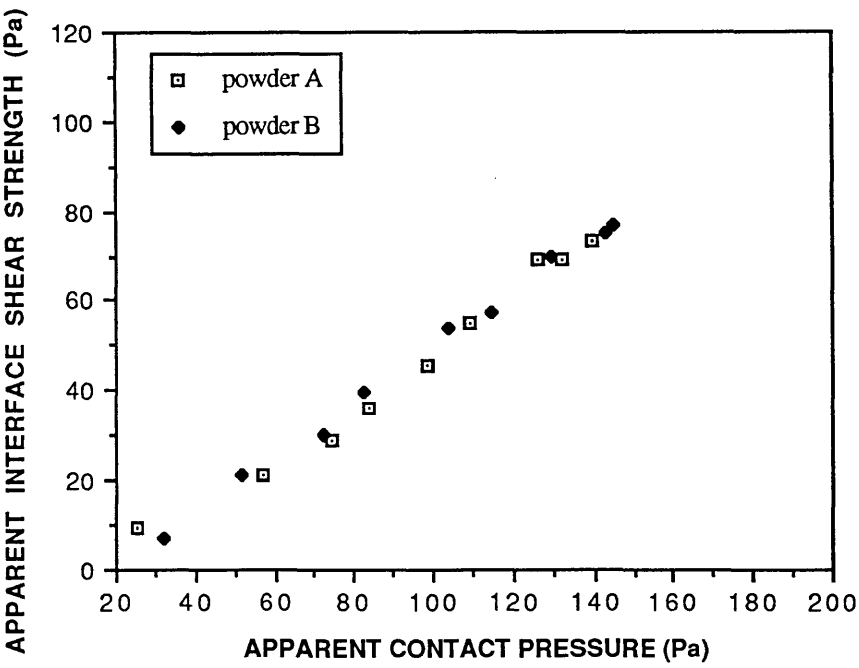

Figure 7.4a Variation of the apparent shear strength with the apparent contact pressure for two "as-received" UO_2 materials. Data from the rolling cylinder experiment.

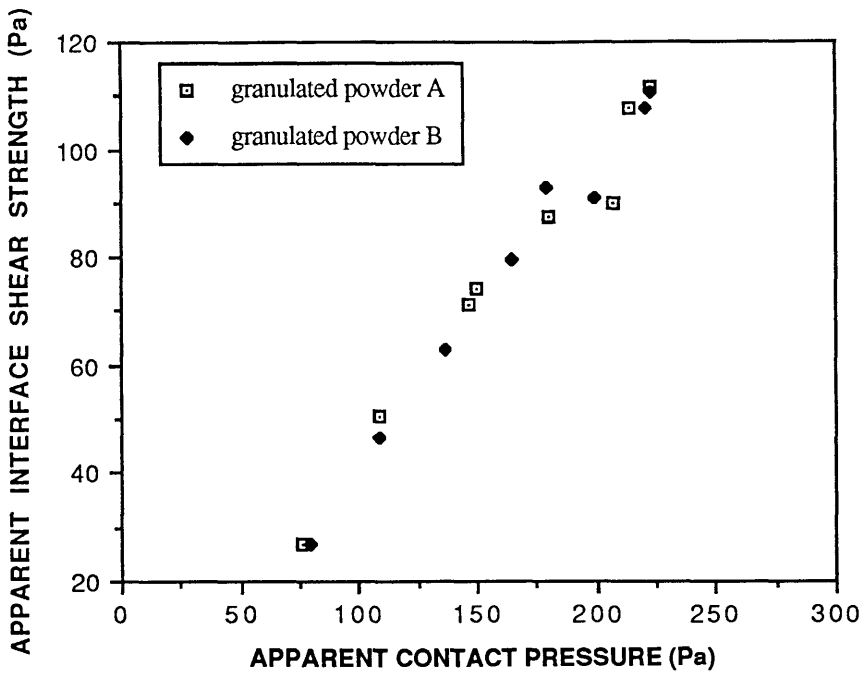

Figure 7.4b Variation of the apparent shear strength with the apparent contact pressure for two granulated UO_2 materials. Data from the rolling cylinder experiment.

granules which contain PVA or PEG as a binder. This value increases to 0.37-0.38 when the binder consists of a mixture PVA/PEG. The systems which contain no binder, unagglomerated alumina and zirconia, present a higher value of α_a than the corresponding agglomerated systems containing a binder. Greater values of α_a indicate more damage during shearing. Under these conditions, and for the systems studied, it seems that the presence of a binder coating the particles and/or the agglomeration of the powders decreases the value of the pressure coefficient; i.e. the magnitude of the work done in the shearing process. The experimental values for τ_{oa} are also seen to be a function of the binder system but in this case the trend is not so clear.

In the case of the uranium dioxide powders the application of equation 7.6 to the shear strength data reveals negative values of τ_{oa} which is physically unacceptable. A more general empirical expression which adequately describes the shear strength-pressure functionality for the case of the uranium dioxide materials is the equation described by Briscoe and Smith, 1983;

$$\tau_a = \tau'_{oa} \exp(\alpha' P_a) \tag{7.7}$$

where τ'_{oa} and α' are constants for a given temperature and strain rate. The experimental data for the uranium dioxide were fitted to this more general exponential relationship. The corresponding values for the parameters τ'_{oa} and α' are included in Table 7.7. This type of pressure dependence of the shear strength has been reported in the literature for the case of some polymers like polystyrene and polycarbonate (Briscoe and Smith, 1983).

7.3.1.1.3 Modelling of the Interface Friction Data

A model will now be developed to interpret these wall friction data. In the interface configuration described here, it is reasonable to assume that adhesion accounts for all of the frictional work which arises from the shearing of junctions formed at the discrete contact points. The adhesion model of friction which was presented in Chapter 3, has been used in conjunction with a simple geometric agglomerate packing to describe the data. Applying this model to the configuration in the rotating cylinder experiment, it may be shown that the friction force is given by (Briscoe *et al.*, 1985);

$$F = \frac{\pi}{4}\tau_o \left(4D\right)^{2/3} \left(\frac{12 R L^2}{\rho g}\right)^{1/9} W^{7/9} + \alpha W \tag{7.8}$$

where R and L are the radius and length of the cylinder respectively and ρ is the specific density of the particles. The constant D is given by;

$$D = \frac{3}{4}\left(\frac{1-\upsilon_1^2}{E_1} + \frac{1-\upsilon_2^2}{E_2}\right) \qquad (7.9)$$

where υ_1, υ_2 and E_1, E_2 are the Poisson's ratio and the modulus of elasticity of the two contact bodies. Equation 7.8 has the general form

$$F = c\,W^{7/9} + \alpha W \qquad (7.10)$$

It has been shown (Adams *et al.*, 1987a) that the value of the load index n in equation 7.5 is given explicitly, to a good approximation, by:

$$n = \left(\frac{7 + 9\,a\,W'^{2/9}}{9 + 9\,a\,W'^{2/9}}\right) \qquad (7.11)$$

where W' is the logarithmic mean of the load range used and $a = \alpha/c$. The values of n were computed from the best available estimates of τ_o, α, υ, and E which are summarised in Table 7.8. The values for the mechanical properties of the different systems are taken from the literature (Parker, 1967 and Briscoe and Evans, 1988). Reasonably accurate values for the interfacial rheological parameters of the organic binders were obtained from previous studies (e.g. Amuzu *et al.*, 1976; and Briscoe and Smith, 1980). In these interface shear strength studies the values of τ_o and α for several organic films were obtained from model single contact experiments. A thin film is sheared between smooth glass substrates; the experimental configuration involves the sliding of a glass spherical indentor of radius r' over a thin film deposited on a hard, smooth glass substrate. Under these conditions the real area of contact A_r, is obtained as a function of the applied normal load W, assuming that the surfaces deform elastically, from the Hertzian equation (Briscoe and Smith, 1980)

$$A_r = \pi\,(D\,W\,r')^{2/3} \qquad (7.12)$$

TABLE 7.8 Bulk Mechanical Properties and Interfacial Rheological Properties of Several Systems.

Material	Modulus of Elasticity (GPa)	Poisson's Ratio	τ_o (MPa)	α	Reference
Alumina	300	0.30	----	----	a
Zirconia	205	0.30	----	----	a
Borosilicate glass	61	0.22	----	----	b
Uranium Dioxide	186	0.30	----	----	b
Ferrite	8	0.30	----	----	a
PVA	0.004	0.10	6.0	0.07	a, c
PEG	---	---	7.0	0.37	c
Stearic Acid	---	---	1.5	0.07	d
Calcium Stearate	---	---	1.0	0.08	d

a: Briscoe and Evans, 1988; b:Parker, 1967; c: Fernando, 1986; d: Briscoe and Smith, 1980

The predicted values of n are next compared with the experimentally obtained values. Table 7.7 shows the values of the friction coefficient k, and the load index n together with the predicted values of the load index. The measured values of the index are close to the predicted values which suggests that these systems may be modelled based on the adhesion model of friction. The adhesion model of friction predicts for particle assemblies in the rotating cylinder configuration that the load index may vary between 7/9 and unity. For the polymeric agglomerated systems the values of n are less than unity and close to 0.8 (n ranges between 0.8 and 0.9) which indicates that these systems may be modelled based on elastic deformation of point contact, smooth spheres. This is reasonable as at these low normal applied loads the point contact stresses are low and an elastic deformation of the agglomerates is most probable. Also, it is observed that the values of k are a function of the binder system. The data show a single asperity elastic response with film shear and that it is the interfacial rheology of

the organic binder coating the granules which primarily controls the wall friction.

In the case of the base particles the experimental values of n for the unagglomerated alumina and zirconia and for the uranium dioxide powders are approximately equal to unity. These values are consistent with a multiple asperity elastic contact at the interface produced by rough particles.

In summary, the smooth agglomerates; i.e. those granules coated with a binder produce load indices, n, of ca. 0.85 (single asperity elastic contact) whilst the rough base particles yield an index of near unity (multiple asperity elastic contact).

7.3.1.2 Internal Friction

The variation of the frictional force with the load, Figures 7.1 and 7.2, is similar to the one observed at low applied normal loads by Briscoe *et al.*, 1983. It is expected that the frictional force increases with the load in an exponential way until a certain load value is reached when the frictional force decreases with the increase of the load. This is explained in terms of the change in the friction mode that is governing the system; there is a change from a particle-wall to a particle-particle friction as the load is increased. Experimentally this would be observed by a change in the mode of motion of the particles inside the cylinder from sliding to cascading which in our case is not observed. In this study, even at the highest applied load, sliding is the only mode of motion observed; in neither case did cascading occur. Therefore, the internal friction could not be determined from the magnitude of the friction force at high loads. The internal friction was estimated from the variation of the mean force required to initiate motion of the cylinder. This variation was interpreted as a measure of the heterogeneities of the internal stress distribution in the powder bed and hence the magnitude of the internal particle-particle friction. The data for the flow angles and the corresponding angle variance reflecting the variation in the sliding force were discussed in Chapter 6 in relation to the flow properties of the bulk powders. That analysis may be extended to include the interparticle friction as the bulk flow properties may be correlated with the particle-particle friction forces.

7.3.2 Interface Sliding Friction of Compacts

The data discussed in the latter Section relates to the interface frictional characteristics of powders at low stresses, during unconstrained flow. In order to analyse the friction characteristics of these ceramic/binder systems at higher loads the sliding friction of compacts under two slightly different geometric conditions has been studied. The data generated from these two model experiments; the sliding of hemispherical compacts over a substrate and the sliding of a sphere over the compact surface, are analysed in the following sections.

7.3.2.1 Interface Sliding Friction of Hemispherical Compacts

Hemispherically shaped compacts were prepared as a means of modelling compact-wall tractions. The frictional force generated during the sliding of hemispherical compacts over a smooth, glass surface was recorded as a function of the applied normal load. The load dependence of the friction force for the two hemispherical compacts of uranium dioxide agglomerated and lubricated powders is shown in Figure 7.5. The data are well described by equation 7.5. The values of the load index, n, and the parameter k were computed for several ceramic/binder systems and for some polymeric samples. These values are obtained from the slope and intercept respectively of the logarithmic curves of the frictional force as a function of the applied normal load (Figure 7.5). These values are presented in Table 7.9.

From the data presented in Table 7.9 it may be observed that the experimental values for the interfacial friction parameter k are dependent on the type of binder used. In all the cases studied PEG presents a higher value of the friction parameter k than PVA, and an intermediate value of k is obtained when the coating is a mixture PVA/PEG. No differences are observed between both the uranium dioxide powders. Two different trends are distinguished regarding the value of the load index n. Some systems; the polymers and the uranium dioxide materials, present a value of the load index close to unity. The alumina and zirconia systems however, present values of n which are less than unity. These two cases are analysed separately in the following

sections.

The friction data corresponding to the sliding friction of green compacts presented in Table 7.9 will be compared with the friction data obtained during the unconstrained flow of the powders presented in Table 7.7 (see Section 7.3.3).

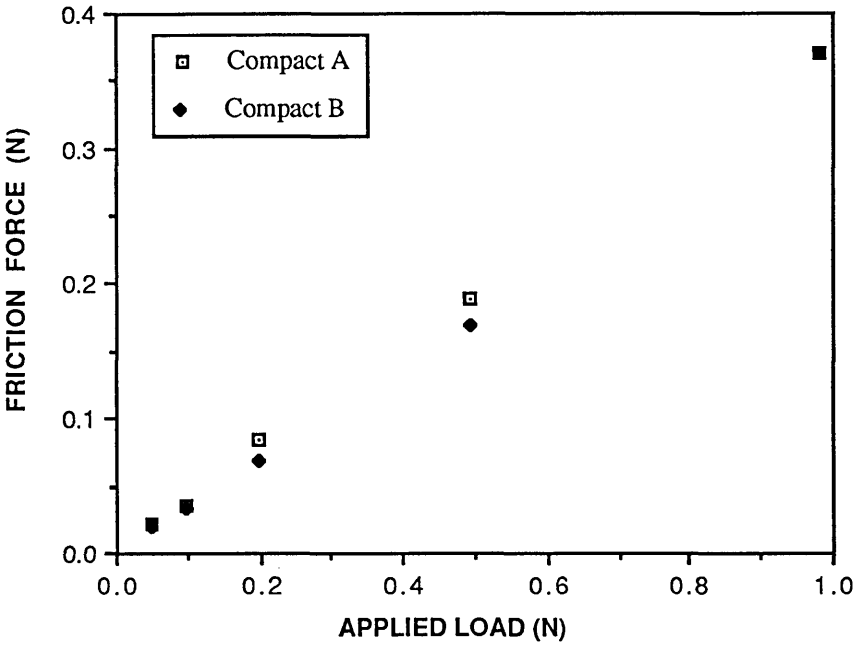

Figure 7.5 Variation of the friction force as a function of the applied normal load for the sliding of hemispherical uranium dioxide compacts pressed to 125MPa over a smooth glass surface.

TABLE 7.9 Interfacial Sliding Friction Parameters for Green Compacts.

Material	Binder	Experimental Values				Predicted
		k	n	τ_{oa} (MPa)	α_a	n
Alumina	PVA 14000	0.26	0.87	6.9	0.47	0.95
Alumina	PEG 400	0.57	0.93	29.1	0.36	0.84
Alumina	50%PVA 1400 50% PEG 400	0.50	0.90	13.6	0.37	0.90
Zirconia	PVA 14000	0.18	0.75	45.9	0.20	0.75
Zirconia	PEG 400	0.29	0.76	74.4	0.13	0.71
PVA 14000		0.13	1.00	-----	-----	-----
PVA 72000		0.09	0.96	-----	-----	-----
PEG 400		0.39	1.04	-----	-----	-----
UO_2 A_{96}		0.37	1.00	-----	-----	-----
UO_2 B_{96}		0.36	0.99	-----	-----	-----
Ferrite	PVA 72000	0.24	0.99	-----	-----	-----
Ferrite	75%PVA 72000 25%PEG 4000	0.20	1.00	-----	-----	-----
Ferrite	50%PVA 72000 50%PEG 400	0.21	0.99	-----	-----	-----
Ferrite	Gohsenol	0.17	0.97	-----	-----	-----

7.3.2.1.1 Alumina and Zirconia Systems; n<1

The experimental results from the sliding of alumina and zirconia compacts pressed from the granulated powders coated with a binder show a value of the load index less than unity. This suggests an elastic deformation of the interface. It seems that the

pressure developed at the contact is below the flow stress of these systems. The situation at the interface has been modelled applying the adhesion model of friction. A similar approach to the one presented in Section 7.3.1.1.3, to model the interface friction of bulk powders against the walls of the rolling cylinder, is followed. In this case it is necessary to consider a different description of the geometry of the contact. The shear strength of these systems was calculated form the measured friction force and the area of contact which was determined applying the Hertz equation (equation 7.12). The observed contact pressure dependence of the shear strength τ was assumed to follow the relationship;

$$\tau = \tau_o + \alpha P \tag{7.13}$$

and the values of the interface parameters τ_o and α were determined from the shear strength-contact pressure curves. These values are presented in Table 7.9.

Introducing these results in the adhesion model of friction the friction force is given by

$$F = \pi \tau_o \left(D r\right)^{2/3} W^{2/3} + \alpha W \tag{7.14}$$

where D is defined by equation 7.9, r is the sphere radius and W is the applied normal load.The load index may be predicted according to

$$n = \left(\frac{2 + 3 a' W'^{2/3}}{3 + 3 a' W'^{2/3}} \right) \tag{7.15}$$

where W' is the logarithmic mean of the load range used, a' = α/c' and c' is given by

$$c' = \pi \tau_o \left(D r \right)^{2/3} \qquad (7.16)$$

The load index was predicted by introducing in equation 7.15 the values of the mechanical properties of the interface found in the literature (Table 7.8) and the experimental interfacial rheological properties, τ_o and α, obtained from the present shear strength data which are shown in Table 7.9. The experimental and predicted values of n for these alumina and zirconia systems are presented in Table 7.9. The predicted values are close to the experimentally obtained load indices. This suggests that these systems may be modelled based on the adhesion model of friction which predicts that for this configuration the load index may vary between 2/3 and unity. These results indicate that these alumina and zirconia systems, under the conditions studied, may be modelled based on the elastic deformation of the hemispherical compact-glass interface. The values of n for the alumina/binder compacts are close to the Archard precursor (n=8/9) indicating a rough contact where all the asperities are of the same height. The interface shear properties of the compact surface govern the interface friction process and these properties are a function of the binder system present in the ceramic material.

7.3.2.1.2 Polymeric and Uranium Dioxide Systems; n=1

All the friction force load indices, n, in the case of the sliding of hemispherical compacts of the bulk polymers and the uranium dioxide granules have a value close to unity (Table 7.9). Accordingly, the friction force is directly proportional to the applied normal load and the k values for these systems correspond to the values of the wall coefficient of friction, μ which is constant in the load range examined. That is, it is not a function of the normal load. Also, it is observed that the experimental values of k, the coefficient of friction, for the sliding of the polymer compacts are similar to the shear strength pressure coefficients of the thin polymer films, α (Table 7.8). As it will be shown later (Section 7.3.3) the value of α is the limiting value of the coefficient of

friction when plastic deformation occurs. These results indicate that the contact is probably plastically deforming in nature. Plastically deforming contacts always produce a value of n equal to unity (Briscoe *et al.*, 1985).

The results for the value of k of the polymer compacts show that the pressure coefficient of the thin films is the limiting value of the coefficient of friction of the bulk material at high loads where plastic deformation occurs. These results suggest that the properties of the interfacial region when a bulk polymeric compact is slid over a hard substrate resemble the rheological properties of thin polymeric films sheared between smooth, hard surfaces.

In summary, during the sliding of these rigid hemispherical compacts on a glass surface high contact pressures develop at the interface inducing plastic deformation of the microasperities on the compact surface. The response of the bulk polymeric compacts may be predicted from the shear properties of the thin polymer films.

In the case of the sliding of the two uranium dioxide hemispherical compacts n is unity. This indicates a plastic deformation of the interface or an elastic, multiple asperity contact. From the value of n it is not possible to distinguish between these two situations. In this case it is most probable that the situation at the interface corresponds to an elastic multiple asperity contact with a distribution of asperity heights. The values of the coefficient of friction obtained in this configuration are close to the corresponding values of k obtained during the unconstrained flow of these powders (Table 7.7) where elastic deformation of the interface occurred. Also, the expected values of the coefficient of friction if the interface deforms plastically would be close to the values of α' (Table 7.7). The experimental values of the coefficient of friction suggest that the compact-glass contact is elastic in nature. The different behaviour of the uranium dioxide compacts compared to the alumina systems, where the Archard precursor was obtained, is probably due to the different properties of the UO_2 and alumina particles.

7.3.2.2 Interface Sliding Friction of a Sphere on a Compact

The results from the second configuration used to describe the sliding friction of compacts, the sliding of a sphere over the compact surface, are presented for several ferrite systems in Table 7.9. The load index, n, in all the cases studied is unity. In this case of a rigid sphere sliding on the compact surface high contact pressures develop at the interface inducing plastic deformation of the surface of the compact. The same analysis as the one used to describe the sliding of hemispherical compacts of the polymers or the uranium dioxide presented in Section 7.3.2.1.1 applies to this case. The friction force is directly proportional to the applied load and therefore k represents the value of the coefficient of wall friction. The value of the coefficient of friction is a function of the binder present in the ferrite system.

7.3.2.3 Summary of Compact Wall Tractions

The sliding friction of compacts against walls has been described using a model experiment under two different configurations; a hemispherical compact sliding over a smooth surface and a sphere sliding over a cylindrical compact surface. In the former case when a ceramic/binder system is considered the contact pressure is not high enough to produce the plastic deformation of the interface; an elastically deforming contact describes the situation at the interface. The behaviour is a function of both the ceramic system and the binder system considered. In the case of the polymeric binder samples, the flow stress of these systems is lower and therefore the contact pressure at the interface is high enough to produce plastic deformation. The properties of the interface are well defined by considering the shear stress properties of thin organic films.

In the second configuration, sphere-on-compact, the contact pressure is quite high and as a result a plastically deforming contact is observed. The interfacial properties are seen to be a function of the binder system coating the ceramic particles.

7.3.3 Coefficient of Friction

The data presented and analysed in the previous sections include several aspects related to the frictional characteristics of ceramic and binder systems under a range of contact conditions and applied loads. One important aspect is the magnitude of the coefficient of friction and its variation with the normal load. The main characteristics of the coefficient of friction, as sensed in the model experiments discussed in this Chapter, are presented in this Section.

In general, the coefficient of wall friction, μ is defined as the interface shear or friction force divided by the normal load

$$\mu = k\, W^{n-1} \tag{7.17}$$

where n is a load index whose numerical value is less than or equal to unity. The friction coefficient for elastic deformation of the interface is characterised as a decreasing function of the load ($n<1$). This is the result obtained in this work for the friction coefficient of the loose powder beds. Figure 7.6 shows the load dependence of the coefficient of friction for the case of two different ferrite/binder loose powder beds sliding against the rolling cylinder walls.

For the case of a plastically deforming contact n is unity and the friction force is a linear function of the load and in this case the coefficient of friction is constant

$$\mu = k \tag{7.18}$$

This is the result found for the case of the polymeric compacts sliding over smooth glass surfaces and for the sliding of a rigid body over the surface of the ferrite compacts. For these two situations plastic deformation of the interface occurs. The values of k given in Table 7.9 for the cases where n=1 correspond to the values of the coefficient of friction. It has been shown that the value of the coefficient of friction is a function of the type of binder.

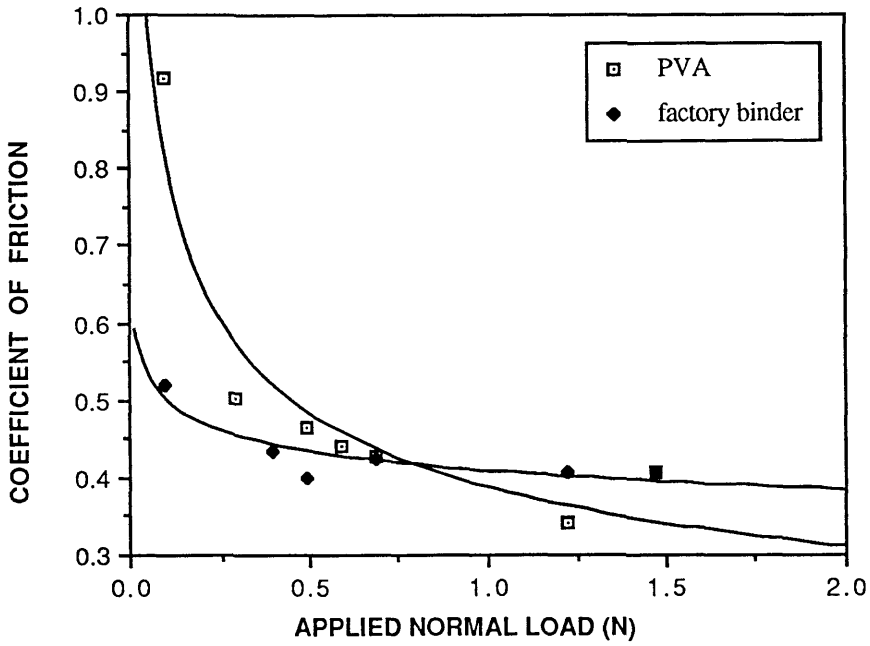

Figure 7.6 Variation of the coefficient of friction with the applied normal load for two ferrite powders (IC2 and IC0) sliding against smooth counterfaces.

The friction data presented in Table 7.9 may be compared with the similar data produced during the unconstrained flow of bulk powders and presented in Table 7.7. In the rotating cylinder configuration the values of n obtained were 0.80-0.90. The corresponding values for k in both configurations (Tables 7.7 and 7.9) show, in general, a higher value of k for the rolling cylinder case. In summary, as the contact pressure increases from an elastic unconstrained flow situation to a plastic case the value of the coefficient k decreases and the value of the load index n increases. The increase of n with the applied pressure has been dealt with many times (Adams *et al.*, 1987a) and is predicted from equation 7.15. The decrease of k, or the coefficient of friction, with the applied load has been shown in this work and is represented in Figure 7.6 and Tables 7.7 and 7.9. This is what is predicted by the expression presented by Adams *et al.*, 1987a (see Section 3.2.2.2.1.1)

$$k = \frac{c + \alpha W'^{1/3}}{W'^{z}} \tag{7.19}$$

and z is given by

$$z = \frac{a W'^{1/3}}{3\left(1 + a W'^{1/3}\right)} \tag{7.20}$$

The coefficient of friction may also be expressed as a function of the contact pressure as it has been explained in Chapter 3. Considering the contact pressure dependence, the friction force is given by

$$F = \left(\tau_o + \alpha P\right) A_r = \left(\frac{\tau_o}{P} + \alpha\right) W \tag{7.19}$$

where A_r is the real area of contact and P is the contact pressure. From equation 7.19 it follows that

$$\mu = \frac{\tau_o}{P} + \alpha \tag{7.20}$$

and the friction coefficient decreases with increasing contact pressure until some asymptotic value is reached which is approximately equal to the pressure coefficient α, or rather $(\tau_o / P_o) + \alpha$ where P_o is the plastic yield pressure or flow stress of the material. For the sliding of the polymeric compacts $(\tau_o / P_o) << \alpha$ and thus $\mu = \alpha$.

7.4 WALL STRESSES IN DIE COMPACTION

This study has also investigated the stress transmission during uniaxial single sided compaction of powders and the resulting stress and density variations in the compacts. The experimental results and the corresponding analysis from the study of the effects of

the particle-wall friction on the stress transmission during powder compaction and green ejection are presented in Chapter 8. Some of the friction properties deduced from the model experiments presented in this Chapter will be applied to describe the situation at the powder-wall or compact-wall interface during compaction and ejection which involve both constrained and unconstrained flow and a broad range of applied loads or contact pressures.

7.5 CONCLUSIONS

The particle-wall friction properties of a range of ceramic and binder systems have been investigated as a function of the applied normal load in two model experiments. From these observations the following conclusions may be drawn:

- There is no evidence of major differences in the interface friction or shear stress in free flow for any of the different uranium dioxide powders studied. The only differences observed correspond to the state of the powder (granulated or "as-received") not to the type of powder (A or B).

- The levels of wall friction and its variation with the normal stress have been to some extent rationalised using the adhesion model of friction in conjunction with a simple contact mechanical model of the powder surface. At low normal stresses, as experienced in unconstrained flow, there is a logarithmic relationship between the friction force and the load and it is observed that the autoadhesion component of the friction is negligible. These systems produce elastic contacts and apparently single asperity contacts in the case of ceramic/binder powders. The load variation follows an extended Hertz model for an assembly. The coefficient of friction is a decreasing function of the applied normal load and it depends on the type of binder. For the base powders the situation is better described considering a rough elastic contact.

- At higher loads the contacts flow plastically at the surface. Under these conditions the adhesion model of friction is still applicable but now a constant, or rather load invariant, coefficient of friction is obtained. Its value is a function of the powder and

binder systems considered.

- Overall, the coefficient of wall friction follows the form $\mu = c^* W^{-1/3} + \alpha$ for contact pressures below the flow stress. Above the flow stress $\mu = c'' + \alpha = (\tau_o/P_o) + \alpha$ where c^* and α are parameters which may be estimated from simple mechanical and rheological characteristics of the particles and coatings produced by the binder selected.

- The friction response, and thus the coefficient of friction, for the systems studied are apparently controlled by the organic binder and they are a strong function of the contact pressure. The organic binders are primarily responsible for the observed wall friction characteristics.

CHAPTER 8

COMPACTION RESULTS AND DATA ANALYSIS

8.1 INTRODUCTION

The experimental data generated from the uniaxial compaction of several oxide powders and from the ejection of the resulting pressed bodies, and the analysis of these data are presented in this Chapter.

Compaction studies are normally conducted by either static (generation of the compaction-pressure curve from static measurements of compaction at several pressures) or dynamic techniques (continuous measurement of the compact height to determine the entire compaction-pressure curve) (Leiser *et al.*, 1970). Data obtained from both the static and the dynamic compaction techniques will be discussed. Consolidation of powders is a complex process; several mechanisms are involved and it is difficult to differentiate the individual stages. Consequently a number of properties are used to indirectly interpret powder compaction; amongst these are the granule yield point, the green density, the compaction ratio, and the green strength of the compact. Most ceramic systems contain an organic binder and all of the above properties of the green pressed body are largely dependent on the properties of the organic binder. The effect of the type of binder on these properties has also been studied. To assist in the pressing of these materials a wall lubricant is usually added. The effect of the presence of lubricant during the compaction and the ejection stages is also covered in this Chapter. The complex, and great volume of information obtained from the study of the compaction process has been divided into four main areas of interest; the densification of the powder, the friction effects during pressing and the transmission of forces, the friction effects during the ejection of the compact, and finally the characterisation of the

resulting green compact. This latter aspect will be presented separately in Chapter 9.

8.2 EXPERIMENTAL DESIGN AND DATA

There are a number of variables that affect the pressing behaviour of powders. Because of this the experimental conditions were carefully controlled. The different sets of experiments that were carried out are summarised in this Section. Also, the main experimental results from the pressing of the different materials are presented. Several aspects of interest; powder densification, friction effects during pressing, and ejection of the pressed body are included. All these three aspects will be analysed separately in the following sections.

8.2.1 Calibration

The main compaction and ejection experiments involved the continuous measurement of the applied and transmitted stresses using the technique described in Chapter 5 (see Section 5.6.4 and Figure 5.11). The two transducers used to monitor the top and bottom forces were calibrated with respect to their charge sensitivity in pcb/lbs and the corresponding calibration curves are shown in Figure 8.1. The equipment was recalibrated on several occasions by applying known dead weights and measuring the corresponding output force. The calibration factor was found to be constant for each load range used. The cross-head speed of the Instron testing machine used to applied the force was calibrated by determining the displacement and the time as a function of the applied voltage. The resulting calibration curve is shown in Figure 8.2.

8.2.2 Ferrite

First, some preliminary studies to determine the general pressing behaviour of several ferrite/binder materials were conducted by a static technique. A fixed amount of powder, Ferrite/Gohsenol was the material selected, was pressed to different applied pressures. The final compact green density was determined for each compacting

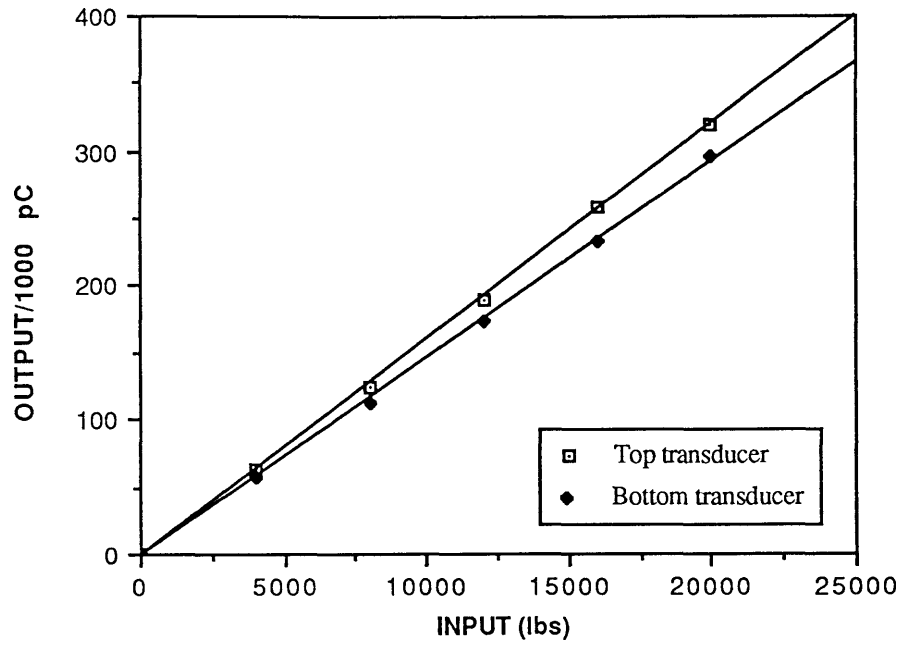

Figure 8.1 Calibration curves of the load transducers used to monitor the applied and transmitted pressures during powder compaction.

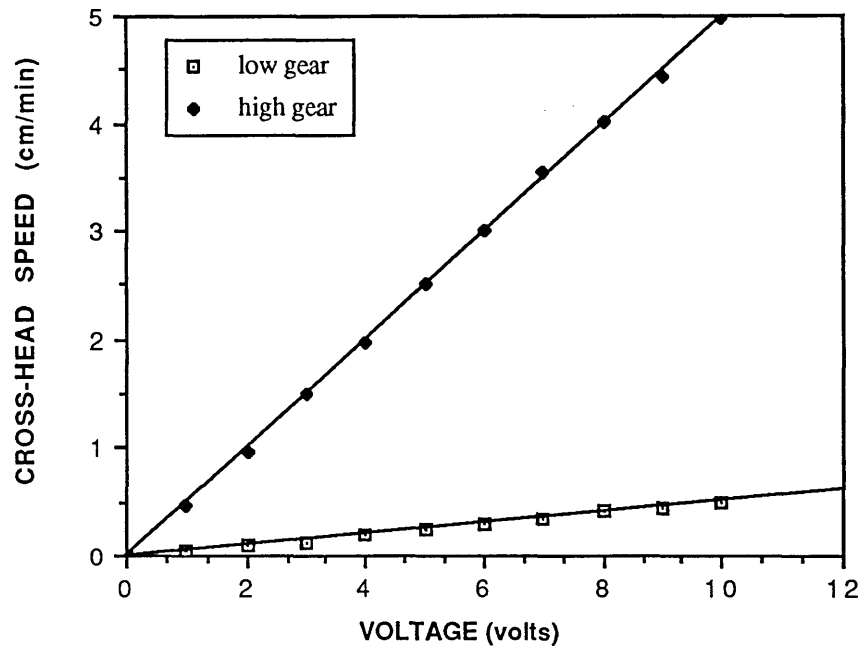

Figure 8.2 Calibration curve of the cross-head speed, at two gear settings, of the Instron testing machine used for the compaction of the powders.

pressure and the compacts were characterised regarding their hardness profiles (see Chapter 9). From these initial studies a range of maximum applied pressures of 15 to 150 MPa, and a maximum amount of powder of 0.040 kg required to produce good quality greens were established.

There are several variables that influence the compaction behaviour of a material and some of them have been studied for some ferrite granulated materials. The influence of the applied load on the compaction of several ferrites containing different binder systems has been studied by measuring the green density of the different pressed specimens as a function of the applied load. Other variables studied include the agglomerate average size, the powder moisture content, the type of binder, the use of lubrication, and the initial amount of powder or sample aspect ratio. Table 8.1 presents a summary of the different sets of experimental conditions selected, regarding all these variables, for the study of the pressing behaviour of some ferrite/binder systems. A powder is classified as dry after having been dried in an oven at 90 °C for 48 hours and then stored over silica gel in a desiccator. The average moisture content was ca. 0.2-0.4%. The granules were single-sided uniaxially pressed using a cylindrical die of 0.0163 m internal diameter mounted in an Instron testing machine using a constant crosshead speed of 2.5×10^{-4} m/sec. The die walls were in some cases lubricated with zinc stearate powder applied evenly onto the die and punch walls. The amount of ceramic powder used varied from 0.0025 to 0.030 kg to produce a range of initial powder bed height/die diameter ratios, $(H/D)_o$, of between 0.5 to 7.0 and compaction pressures of up to 150 MPa were applied. The applied and transmitted pressures were monitored continuously as a function of the punch displacement.

It may be seen from Table 8.1 that the type of binder, the initial amount of powder, the agglomerate size, the humidity conditions (i.e. whether the material had been previously dried in an oven at 90 °C or kept under atmospheric conditions), the maximum applied pressure, and the lubrication were the factors considered.

TABLE 8.1 Experimental Conditions Selected in the Compaction Experiments for Ferrite Systems.

Binder	Mean Size (μm)	Amount /10^{-3} kg	Humidity	Applied Pressure (MPa)	Lubricant
Gohsenol	212-425	5.0-20.0	dry	60	Zn-stearate
Gohsenol	212-425	5.0-20.0	dry	60	no
Gohsenol	212-425	5.0	dry	22-106	Zn-stearate
Gohsenol	212-425	5.0	dry	21-88	no
Gohsenol	212-425	2.5-5.0	dry	60	no
	425-600	2.5-5.0	dry	60	no
	600-850	2.55-5.0	dry	60	no
Gohsenol	212-425	2.55-5.0	dry	60	Zn-stearate
	425-600	2.55-5.0	dry	60	Zn-stearate
	600-850	2.55-5.0	dry	60	Zn-stearate
PVA 14,000	212-425	2.5-12.5	dry	60	Zn-stearate
PVA 14,000	212-425	2.5-12.5	dry	60	no
PVA 14,000	212-425	5.0	dry	22-85	no
PVA 14,000	212-425	5.0	dry	22-107	Zn-stearate
PVA 14,000	212-425	10.0	dry	22-102	Zn-stearate
PVA 14,000	> 425	10.0-30.0	atmospheric	30-127	Zn-stearate
PVA 14,000	212-425	10.0-20.0	atmospheric	47-83	Zn-stearate

Several experiments were carried out using selected ferrite systems and conditions. The data generated comprise the applied and transmitted pressures, the piston displacement, the compact final density and the ejection pressure. A typical example of the type of results generated from the pressing and the ejection of a Ferrite/Gohsenol system are shown in Tables 8.2 and 8.3 respectively.

TABLE 8.2 Summary of Results from the Pressing Stage of the Compaction-Ejection Cycle for Ferrite/Gohsenol Pressed at 60 MPa Using a Variable Initial Powder Mass.

Amount (kg)	$(H/D)_o$	Piston Displacement (m)	Max. P_a (MPa)	Time (sec)	Compact Density (g/cm^3)
0.0050	1.05	0.0090	62.51	36.3	2.54
0.0100	2.14	0.0160	62.55	66.7	2.46
0.0125	2.63	0.0199	62.11	80.7	2.50
0.0150	3.23	0.0227	60.94	94.1	2.42
0.0200	4.27	0.0299	60.13	122.8	2.34

TABLE 8.3 Summary of Results from the Ejection Stage of the Compaction-Ejection Cycle for Ferrite/Gohsenol Pressed at 60 MPa Using a Variable Initial Powder Mass.

Amount (kg)	Piston Displacement (m)	Max. Pejection (MPa)	Time (sec)
0.0050	0.0199	1.05	39.8
0.0100	0.0305	3.83	61.0
0.0125	0.0352	4.20	70.4
0.0150	0.0407	6.39	81.4
0.0200	0.0510	19.80	102.0

In these series of experiments the influence of the initial amount of powder on the pressing and ejection behaviour was studied. These types of tables were generated for each of the experimental sets described in Table 8.1.

8.2.3 Uranium Dioxide

In the case of the uranium dioxide powders the main interest was the possibility of determining any differences in the pressing behaviour of the two available uranium dioxide materials A and B. The powders were pressed under constant experimental conditions.

8.2.3.1 "As-Received" Materials

The compaction behaviour of the "as-received" uranium dioxide powders A and B has been evaluated using single sided die compaction. The materials were pressed in a 0.019 m internal diameter cylinder. The die was filled with a fixed amount of powder (0.012 kg) and a load varying from 22.65 to 4,530 kg was applied to compact the powder. The compaction pressure ranged from 0.8 to 157 MPa. The green density of the resulting pressed bodies was determined in each case.

8.2.3.2 Granulated Materials

The lubricated uranium dioxide granules were pressed in a 0.019 m internal diameter die at an applied pressure of 157 MPa. Different initial masses were used, from 0.021 to 0.036 kg with 0.005 kg intervals. The maximum applied pressure and the final compact dimensions were determined. These granulated materials which had been admixed with a lubricant, zinc stearate powder, were also pressed using the dynamic compaction technique where both the applied and transmitted forces were monitored in a continuous way. 0.106 kg were pressed in a 0.022 m internal diameter cylindrical die at a crosshead speed of 5.6×10^{-5} m/sec. The two continuously recorded compaction curves corresponding to the uranium dioxide lubricated granules $A_{96\text{-}L}$ and $B_{96\text{-}L}$ pressed under these conditions are presented in Figure 8.3.

The experimental data generated during the pressing of the granulated uranium dioxide powders are summarised in Tables 8.4 and 8.5.

TABLE 8.4 Experimental Results for the Compaction of Uranium Dioxide.

Powder	Amount (kg)	$(H/D)_o$	Max. Applied Pressure (MPa)	Time (sec)
lubricated granules, 0.022 m die				
$A_{96\text{-}L}$	0.106	4.5	113	745
$B_{96\text{-}L}$	0.106	4.4	130	633

TABLE 8.5 Variation of the Grcen Density for Compacts Pressed up to 156 MPa Using Different Masses of Lubricated UO_2 Granules.

INITIAL MASS (kg)	GREEN DENSITY (g/cm^3)	
	POWDER $A_{96\text{-}L}$	POWDER $B_{96\text{-}L}$
0.036	5.05	5.06
0.031	5.42	5.07
0.026	4.99	5.10
0.021	5.05	5.41

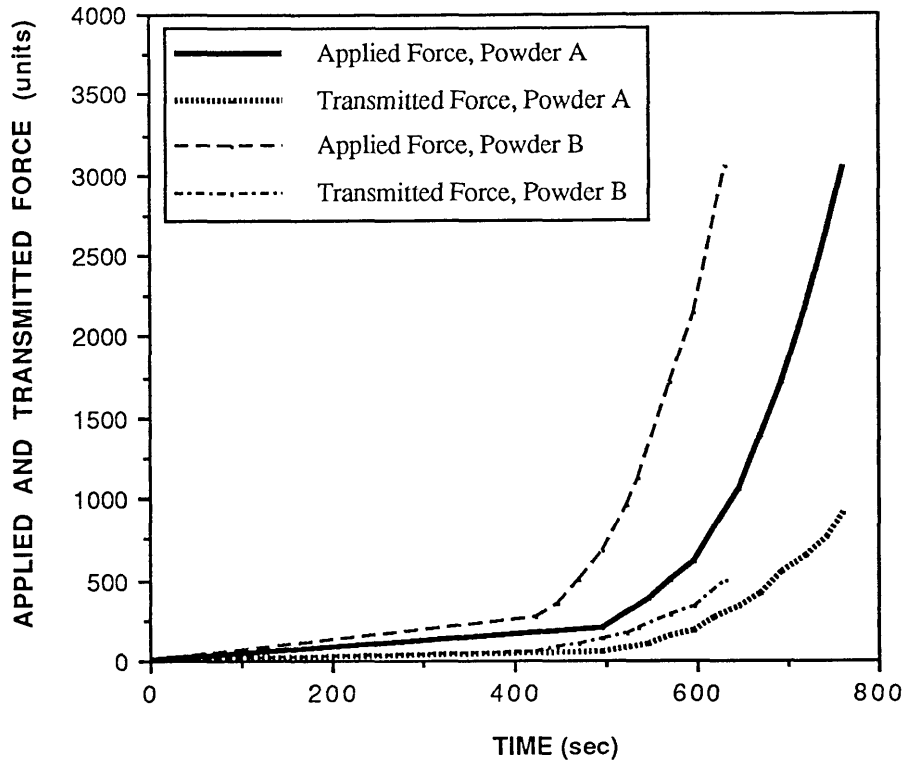

Figure 8.3 Experimental curves of the applied and transmitted forces as a function of time for the pressing of 0.106 kg of the lubricated UO_2 granules at a crosshead speed of 5.6×10^{-5} m/sec in a 0.022 m diameter cylindrical die.

8.2.4 Alumina and Zirconia

The pressing behaviour of these powders was studied under a series of different experimental conditions. The aim was to analyse the effect of the use of a lubricant and the influence of the initial aspect ratio, i.e powder bed height/diameter ratio, on the transmission of forces during the compaction of several selected alumina and zirconia granulated materials. Table 8.6 presents the variables studied.

The compacts were prepared by using powders weights from 0.0010 to 0.050 kg which produced initial powder bed height/diameter ratios of between 0.5 to 5.0. Compaction pressures of up to 80 MPa were applied using unlubricated dies and up to 150 MPa for calcium stearate lubricated die walls.

TABLE 8.6 Experimental Conditions for the Compaction of the Alumina and Zirconia Powders.

Powder	Mean Size (μm)	$(H/D)_o$	Final Applied Pressure (MPa)	Lubricant
Alumina/PVA	212-425	4.7	154	Ca Stearate
		2.5	162	Ca Stearate
		2.5	81	unlubricated
		1.0	162	Ca Stearate
		1.0	81	unlubricated
Alumina/PVA-PEG	212-425	1.2	162	Ca Stearate
		2.4	162	Ca Stearate
		4.7	162	Ca Stearate
Zirconia/PVA	212-425	4.6	162	Ca Stearate
		2.4	162	Ca Stearate
		1.1	162	Ca Stearate

*(PVA 14,000, PEG 400)

8.3 DATA ANALYSIS

It has been mentioned in the Introduction that the data generated during the pressing of the powders have been divided into three different areas; powder densification, friction effects, and compact ejection. These three aspects are treated in the following sections.

8.3.1 Green Compact Density

The first step in designing a procedure to prepare dry pressed products is the establishment of the relationship between the compacting pressure and the resulting pressed density. The generation of the pressure-volume curves during compaction was

discussed in Chapter 5. The pressure-density relationships were obtained from the continuous monitoring of the applied force and the punch displacement and also, in a separate series of experiments, from the mass and dimensions of ejected specimens which were compacted to different pressures. These pressure-density compaction curves were used to analyse the compaction behaviour of the powders.

The green density was generally found to increase with the logarithm of the applied compaction pressure in a linear way for all the ceramic systems studied. The compaction results can be represented by semilogarithmic plots; the compact density being linearly related to the logarithm of the compaction pressure;

$$\rho - \rho_y = m \ln \frac{P}{P_y} \qquad (8.1)$$

where ρ is the density, P is the applied pressure, P_y and ρ_y are the pressure and density at the point of yielding, and m is an empirical constant called the compressibility factor. The tap density of the powder is close to the density at the point of yielding, ρ_y. This linear relationship between the density and the logarithm of the pressure is shown in Figure 8.4 for the ferrite systems IC2 (PVA 14,000) and IC12 (Gohsenol). The plotted data corresponds to the compaction of 0.005 kg of the dried powders to 60 MPa in a non lubricated 0.019 m internal diameter cylindrical die. This type of behaviour is widely reported in the literature (see Section 4.2.6.1, Chapter 4). From the analysis of this type of relationships several authors have identified the different stages in the densification process from the slopes of the several straight line segments in the curve. In the range of pressure used in this work two and sometimes three compaction stages are apparent. The pressure at which this change in slope takes place may be determined from these plots. Each region corresponds with a different mechanism believed to control the compaction in that pressure region. The data were, generally, fitted to two linear portions. A low pressure region, where compaction is due to particle rearrangement is controlled by particle-particle friction. At pressures above the break point; particle deformation, aggregate breakup or crushing occurs and is controlled by

the strength of the agglomerates. In some cases a second change of slope in the density-pressure semilogarithmic curve is observed. This third region may be identified with the breakdown of stable structures or the deformation of the basic ceramic particles themselves.

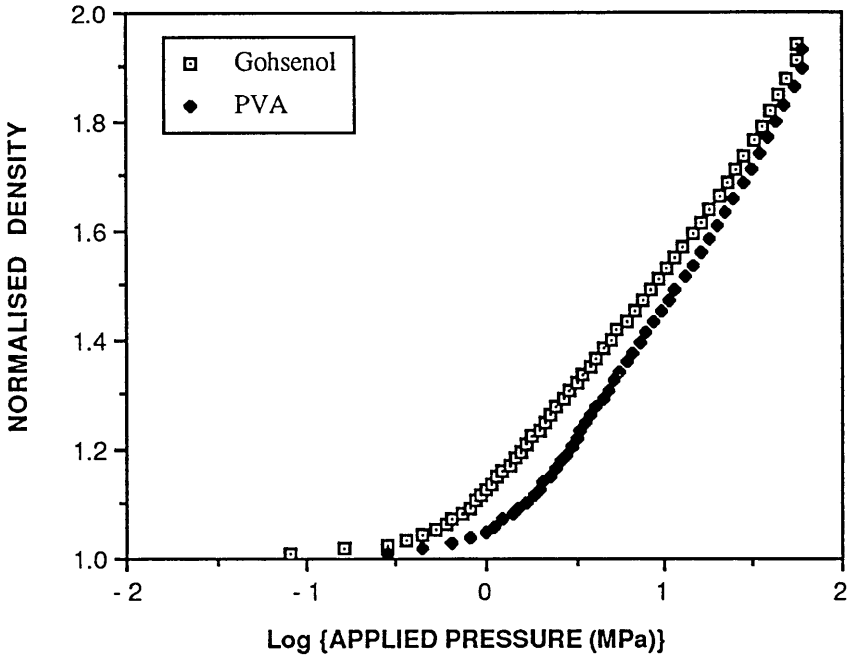

Figure 8.4 Semilogarithmic plots of the compact bulk density normalised by the initial powder density as a function of the applied pressure for two ferrite systems. 0.0050 kg, 212-424 μm dried granules pressed to 60 MPa at 2.5×10^{-4} m/sec in a non lubricated 0.019 m diameter cylindrical die.

8.3.1.1 Yield Point

An important value obtained from these curves is the breakpoint or yield point; i.e. the pressure at which the first change in slope is observed, which is believed to correspond to the beginning of granule crushing. The granule yield point is defined as the pressure at which granule rearrangement is essentially complete and granule deformation and/or fracture begins (Nies and Messing, 1984). It seems to relate to the granule strength. According to Niesz et al., 1978 and other authors the breakpoint

observed in the logarithm representation of the pressure versus the green density is a measure of the compression strength of the agglomerates in the powder. In contrast Ciftcioglu *et al.*, 1986 stated that the pressure-density compaction curves may give qualitative information about the nature of any agglomerates present but are of limited value in providing information about agglomerate strength. Table 8.7 shows the values obtained experimentally for the granule strength (single granule crushing experiment) and the corresponding values obtained from the breakpoint of the density-pressure semilogarithmic curves where such a point was distinguishable. It may be seen that a detectable correlation exists between both set of data. Unless otherwise stated, all the samples were dried in an oven at 90 °C and stored over silica gel. The samples labelled "saturated" were stored over water for four days. The materials were pressed in a 0.019m diameter die whose walls were lubricated with zinc stearate in the case of the ferrite powders and with calcium stearate for the alumina and zirconia samples.

8.3.1.1.1 Effect of Type of Binder

It is apparent from these data that the granule yield point gradually decreases with increasing PEG content. The plasticity of the binder becomes important when granule deformation and fracture occurs during compaction; the added deformability of the binder leads to a lower granule yield point. The effect of adding a plasticising, PEG, to PVA appears to be that the granule strength and consequently the granule yield point decreases enhancing the pressing. It was observed that the change in slope (green density vs. log (applied pressure) curves) occurred at approximately the tapped bulk density of the material which corresponds to the onset of granule deformation.

8.3.1.1.2 Effect of Water Content

Comparing dry samples with material saturated with water, it is observed that the saturated samples press to higher densities and the agglomerate yield point is reduced. The effect of water is similar to that of a plasticiser; water may be considered a plasticiser. The presence of water reduces the granule strength and a lower granule yield point is observed.

TABLE 8.7 Granule Strength and Granule Yield Point Values.

Material	Conditions	Granule Strength (MPa)	Yield Pressure (MPa)	Density 100MPa (g/cm^3)
Ferrite				
Factory binder	300-500 μm, dry	----	0.10	2.85
	300-500 μm, sat 0.99%	----	0.11	3.16
PVA 72,000	<200 μm, dry	----	2.80	2.68
	<200 μm, sat 1%	----	0.30	3.20
	300-500 μm, dry	2.17	0.70	2.87
	300-500 μm, sat	2.05	0.30	3.20
PVA 14,000	dry	1.64	----	----
1:1 PVA 72,000	<200 μm, dry	----	0.31	2.93
PEG 4,000	<200 μm, sat 1.33%	----	0.17	3.29
1:1 PVA 72,000	300-500 μm, dry	1.03	0.06	3.04
PEG 4,000	300-500 μm, sat 1.33%	0.79	0.05	3.21
3:1 PVA 14,000	dry	1.17	----	----
PEG 400				
Alumina				
no binder	100-200 μm, dry	----	6.7	1.92
	100-200 μm, sat	----	----	1.92
PVA 14,000	300-400 μm, dry	1.20	5.0	----
	100-200 μm, dry	----	6.9	1.62
	100-200 μm, sat 2.2%	---	5.0	2.18
PVA 72,000	100-200 μm, dry	----	7.0	1.85
	100-200 μm, sat 1%	----	4.5	2.00
PEG 400	300-400 μm, dry	0.44	----	----
Zirconia				
PVA 14,000	300-400 μm, dry	0.80	0.6	---
PVA 72,000		----	0.5	3.20
PEG 400	300-400 μm,dry	0.19	----	----
PVA 14,000	100-200 μm, dry	----	2.2	----

8.3.1.1.3 Effect of Particle Size

Particle size and size distribution have an important effect on the compaction of some of these powders. The proportion of voids in the packing will be affected by the ratio of the particle size of the powder to the diameter of the die in which it is compacted. The number and the total area of the contacts between particles will be influenced by the particle size, the size distribution, and the packing arrangement within the powder. For the two different particle size distributions studied, in all the cases the 300-500 μm size material presents a lower yield point than the corresponding undersize batch (<200 μm). This behaviour is consistent with the single granule crushing results; smaller granules present a higher strength.

These findings and the correlation between the yield point and the density attained at a given pressure support the hypothesis that the yield point in the density curve reflects the strength of the granules in the material.

8.3.1.2 Kawakita Relationship

The compressibility of the samples may also be examined by applying the Kawakita equation,

$$\frac{P}{C} = \frac{1}{a\,b} + \frac{P}{a} \qquad (8.2)$$

where P is the applied pressure, a and b are constants, and C is the degree of volume reduction which is defined as $(V_o\text{-}V)/V_o$; V_o being the initial volume and V the volume at any given pressure. The pressing data were plotted in this way as it is shown in Figure 8.5, where P/C is plotted against pressure for the ferrite systems IC2 (PVA 14000) and IC12 (Gohsenol). This equation takes into account the initial bulk density of the material since C is the fractional volume change on compression. The constant a is a measure of the initial packing, while b is a measure of the resistance to compaction of the material. The values for the constants a and b in the Kawakita expression are

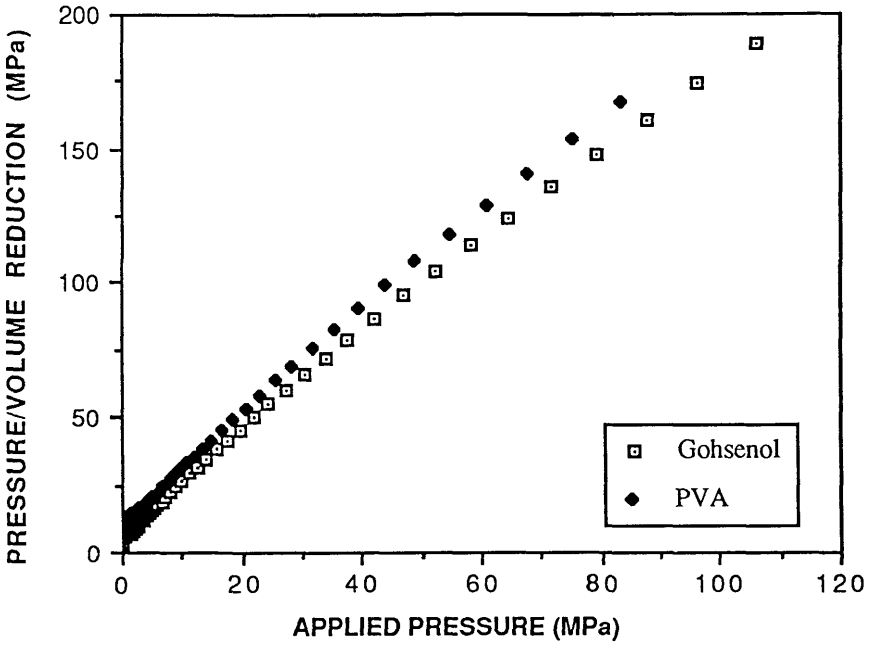

Figure 8.5 Compaction data plotted according to the Kawakita equation for the compaction of 0.0050 kg of Ferrite/Gohsenol and Ferrite/PVA 14,000 granules in a lubricated 0.0163 m diameter die.

given in Table 8.8 for the case of Ferrite/Gohsenol granules as a function of the particle mean size, the amount of powder being compacted and the lubricating conditions during pressing.

From the results in Table 8.8 several general trends in the data are observed. First, the values of the constants a and b are seen to decrease as the amount of powder increases. Secondly, considering the effect of the particle size on the values of a and b it may be observed from the presented data that as the particle average size decreases both constants decrease in value.

TABLE 8.8 Kawakita Constants Values.

Material and Conditions	Variable Size or Amount	a	b
Ferrite /Gohsenol			
0.0025 kg, 60 MPa, unlubricated			
different granule size fractions	600-850 μm	0.62	0.33
	425-600 μm	0.58	0.25
	212-425 μm	0.57	0.23
Ferrite/Gohsenol			
212-425 μm, 60 MPa, unlubricated			
several amounts	0.0050 kg	0.51	0.31
	0.0100 kg	0.48	0.25
	0.0125 kg	0.46	0.18
	0.0150 kg	0.45	0.18
	0.0200 kg	0.45	0.12
Ferrite/Gohsenol			
212-425 μm, 60 MPa, lubricated			
several amounts	0.0050 kg	0.54	0.31
	0.0100 kg	0.48	0.25
	0.0125 kg	0.48	0.26
	0.0150 kg	0.46	0.23
	0.0200 kg	0.46	0.20

Finally, the effect of the presence of a lubricant during the pressing stage on the values of the Kawakita constants was studied. The value b was higher in the lubricated case; the value of a does not seem to be greatly affected by the presence of a lubricant. The same trends are observed for the compaction of Ferrite/PVA 14,000 under the same conditions. These observed data trends may be explained by considering the constant a as an indicator of the initial porosity of the powder bed. As the amount of powder in the initial powder bed increases the porosity of the bed decreases. It also decreases as the size of the particles decreases. No variation in the initial porosity is expected when a

lubricant is employed. The constant b may be considered as representing the cohesivity of the material. According to the experimental results obtained under the conditions studied b increases when a lubricant is used, and it is well known that a lubricant facilitates the pressing. b increases as the size of the granules increases and in this work when fine powders were used the pressing was not so satisfactory; the quality of the pressing stage improved when a bigger average particle size was selected. Also, b decreases with the increase in the initial amount of powder and when a higher amount of powder is used the pressing presents serious problems of force transmission due to the increase in friction forces as will be presented in Section 8.3.2. All these results of the trends on the values of the constant b are an indication of the possible use of b as a parameter indicating the "ease" of pressing and in particular the level of the friction effects taking place during the compaction. In this context the word "ease" may be interpreted as a measure of the compressibility of the sample. This is a function of the powder and the wall friction. For a given powder b will scale with the magnitude of the wall friction. In general, and under the experimental conditions studied, a higher value of b is an indication of a "better" pressing behaviour.

8.3.1.2.1 Effect of Binder

Several ferrite/binder systems varying in the type and content of PVA and PEG were pressed under the same experimental conditions and the values of the Kawakita constants a and b were determined from the density-pressure curves. The results are shown in Table 8.9.

These data show that the addition of PEG to PVA increases the values of both a and b. These results support the idea presented in the previous Section that the value of the constant b is related to the quality of the pressing stage. Additional data, presented in this Chapter, Tables 8.7 and 8.11, on the pressing behaviour of a material as a function of the presence of PEG indicate that when PEG is substituted for PVA the resulting green density increases and the friction at the die walls decreases.

TABLE 8.9 Compaction Parameters for Several Ferrite/Binder Systems.

BINDER	a	b
PVA 14,000	0.54	0.21
PVA 72,000	0.53	0.21
3:1 PVA 72,000/PEG400	0.57	0.30
1:1 PVA 72,000/PEG400	0.57	0.29
1:1 PVA 72,000/PEG4000	0.57	0.34

8.3.1.3 Variables Affecting the Densification of Selected Ferrite Materials

The influence of the applied load on the compaction of the ferrites IC2 and IC12 has been studied by measuring the green density of the different cylindrical specimens as a function of the applied load. These results have been presented in previous sections. Other variables studied include the average agglomerate size the powder moisture content, the type of binder, the use of lubrication, and the initial amount of powder or aspect ratio. These aspects have been studied by compacting a powder under a set of different conditions regarding all these variables. The compacts were prepared by using powders weights from 0.0025 to 0.050 kg which produced initial powder bed height/diameter ratios of between 0.5 to 5. Compaction pressures of up to 80 MPa were applied using unlubricated dies and up to 150 MPa for zinc stearate lubricated die walls.

8.3.1.3.1 Particle Size

Figure 8.6 presents the densification curves corresponding to the compaction of different sizes Ferrite IC12 (Gohsenol) granules under the same conditions. 0.0025 kg of dry material were compacted in a 0.0163 m internal diameter die lubricated with zinc

stearate at a crosshead speed of $2.5x10^{-4}$ m/sec. Three different granule size ranges were selected; 212-425 μm, 425-600 μm and 600-850 μm.

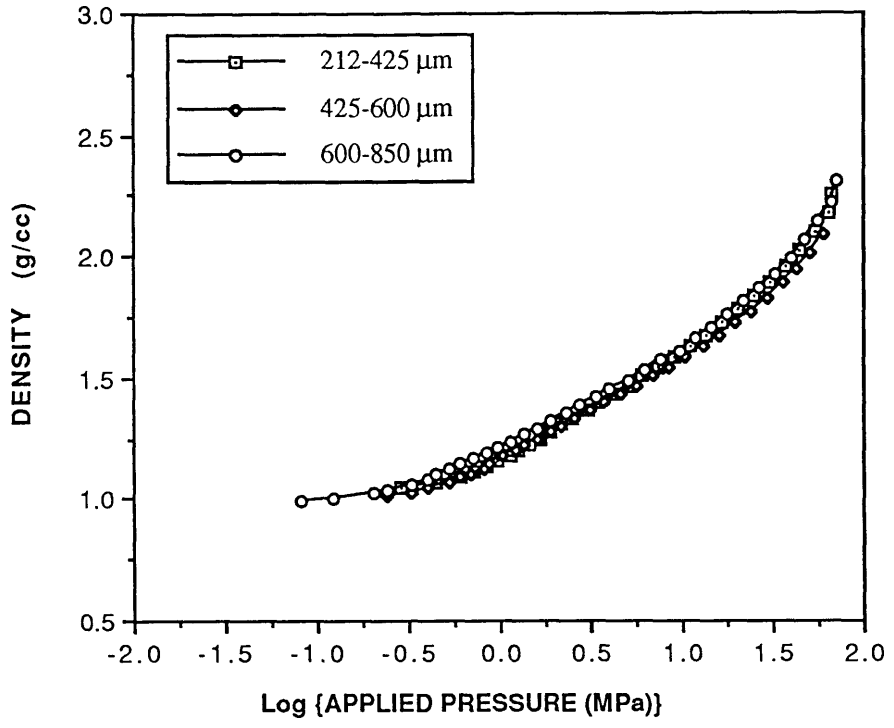

Figure 8.6 Semilogarithmic plot of the green density as a function of the applied pressure for three different size ranges of Ferrite/Gohsenol granules. 0.0025 kg of dry material pressed up to 66 MPa in a 0.0163 m diameter lubricated die at $2.5x10^{-4}$ m/sec.

From the densification curves no apparent effect of the granule size on the compact density is evident.

8.3.1.3.2 Moisture Content

Two sets of ferrite IC2 granules were pressed under the same experimental conditions. 0.010 kg of 212-425 μm granules were compacted in a 0.0163 m internal diameter die lubricated with zinc stearate at a cross-head speed of $2.5x10^{-4}$ m/sec. One of the batches had been previously dried.

Figure 8.7 represents the corresponding semilogarithmic densification curves. The density is normalised by the initial powder density.

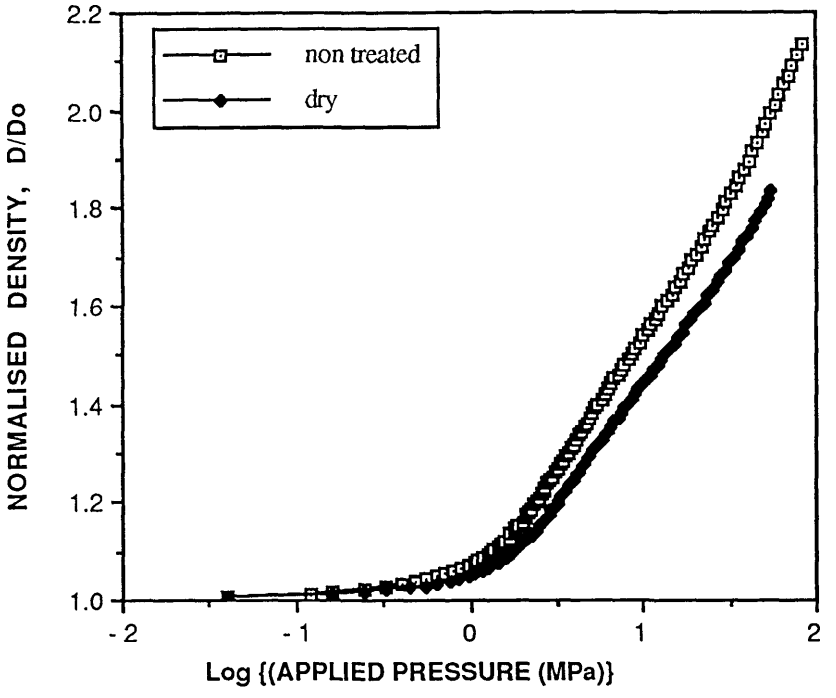

Figure 8.7 Semilogarithmic plot of the green density as a function of the applied pressure for Ferrite/PVA 14000 dry and non treated powders. 0.010 kg of the material pressed at 2.5×10^{-4} m/sec in a lubricated die, D=0.0163 m.

It may be observed from the densification curves that in the case of the powder with a higher content of water the density at any given pressure is higher than that for the dry powder. This different behaviour may be due to the lubricating properties of the water which reduces the interparticle friction effects resulting in a higher densification of the powder. Also, water plasticises the coating and will generally reduce the shear strength (Briscoe and Smith, 1983). Hence, the coefficient of friction will decrease (Section 3.2.2.2.3) and a higher densification is obtained.

8.3.1.3.3 Initial Height/Diameter Ratio

The effect of the initial amount of powder in the die or the initial aspect ratio, $(H/D)_o$, was analysed. Figure 8.8 shows the results for a series of initial aspect ratios for the pressing of ferrite IC12 granules. Three different amounts of dry powder; 0.005, 0.010 and 0.015 kg, producing a range of initial aspects ratios of 1.04, 2.09 and 3.10 were pressed to 60 MPa in a 0.0163 m internal diameter die no lubricated, at a cross-head speed of 2.5×10^{-4} m/sec.

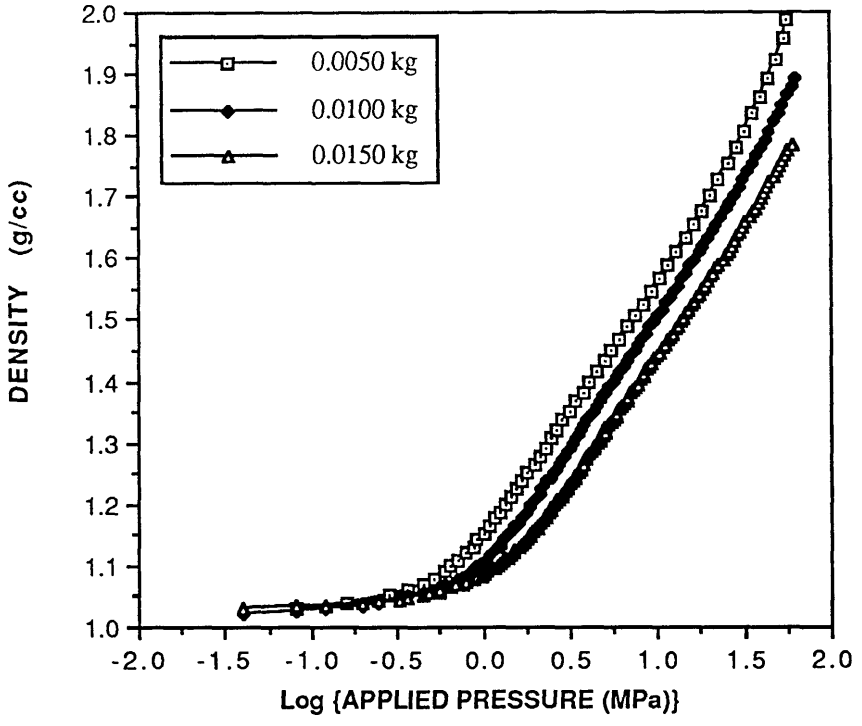

Figure 8.8 Semilogarithmic plot of the density as a function of the applied pressure for a range of Ferrite/Gohsenol masses. Maximum applied pressure of 60 MPa at a speed of 2.5×10^{-4} m/sec, unlubricated 0.0163 m diameter die.

From the densification curves it may be observed that at any given applied pressure the corresponding density is higher for the smallest amount of powder. As the amount of powder in the die increases the friction effects between the powder and the die walls and between the granules themselves become more important and the resulting effect is a decrease in the degree of densification obtained.

8.3.1.3.4 Lubricant

The use of a lubricant has no clear effect on the densification of the materials studied. This may be observed in Figure 8.9 where the densification curves for the pressing of ferrite IC12 under lubricated wall and unlubricated conditions are shown. 0.010 kg of dry material was pressed to 60 MPa at a cross-head speed of 2.5×10^{-4} m/sec, in a 0.0163 m internal diameter die. In one case no lubricant was used and in a second case the die walls were lubricated with zinc stearate. When a lubricant is used a slightly higher densification for a given applied pressure is observed. The presence of the lubricant reduces the friction between the powder and the die walls and consequently a higher proportion of the applied force is employed in densifying the material.

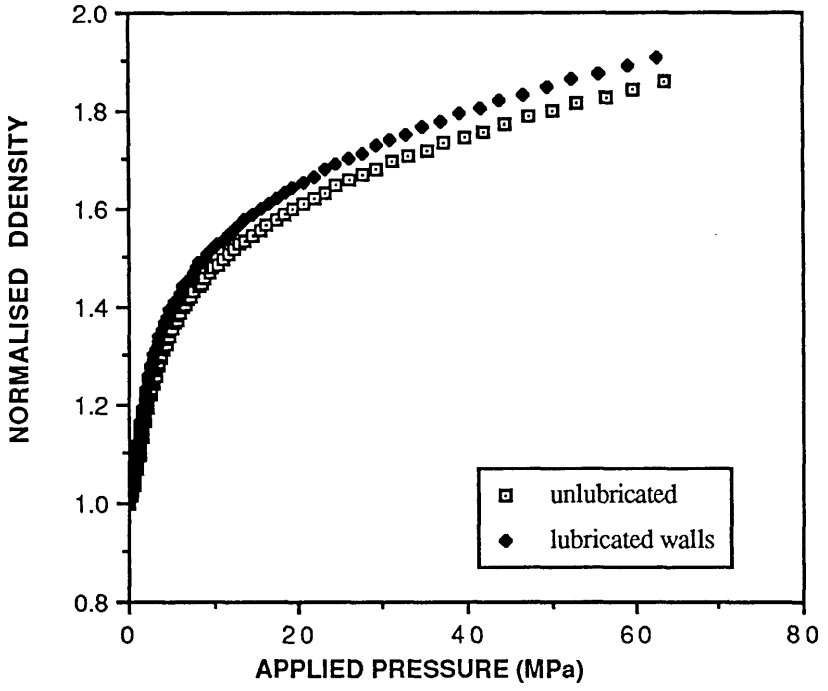

Figure 8.9 Variation of the density normalised by the initial density as a function of the applied pressure for the pressing of Ferrite/Gohsenol under lubricated and unlubricated conditions. Dry powder, 0.0100 kg, D=0.0163 m.

8.3.1.4 Densification of Uranium Dioxide Powders

Figure 8.10 shows the compaction behaviour of the uranium dioxide base powders as the variation in green density with the applied pressure. No major differences in the compaction behaviour of these two powders were observed. The green density has been normalised by the initial loose powder density; 0.91 g/cm^3 in the case of powder A and 0.98 g/cm^3 in the case of powder B. Powder A attains a higher relative green density than powder B (these systems were not lubricated).

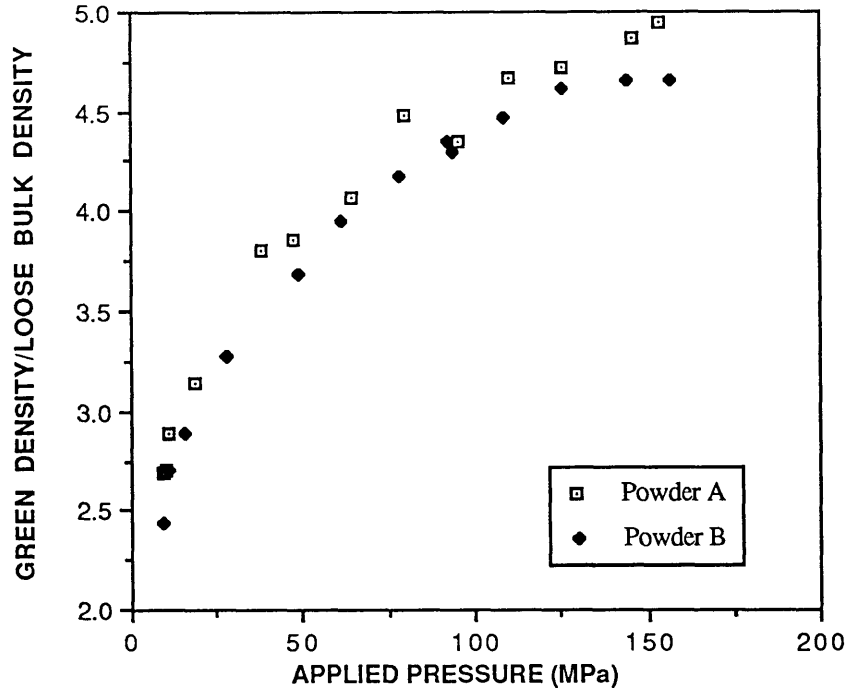

Figure 8.10 Variation of the green density normalised by the powder bulk density as a function of the maximum applied compaction pressure for the two "as-received" UO_2 materials. 0.012 kg were pressed with no lubrication, D=0.019 m.

The granulated powders A_{96} and B_{96} were admixed with 0.2% wt. zinc stearate. The compaction data for the lubricated granules (green density as a function of the initial mass) were shown in Table 8.5. It may be seen that the final density is not a marked function of the initial mass in the range examined. When non granulated material was used a green density of ~4.5 g/cm^3 was obtained for the same applied pressure, 156 MPa.

8.3.2 Friction Effects: Transmitted Stress

During die compaction of powders frictional forces arise from two main sources; between the material and the die wall and between the particles of the material. The latter is generally restricted to the first stage of compaction. The major source of friction in the compaction process is that between the powder and the die wall. The level depends on the surface condition of the die, the surface characteristics of the feed material and the area of contact between the material and the die wall (MacLeod, 1983).

8.3.2.1 Uranium Dioxide

The uranium dioxide lubricated granules were compacted and the ratio of applied and transmitted stress was measured. The experimental curves showing the transmitted and applied stresses during compaction of these two materials A_{96} and B_{96} were shown in Figure 8.3.

These data were treated following the Janssen analysis (Nedderman, 1982) (see Section 4.2.5) which proposes that:

$$P_t = P_a \exp\{ - 4 \mu_w K_w \frac{H}{D} \} \tag{8.3}$$

where P_t is the transmitted pressure, P_a is the applied pressure, H is the powder height at P_a, D is the die diameter, μ_w is the coefficient of wall friction, and K_w is the ratio of horizontal to vertical stress at the wall. In the logarithmic form equation 8.3 becomes

$$\frac{D}{H} \ln P_t = \frac{D}{H} \ln P_a - 4 \mu_w K_w \tag{8.4}$$

In Figure 8.11 the experimental data have been plotted according to equation 8.4 as (D/H) ln P_t versus (D/H) ln P_a. The Janssen plots for both lubricated powders are quite non linear although the data for powder B are detectably more curved than those of A, which suggests that the values of the coefficient of friction and/or K_w depend on the

pressure field. The analysis is correct in principle but does assume that μ_w and K_w are not functions of the other variables (P_t, P_a, D and H). The data suggest that $\mu_w K_w$ is not a constant and Figure 8.12 illustrates how μ_w varies with the applied pressure if a constant value of the horizontal to vertical stress ratio, K_w= 0.4, is considered.

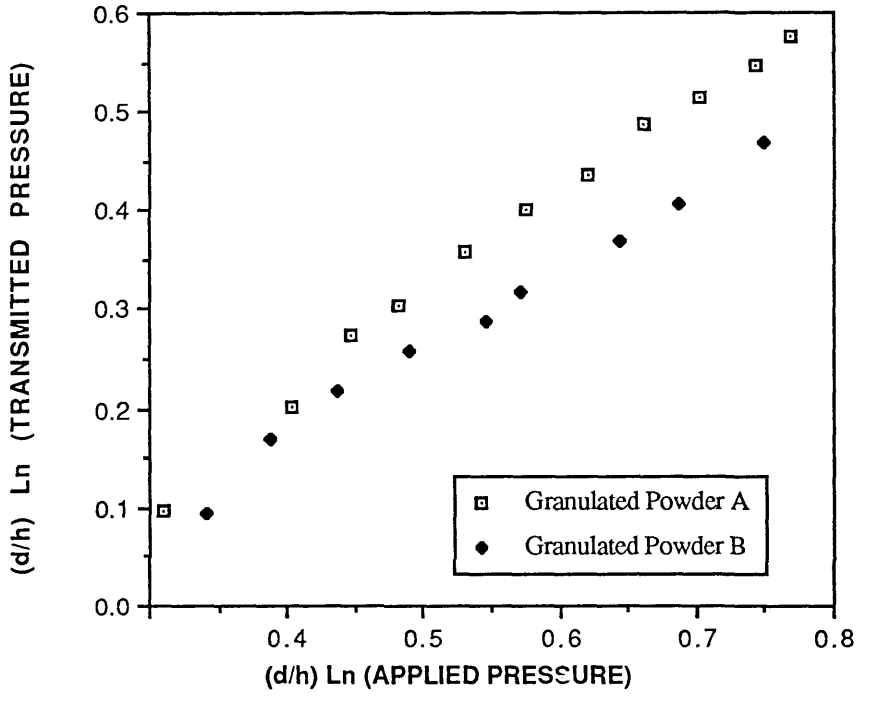

Figure 8.11 Compaction data plotted according to the Janssen equation for the two granulated uranium dioxide powders.

For a very low applied pressure the value of μw decreases with increasing pressure until it reaches a minimum, which corresponds to an applied pressure of 20 MPa. A further increase of the applied pressure causes the value of μ_w to remain almost constant in the case of powder A. The trend in the case of powder B is an increase of the coefficient of friction with pressure. The variation of μ_w with pressure is more pronounced in the case of B. The value of μ_w for A is in all the pressure range smaller than the corresponding value for B.

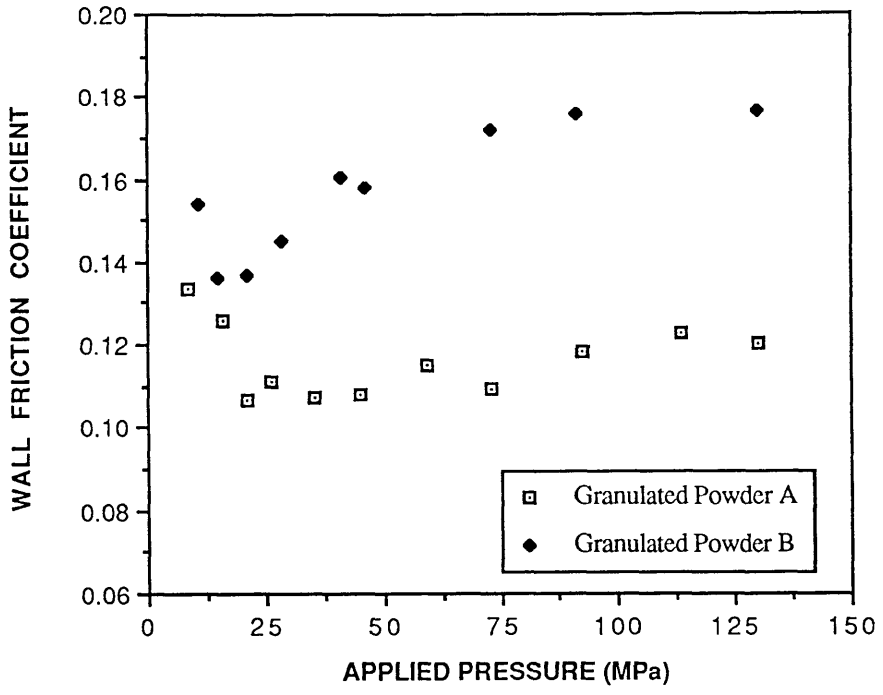

Figure 8.12 Variation of the wall coefficient of friction, μ_w with the applied pressure during the compaction of the two granulated UO_2 powders.

Applying this approximate Janssen analysis to the experimental data and taking the average value of the wall coefficient of friction over the whole pressure range μ_{wA}=0.11(standard deviation 0.0084) and μ_{wB}=0.16 (standard deviation 0.015). These values may be compared with the coefficients of friction obtained for these uranium dioxide systems under lower contact pressure conditions (cf. unconstrained flow of powders and sliding of hemispherical compacts) (Sections 7.3.1 and 7.3.2.1.2). During compaction a lower wall coefficient of friction is obtained due to the higher contact pressures developed during this process.

The ratio transmitted/applied stress is less in the case of B than for A. For A about 1/3 of the applied force is transmitted to the bottom face of the compact. This means that one would expect a greater variation in the stress distribution within the compact of B. It will be shown that this is the case from the results on green characterisation which

are included in Chapter 9. The applied force is not transmitted so easily through the body as a higher proportion of the applied force is being dissipated as frictional force on the walls. This material does not transmit pressure so efficiently probably due to the higher frictional forces which exist between the uranium dioxide particles themselves and the particles and the wall. The data for the case of the uranium dioxide agglomerates, where the lubricant was admixed with the granules instead of coating the die walls as in the case of alumina, zirconia and ferrite materials, show a different pressure ratio for these two uranium dioxide powders. This may be attributed to the less efficient action of the dry mixed lubricant in the case of powder B, and this may arise because of a less effective lubricant distribution.

8.3.2.2 Alumina, Zirconia and Ferrite Powders

This Section considers the role of particle-wall friction in the compaction of some granulated ceramic powders. Alumina, zirconia and ferrite particles coated with two organic polymeric materials (PVA 14,000 and PEG 400) are described.

The dry granules, 212-425 μm, were single-sided pressed using a cylindrical die of 0.0163 m internal diameter. The die walls were in some cases lubricated with zinc or calcium stearate applied evenly onto the die. The amount of ceramic powder used varied from 0.0025 to 0.030 kg to produce a range of initial powder bed height/die diameter ratios, $(H/D)_o$, of between 1 to 7 and compaction pressures of up to 150 MPa were applied. Several experiments were carried out using different materials and conditions. The main experimental variables affecting the transmission of forces studied include: the type of material, the particle size, the type of binder, the use of a lubricant, the initial powder bed height/die diameter ratio and the maximum applied pressure.

The analysis of the experimental compaction data has been carried out using the two different analyses due to Janssen (modified by Walker) and to Spencer. The data have been plotted according to the expression:

$$\ln \frac{P_t}{P_a} = -4 \mu_w K_w \Delta \frac{H}{D} \qquad (8.5)$$

where P_t is the transmitted pressure, P_a is the applied pressure, H is the powder height at P_a, D is the die diameter, μ_w is the coefficient of wall friction, K_w is the ratio of horizontal to vertical stress at the wall, and Δ is the distribution factor. Δ is defined as the ratio between the vertical stress at the wall and the mean vertical stress. This expression is similar to equation 8.4, the only difference is the introduction of the factor Δ.

Figure 8.13 shows that the ratio of transmitted/applied pressure P_t/P_a is not a constant during the whole of the compaction process but it depends on the actual height of the powder bed being compacted. The data correspond to the compaction of Ferrite/Gohsenol and Ferrite/PVA 14,000 granules; the same trend was observed for all the other cases studied. The model proposed by Spencer does not explain the variation of the transmitted ratio observed experimentally as it predicts a constant pressure ratio. Thus, the model proposed by Janssen will be chosen to represent these systems during compaction. It is observed, in Figure 8.13, that as the height decreases, that is as the applied pressure is increased, the transmitted/applied pressure ratio is not constant but follows a peculiar trend. Also a different behaviour for the two different systems is observed. These systems differ only in the type of binder used to coat the ferrite particles.

During compaction the nature of the sliding interface will change as consolidation proceeds and, because of pressure transmission effects, will vary along the length of the compact. In order to describe the microscopic situation at the wall during compaction the adhesion model of friction has been applied to the Janssen-Walker analysis in a semiquantitative manner. On a microscopic scale the interface between material and die wall is not smooth but consists of a series of interacting asperities so that the effective area of contact is only a small fraction of the total surface area. When a normal load is applied across the interface, stresses induced at the asperities cause them to yield, increasing the effective area of contact and thereby supporting the applied load.

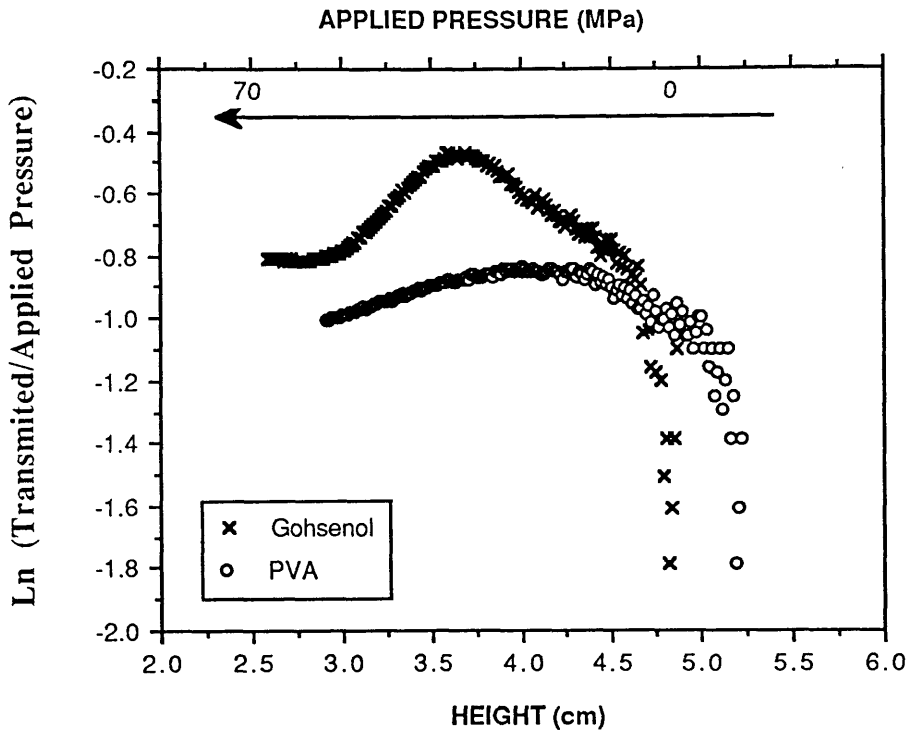

Figure 8.13 Variation of the transmitted/applied pressure ratio with applied pressure shown is the current value of the compact height, H.

As the radial normal stresses increase there will be a corresponding increase in the effective area of contact depending on the yield strength of the material. The effective or real area of contact (A_r) cannot be measured conveniently in practice; this is why much of the published work relating to die wall friction refers to the geometric or apparent surface area, A_{app}, of the die defined by πDH. The use of this geometric area in deriving frictional relationships poses several problems since the ratio A_r/A_{app} varies with the material yield properties as well as with the radial normal stresses (MacLeod, 1983). The adhesion model of friction (Bowden and Tabor, 1950) assumes that the local contact area particle-wall is defined by the type of contact which can be elastic or plastic and the friction force is not generally proportional to the load. From the microscopic analysis one may then proceed to the situation at the wall, i.e., from a single to a multiple contact case. For this analysis it is necessary to estimate the area of contact and the ratio between the real and the apparent area of contact. This ratio is expressed by ζ. The introduction of the adhesion model of friction for the treatment of powder compaction permits a more exact description of the wall coefficient of friction.

The value of μ_w introduced in equation 8.5 is an average value over the whole pressure range and a local value of the coefficient of friction at the wall may be substituted for μ_w. According to the adhesion model of friction

$$\tau = \tau_o + \alpha P \tag{8.6}$$

where τ is the interface shear stress, τ_o and α are material constants, and P is the contact pressure. This equation may be rewritten as

$$\frac{\tau_{wr}}{\zeta} = \frac{(\tau_o + \alpha\, \sigma_{(xx)m})}{\zeta} \tag{8.7}$$

where τ_{wr} is the shear stress at the wall considering the real area of contact, ζ is the real to apparent area ratio, and $\sigma_{(xx)m}$ is the mean radial stress at the wall. The wall coefficient of friction may then be expressed as a function of certain interfacial parameters according to :

$$\mu_w = \frac{\tau_w \zeta}{\sigma_{xx}} \tag{8.8}$$

where τ_w is the apparent wall shear stress. Introducing this expression in equation 8.5 the dependence of the stress transmission ratio on these microscopic characteristics is obtained:

$$\text{Ln}\, P_t = \text{Ln}\, P_a - 4 \frac{\tau_w \zeta}{\sigma_{xx}} K_w \Delta \frac{H}{D} \tag{8.9}$$

An attempt to interpret the observed experimental trends in P_t/P_a, by deducing the variation of the different parameters involved as pressure increases, is now proposed. Figure 8.14 shows qualitatively, the variation of each of these parameters as

compaction proceeds. It is uncertain how the coefficient of pressure at the wall, K_w and Δ, the distribution factor, behave as the radial stress at the wall increases.

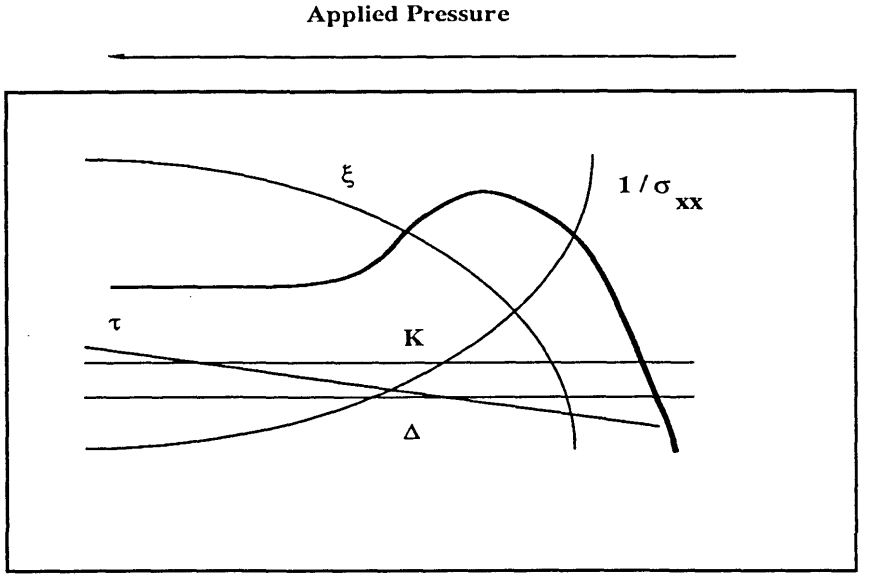

Figure 8.14 Qualitative description of the variation with pressure of several parameters.

The precise definition of the constant K_w is currently contentious. Jenike suggested that it has a value of 0.4 for most materials (Jenike and Johanson, 1969). The variation of the distribution factor, Δ, with the applied pressure is unknown but values of Δ have been calculated when the value of the mean axial stress has reached its asymptotic value. For most systems Δ is close to unity. The real area of contact of the particles-wall interface will increase as the applied pressure increases and as the individual granules are broken down so that the factor ζ most certainly increases with the extent of the compaction. The radial stress at the wall obviously increases as compaction proceeds and the specific shear stress can be expected to increase slightly. As a result, from the combination of all these factors, it can be seen that if one considers the effect

of increased applied pressure on these variables the experimental trend observed may be qualitatively explained. These data obtained from the pressure transmission ratios during the compaction experiment will be correlated with the final properties of the green as assessed by results from the hardness mapping and attrition of compacts (Chapter 9) and it will be shown that the type of surface coating, i.e. the type of binder system applied to the powder, affects the final properties of the compact.

8.3.2.3 Effect of Some Variables on the P_t/P_a Values

The data in Table 8.10, which correspond to the compaction of several materials in a lubricated die under similar conditions, show that the pressure ratio is rather independent of the organic binder which suggests that the frictional force at the wall-agglomerates interface is governed by the lubricant. In the case of the unlubricated dies the pressure ratio is higher for the system that contains PEG (see Table 8.11).

TABLE 8.10 Average Pressure Transmission Ratio Values. Powders Compacted in Lubricated Dies.

SYSTEM	AVERAGE P_t/P_a	$(H/D)_o$
Zirconia/PVA 14,000	0.75	2.5
Zirconia/PEG 400	----	----
Ferrite/PVA 14,000	0.58	2.0
Ferrite/Gohsenol	0.53	2.1
Alumina/PVA 14,000	0.82	1.0
Alumina/PEG 400	0.84	1.1

The effects of the experimental conditions on the average value of the transmitted/applied pressure ratio are summarised in Table 8.11.

TABLE 8.11 Effect of Size, Humidity, Mass, and Lubrication on the Average Transmitted Pressure Ratio.

MATERIAL	SIZE (μm)	$(H/D)_o$	P_t/P_a No Lubrication	P_t/P_a Die Lubrication*
Ferrite				
PVA 14,000	200-425	2.0	0.58	----
Gohsenol	200-425	2.1	0.53	----
Alumina				
PVA 14,000	200-300	4.7	<0.05	0.27
		2.5	0.12	0.58
		1.0	0.41	0.82
PEG 400	200-300	4.7	<0.05	0.26
		2.8	0.17	0.57
		1.1	0.53	0.84
50% PVA 14,000		4.7	0.28	----
50%PEG 400		2.4	----	0.65
		1.2	----	0.79
Zirconia				
PVA 14,000		4.6	0.53	0.29
		2.4	0.77	0.63
		1.1	0.94	----
PEG 400		4.3	0.58	0.25-0.60
		2.7	0.84	0.55-0.85
		1.2	----	0.63-0.91

* Zn stearate in the case of ferrite materials and Ca stearate for alumina and zirconia

There is a clear difference between the case of lubricated and unlubricated dies. Some of these data are also presented graphically showing the variation of the P_t/P_a ratio as a function of the applied pressure for several selected experimental conditions. The same variables were considered in the study of the densification of these powders, see Section 8.3.1.1.1. The granule mean size, Figure 8.15; the humidity content of the powder, Figure 8.16; the initial aspect ratio, Figure 8.17; and the effect of the presence of a lubricant, Figure 8.18 are the aspects considered in this study of the stress transmission.

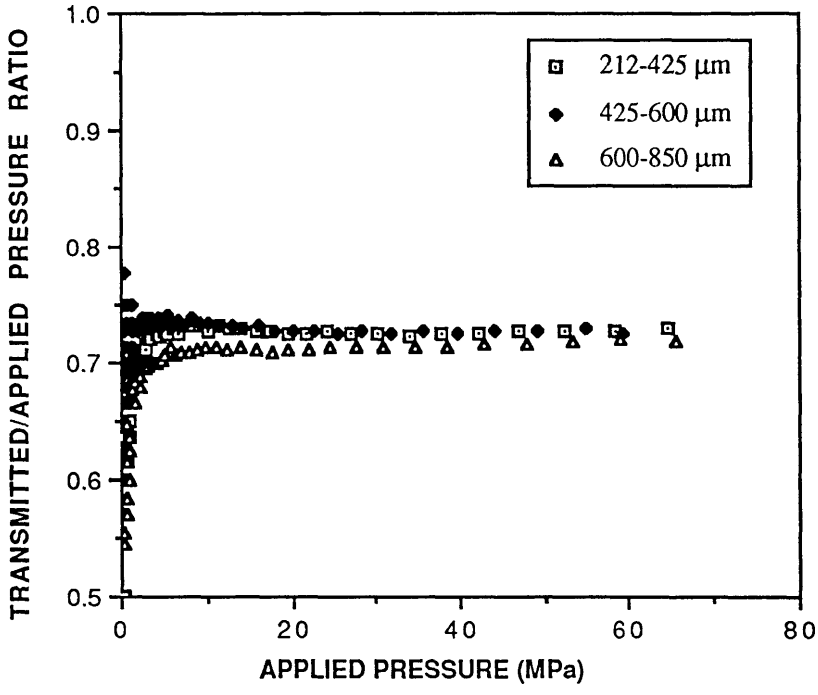

Figure 8.15 Variation of the pressure ratio with the applied pressure for different size fractions of Ferrite/Gohsenol granules. 0.0050 kg pressed to 60 MPa in a lubricated 0.0163 m diameter die.

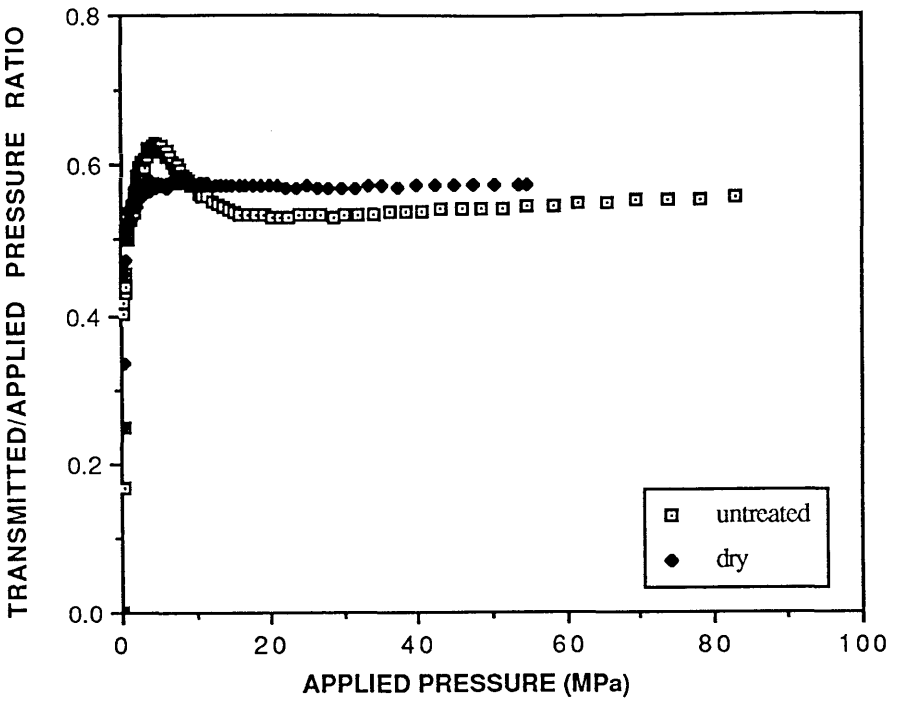

Figure 8.16 Variation of the pressure ratio with the applied pressure for Ferrite/PVA 14,000 untreated and dry granules. 0.0100 kg, 212-425 μm pressed in a lubricated 0.0163 m diameter die.

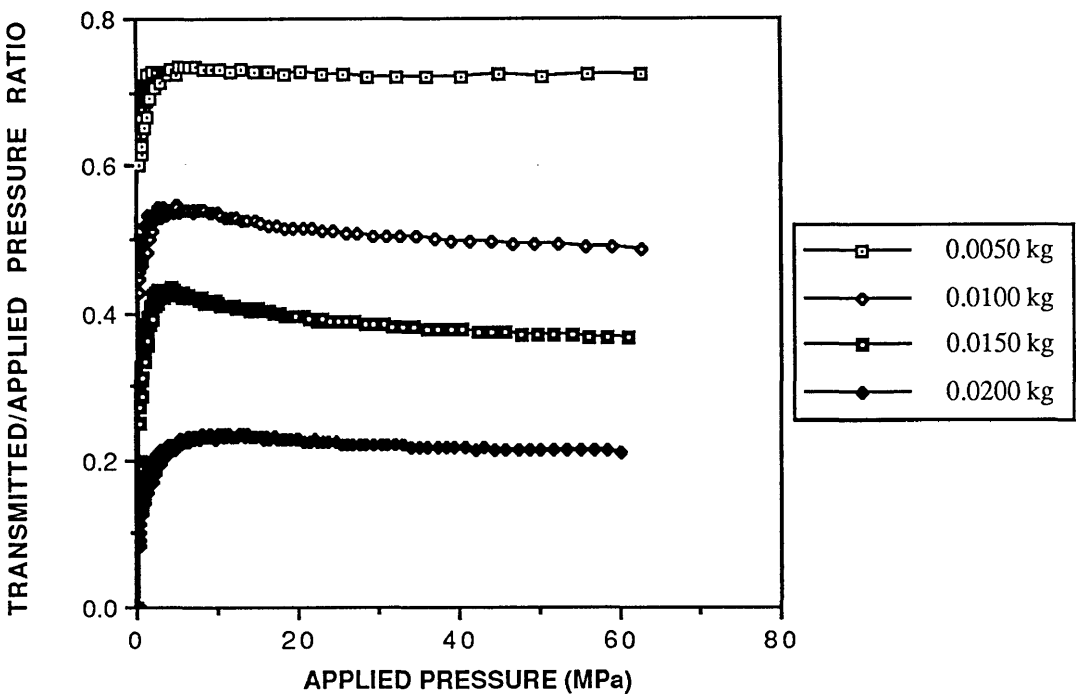

Figure 8.17 Variation of the pressure ratio with the applied pressure for a range of initial amounts of Ferrite/Gohsenol powder pressed up to 60 MPa in a lubricated 0.0163 m diameter die.

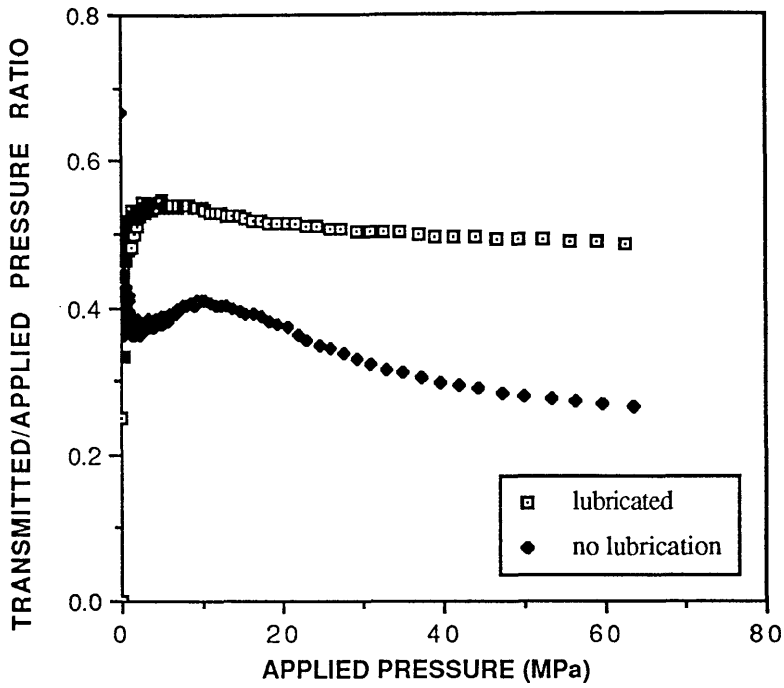

Figure 8.18 Variation of the pressure ratio with the applied pressure for dry, 212-425 μm Ferrite/Gohsenol granules. 0.0100 kg pressed to 60 MPa in a lubricated 0.0163 m diameter die.

8.3.2.3.1 Particle Size

The pressure transmission ratio is not seen to be a strong function of the granule size in the range studied, Figure 8.15. The densification curves corresponding to these three different size range materials, see Figure 8.6, were also similar.

8.3.2.3.2 Moisture Content

In the case of a dry material the transmission pressure ratio is slightly lower than for the case of the non-treated material at low applied pressures but it becomes slightly greater at higher pressures. A plausible explanation to this observed behaviour, Figure 8.16, might be that the lubricating effect of the water present in the material is important only in the initial stages of compaction, during the granule rearrangement process. The

differences observed between both cases, dry material and material kept under atmospheric conditions, regarding not only the pressure transmission but also the densification curves, see Figure 8.7, are not very great. The water content of the untreated material was ca. 0.22%.

8.3.2.3.3 Height/Diameter Ratio

The effect of the initial amount of powder on the transmission of forces is very significant, Figure 8.17. The corresponding densification curves also show this effect, see Figure 8.8. An increasing powder bed height means that the area of contact powder-die wall, where most of the energy dissipation due to frictional effects takes place, increases and as a result the force transmitted to the powder body decreases.

8.3.2.3.4 Lubrication

The effect of adding a lubricant to the die walls on the pressure transmission, Figure 8.18, is an increase on the transmitted/applied pressure ratio and this effect becomes more important as the applied pressure increases. This is a consequence of the increased friction at the die walls when no lubricant is added and the increase in wall friction becomes greater at higher the applied pressures. Also, the presence of a lubricant might facilitate the powder flow during the filling of the die producing a more homogeneous powder bed.

Summarising the findings from these studies regarding the effect of several variables on the pressure transmission as a function of the applied pressure, it has been shown that the two most important variables are the powder aspect ratio and the presence of a lubricant. In order to obtain the most effective transmission of stresses during single sided pressing an effective lubricant and a low aspect ratio should be used. This is exactly the prediction of the P_t/P_a ratio in either model (Janssen and Spencer). The effect of the other variables studied is not so important.

8.3.3 Wall Stresses During Green Ejection

Frictional forces are also present during the ejection process between the compact and the die wall. The same experimental technique used to measure the stresses during the pressing of the powder was used to determine, as a function of time, the force applied to eject the compact. In all the cases the compact was ejected from the same direction as it had been compacted.

8.3.3.1 General Ejection Profile

The profiles of the ejection pressure, P_e, as a function of time were not similar for all the conditions examined, two extremes are shown schematically in Figure 8.19. In certain cases, as pressure was applied, the ejection pressure corresponding to the first compact movement rose steeply to a maximum at point A. This was the recorded value of P_e and defined as static ejection pressure. After movement was initiated, the pressure fell to a new value which remained almost constant throughout part of the ejection process until approximately the compact begins to be ejected out of the die at point B. From this point the ejection pressure decreases steadily until the final compact ejection where it fell abruptly to zero. The values of A and B were dependent on compact H/D ratio, lubrication conditions and compaction pressure. MacLeod and Marshall, 1977 found that point B, which defines the dynamic ejection pressure, is additionally dependent on the rate of pressure application. In the second case encountered, the ejection pressure rose steeply to a first maximum at point a, then the ejection first decreases and then increases to reach a maximum, constant value b, then it drops continuously until the ejection is completed. The difference with the previously described trend is that the pressure in the plateau is higher than the static value. These two experimentally observed trends were of a general character, the second type of behaviour was found when a higher amount of material had been pressed. The two examples presented in Figure 8.19 correspond to the ejection profiles of two Ferrite/PVA 14,000 compacts pressed from 212-425 μm material in a lubricated die to a maximum applied pressure of 75 MPa. In Figure 8.20 the ejection pressure is plotted as a function of the compact displacement from its pressed position in the die. The vertical

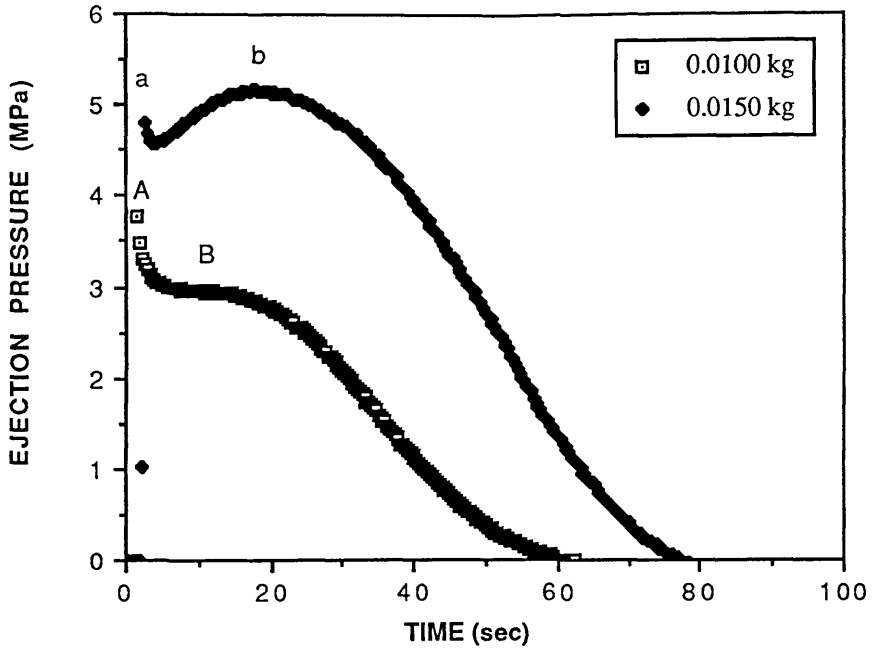

Figure 8.19 Typical profiles of the variation of the ejection pressure as a function of time. Data correspond to the ejection of two Ferrite/PVA 14000 compacts of different mass pressed to 75 MPa with wall lubrication.

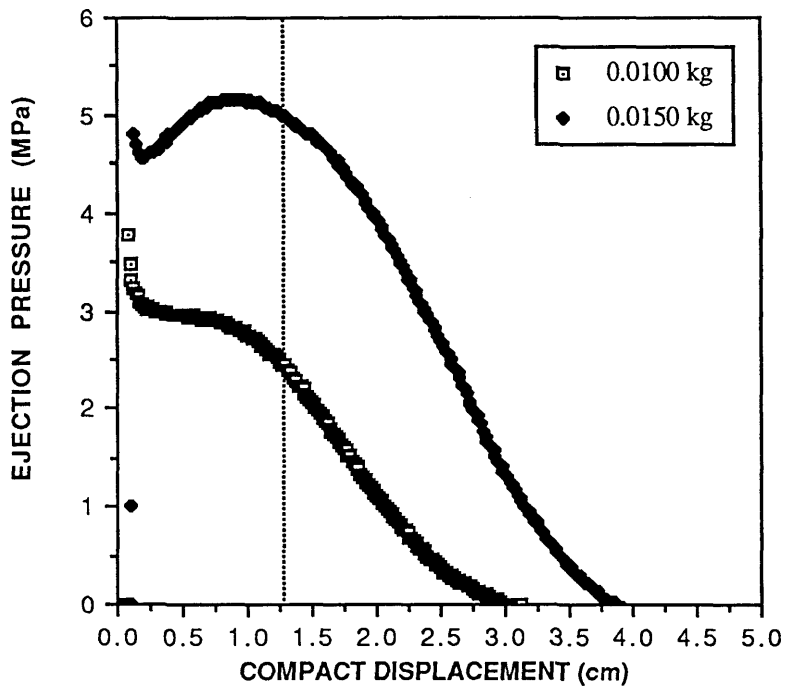

Figure 8.20 Ejection profiles as a function of the compact movement from its pressed position for two Ferrite/PVA 14000 compacts pressed to 75 MPa with wall lubrication.

line indicates the moment when the bottom of the compact begins to emerge from the die. The maximum pressure required for the ejection of each compact from the die, P_e, was recorded and is shown in Table 8.3. The value of P_e varied directly with die-wall frictional forces and was dependent on the compact H/D ratio, the lubrication conditions and on the compaction pressure.

In summary, the trend seen for the high wall friction and high aspect ratio compacts (low stress transmission ratios in compaction) is an increase in the ejection force with increasing displacement prior to the sample leaving the cavity. The inference is that this wall constraint continues to induce a compaction in the sample, or at least maintains a reasonable level of normal wall stress, even when the base platen is removed. The slug may wear as it slides in the die and it may be this loss of material which releases the normal stress as the sample moves towards the exit of the die. The normal wall stresses may of course be released by a slow stress relaxation during the ejection period. In contrast, the low aspect ratio and low wall friction systems in compaction do not appear to be able to maintain the radial wall stress component. The ejection forces show a gradual almost monotonic decrease as the slug moves to the exit of the die. The system is apparently releasing the normal stress on the wall or alternatively the wall traction is not sufficient to induce the compaction process when the base platen is completely removed. In both cases once the samples emerge from the base of the die there is an almost linear decrease in the ejection force with the reduction in the compact-die surface area.

Two sets of experiments were performed to study the influence of the initial powder mass and of the applied compacting pressure on the ejection pressure. Also, the ejection profiles for the case of unlubricated conditions and lubricated die wall under otherwise identical pressing conditions, were studied.

8.3.3.2 Constant Compaction Pressure; Variable Powder Mass

Die-wall friction effects of different binders have been investigated by pressing under a constant maximum applied pressure of 60 MPa compacts of several masses and

recording the ejection force. Ferrite/Gohsenol and Ferrite/PVA 14,000 granules were selected to carry out these experiments. For some cases the dies were not lubricated so that the interfacial friction properties of the binders could be investigated. The effect of compacting the powders under lubricated conditions on the ejection force was also investigated.

8.3.3.2.1 Ejection Profiles

Figures 8.21 and 8.22 show the ejection profiles as a function of the compact displacement for the case of Ferrite/Gohsenol compacts pressed using a die wall lubricant and without a lubricant respectively. The curves correspond to different masses of powder. Several features are worth noting. The maximum ejection pressure is displaced towards higher time or displacement values as the compact mass increases; i.e. it takes longer to reach the maximum ejection force for higher compact masses. The rate at which the ejection force decreases as the compact is being forced out of the die is a function of the compact mass, it increases as the compact mass increases. This is observed for both lubricated and unlubricated compaction conditions. At low compact masses, less than 0.010 kg, the maximum ejection pressure occurs at the beginning of the ejection cycle; it corresponds to the initial movement of the compact in the die. For the higher weight compacts the ejection pressure increases steadily to reach a maximum value as the compact moves toward the end of the die and then it decreases. These correspond to the two general ejection profile types described in Section 8.3.3.1.

In the case of compaction in a lubricated die and a high compact weight, there is an initial decrease in the ejection force; this minimum disappears when the corresponding no lubrication cases are considered. This may be due to the fact that there is no lubricant in that region to decrease the ejection pressure. Leopold and Nelson, 1965 observed a similar result but they only considered the effect of the lubrication conditions and did not take into account the effect of the compact weight on the ejection profile. They explained the differences observed only as a result of lubricating effects. In this work it is shown that the ejection profile is a result of both the compact weight and the lubrication conditions under the constant compaction conditions examined.

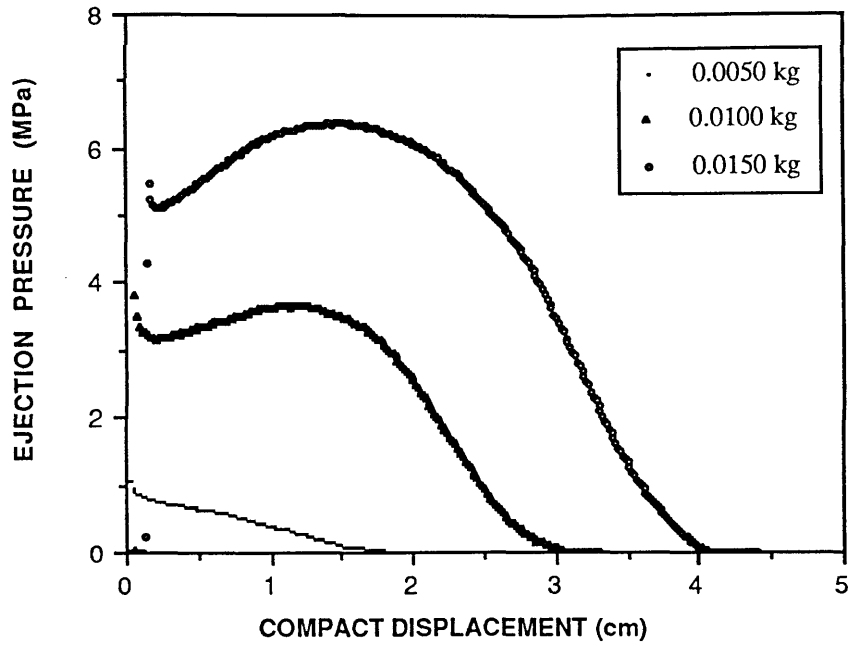

Figure 8.21 Ejection profiles as a function of the compact movement for Ferrite/Gohsenol compacts of several masses pressed to 60 MPa in a lubricated 0.0163 m diameter die.

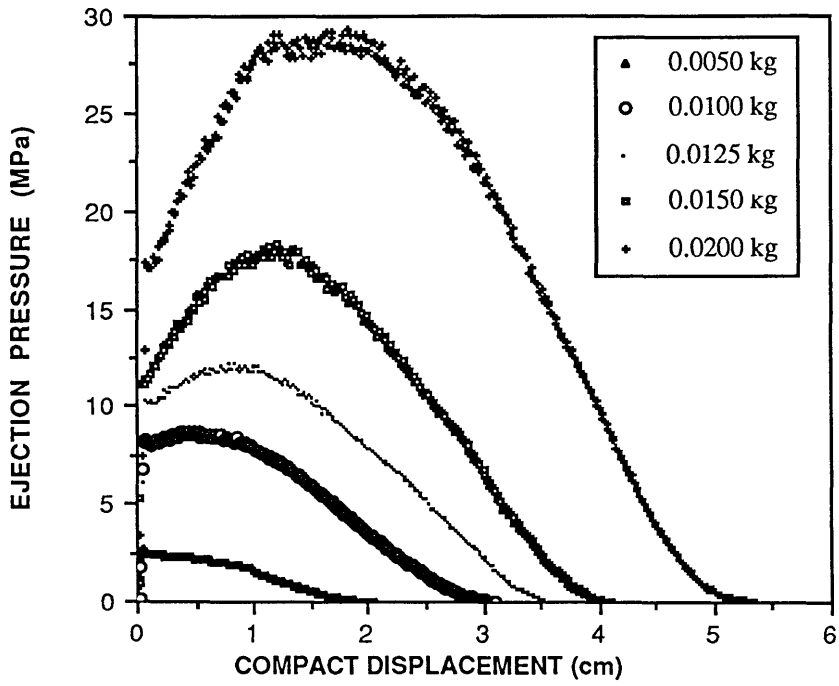

Figure 8.22 Ejection profiles as a function of the compact movement for Ferrite/Gohsenol compacts of several masses pressed to 60 MPa with no lubrication in a 0.0163 m diameter die.

8.3.3.2.2 Area of Contact

The maximum ejection pressure is plotted as a function of the compact surface area in contact with the die wall in Figure 8.23.

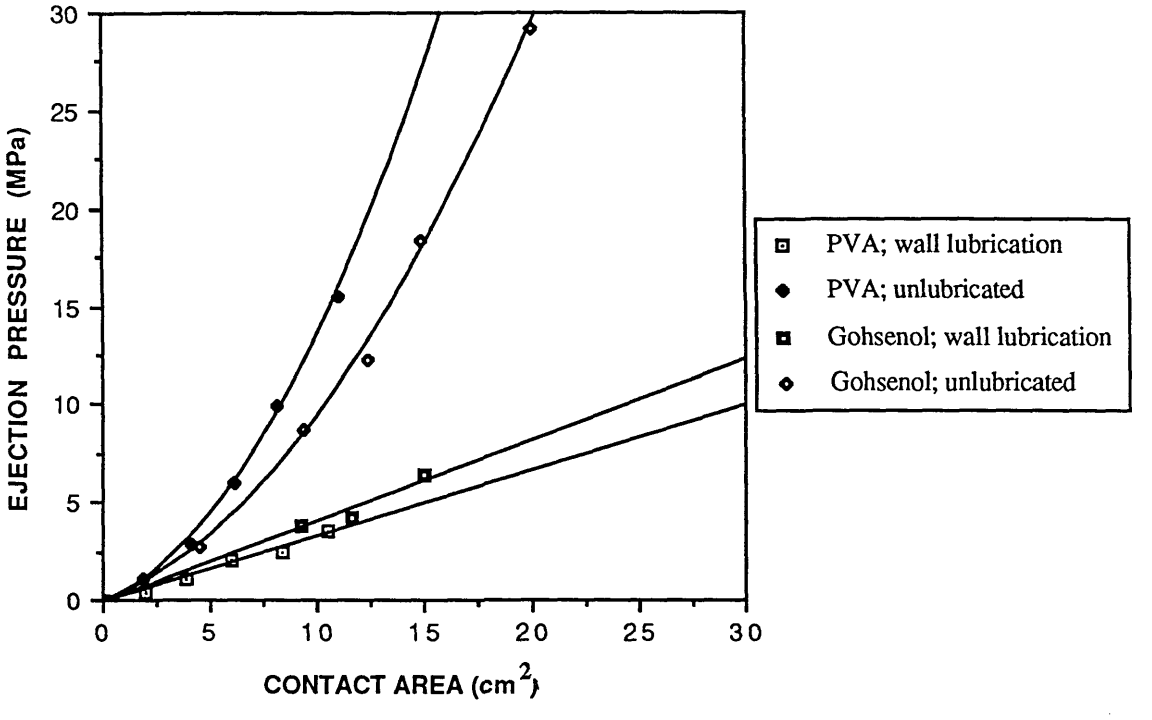

Figure 8.23 Maximum ejection pressure plotted as a function of the geometric area of contact compact-wall for Ferrite/PVA 14,000 and Ferrite/Gohsenol compacts of several masses pressed to 60 MPa under lubricated and unlubricated conditions.

These data correspond to the ejection of Ferrite/PVA14,000 and Ferrite/Gohsenol compacts of several masses pressed to 60 MPa under lubricated and unlubricated conditions. Under constant compact conditions as is the case in the data being discussed in this Section, the area of contact compact-die wall is directly proportional to the powder or compact mass. The use of a lubricant during the pressing stage not only assists the compaction step but also reduces the ejection force.

For die wall lubricated compaction, the relationship between the ejection pressure and the area of contact is nearly linear. Since the surface area is a function of the weight of the compact, this graph indicates that, for lubricated conditions, the ejection pressure is directly related to the area over which the friction is acting and that the wall coefficient of friction is constant. On the basis of a simple analysis the ejection pressure, P_e, may be expressed as

$$P_e = 4\,\tau\frac{H}{D} \tag{8.10}$$

where τ is some mean interfacial shear strength over the whole compact/wall interface, H is the compact height, and D is the compact diameter. τ is sensitive to the contact conditions, such as temperature, velocity of ejection, and pressure. The derivation of this expression assumes that the radial stress normal to the die wall is constant and not a function of compact height and also does not take account of the stress relaxation on unloading. The relationship between τ and pressure is given by:

$$\tau = \tau_o + \alpha\, P = \mu_e\, \sigma_{xx} \tag{8.11}$$

where τ_o and α are material constants, μ_e is the coefficient of friction during ejection and σ_{xx} is the radial stress. On the basis of equation 8.10 a graph of ejection pressure versus H/D or the contact area was plotted (Figure 8.23) for the different binder systems studied. For a powder mass compacted with no lubrication the data is clearly no linear. For the lubricated compaction a linear relationship is obtained. This allows an average value of the interface shear stress to be obtained from the slope of the curve. Inputting this value of τ in equation 8.11 and considering the Janssen analysis to determine the radial stress an approximate value for the coefficient of friction during the ejection of these compacts under these experimental conditions may be obtained. For the ejection of the Ferrite/PVA 14,000 compacts a value of μ_e = 0.05 was thus determined and in the case of the Ferrite/Gohsenol compacts μ_e = 0.07.

For the compaction with no lubrication this relation is not linear, and a non constant coefficient of friction must be assumed in the unlubricated cases. The coefficient of friction does not appear to be linear with either the weight or the surface area of the compact in contact with the die.

The increase of the ejection pressure with the mass of powder pressed may be explained in terms of an increase in the area where the friction forces are acting and subsequently the force necessary to overcome these frictional forces is higher.

8.3.3.3 Constant Powder Mass; Variable Compaction Pressure

In another set of experiments the force required to eject compacts pressed at a range of pressures from a constant amount of powder was recorded. The data presented correspond to the ejection of Ferrite/PVA 14,000 and Ferrite/Gohsenol compacts pressed under lubricated and unlubricated conditions to a range of applied pressures.

8.3.3.3.1 Ejection Profiles

Figures 8.24 and 8.25 show these experimental results for Ferrite/PVA 14,000 and Ferrite/Gohsenol compacts respectively. For a given powder mass the general shape of the ejection profile does not depend on the lubricating conditions existing during the powder compaction or on the compaction pressure applied. When a higher compact weight is considered, Figure 8.24c, the only change in the ejection profile is the development of a small plateau or region where the ejection pressure is constant. This region is not evident for small compact weights, Figure 8.24 a and b and 8.25 a and b. Comparing these curves with the ejection profiles corresponding to compacts of a variable powder mass and a constant compaction pressure presented in Section 8.3.3.2, it may be seen that the resulting ejection curve is a complex function of the compact mass, applied compaction pressure and state of lubrication.

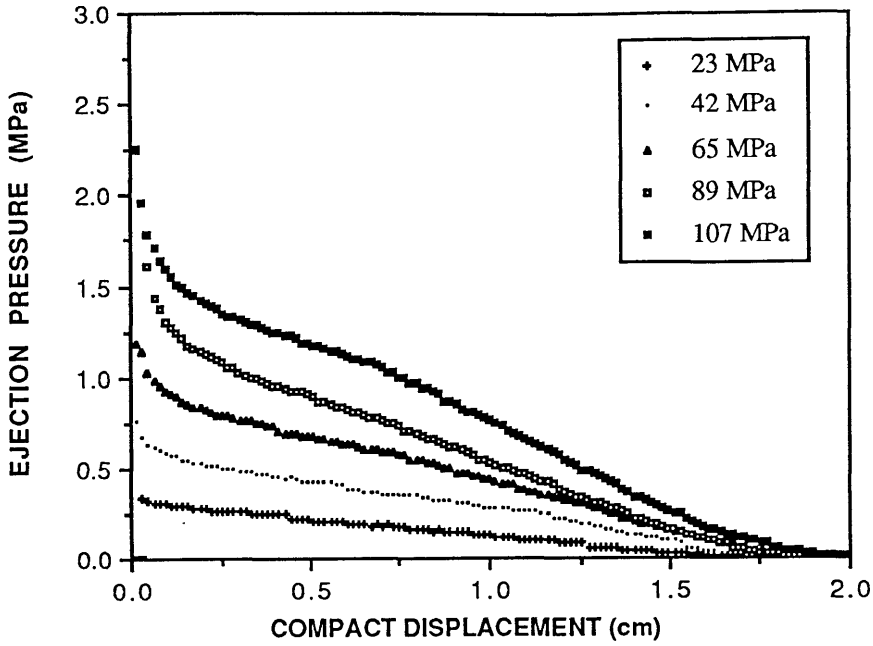

Figure 8.24a Ejection profiles as a function of the compact displacement for a group of 0.0050 kg Ferrite/PVA compacts pressed to several applied pressures in a 0.0163 m diameter lubricated die.

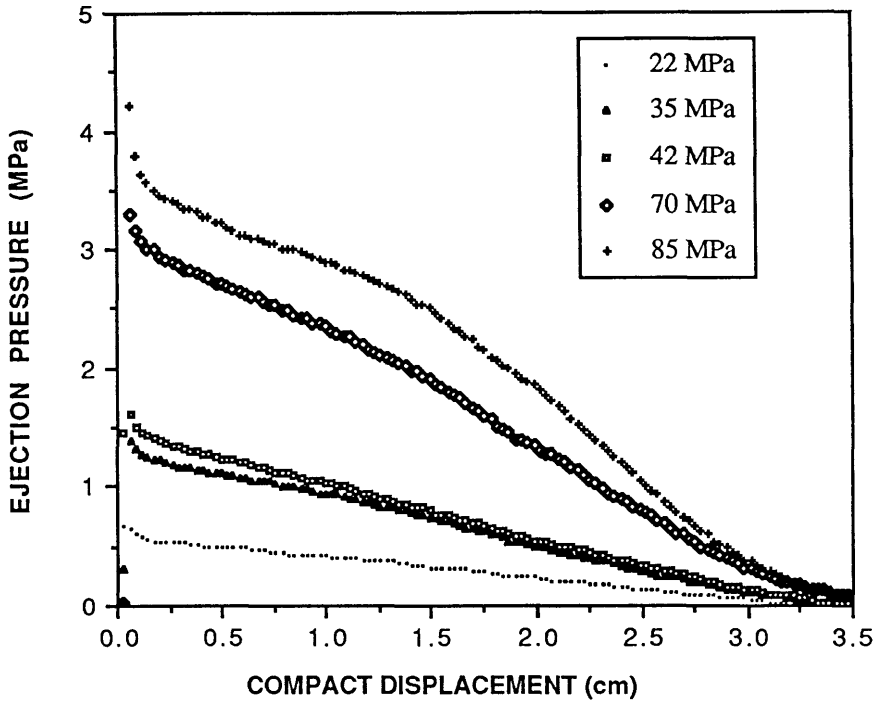

Figure 8.24b Ejection profiles as a function of the compact displacement for several 0.0050 kg Ferrite/PVA compacts pressed to a range of applied pressures under no lubrication in a 0.0163 m diameter lubricated die.

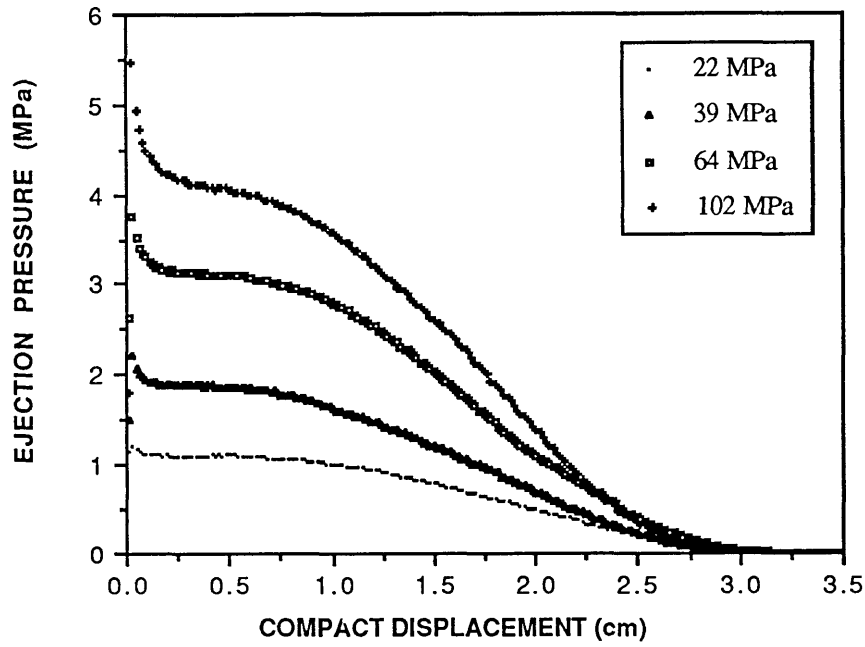

Figure 8.24c Ejection profiles as a function of the compact displacement for 0.0100 kg Ferrite/PVA compacts pressed to a range of applied pressures in a 0.0163 m diameter lubricated die.

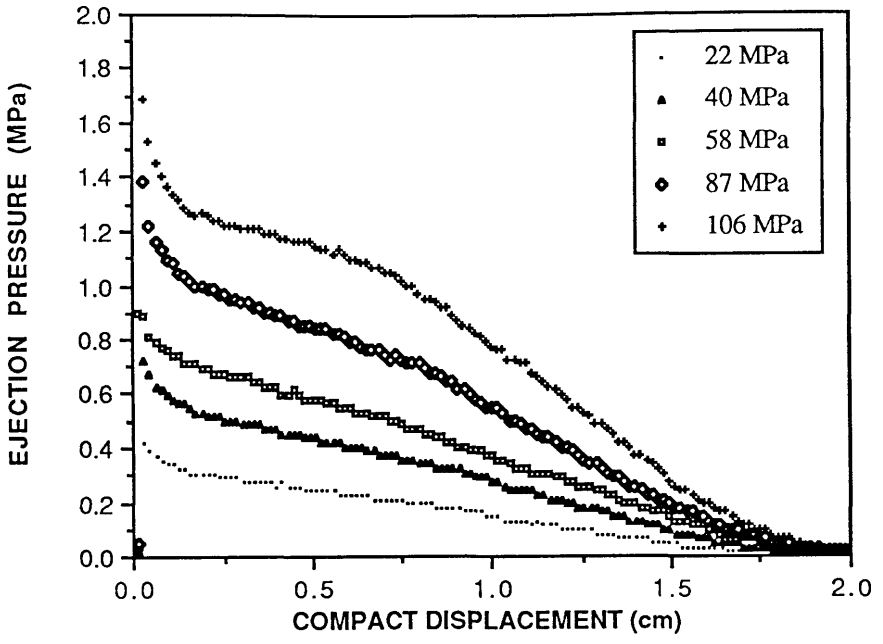

Figure 8.25a Ejection profiles as a function of the compact displacement for a series of 0.0050 kg Ferrite/Gohsenol compacts pressed to several applied pressures in a 0.0163m diameter lubricated die.

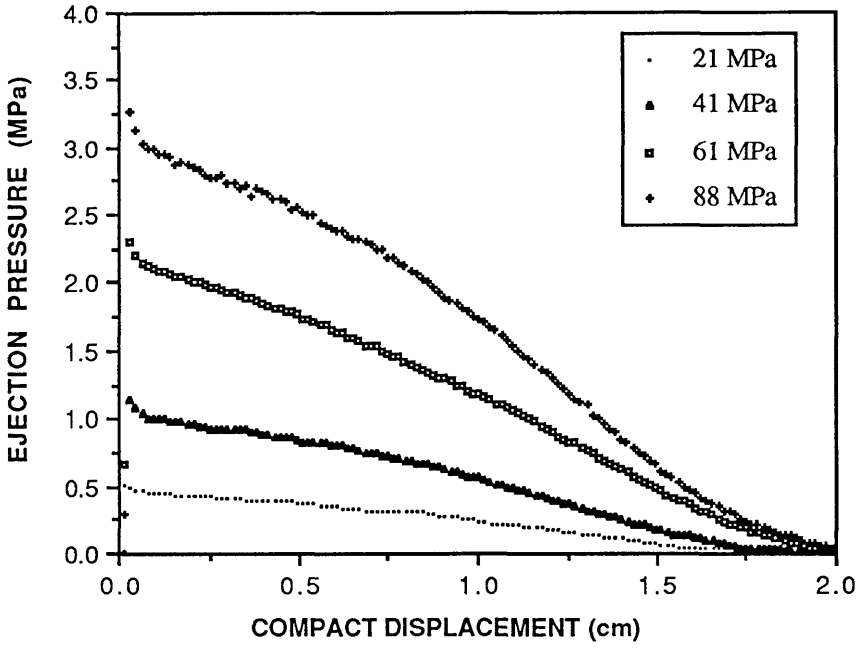

Figure 8.25b Ejection profiles as a function of the compact displacement for several 0.0050 kg Ferrite/Gohsenol compacts pressed to a range of applied pressures under no lubrication in a 0.0163m diameter die.

8.3.3.3.2 Compaction Pressure

Figures 8.26 show the variation of the maximum ejection pressure as a function of the pressure applied to compact the powder for a constant powder mass pressed under wall lubrication and unlubricating conditions. In all the cases studied the ejection pressure increases in a non linear way with the compaction pressure and as it is expected the ejection pressure for unlubricated compaction was higher than when a lubricant was used, Figures 8.26a and c. Also, from Figure 8.26b the effect of powder mass on increasing the ejection pressure is observed. The ejection pressure was normalised by the compaction pressure and the results were plotted as a function of the compaction pressure, Figure 8.27a and b. In general, it is observed that the ejection/compaction pressure ratio is almost constant for the lubricated cases and increases with the compaction pressure for the unlubricated conditions.

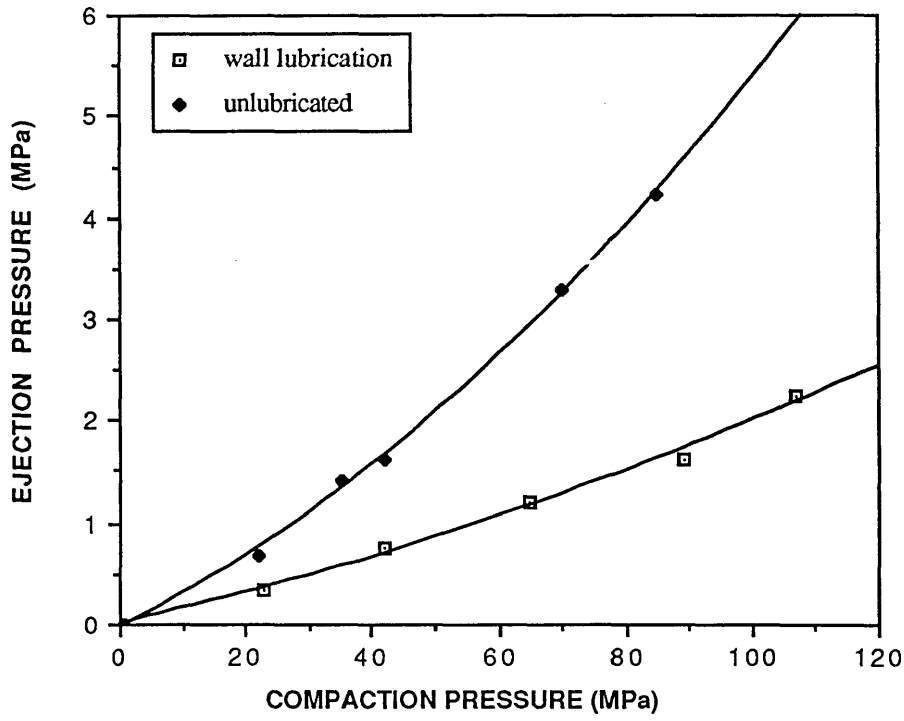

Figure 8.26a Ejection pressure plotted as a function of the applied compaction pressure for Ferrite/PVA 14,000. 0.0050 kg compacts pressed to several pressures under lubricated and unlubricated conditions in a 0.0163 m diameter die.

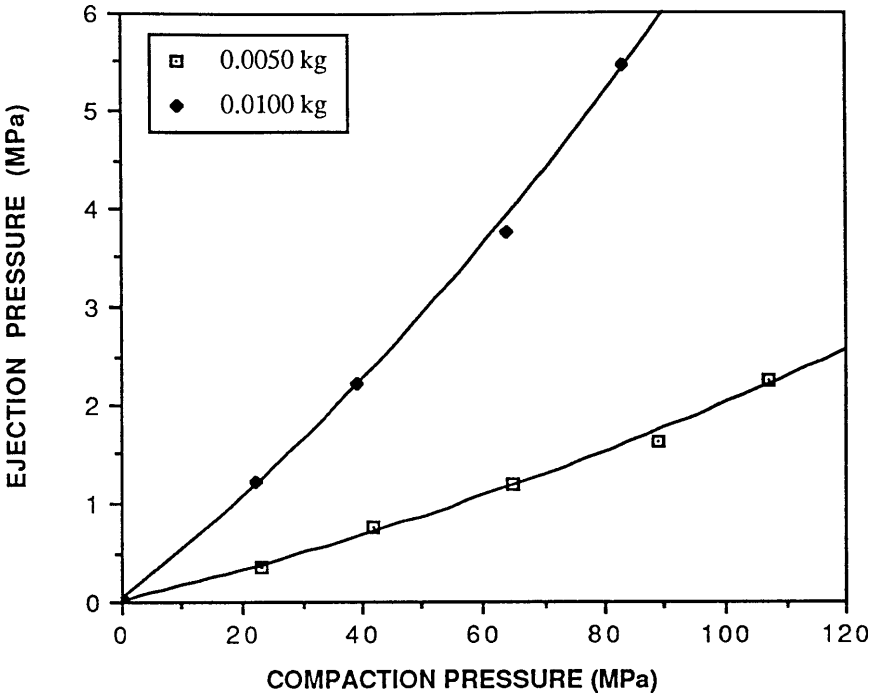

Figure 8.26b Ejection pressure plotted as a function of the applied compaction pressure for two Ferrite/PVA compacts of different weight pressed to several pressures in a lubricated 0.0163 m diameter die.

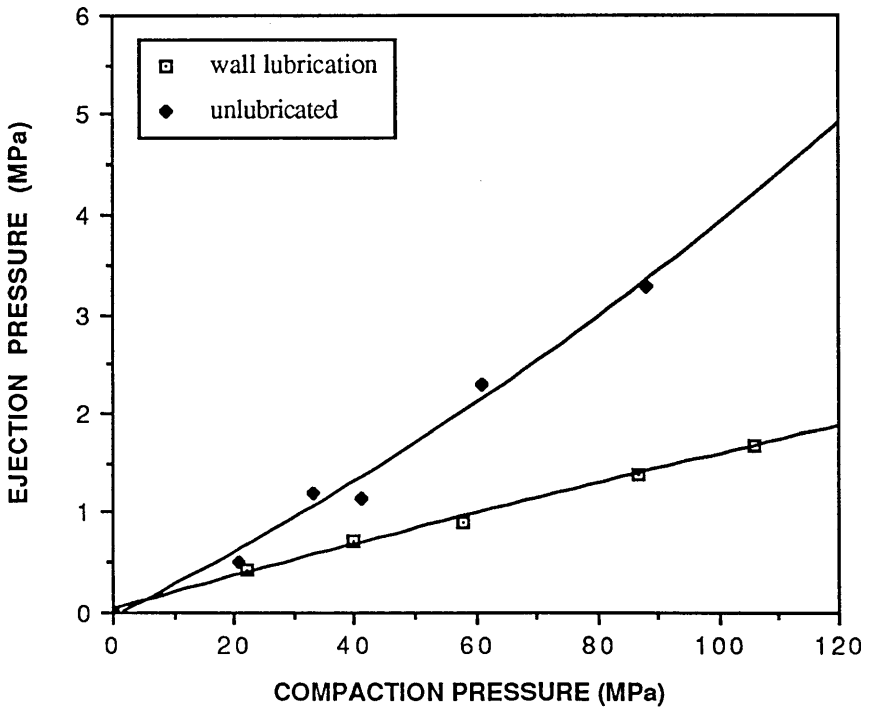

Figure 8.26c Ejection pressure plotted as a function of the applied compaction pressure for Ferrite/Gohsenol compacts. 0.0050 kg pressed to several pressures under lubricated and unlubricated conditions. D=0.0163 m.

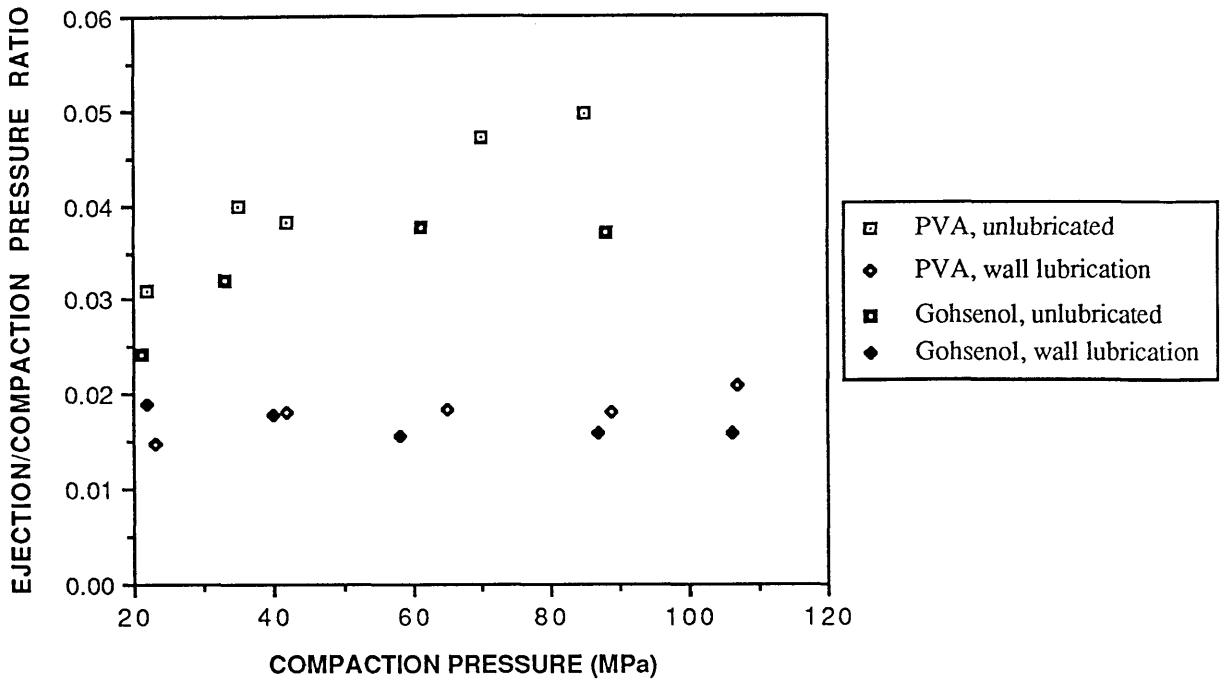

Figure 8.27a Ejection/compaction pressure ratio plotted as a function of the compaction pressure for 0.0050 kg Ferrite/PVA and Ferrite/Gohsenol compacts pressed under lubricated and unlubricated conditions.

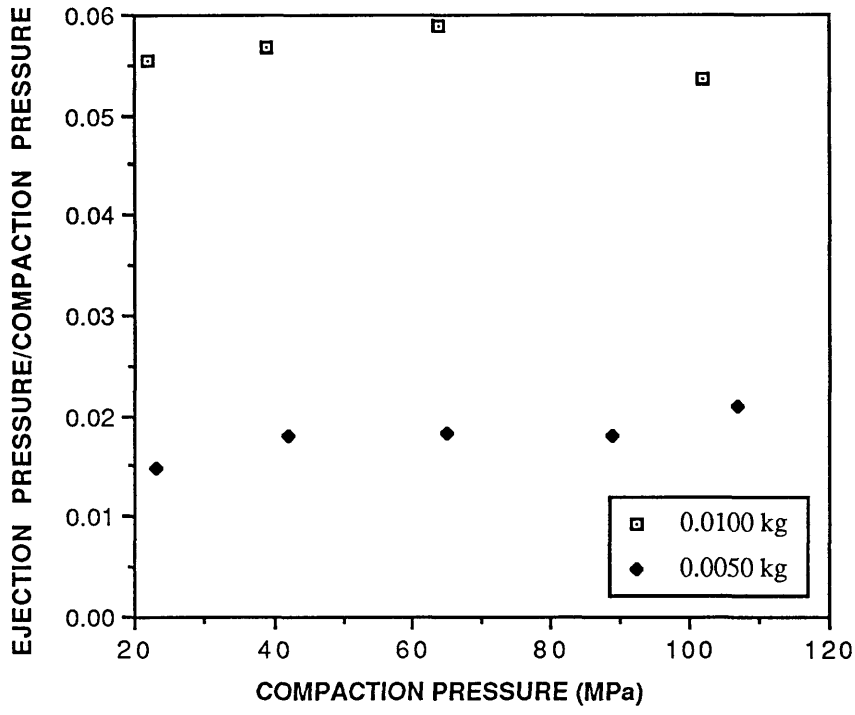

Figure 8.27b Ejection/compaction pressure ratio plotted as a function of the compaction pressure for two Ferrite/PVA14000 compacts pressed in a lubricated 0.0163 m diameter die.

8.3.3.3.3 Area of Contact

When a constant compaction pressure was applied to press different amounts of powder it was noted, Section 8.3.3.2.2, that the ejection pressure increased with the area of contact compact-die wall. For compacts of a constant mass pressed to a range of compaction pressures, the opposite is observed. The ejection pressure increases as the area of contact compact-die wall decreases, Figure 8.28. As the powder is pressed to higher pressures, the compact height decreases but the compact density increases and a higher force is required to eject the compact. Also, the ejection process takes a longer time to complete. This is observed for both lubricated and unlubricated compaction conditions. In these cases the situation may be better described in terms of the radial stresses developed during the compaction. A higher compaction pressure involves higher radial and friction stress at the die walls. During the ejection process these two stresses have to be overcome and consequently the force necessary to eject the compact is higher for higher compaction pressure as the stresses developed during compaction were higher.

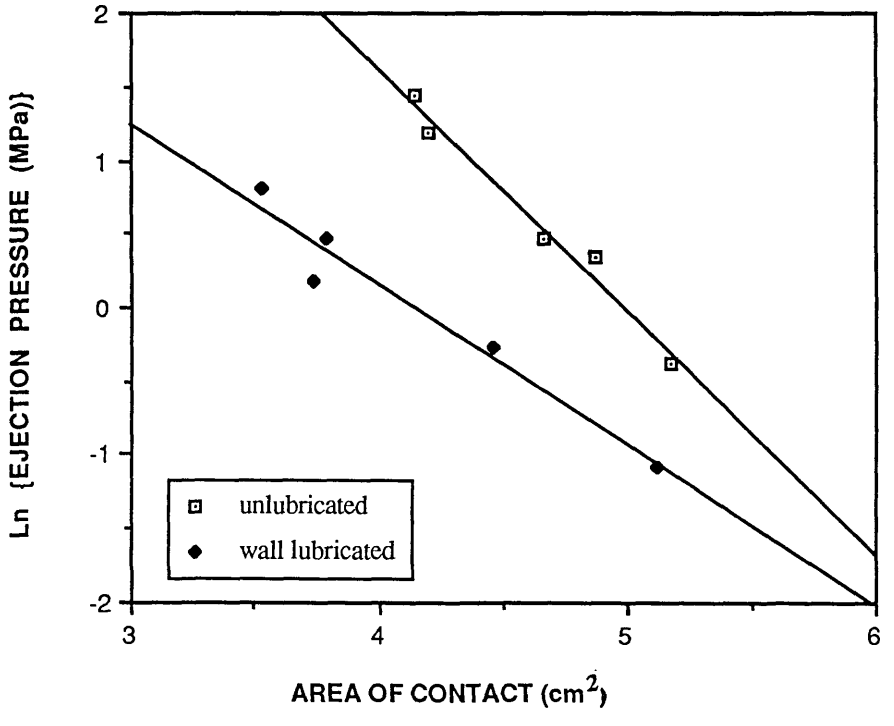

Figure 8.28a The logarithm of the ejection pressure is plotted as a function of the area of contact for 0.0050 kg Ferrite/PVA 14,000 compacts pressed to several compaction pressures in a lubricated and unlubricated die.

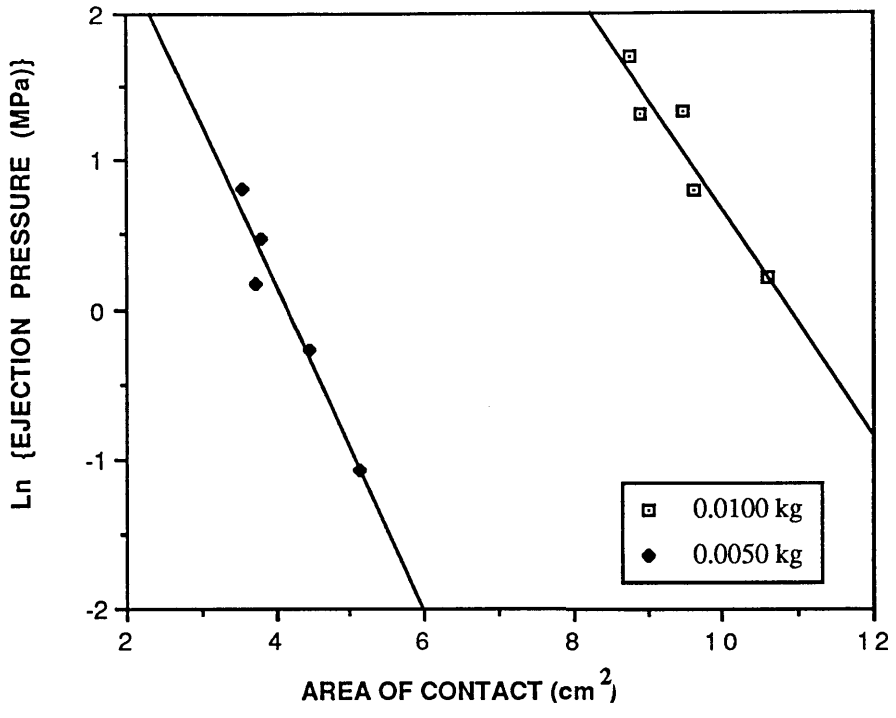

Figure 8.28b The logarithm of the ejection pressure is plotted as a function of the area of contact for Ferrite/PVA 14,000 compacts of two different weights pressed to several pressures in a lubricated 0.00163 m diameter die.

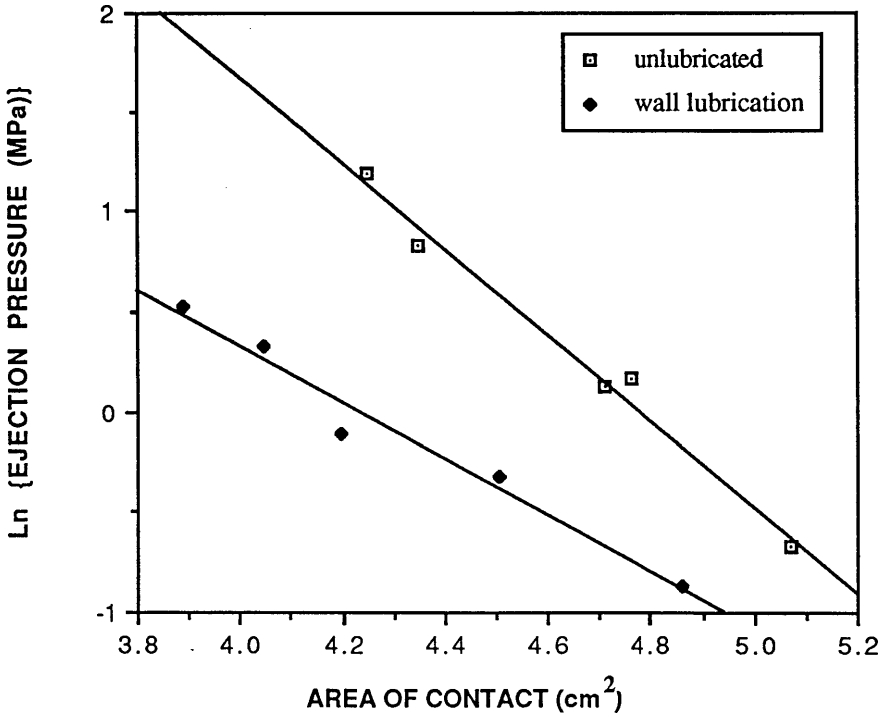

Figure 8.28c The logarithm of the ejection pressure is plotted as a function of the area of contact for 0.0050 kg Ferrite/Gohsenol compacts pressed to several pressures under lubricated and unlubricated conditions. D=0.00163 m.

The ejection pressure may be expressed as a function of the area of contact as

$$\text{Ln } P_e = -k \pi D H \tag{8.12}$$

where k is a constant, D is the die diameter and H is the compact height. This expression is similar to that proposed for constant compaction conditions by MacLeod and Marshall, 1977 who observed that

$$\text{Ln } P_e = k' H/D \tag{8.13}$$

From these two types of experiments the effects of compaction pressure and mass of powder on the ejection pressure both under lubricated and unlubricated conditions have been investigated.

8.3.3.4 Granule Size

Ferrite/Gohsenol granules of three different size ranges; 212-425; 425-600 and 600-850 μm were pressed to a constant compaction pressure of 60 MPa. Two different initial powder masses, 0.0025 and 0.0050 kg were used. The data corresponding to the ejection of these compacts pressed under die wall lubrication and unlubricating conditions are presented in Figures 8.29 and 8.30 respectively.

The shape of the ejection profiles is quite similar for all the cases studied. The ejection pressure is maximum at the beginning of the ejection process. The effect of a lubricant in reducing the pressure required to eject the compact is also evident. The ejection pressure is higher in the case of a higher compact weight. A small plateau or region of constant ejection pressure is observed only in the lubricated cases, Figure 8.29.

The effect of particle size on the ejection pressure values is considered negligible for the lubricated compacts, Table 8.12. A very similar force is required to eject these compacts. When the data corresponding to the ejection of unlubricated compacts are

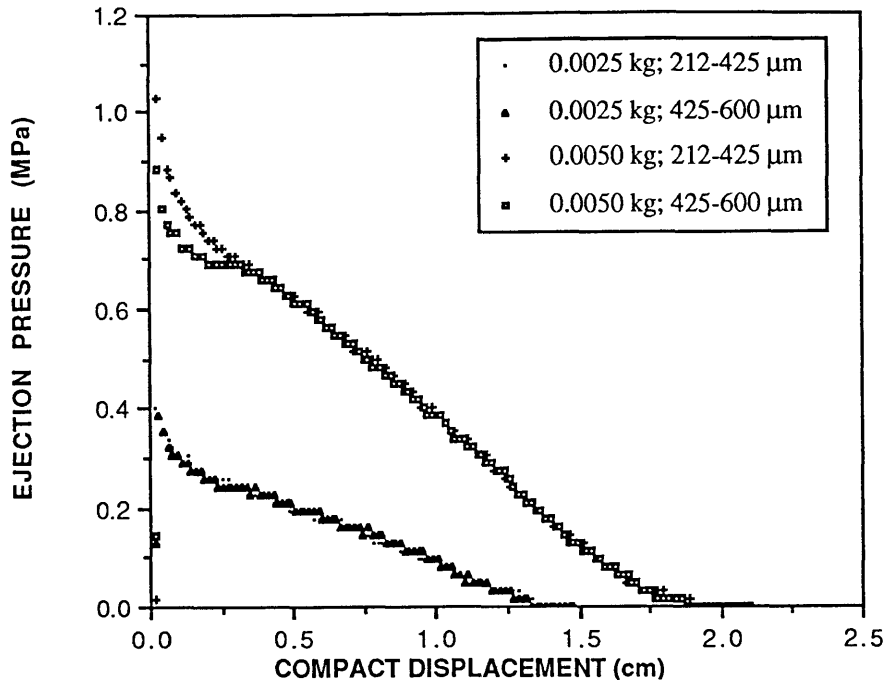

Figure 8.29 Ejection profiles as a function of the compact displacement for several Ferrite/Gohsenol compacts pressed in a lubricated die to 60 MPa. Data correspond to different compact masses and different powder sizes.

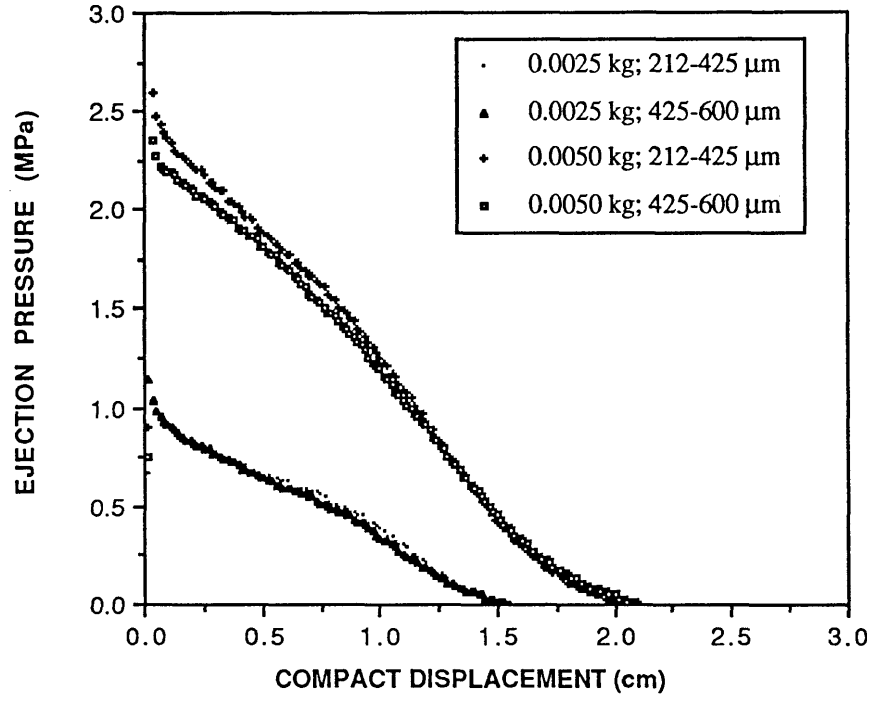

Figure 8.30 Ejection profiles as a function of the compact displacement for Ferrite/Gohsenol compacts pressed to 60MPa under no lubrication. Data correspond to different compact masses and different powder sizes.

considered, the ejection pressure is maximum for the compact pressed from the medium sized granules; 425-600 μm.

TABLE 8.12 Ejection Pressure Values for Compacts Pressed from Several Sized Particles.

Mass (kg)	Granule Size (μm)	Ejection Pressure Lubricated (MPa)	Ejection Pressure No Lubricated (MPa)
0.0025	212-425	0.40	1.05
	425-600	0.39	2.24
	600-850	0.43	1.14
0.0050	212-425	1.03	2.59
	425-600	0.88	3.14
	600-850	1.05	2.35

8.4 SUMMARY AND CONCLUSIONS

This Chapter has dealt with the compaction of some selected ceramic/binder systems. The interface friction and deformation characteristics of the organic species and of the agglomerated powders at high contact stresses, the pressure-volume relationship and stress transmission in single sided die compaction have been investigated. The ejection of the compacts from the die has also been studied under several experimental conditions. Two established models, due to Janssen and to Spencer, have been used to describe the compaction data in conjunction with a simple friction model. A first order estimate of the role and magnitude of the wall friction in compaction has been modelled by adopting a modified friction model based upon the interfacial shear of the organic coating at the walls of the containers or dies. The results

have shown that there seem to be several relationships between the agglomerate strength and their pressure-density behaviour in compaction. In addition there is an interrelationship between the interface properties of the agglomerates and their stress transmission during compaction. The data indicate that the processing aids significantly modify the stress transmission during compaction.

The ejection of the compacts from the die has also been investigated under several different conditions.

From this analysis the following conclusions can be drawn:

- The effect of several variables on the pressing of several powders and on the green ejection has been determined. The variables considered include the particle size, the moisture content, the type of binder, the lubricating conditions, the aspect ratio and the applied load.

- A semilogarithmic linear relationship between the green density and the applied compaction pressure accurately describes the compaction behaviour of the ceramic powders under the conditions studied. The yield pressure values deduced from this empirical relationship reflect the strength of the granules.

- The Kawakita constants a and b are valid parameters to describe the pressing behaviour of a system. The value of b is directly related to the level of friction during compaction.

- The variation of the transmitted/applied pressure ratio with height during compaction may be explained using the Janssen theory allowing for the variation of the friction coefficient with applied pressure. The interface friction may be modelled by using a simple mechanical model of the interface and the adhesion model of friction. The interfacial wall-particle friction is defined by the surface coating. A proper choice of processing aids to coat the ceramic particles will optimise the pressure transmission during compaction.

- The prediction of the stress/density variations as described by the pressure transmission ratio requires the knowledge of the shear stress at the wall, the real to apparent area of contact ratio, the radial stress at the wall, the distribution factor and the coefficient K_w. It is believed that it is the real to apparent area of contact ratio that has a greater influence.

- The force necessary to eject the compact from the die is a complex function of the pressing conditions, mainly the amount of powder, the compaction pressure, and the lubricating conditions. The shape of the ejection profile depends mainly on the powder mass. Two general types of ejection profiles have been described.

- For a constant compaction pressure, the ejection pressure increases with the mass of the compact, i.e. with the area of contact compact-die wall. In the case of lubricated walls a constant coefficient of friction may be assumed. Approximate values of 0.05 and 0.07 for the coefficient of friction during ejection of lubricated Ferrite/PVA 14,000 and Ferrite/Gohsenol compacts respectively were determined.

- For a constant mass of powder pressed, the ejection pressure increases with the compaction pressure, due probably to the higher radial stresses developed during the pressing stage or higher real contact area.

- The presence of a lubricant during the compaction decreases the ejection pressure due to the reduction of frictional effects at the powder die interface.

CHAPTER 9

GREEN CHARACTERISATION

9.1 INTRODUCTION

The ceramic powders have been uniaxially pressed into cylindrical shapes to produce a compact or "green". The area of interest in this study was to characterise the green piece and to correlate the properties of the pressed component with the characteristics of the initial powder and with the pressing process variables. The green body is the precursor of the fired body, and consequently the quality of the final product depends heavily on the detailed characteristics of the unfired body.

There are several well established methods to characterise the green and many attempts have been made to relate the green quality to the previous processing steps. Two types of experimental measurements have been applied to the present study of the compaction process:

1.- The measurement of the change of properties whilst the pressing process is in operation such as force-displacement characteristics and stress transmission.

2.- The examination of the end product after the forming pressure has been applied and released and the compact extruded from the die. This includes measurements such as the density and the hardness of the compact. To cover the whole pressure range these measurements are taken from compacts pressed to various levels of pressure and the necessary interpolations made.

The first group of measurements was reviewed in Chapter 4. This Chapter will concentrate on the latter type of measurements. A review of the main methods proposed in the literature will be presented and a new method based on the controlled attrition of the green will be introduced. Also, some experimental results will be presented. These data will be correlated with the friction characteristics of the powders, especially during compaction. The effect of the stress transmission during die-pressing on the resulting density distribution in the compact will be analysed.

9.2 LITERATURE REVIEW

9.2.1 Types of Measurements

The compact produced by pressing must have an adequate physical durability to withstand the stresses generated during handling, transportation, etc. One of the main properties of interest for the overall quality of the green piece is the strength or toughness which is usually measured by means of a diametral compression test (Carstensen, 1984). Brewer *et al.*, 1981 examined the densification and green strength of compacts pressed from manganese zinc ferrite agglomerates containing different levels of PVA and absorbed moisture. The green fracture tensile strength of specimens was determined in diametral compression and in three-point bending of pressed bars. It was observed that the green strength increased with compact density and was higher for compacts initially pressed from powders stored at a greater %rh, and with greater concentration of PVA. This type of study attempted to interrelate the applied external pressure and the average density/porosity of the compacted mass. An important drawback to this type of approach is that it only provides an average value of a property to characterise the green which is invariably an inhomogeneous entity. Thus, a more complete study of the characteristics of the resulting green involves the evaluation of the stress and density distributions inside the compact.

Several authors have approached the problem of determining the density gradients developed in the green as a result of the die wall friction which restricts flow on compaction. These effects cause the stress gradients and hence the density gradients to

be produced throughout the compact. The assessment of the pressure fields within a compact without interfering with the consolidation process itself requires special precautions. The problem has been approached from evaluating external measurements. This has involved sensing punch pressures, piston displacement and die distortion for various die geometries (Spencer *et al.* 1950; Walker, 1923a, b, c; Duwez and Zwell, 1949; Huffine and Bonilla, 1962). Measurements on the compact after forming and being extruded from the dies have included measurements of microhardness and density determinations (Van Groenu, 1983; MacLeod and Marshall, 1977; Walker, 1923; Kandeil *et al.*, 1977); the observation of the distortion of easily detected heterogeneities, usually in the form of a grid or network of lead particles inserted before compaction and measurements of the stresses during the pressing process (Reed and Runk, 1976; Kandeil *et al.*, 1977; Orr, 1966). This latter approach has been followed by Train, 1957 and by Takada *et al.*, 1976 who used a scattered-light photoelastic technique to measure the distribution of normal stresses at the die wall. Other authors have made calculations based on the limiting stress state assumption on regarding the compacting powder as a rigid-plastic material (Schwartz and Weinstein, 1965); and Strijbos and Vermeer, 1978 used a model based on the finite element method to calculate the boundary stresses occurring during one-sided die compaction for a theoretical, two-dimensional compact. A review of the study of pressure transmission during compaction is given by Orr, 1966. Also, Kandeil *et al.*, 1977 made a critical evaluation of a number of experimental techniques used in the study of density distributions.

9.2.2 Stress/Density Pattern Distributions in a Compact

Train, 1957 has made a definitive contribution to this area of research. It is of interest for me to note that he carried out his research in the Department of Chemical Engineering, Imperial College in all probability just a few metres away from where I carried our my research (Oackley, 1987). He developed a manganin wire resistance gauge to measure the pressure response developed at selected points within a particulate mass under compaction. He carried out the first recorded experimental measurements within a powder mass during the compaction process. Before, only indirect methods,

mainly the measurement of apparent density and hardness, were available to determine the pressure developed at a point within a compact. Evidence for the development of a complex stress pattern in a mass of particulate material when compacted in a cylindrical die was confirmed by determining the relative density distributions in a number of compacts pressed to various levels within the pressure range. A close relationship was found to exist between the local pressure developed and the apparent density produced at a given point within a compact.

The measurements of pressure distributions for the single sided compaction of powders obtained by different authors (Train, 1957; MacLeod and Marshall, 1977; Kandeil *et al.*, 1977; MacLeod, 1983) revealed that the density is at a minimum at the outer circumference of the compact adjacent to the bottom, stationary punch. The mean density decreases with increasing distance from the moving punch, but a dense core of material exists on the compact axis near the stationary punch which is in many cases denser than the material directly between it and the moving punch. Those parts of the compact subjected to little movement, such as the peripheral zone adjacent to the bottom stationary punch and the axial zone adjacent to the top moving punch, are the less dense due to the absence of shear forces. While the denser areas correspond to the zones where conditions of strong shear forces are developed.

9.2.3 Explanation of the Development of the Pressure Pattern

The development of pressure during pressing has been explained by Train, 1957 who proposed a simple explanation for the observed patterns of density distribution based on the development of high density wedges of material owing to high shearing forces at the die wall adjacent to the moving punch. Figure 9.1 represents the forces developed in the compact as described by Train. The pressure develops as it does largely because of the resisting and frictional effects of the walls. If the die were of infinite extent laterally, the pressure distribution would follow the "pressure bulb" profiles advanced by Boussinesq, 1876 (in Train, 1957). In essence the pressure would radiate in approximately hemispherical lines from the source of the force. The walls of a die, however, prevent such an expansion, and the sliding of the powder

along them creates resisting forces. As the top punch descends, material is forced into the zones around the top corners giving rise to the intense local stresses. Because of symmetry, the tangential forces cancel one another. At equilibrium conditions the upwards component of the axial force, z, is resisted by the punch and that downward, y, by the reaction of lower layers of particles. For the case of the radial force, the radial component outward x is supported by the die and the inward one w by the reaction of the central powder mass. The resultant force v of the reactions w and y is directed diagonally toward the lower centre of the compacting mass. There the v forces combine to give the resultant t that is greater than the individual components and create the region A of high pressure and density. The region B is established at the same time as one of low pressure and density because this area is subjected to negligible shearing forces and is partially protected from the axial normal pressures by the vaulting effect of the high density wedges. Area C adjacent to the stationary punch undergoes no movement relative to the die wall so shearing forces will be absent and the density will be low since consolidation will depend on transmitted axial forces only.

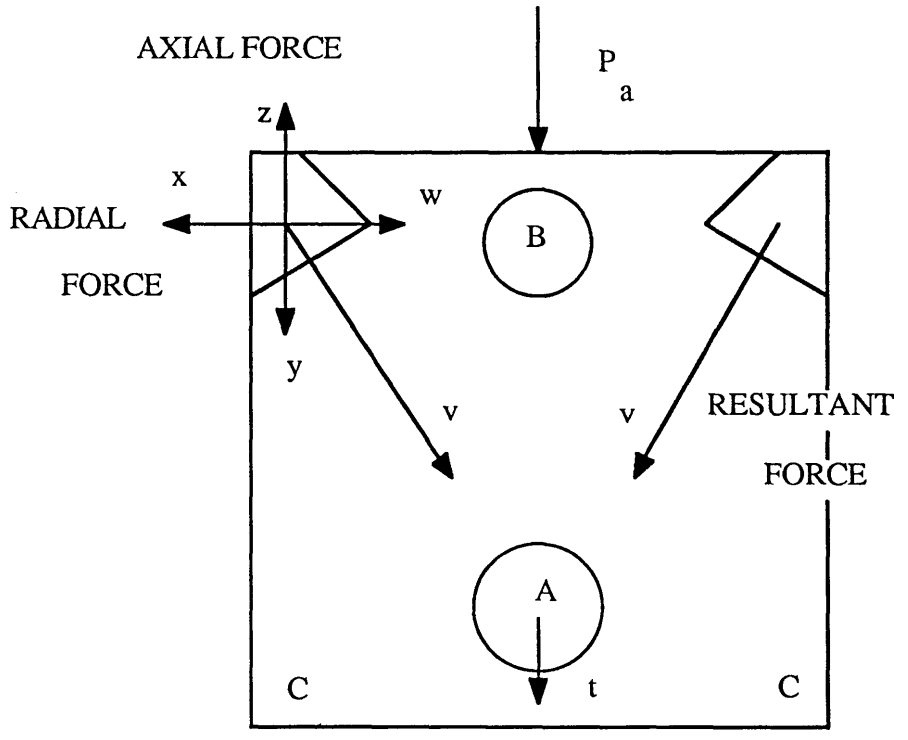

Figure 9.1 Transmission of forces through a powder during the process of uniaxial pressing (after Train, 1957).

9.2.4 Summary

When a powder is confined in a die the pressure is not transmitted uniformly through the mass but conforms to a stress pattern imposed by die-wall friction. As a result, density gradients are set up within the powder compact which have a significant effect on its physical and mechanical properties. The density distribution in green compacts is the controlling factor on shrinkage during sintering, and on the homogeneity of the final product. It is therefore important to be able to control and measure the green density within samples. There are a variety of methods to study the density distributions. It has also been shown that the predicted density variations within the compact are such that the maximum densities are at the top outside perimeter close to the piston-cylinder interface and in the lower central zone of the compact (Kandeil *et al.*, 1977). The importance of determining the density distributions has been established not only to characterise the green but to provide an insight into the pressing process per se.

The resulting compact must have adequate strength to survive ejection intact and for handling prior to sintering. The mechanical interlocking of particles and short range attractions between molecular groups of absorbed polymer binders contributes to the strength (Reed and Runk, 1976).

9.3 DATA AND ANALYSIS

Train, 1957 showed that the density distributions within a compact are a result of the stress distributions occurring during pressing. Apart from the measurement of the applied and transmitted forces during compaction, the stress distribution in a compact may be determined from hardness mapping of the top and bottom surfaces and along the side of the green. Also, attrition experiments in which the compact is placed on a bed of abrasive material which is rotated in a rolling mixer provide a measure of the density distributions. The values of the change in dimensions (height and diameter) and the weight loss will indicate the density distributions within the compact as a result of the stress transmission during compaction.

The results from these two types of experimental techniques of green evaluation are presented in this Section.

9.3.1 Hardness

The hardness measurement is a means of evaluating the surface pressure distributions that arise during the compaction. Microhardness measurements were carried out on some selected samples. Two types of measuring techniques were used; indentation hardness and scratch hardness. The hardness values are calculated from the measured indentation or scratch width. The values were typically 10-30 MPa and were found to vary over the compact surfaces.

9.3.1.1 Ferrite

The hardness of the several ferrite compacts has been measured as a function of the radius on the top and bottom surfaces and as a function of the height along the side of the compact. The hardness profiles in both top and bottom surfaces and along the side corresponding to a Ferrite/PVA 72,000 (IC1) cylindrical specimen are shown in Figure 9.2 for the case of indentation hardness measurements. The scatter of the data is evident but in general it may be observed that for the top surface the hardness near the edges is greater than in the middle of the top face; whilst in the case of the bottom face the opposite is true; the hardness is lower at the edges than at the centre of the face. This agrees with the predictions made in Section 9.2.2 on the development of stresses during compaction and the resulting stress and density distributions within a compact. Also in Figure 9.2, the variation of the hardness along the side of the compact is shown. The hardness increases as a function of height, being lower near the static face and greater near the moving face.

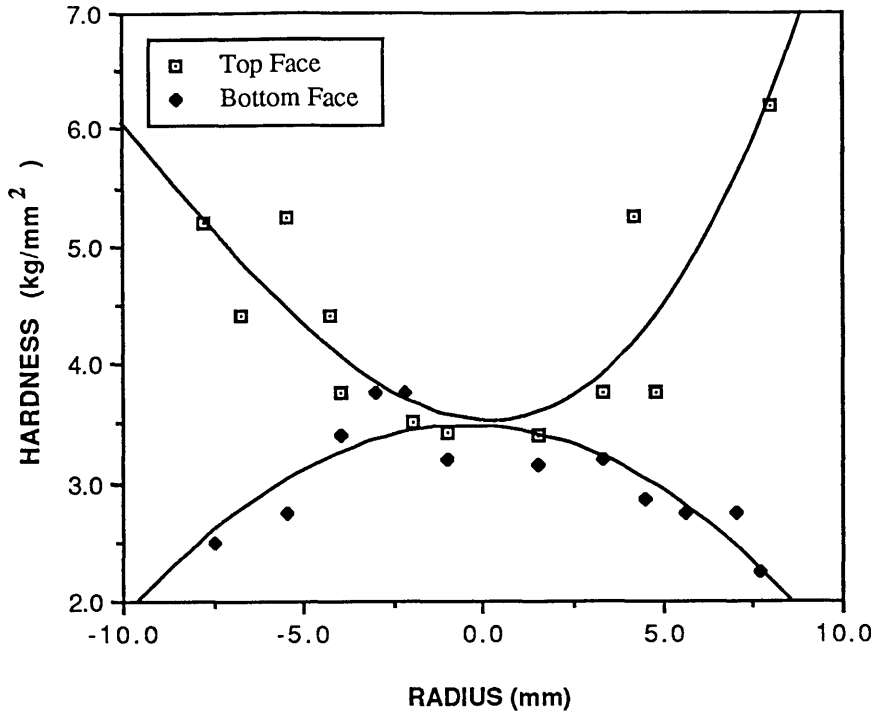

Figure 9.2a Hardness profiles across the top and the bottom faces for a Ferrite/PVA 72,000 compact pressed at 135 MPa in a 0.019 m diameter die.

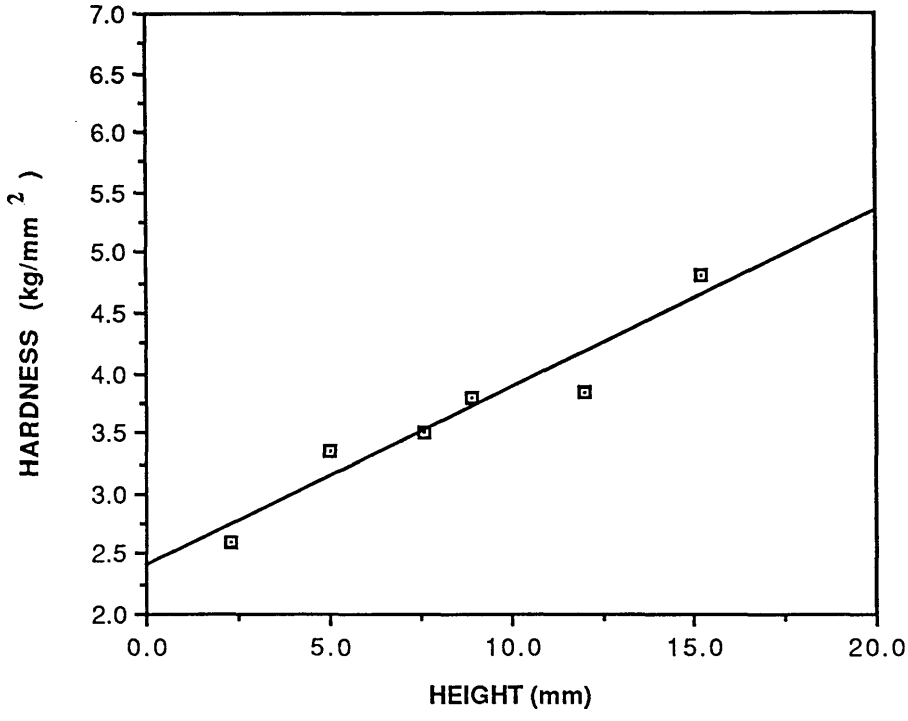

Figure 9.2b Variation of the hardness along the side of a Ferrite/PVA 72,000 compact pressed at 135 MPa in a 0.019 m diameter die.

In all the cases examined, and as it was expected, the hardness is greater on the top surface than on the bottom. This non-uniform distribution of hardness along the compact surfaces is a clear evidence of the generation of a pressure gradient along the compact during pressing. This appears always to be the case with powders confined in a die. In a compaction system like the one that has been used (one side pressure application using stationary lower punch and a moving upper punch), the generation of a pressure gradient is inevitable. This phenomenon of non-uniform density distribution can be attributed to the friction between the powder and the die walls. Another possible cause of non-uniform compaction can be the non-uniformity of die filling which causes variations in the initial bulk density in the die.

One of the notable features of these hardness data are the marked fluctuations in hardness observed in some cases. This is particularly apparent on the platen faces; see Figure 9.3. This is not believed to be an experimental artifact. Such variations have not

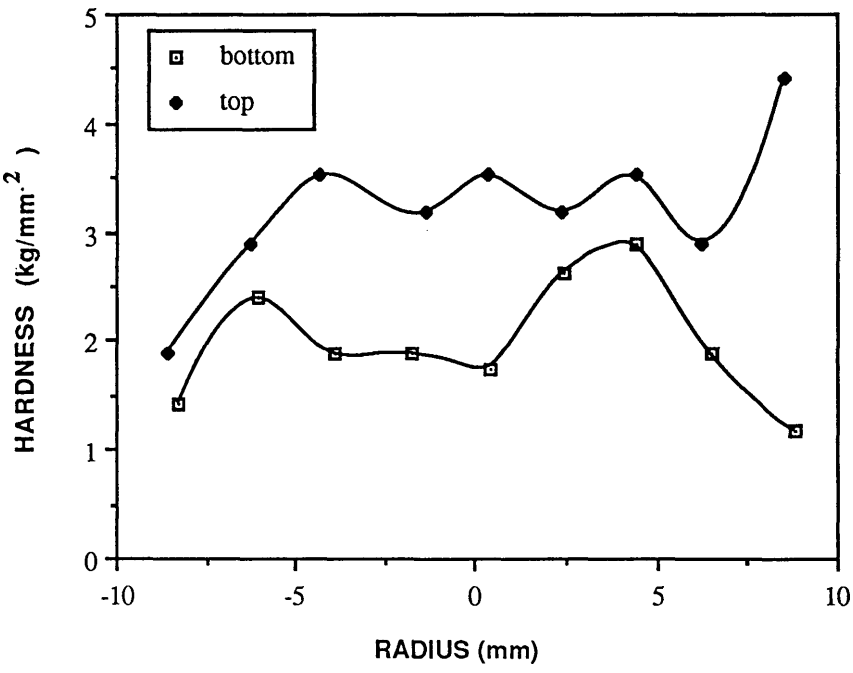

Figure 9.3 Hardness profiles for a 0.01620 kg Ferrite/Gohsenol compact pressed to 31 MPa in a 0.0019 m diameter die without lubrication.

been reported in the literature. It may be that these variations reflect the local internal slip lines in the compact during compaction. Such features would be predicted by slip-line field analysis on the die wall at least. Nedderman, 1982 has noted this for hopper wall stresses. The variations on the die platen faces is at first sight less readily explained as the formation of the Rankine zone might suggest a continuous variation in pressure and hence hardness. However several authors; Briscoe *et al.*, 1984 for example, have noted pressure fluctuations at walls for powders under gravity forces during flow. These variations seem to be a reflection of the influence of the internal angle of friction of the powder and its slip lines.

The influence of the applied load on the compaction of several ferrites has been studied by measuring the hardness profiles of different cylindrical specimens as a function of the normal load applied to compact the powder. An example is presented in Figure 9.4 which corresponds to the scratch hardness profiles on the top and bottom surfaces for the case of Ferrite/50%PVA 72,000-50%PEG 400 (IC5) compacts pressed at a range of applied pressures. The variation of the average hardness of the top surface as a function of the applied load for two ferrite systems is shown in Figure 9.5. These curves indicate, that in general the hardness increases with the increase of the compaction pressure.

9.3.2 Attrition

The attrition of some selected compacts has been studied. In the case of the uranium dioxide powders the aim was to establish if, due to the different stress distributions that occur during the compaction of both powders, the compacts A and B would behave differently during attrition.

The lubricated granules $A_{96\text{-}L}$ and $B_{96\text{-}L}$ were single-sided compacted at different pressures using the same amount of powder and at a fixed pressure using different amounts of powder to obtain compacts with a range of sizes and compaction pressures.

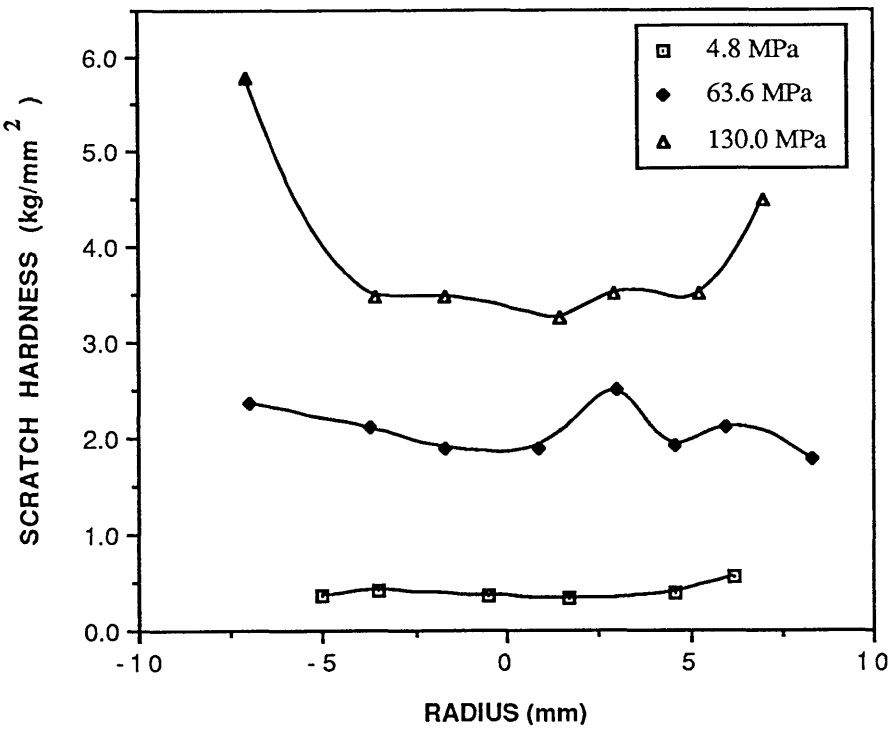

Figure 9.4a Scratch hardness profiles for the top surface of several Ferrite/50%PVA-50%PEG (IC5) compacts pressed at a range of loads.

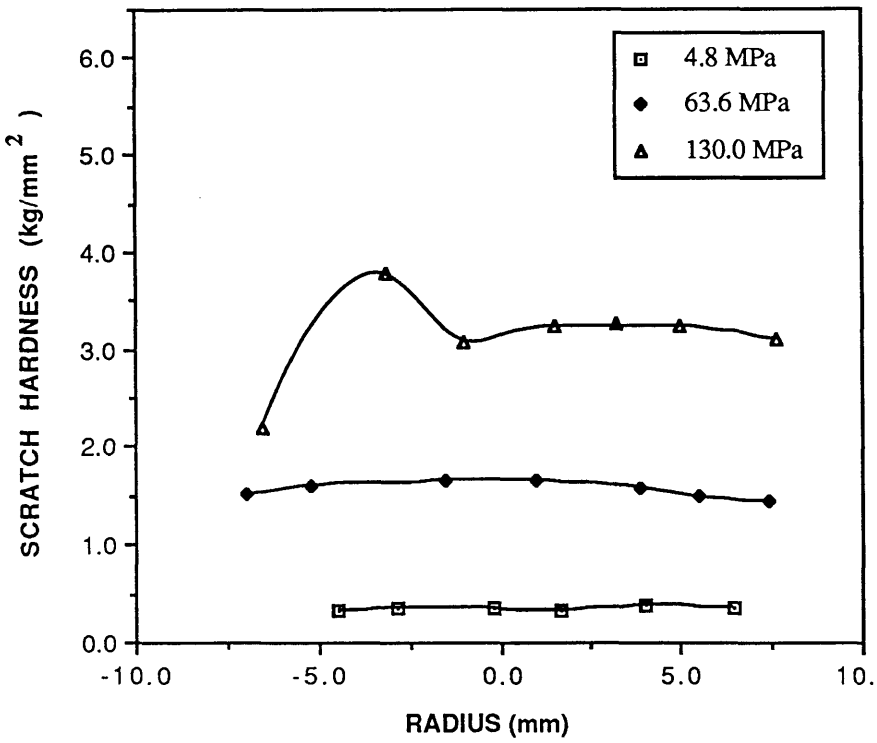

Figure 9.4b Scratch hardness profiles for the bottom surface of several Ferrite/50%PVA-50%PEG (IC5) compacts pressed at a range of loads.

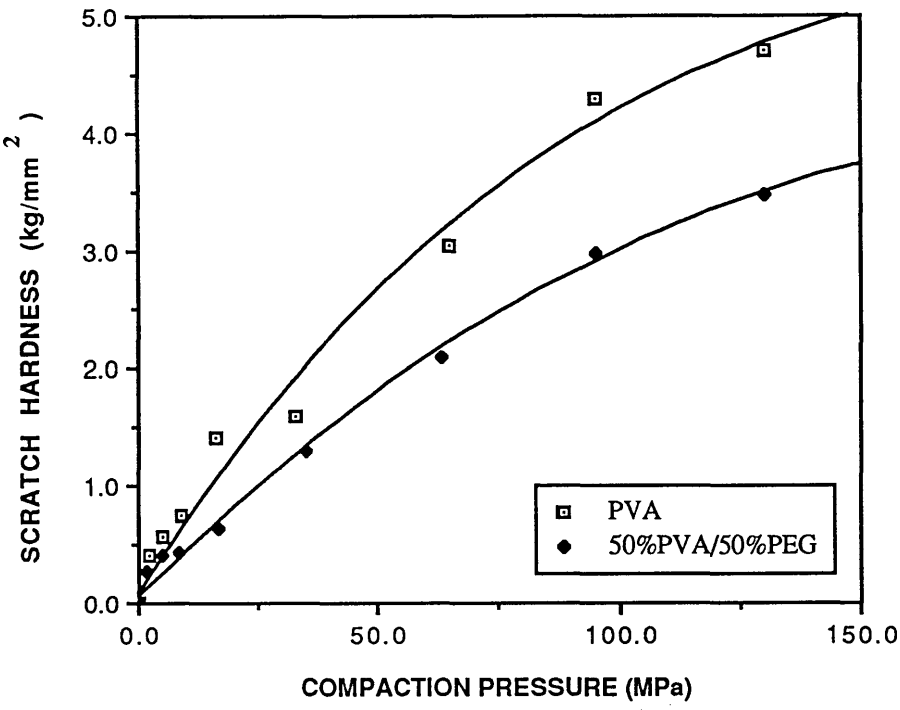

Figure 9.5 Variation of the average scratch hardness on the top surface as a function of the compaction pressure for Ferrite/PVA 14,000 and Ferrite/50%PVA 72,000-50%PEG 400 green compacts.

The following compacts, from $A_{96\text{-}L}$ and $B_{96\text{-}L}$ granules, were prepared with the following mass and compaction pressure:

- 0.031 kg, 94 MPa
- 0.031 kg, 125 MPa
- 0.031 kg, 157 MPa
- 0.019 kg, 157 MPa

The observed weight loss as a function of time for the two compacts, A and B, pressed at different pressures is represented in Figure 9.6. The corresponding wear rate variation as a function of time is presented in Figure 9.7. The change in the dimensions, diameter and height of the cylindrical compacts as a function of time is represented in Figure 9.8. All the data have been normalised by the initial weight and dimensions of the compacts.

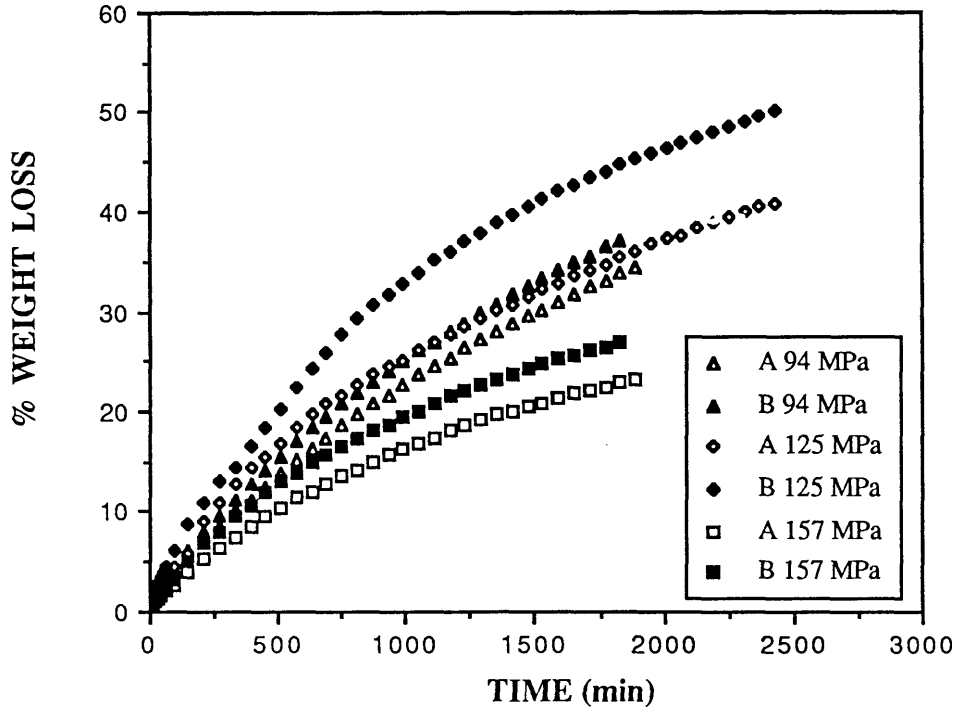

Figure 9.6 Weight loss as a function of attrition time for uranium dioxide compacts pressed at different pressures.

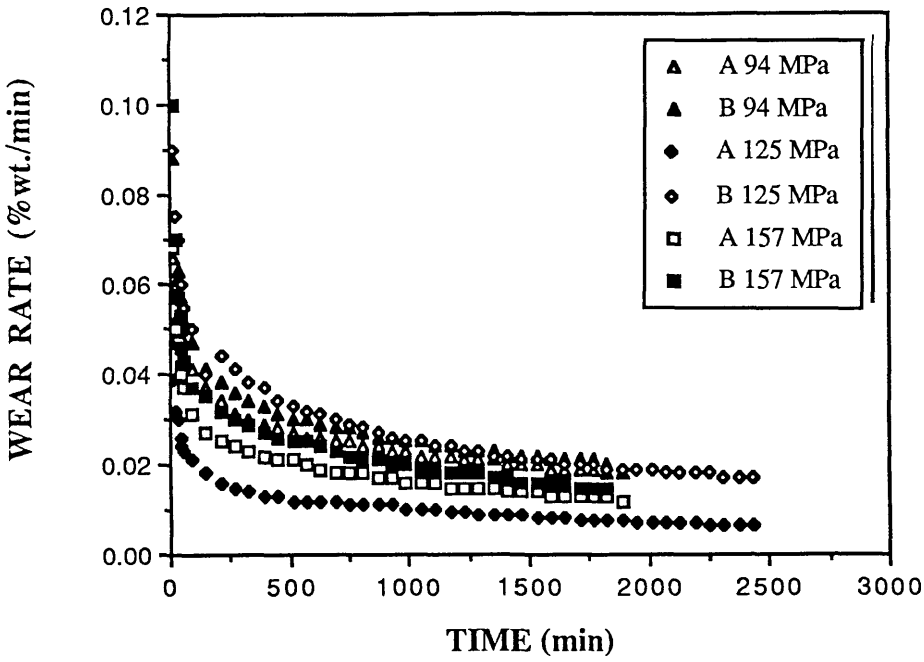

Figure 9.7 Variation of the wear rate as a function of the attrition time for uranium dioxide compacts pressed at different pressures.

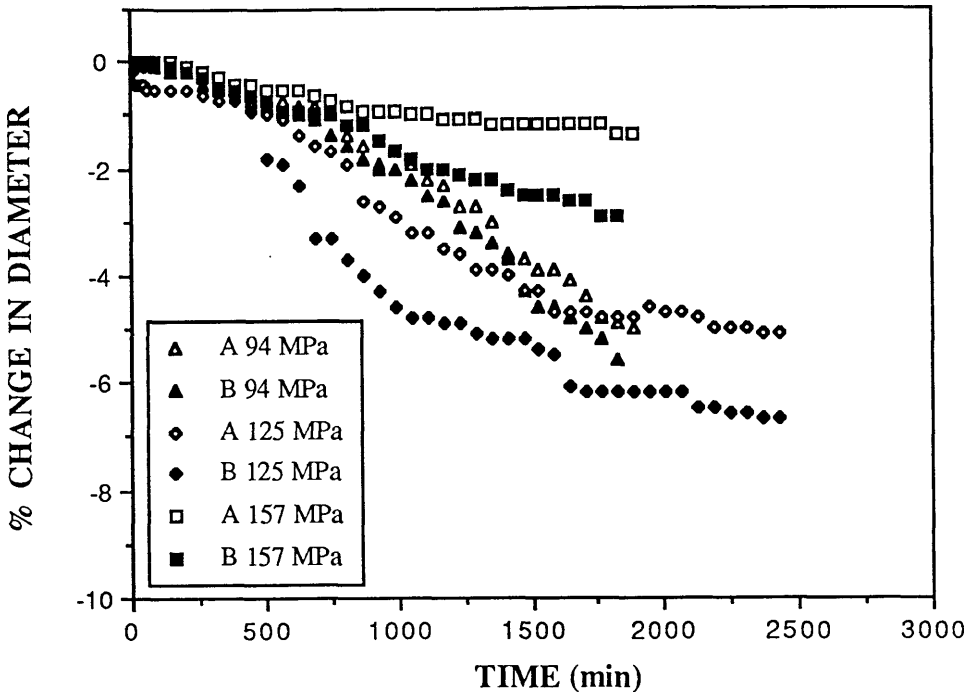

Figure 9.8a Change in the diameter of the uranium dioxide compacts as a function of the wear time.

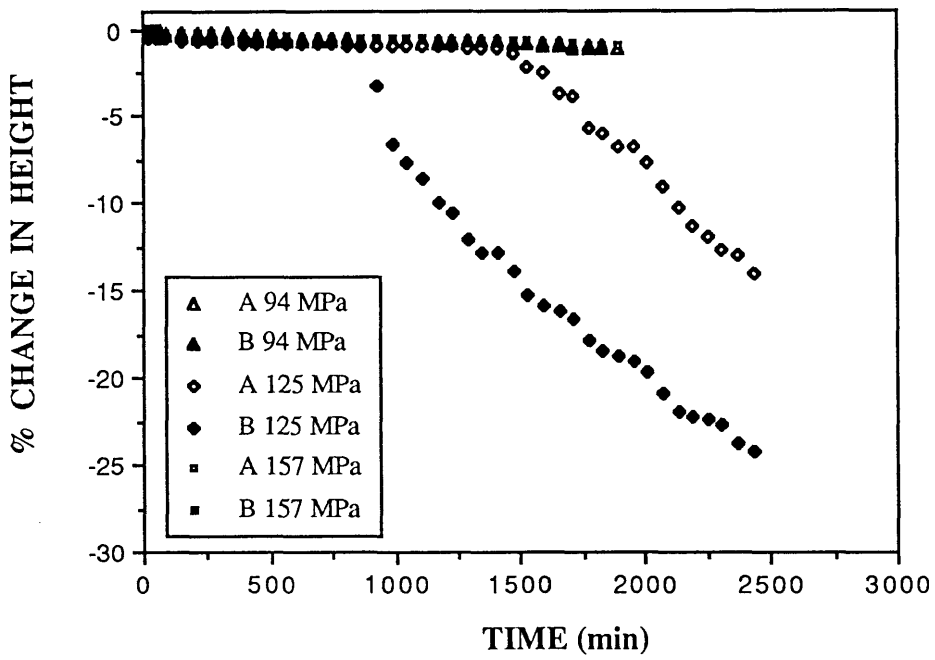

Figure 9.8b Change in the height of the uranium dioxide compacts as a function of the wear time.

It can be observed that all the experimental curves follow the same trend so it can be said that the wear mechanism is probably the same in all the cases. It does not appear to depend on the type of powder, the initial amount of powder or the compaction pressure.

The amount of wear observed for each powder depends on the pressure applied to compact the powders. B wears at a greater rate than A in all the cases tested. The difference in the wear of both powders is greater for the case of the compacts pressed at 125 MPa which corresponds with the higher degree of wear observed.

Two important facts are noted. For a given pressure, B wears more than A and for both powders the wear as a function of the compaction pressure follows this trend 125MPa>94MPa>157MPa.

This last fact could be explained considering that the Janssen's coefficient, K_w is a function of the applied pressure; the effects of the stresses at the wall during compaction depend on the applied pressure in a non simple way. A similar result has been found in the case of the variation of the average hardness of a uranium dioxide type B compact as a function of the applied pressure; the hardness is not a simple function of the applied pressure. Figure 9.9 shows these hardness results for the case of the average hardness of the compact but the same trend is observed for the variation of hardness on the top and bottom faces as a function of the applied pressure.

In general compacts prepared from A present a lower degree of diameter reduction than those prepared from powder B.

The influence of the compact size on the wear has been analysed by studying the attrition of two uranium dioxide compacts. These compacts were pressed to the same final pressure but different amounts of powder were used. It has been observed that the smaller compacts suffer a greater amount of wear and exhibit a higher wear rate.

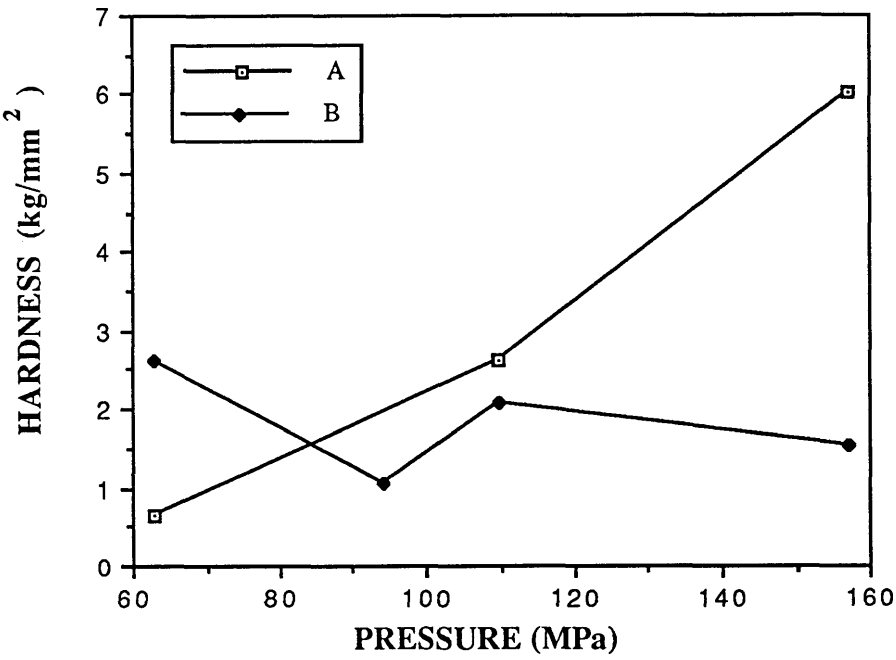

Figure 9.9 Variation of the average hardness of uranium dioxide compacts as a function of the applied compacting pressure.

Compacts pressed from other materials; ferrite, alumina, and zirconia coated with different binder systems have also been studied. The same type of wear curves as for the case of the uranium dioxide are obtained. In Figure 9.10 the weight loss and the dimensional changes for a Ferrite/PVA 14,000 compact pressed to 47 MPa in a wall lubricated die are presented. It has been observed that the wear rate depends on the ceramic material and type of binder used. The effect of the type of binder on the wear of some alumina and zirconia compacts is shown in Table 9.1.

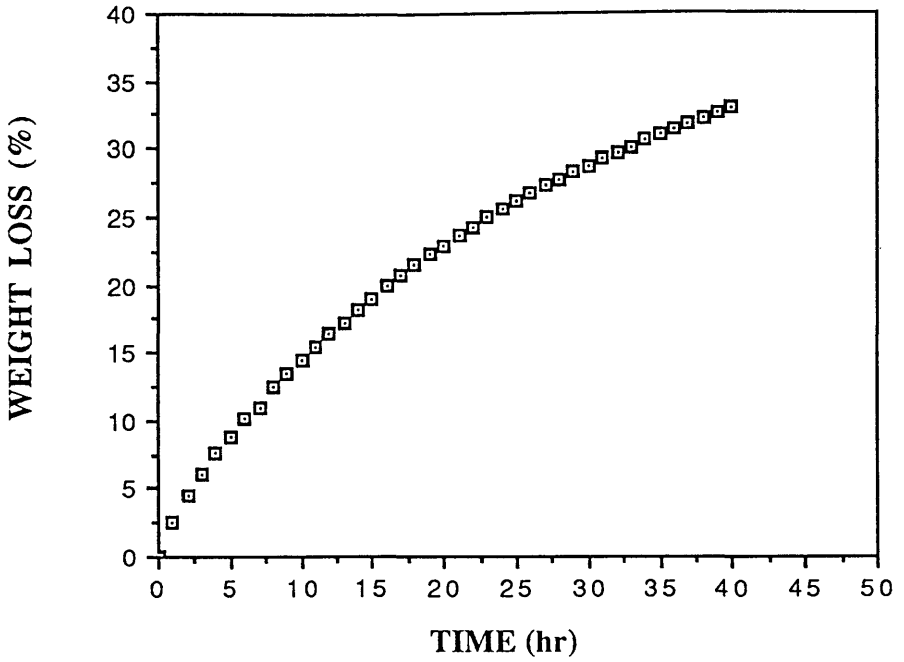

Figure 9.10a Weight loss as a function of time during the attrition of a Ferrite/PVA 14,000 compact pressed to 47 MPa in a lubricated 0.019 m diameter die

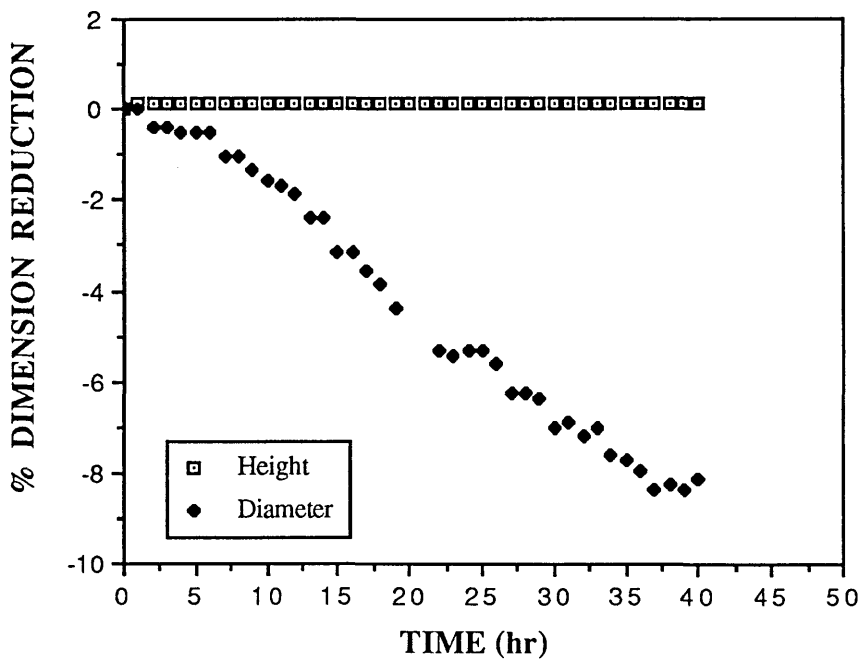

Figure 9.10b Dimensional changes, height and diameter, as a function of time during the attrition of a Ferrite/PVA 14,000 compact pressed to 47 MPa.

TABLE 9.1 Weight Loss During the Attrition of Several Ceramic/Binder Systems.

CERAMIC SYSTEM	%WEIGHT LOSS	TIME (hrs.)
Alumina/PVA 14,000	2.6	10
Alumina/PEG 400	2.0	10
Alumina/PVA14,000-PEG400	1.0	10
Zirconia/PVA 14,000	0.6	20
Zirconia/PEG 400	5.2	20
Ferrite/PVA 14,000 (IC2)	23.0	20

The trend in the change in shape for two uranium dioxide compacts as observed photographically, Plates 9.1, may be described as follows: first the material removal takes place from the borders of the bottom face and then from the bottom face itself. A higher degree of material removal takes place on the bottom face than on the top one as it was expected, showing that the top face is tougher than the bottom one due to the stress distributions generated during the compaction. The way these changes occur is different for the two uranium dioxide compacts analysed, A and B, as shown schematically in Figure 9.11. These compacts were prepared by pressing to 125 MPa the lubricated granules $A_{96\text{-}L}$ and $B_{96\text{-}L}$. In the case of compact B there is a difference in the relative amount of material removed from the area close to the bottom and to the top faces. For A there is little difference in the attrition values of the two surfaces.

Taking the samples compacted at 125 MPa (the ones that show a greater degree of wear) it is observed (Figure 9.8) that the change in diameter is only about 7% while the change in height reaches 25%. Another important fact is that the diameter begins to decrease from the beginning but the height remains constant until a certain time is reached and from then on it changes very rapidly. The material removal in the first

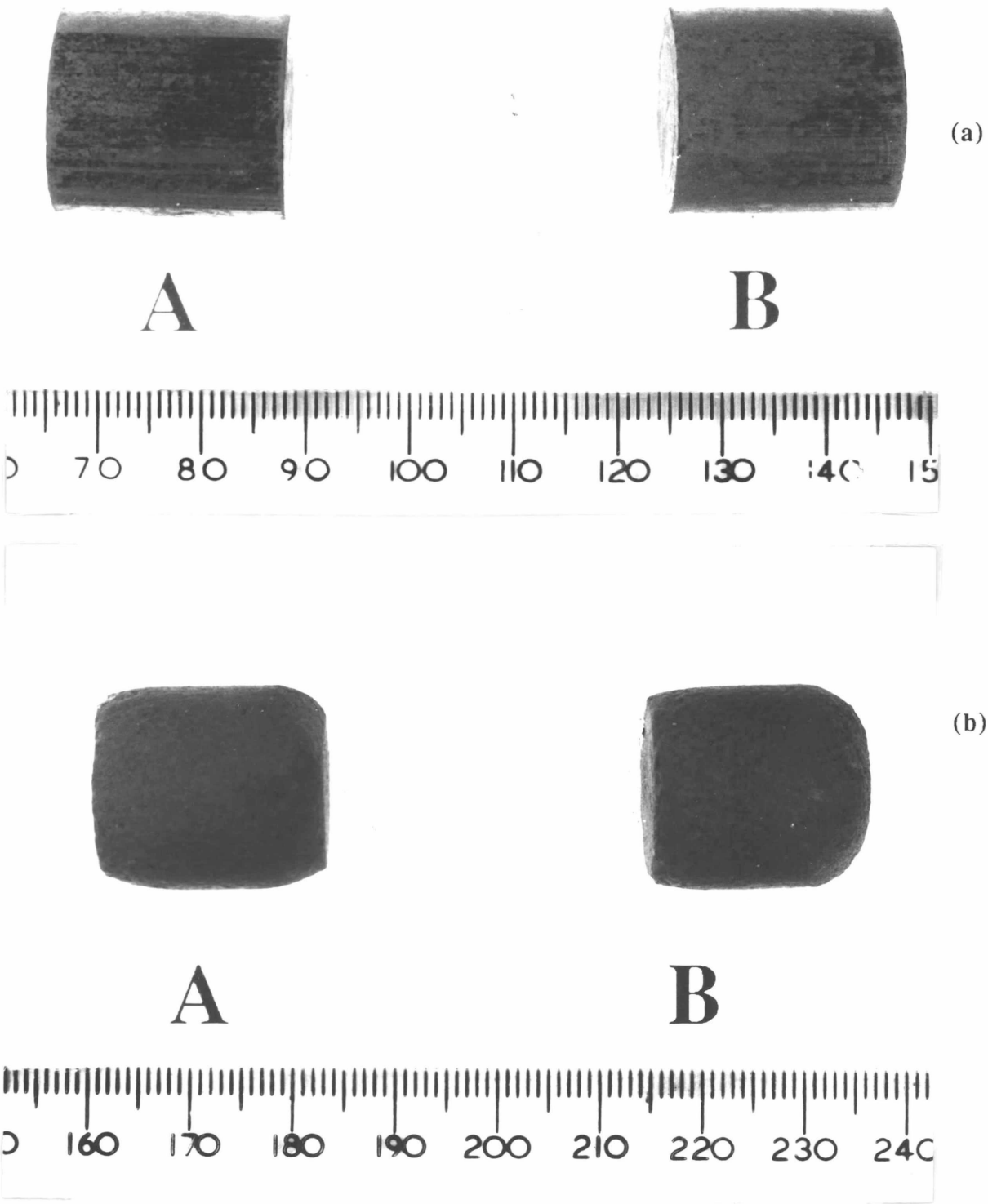

Plate 9.1 Photographic sequence showing the changes in shape for the two uranium dioxide compacts pressed to 125 MPa as a function of the attrition time. (a) initial samples, (b) after 210 min., (c) after 450 min., (d) after 1110 min., (e) 1530 min., (f) 2430 min.

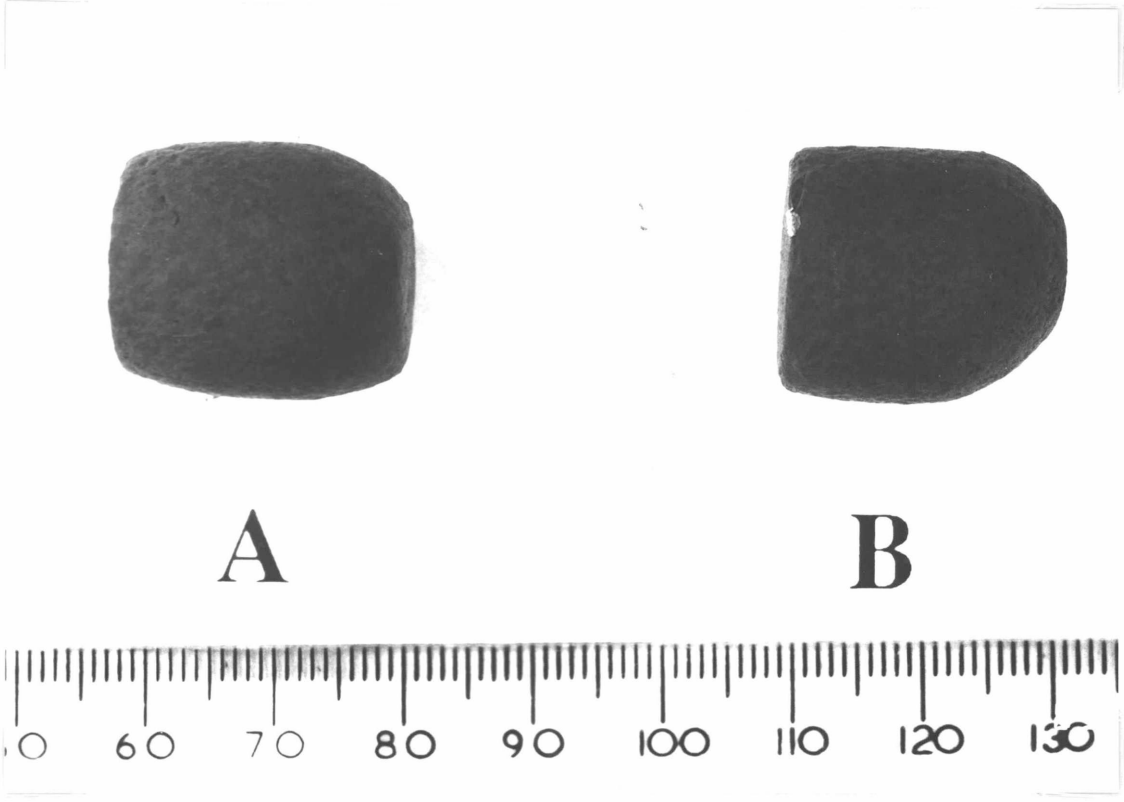

(c)

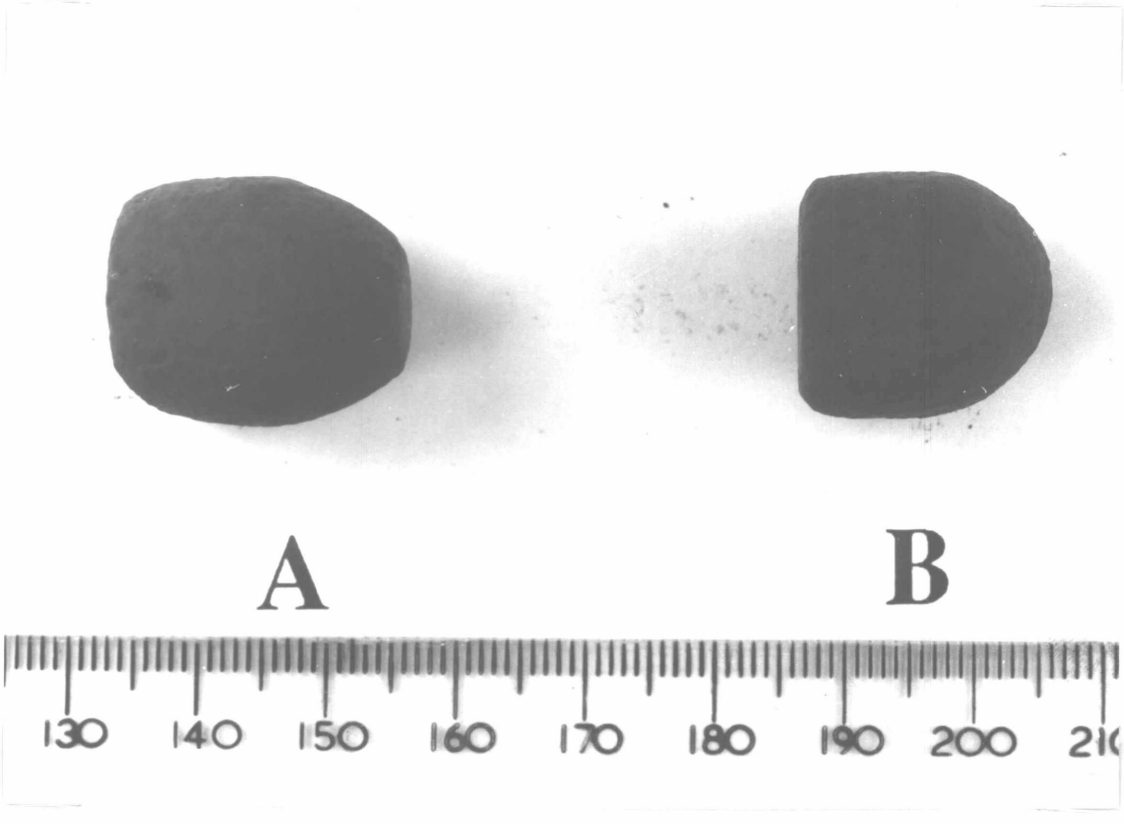

(d)

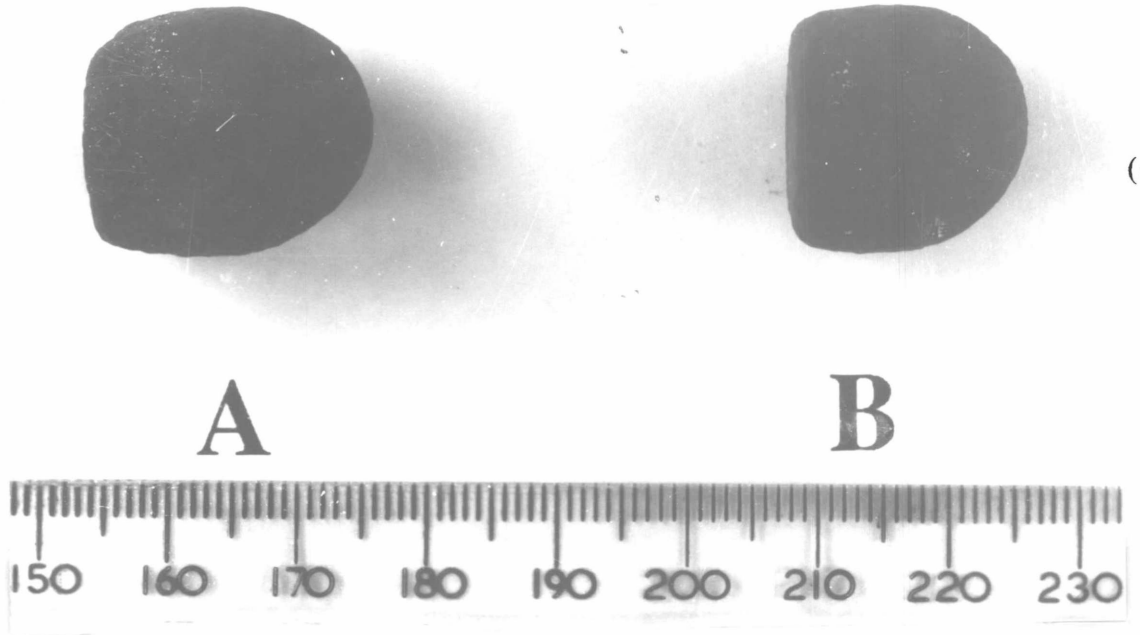
A
B
150
160
170
180
190
200
210
220
230

(e)

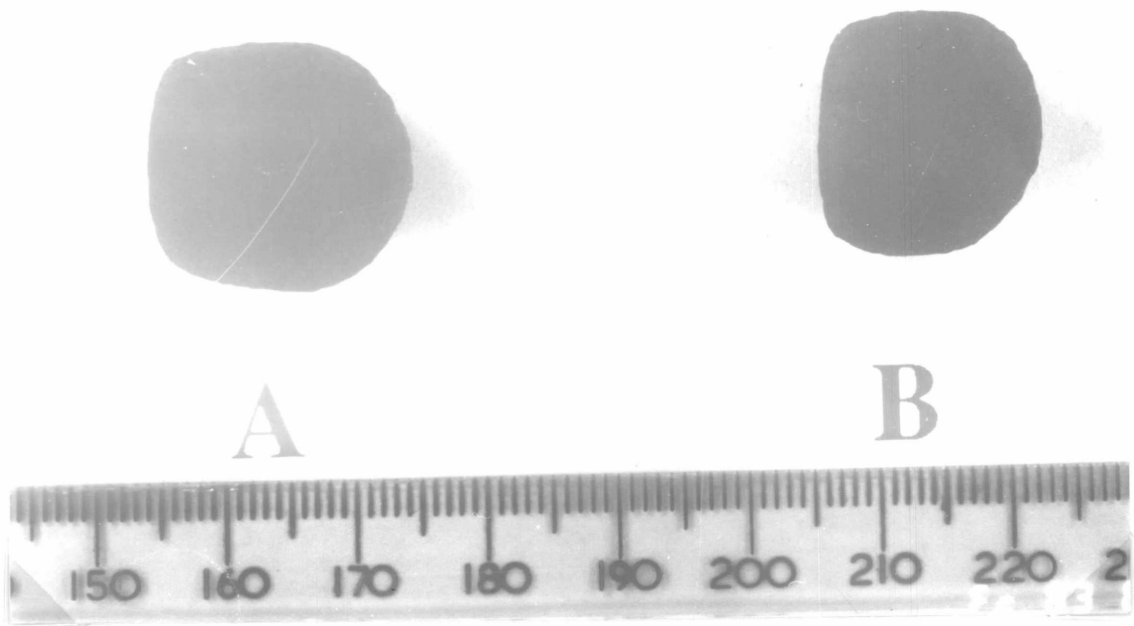
A
B
150
160
170
180
190
200
210
220

(f)

instance is along the sides (change in diameter, no change in height). Once this outer layer has been worn away the inner parts of the compacts are exposed. This is tougher so the wear begins to take place in such a way that produces a decrease in height of the compact. For the case of the other compacts the same trends would be expected.

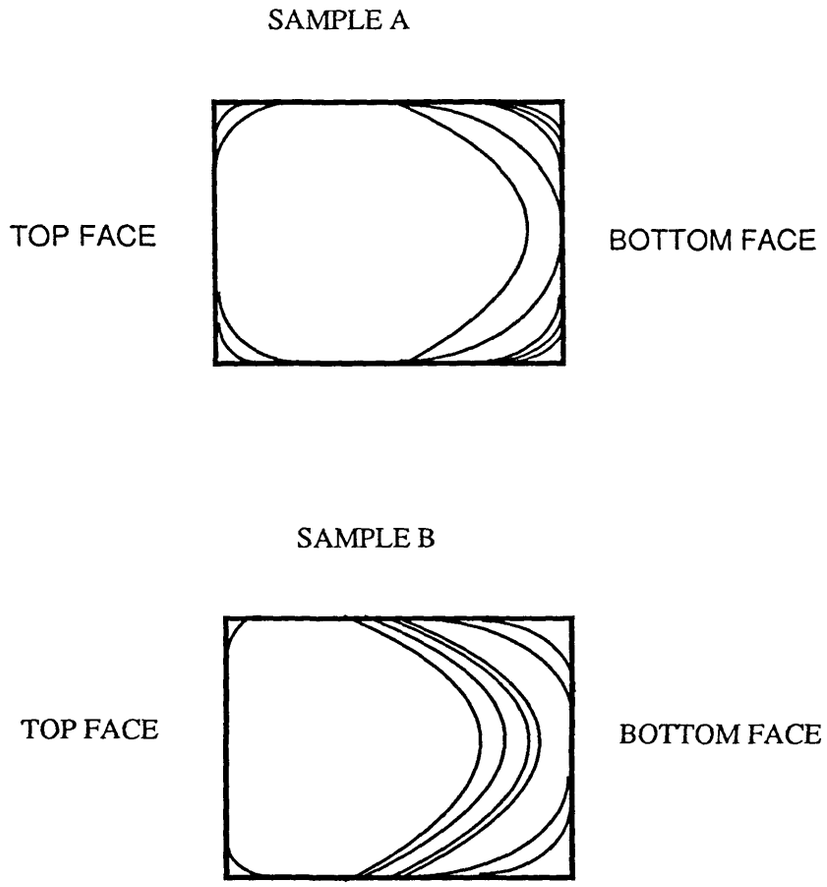

Figure 9.11 Schematic representation of the changes in shape that occur during the attrition of the two uranium dioxide compacts.

9.3.3 Stress Distribution

The results from the hardness mapping and attrition of compacts are correlated with the data obtained from the transmission ratios during the compaction experiment in

Table 9.2. The values of the change in dimensions (height and diameter) and the weight loss indicate the density distributions within the compact as a result of the stress transmission during compaction.

TABLE 9.2 Several Means of Assessing the Non Homogeneous Transmission of Stress During Compaction.

SYSTEM	P_t/P_a (average)	$(H/D)_o$	HARDNESS (kg/mm^2)	ATTRITION (%Weight Loss)
UO_2 ($A_{96\text{-}L}$)	0.30	4.5	3.08 [157]	40.9
UO_2 ($B_{96\text{-}L}$)	0.15	4.5	1.80 [157]	50.0
Zirconia/PVA lubricated die	0.75	2.5	----	0.63 [47]
Zirconia/PEG lubricated die	----	----	----	5.20 [47]
Ferrite/PVA lubricated die	0.58	2.0	3.30 [64]	----
Ferrite/Gohsenol lubricated die	0.53	2.1	1.96 [64]	----
Alumina/PVA lubricated die	0.82	1.0	----	14.24 [47]
Alumina/PEG lubricated die	0.84	1.1	----	2.62 [47]

[ ] indicates the compaction Pressure (MPa).
PVA 14,000; PEG 400

There is a clear difference between the case of lubricated and unlubricated dies. The data show that the pressure ratio is rather independent of the organic binder which suggests that the frictional force at the wall-agglomerates interface is governed by the lubricant. In the case of the unlubricated dies the pressure ratio is higher for the system that contains PEG. The data for the case of the uranium dioxide agglomerates, where the lubricant was admixed with the granules instead of coating the die walls, show a different pressure ratio for those two powders, this may be attributed to the less efficient action of the dry mixed lubricant in the case of powder B. This may arise because of a less effective lubricant distribution. The observed changes during the attrition of these compacts, and the differences observed in the transmission of pressure during compaction, suggest that the different behaviour of the powders could be due to the different stress distributions within the compacts which occur during the compaction process. This difference may arise from different distributions of the lubricant particles around the uranium dioxide granules. There is no direct evidence that this is the case.

The type of surface coating, i.e. the type of binder system applied to the powder, affects the final properties of the compact and it can be seen that there is a tentative correlation between the pressure transmission during compaction and the final properties of the green as assessed by the hardness and the rate of attrition.

9.4 CONCLUSIONS

The applied pressure during compaction is not transmitted uniformly through the body and this is evidenced by a non-uniform distribution of hardness over the compact surfaces and the attrition profiles. The trends in these measurements correlate directly with the pressure transmission data presented. The source of this non-uniform density distribution may be attributed to the friction between the powder and the die-walls. Another possible cause may be the non-uniformity of die filling which causes variations in the initial bulk density in the die.

In general, the average hardness of the compact increases with the increase of the compaction pressure. The marked fluctuations in hardness data may reflect the local internal slip lines in the compact during compaction.

The results have shown there to be several relationships between the mean transmitted stress ratio and the green density variations sensed in the attrition experiment. This experiment exposes density and pressure variations generated during compaction.

CHAPTER 10

CONCLUSIONS

The aim of the work described in this Thesis was to evaluate the interface friction and lubricating characteristics at certain distinct stages during the processing of several ceramic powders. These materials, in agglomerated form, have been treated with a range of organic materials which modify the ceramic powder's surface properties. The interface friction and the deformation characteristics of the organic species and of the agglomerated ceramic powders in free flow and during constrained flow have been investigated. Several model experiments have been used to study the particle-wall friction effects under a wide range of applied normal loads. An attempt to model these effects by examining the properties of individual particles and their interactions with their neighbours and the confining walls by describing the situation at the wall-powder interface has been presented.

From the experimental data generated in this study the following conclusions may be drawn:

1. The flowability of the different ceramic powders examined and the magnitude of the wall friction in unconstrained flow are effectively sensed by the gross bulk powder flow in cylinders down an inclined plane. The bulk powder flow studies have been shown to be able to distinguish between free-flowing and poor flowing powders in the case of several ferrite/binder systems and some uranium dioxide materials. A narrow frequency distribution of the sliding angle indicates a good free-flowing powder and a more broad frequency distribution of the sliding angle characterises poor flowing powders. The different ferrite/binder systems were classified in relation to their free flow behaviour according to their flow angle variance and the corresponding flow angle value.

2. The main features related to the uniaxial single-sided dry pressing of ceramic powders have been presented. The friction effects during powder compaction have been analysed in a number of different ways. The stress-volume relationship, the granule yield point, the stress transmission, and the characteristics of the resulting compact (hardness variation over the compact surface and green attrition characteristics) are all indicative of the level of the wall friction generated during the pressing process. It has been shown that these different properties are interrelated. The wall friction is directly sensed by the stress transmission ratio. Low stress transmission ratios correlate directly with large surface hardness variations, asymmetric attrition shapes and less dense greens for a given imposed surcharge.

Also, these data generated during compaction have been correlated with other properties of the ceramic/binder systems. The granule strength and the various flow and friction data obtained during unconstrained flow correlate with the yield pressure and pressure-volume parameters. In addition, there is an interrelationship between the interface properties of the agglomerates and their stress transmission during compaction.

3. The effect of several variables on the pressing of ceramic powders has been determined. The variables considered include; the particle size, the moisture content, the type of binder, the lubricating conditions, the aspect ratio and the applied load. The two variables having a greater influence are the initial powder aspect ratio and the presence of a specific lubricant coating at the die walls. The presence of a lubricant at the the die wall surface significantly reduces the frictional effects at the wall interface both during pressing and during the green ejection stage.

4. An empirical semilogarithmic linear relationship between the green density and the applied compaction pressure accurately describes the compaction behaviour of the agglomerated ceramic powders under the conditions studied. The yield pressure values deduced from this empirical relationship reflect the corresponding measured strength values of the granules.

5. The Kawakita constants a and b are valid parameters to describe the pressing behaviour of these systems. The value of b is directly related to the "ease" of pressing the powder and in particular to the level of the wall friction during the compaction and its magnitude is hence dependent on the binder system.

6. The interface wall friction prevailing during uniaxial compaction, as sensed by the transmitted/applied pressure ratio, has been found not to be constant but to vary with the change in powder height during the compaction process. This has been explained by invoking a simple mechanical model of the interface and the adhesion model of friction, which describes the normal pressure dependence of the friction coefficient, in the Janssen-Walker theory. The qualitative predictions of the stress/density variations during compaction, as described by the pressure transmission ratio, are in good agreement with experiment. The quantitative prediction requires the knowledge of the shear stress at the wall, the real to apparent area of contact ratio, the radial stress at the wall, the distribution factor and the axial/radial stress ratio, K_w. It is believed that it is the real to apparent area of contact ratio that has a greater influence.

7. The force necessary to eject the compact from the die is a complex function of the pressing conditions, mainly the amount of powder, the compaction pressure, and the lubricating conditions. Two general types of ejection profiles, depending on the amount of powder, have been described.

For a constant compaction pressure, the ejection pressure increases with the mass of the compact, i.e. with the apparent area of the contact compact-die wall interface. In the case of lubricated walls a constant coefficient of friction may be assumed. The determined values of the coefficient of friction during the ejection of lubricated Ferrite/PVA and Ferrite/Gohsenol compacts under these conditions are close to the values computed from the established intrinsic shear strength characteristics of the lubricating species, in particular the pressure coefficient of the shear strength, α.

For a constant mass of powder, the ejection pressure increases with the compaction pressure due probably to the higher radial stresses developed during the pressing stage

and a higher real area of contact.

8. The applied pressure imposed during compaction is not transmitted uniformly through the body. The source of this non-uniform stress and density distribution may be attributed to the friction between the powder and the die walls. Another possible cause may be the non-uniformity of die filling which causes variations in the initial bulk density in the die. These pressure variations are evidenced by a non-uniform distribution of hardness over the compact surfaces. A new method which exposes these density and pressure variations generated during compaction based on the controlled attrition of the green has been introduced. These variations are seen to be a function of the lubricating characteristics of the processing aid. The trends in these measurements (hardness and attrition profiles) correlate directly with the frictional characteristics evident during the compaction; i.e the mean transmitted stress ratio and the characteristics of the initial powder and the processing variables.

9. The friction force is found to be normal load dependent in many cases and follows nearly the expected trends. At low normal stress, as experienced in unconstrained flow, there is a logarithmic relationship between the friction force and the normal load and the autoadhesion component of the friction is negligible. These systems produce elastic contacts and apparently nearly single asperity contacts in the case of many of the present ceramic/binder powders. The load variation follows an extended Hertz model for a wall assembly. Typically, under these experimental conditions the coefficient of friction is a decreasing function of the applied normal load and it depends on the type of binder. For higher normal stresses, as sensed during compact ejection and simulated by the sliding of hemispherical compacts, the contacts flow plastically at the surface. Under these conditions the adhesion model is still applicable but now there is no detectable normal load variation and a constant coefficient of friction is a sufficient description of the friction process.

10. The organic films coating the ceramic particles or walls markedly alter the rheology of the powder and its interaction with its containers, modifying the flow and the friction properties of the powder during unconstrained and constrained flow. It is the surface

coating characteristics which control the interfacial wall friction.

11. A first order estimate of the role and magnitude of the wall friction in powder flows is obtained by adopting a modified friction model based upon the interfacial shear of the organic coating at the walls of the containers or dies. It appears that a single interfacial characterisation of the coating in a model experiment where the coating is sheared between highly elastic contacts provides much of the essential information required to interpret the various features of the unconstrained and constrained flow behaviour of the systems studied.

In final conclusion, these various specific conclusions may be summarised succinctly as follows. The interface friction characteristics of these discrete entities, the powders and the granules, are clearly substantially responsible for the flow characteristics of powders and the products derived from these powders. The contact conditions at the particle-wall interface and in the interparticle contacts are not predicted with great confidence. The forces at all the various contacts propagate in a subtle way throughout the assembly as its properties evolve. However, a first order description of these frictional forces based upon established friction models, does provide a generally sensible and sometimes concise account of the overall magnitude of the frictional forces involved. The fundamental interface characteristic is the interface rheology which may be described by economic empirical expressions. The critical parameter for many purposes is the pressure coefficient of the interface shear strength of the interface layer, α. This parameter, combined with the intrinsic interface shear parameter, τ_o, provides a useful basis for interpreting the processing potential of a coating or processing aid and its likely influence upon the quality of the product and the viability of the process. Clearly certain factors such as the mean particle size, the particles size distribution, the particle strength, the particle shape and topography, are important and influential characteristics. Nevertheless, to a good first order approximation it is the interface rheological characteristics which play the dominant role in the various processing operations. This is the major conclusion of the present study.

REFERENCES

Adams, M.J.; Briscoe, B.J. and Pope, L., 1987a: "A contact mechanics approach to the prediction of the wall friction of powders" in "Tribology in Particulate Technology", Ch.1.1; Briscoe, B.J and Adams, M.J. Eds.; Adam Hilger, UK.

Adams, M.J.; Mullier, M.A. and Seville, J.P.K., 1987b: "Agglomeration" in "Tribology in Particulate Technology", Ch.4.5; Briscoe, B.J and Adams, M.J. Eds.; Adam Hilger, UK.

Amuzu, J.K.A., 1976: "Mechanical properties of polymeric films"; Ph.D. Thesis, University of Cambridge.

Amuzu, J.K.A.; Briscoe, B.J. and Tabor, D., 1977: "Friction and shear strength of polymers"; *Trans. Amer. Soc. Lubr. Engrs*., **20** (40), pp. 354-357.

Archard, J.F, 1957: "Elastic deformation and the laws of friction"; *Proc. Roy. Soc.*, **A243**, pp. 190-205.

Bates, L., 1977: "Solids properties and mechanical handling"; Proc. 4th Int. Powder Tech. and Bulk Solids Conf., "Powtech'77"; Powder Technology Publication Series, No. 7, 34-41; Goldberg, A.S. Ed., Heyden, UK.

Beddow, J.K., 1983: "Theory and applications of morphological analysis" in "Advances in the Mechanics and the Flow of Granular Materials"; Vol. I, 107-127; Shahinpoor, M. Ed.; Trans. Tech. Public., USA.

Berrin, L.; Johnson Jr., D.W. and Nitti, D.J., 1972: "High purity reactive alumina powders: I, Chemical and powder density"; *Am. Ceram. Soc. Bull.*, **51**(11), pp. 840-844.

Blazek, A., 1973: "Thermal Analysis", Van Nostrand Reinhold Co., Czechoslovakia.

Bowden, F.P. and Tabor, D., 1950: "Friction and Lubrication of Solids"; Part I, Clarendon Press, UK.

Bowden, F.P. and Tabor, D., 1964: "Friction and Lubrication of Solids"; Part II, Clarendon Press, UK.

Brewer, J.A.; Moore, R.H. and Reed, J.S; 1981: "Effect of relative humidity on the compaction of barium titanate and manganese zinc ferrite agglomerates containing polyvinyl alcohol"; *Am. Ceram. Soc. Bull.*, **60** (2), pp. 212-220.

Briscoe, B.J.; Scruton, B. and Willis, F.R., 1973: "The shear strength of thin lubricant films"; *Proc. Roy. Soc.*, **A333**, pp. 99-114.

Briscoe, B.J. and Smith, A.C., 1980: "The shear properties of thin organic films"; *Rev. on the Deform. Behav. of Mater.*, **3** (3), pp. 151-191.

Briscoe, B.J., 1981: "Friction and wear of organic solids and the adhesion model of friction"; *Phil. Mag.*, **A43** (3), pp. 511-527.

Briscoe, B.J.; Radwan, H. and Streat, M, 1983: "Model experiments on sliding friction for application in hydraulic conveying of solids"; *Canad. J. Chem. Eng.*, **61** (6), pp. 769-775.

Briscoe, B.J. and Smith, A.C., 1983: "Rheology of Solvent-Cast Polymer Films"; *J. Appl. Polym. Sci.*, **28**, pp. 3827-3848.

Briscoe, B.J.; Pope, L. and Adams M.J., 1984: "Interfacial friction of powders on concave counterfaces"; *Powder Tech.*, **37**, pp. 169-181.

Briscoe, B.J.; Pope, L. and Adams, M.J., 1985: "The influence of particle surface topography on the interfacial friction of powders"; *I.Chem.E. Symposium Series* No. 91.

Briscoe, B.J., 1987: "Discrete particle-wall interactions in powder flow"; *Chem. Eng. Sci.*, **42** (4), pp. 713-723.

Briscoe, B.J.; Fernando, M.S.D. and Smith, A.C., 1987: "The role of interface friction in the compaction of maize" in "Tribology in Particulate Technology", Ch.3.2; Briscoe, B.J and Adams, M.J. Eds.; Adam Hilger, UK.

Briscoe, B.J and Evans, P.D., 1988: "The characterisation of friction in ceramic powder processing" in "Ceramic Transactions" Vol. 1, Ceramic Powder Science II, pp. 758-766; Messing, G.L.; Fuller Jr., E.R. and Hausner, H. Eds.; Am. Ceram. Soc., USA.

Briscoe, B.J., 1990: "The interfacial friction of powder wall contacts" (to be published)

Briscoe, B.J and Evans, P.D. 1990: "Wall friction in the compaction of agglomerated ceramic powders"; *Powder Tech.* (to be published).

Brostow, W., 1979: "Science of Materials"; Wiley-Interscience, USA.

Cahn, D.S. and Karpinski, J.M., 1986: "Compression testing of green and dry iron ore pellets"; *Trans. AIME*, **241**, pp. 475-480.

Capes, C.E., 1971/72: "The correlation of agglomerate strength with size"; *Powder Tech.*, **5**, pp. 119-125.

Capes, C.E., 1980: "Particle Size Enlargement". Handbook of Powder Technology, Vol.1, Williams, J.C. and Allen, T. Eds.; Elsevier, The Netherlands.

Carson, J.W., 1988: "Powder handling in the ceramic industry"; *Am. Ceram. Soc. Bull.*, **67** (5), pp. 874-877.

Carstensen, J.T., 1984: "Tableting and pelletization in the pharmaceutical industry" in "Handbook of Powder Science and Technology", Ch. 7.3; Fayed, M.E. and Otten, L. Eds.; Van Nostrand Reinhold Co., USA.

Carter, A-L, 1988: "The durability of organic films" (Private Communication).

Ciftcioglu, M.; Akinc, M. and Burkhart, L., 1986: "Measurement of agglomerate strength distribution in agglomerated powders"; *Am. Ceram. Soc. Bull.*, **65** (12), pp. 1591-1596.

Cooper, J.R. and Eaton, L.E., 1962: "Compaction behavior of several ceramic powders"; *J. Am. Ceram. Soc.*, **45** (3), pp. 97-101.

Cross, M., 1979: "The transverse motion of solids moving through rotary kilns"; *Powder Tech.*, **22**, 187-190.

Czichos, H., 1978: "Tribology-A Systems Approach to the Science and Technology of Friction, Lubrication and Wear"; Elsevier, The Netherlands.

Daniels, T., 1973: "Thermal Analysis"; Kogan Page Ltd., UK.

Davies, R., 1984: "Particle size measurement experimental techniques" in "Handbook of Powder Science and Technology", Ch. 2; Fayed, M.E. and Otten, L. Eds.; Van Nostrand Reinhold Co., USA.

Deming, W.E. and Mehring, A.L., 1929: "The gravitational flow of fertilizers and other comminuted solids"; *Industr. Engng. Chem.*, **21**, pp. 661-665.

DiMilia, R.A. and Reed, J.S., 1983: "Dependence of compaction on the glass transition temperature of the binder phase"; *Am. Ceram. Soc. Bull.*, **62**, pp. 484-488.

Dowson, 1979: "History of Tribology"; Longman, USA.

Doyle, C.D., 1961: "Estimating thermal stability of experimental polymers by empirical thermogravimetric analysis"; *Anal.Chem.*, **33** (1), pp. 77-79.

Fernando, M.S.D., 1986: "Traction induced compaction of maize powder"; Ph.D. Thesis; University of London.

Fisher, J.R. and Potter, J.F., 1955: "Factors affecting the physical structure of dry pressed steatite"; *Am. Ceram. Soc. Bull.*, **34** (6), pp. 177-181.

Goldman, A.S. and Lewis, H.D., 1984: "Particle Size Analysis: Theory And Statistical Methods" in "Handbook of Powder Science and Technology", Ch. 1; Fayed, M.E. and Otten, L. Eds.; Van Nostrand Reinhold Co., USA.

Grey, R.O and Beddow, J.K., 1968/69: "On the Hausner ratio and its relationship to some properties of metal powders"; *Powder Tech.*, **2**, pp. 323-326.

Halloran; J.W., 1984: "Agglomerates and agglomeration in ceramic processing" in "Ultrastructure Processing of Ceramics, Glasses and Composites", Ch. 3.2; Hench, L.L. and Ulrich, D.R. Eds., Wiley, USA.

Harnby, N., 1987: "The influence of particle adhesion on powder mixing" in Tribology in "Particulate Technology", Ch.2.6; Briscoe, B.J and Adams, M.J. Eds.; Adam Hilger, UK.

Harvey, J.W. and Johnson Jr., D.W., 1980: "Binder systems in ferrites"; *Am. Ceram. Soc. Bull.*, **59** (6), pp. 637-645.

Hausner, H.H., 1967: "Friction conditions in a mass of metal powder"; *Int. J. Powder Metall.*, **3**, pp. 7-13.

Hersey, J.A. and Rees, J.E., 1970: "The effect of particle size on the consolidation of powders during compaction" in "Particle Size Analysis 1970", pp. 33-41; Groves M.J. and Sargent, W. Eds.; Soc. Anal. Chem., UK.

Hoffman, E.R., 1972: "Importance of binders in spray dried pressbodies"; *Am. Ceram. Soc. Bull.*, **51** (3), pp. 240-242.

Holt, C.B., 1981: "The shape of particles produced by comminution. A review"; *Powder Tech.*, **28**, pp. 59-63.

Isherwood, D.P., 1987: "Die wall friction effects in the compaction of polymer granules" in "Tribology in Particulate Technology", Ch.3.3; Briscoe, B.J and Adams, M.J. Eds.; Adam Hilger, UK.

Jenike, A.W. and Johanson J.R., 1969: "On the theory of bin loads"; *Trans. ASME*, **5**, pp. 339-344.

Johanson, J.R., 1971/72: "Modeling flow of bulk solids"; *Powder Tech.*, **5**, pp.93-99.

Kanatani, K-I., 1983: "Macroscopic and microscopic descriptions of the mechanics of granular materials" in "Advances in the Mechanics and the Flow of Granular Materials", Vol. I, pp. 273-284; Shahinpoor, M. Ed.; Trans. Tech Publications, USA

Kandeil, A.; De Malherbe, M.C.; Critchley, S. and Dokainish, M., 1977: "The use of hardness in the study of compaction behaviour and die loading"; *Powder*

Tech., **17**, pp. 253-257.

Katz, R.N., 1976: "Characterization of ceramic powders" in "Treatise on Materials Science and Technology", Vol.9: Ceramic Fabrication Processes,pp. 35-49; Wang, F.F.Y. Ed.; Academic Press, USA.

Kawakita, K. and Lüdde, K-H., 1970/71: "Some considerations on powder compression equations"; *Powder Tech.*, **4**, pp. 61-68.

Kim, Y.S., 1976: "Effects of powder characteristics" in "Treatise on Materials Science and Technology", Vol.9: Ceramic Fabrication Processes, pp. 51-70; Wang, F.F.Y. Ed.; Academic Press, USA.

Kingery, W.D.; Bowen, H.K. and Uhlman, D.R., 1976: "Introduction to Ceramics"; 2nd ed.; Wiley-Interscience, USA.

Lange, F.F., 1984: "Sinterability of agglomerated powders"; *J. Am. Ceram. Soc.*, **67** (2), pp. 83-89.

Leiser, D.B. and Whittemore Jr., O.J., 1970: "Compaction behavior of ceramic particles"; *Am. Ceram. Soc. Bull.*, **49**, pp. 714-717.

Leopold, P.M. and Nelson, R.C., 1965: "The effect of die-wall lubrication and admixed lubricant on the compaction of sponge-iron powder. Part II: Effect of lubrication on ejection pressure"; *Int. J. Powder Metall.*, **1** (4), pp. 37-40.

Levine, S.L., 1969: "A quantitative determination of binder and lubricant in ceramic materials by TGA"; *Am. Ceram Soc. Bull.*, **48** (2), pp. 230-231.

Lo, W.C., 1976: "Methods of measuring surface texture; in "Treatise on Materials Science and Technology", Vol.9: Ceramic Fabrication Processes, pp. 265-294; Wang, F.F.Y. Ed.; Academic Press, USA.

Lukasiewicz, S.J. and Reed, J.S., 1977: "Evaluation of microstructure on compacting spray dried agglomerates" in "Ceramic Microstructures'76", pp. 196-207; Fulrath, R.M. and Pask, J.A. Eds.; Westview Press; USA.

Lukasiewicz; S.J. and Reed, J.S., 1978: "Character and compaction response of spray-dried agglomerates"; *Am. Ceram. Soc. Bull.*, **57** (9), pp. 798-805.

MacLeod, H.M. and Marshall, K., 1977: "The determination of density distributions in ceramic compacts using autoradiography"; *Powder Tech.*, **16**, pp. 107-122.

MacLeod, H.M., 1983: "Compaction of ceramics" in "Enlargement and Compaction of Particulate Solids", Ch. 11; Stanley-Wood, N. Ed.; Butterworths, UK.

McClung, R.W. and Johnson, D.R., 1988: "On-line NDE for control and modeling of ceramic processing"; *MRS Bull.*, **13** (4), pp. 34-39.

Meloy, T.P., 1984: "Particle characterization: Future approaches" in "Handbook of Powder Science and Technology", Ch. 3; Fayed, M.E. and Otten, L. Eds.; Van Nostrand Reinhold Co., USA.

Meloy, T.P.; Mani, B.P. and Clark, N.N., 1986: "Particle shape analysis and separation techniques: A critical review"; *J. Powder and Bulk Solids Technol.*, **10** (1), p. 15-20.

Messing, G.L.; Markhoff, C.J. and McCoy, L.G., 1982: "Characterization of ceramic powder compacts"; *Am. Ceram. Soc. Bull.*, **61** (8), pp. 857-860.

Motamedi, F.;, 1985: "Interface traction of coal particles", MSc Thesis, Imperial College, Univ. of London.

Nedderman, R.M., 1982: "The theoretical prediction of stress distributions in hoppers"; *Trans. I.Chem.E.*, **60**, pp. 259-275.

Nies, C.W. and Messing, G.L., 1984: "Effect of glass-transition temperature of polyethylene glycol-plasticized polyvinyl alcohol on granule compaction"; J. Am. Ceram. Soc.; **67** (4), 301-304

Niesz, D.E.; McCoy, L.G. and Wills R.R, 1978: "Handling and green forming of fine powders" in "Processing of Crystalline Ceramics". Materials Science Research Vol. 11, pp. 41-48; Palmour, III, H.; Davis, R.F. and Hare, T.M. Eds.; Plenum Press, USA.

Oackley, J., 1987: Private Communication.

Orr, Jr., C., 1966: "Particulate Technology"; The Macmillan Company, USA.

Ōyama, Y., 1980: "Particle motion in a horizontal rotating cylinder";*Int. Chem. Eng.*, **20** (1), pp. 36-55.

Parker, E. R., 1967: "Materials Data Book for Engineers"; McGraw-Hill, USA.

Perry, R.H. and Chilton, C.H., 1973: "Chemical Engineers Handbook", 5th ed.; McGraw-Hill, USA.

Pospech, R. and Schneider, P., 1989: "Powder particle sizes from mercury porosimetry"; *Powder Tech.*, **59**, pp. 163-171.

Prior, M.K.J. and Sharma, M.M., 1987: "Study of spartan drum granulator"; Link Project; Imperial College.

Reed, J.S. and Runk, R.B., 1976: "Dry pressing" in "Treatise on Materials Science and Technology", Vol.9: Ceramic Fabrication Processes, pp. 71-93; Wang, F.F.Y. Ed.; Academic Press, USA.

Ruiz de Gordoa, E.; Ortiz, M.I. and Irabien, J.A., 1986: "Correlation for gas-solid and wall-solid areas in rotary cylinders"; *J. Powder and Bulk Solids Tech.*, **10** (1), pp. 1-4.

Rumpf, H., 1962: "The strength of granules and agglomerates" in "Agglomeration", pp. 374-418; Knepper, W.A. Ed.; Interscience, USA.

Scheiffele, G.W. and Sacks, M.D., 1988: "Pyrolysis of poly(vinyl butyral) binders:II, Effects of processing variables" in "Ceramic Transactions"; Vol. 1, Ceramic Powder Science II, pp. 559-566; Messing, G.L.; Fuller Jr., E.R. and Hausner, H. Eds.; Am. Ceram. Soc., USA.

Schwartz, E.G. and Weinstein, A.S., 1965: "Model for compaction of ceramic powders"; *J. Am. Ceram. Soc.*, **48** (7), pp. 346-350.

Schwedes, J. and Schulze, D., 1990: "Measurement of flow properties of bulk solids; *Powder Tech.*, **61**, pp. 59-68.

Schweiwiller, T. and Hutter, K., 1983: "On shear flow of cohesionless granular materials down an inclined chute" in "Advances in the Mechanics and the Flow of Granular Materials"; Vol. II, pp. 613-639; Shahinpoor, M. Ed.; Trans. Tech Publications, USA.

Shahinpoor, M. and Ahmadi, G., 1983: "A kinetic theory for the rapid flow of rough inelastic spherical particles and the evolution of fluctuations" in "Advances in the Mechanics and the Flow of Granular Materials"; Vol. II, pp. 641-667; Shahinpoor, M. Ed.; Trans. Tech Publications, USA.

Sherrington, P.J. and Oliver, R., 1981: "Granulation"; Monograph in Powder Science and Technology Series; Goldberg, A.S. Ed.; Heyden & Son, UK.

Shih, W-K.; Sacks, M.D.; Scheiffele, G.W.; Sun Y-N and Williams, J.W., 1988: "Pyrolysis of poly(vinyl butyral) binders: I, Degradation mechanisms" in "Ceramic Transactions"; Vol. 1, Ceramic Powder Science II, 549-558; Messing, G.L.; Fuller Jr., E.R. and Hausner, H. Eds.; Am. Ceram. Soc., USA.

Spencer, R.S; Gilmore, G.D. and Wiley, R.M., 1950: "Behavior of granulated polymers under pressure"; *J. Appl. Phys.*, **21**, pp. 527-531.

Spiegel, M.R., 1972: "Theory and Problems of Statistics"; SI edition; McGraw-Hill, USA.

Strijbos, S. and Vermeer, P.A., 1978: "Stress and density distributions in the compaction of powders" in "Processing of Crystalline Ceramics". Materials Science Research Vol. 11, pp. 113-124; Palmour, III, H.; Davis, R.F. and Hare, T.M. Eds.; Plenum Press, USA.

Sundaram, V. and Cowin, S.C, 1985: "The experimental evaluation of the effect of material consolidation on static bin pressures"; *Powder Tech.*, **42**, pp. 241-247.

Tabor, D., 1975: "Interaction between surfaces: Adhesion and friction" in "Surface Physics of Materials", Vol.II, Ch. 10; Blakely, J.M. Ed.; Academic Press, USA.

Takada, T., Kuramoto, M.; Kunio, T. and Kuno, H., 1976: "A feasibility study of scattered-light photoelasticity in the determination of the side pressure distribution of the pressed powder bed"; *Powder Tech.*, **14**, pp. 51-60.

Timoshenko, S.P. and Goodier, J.N., 1970: "Theory of Elasticity", 3rd ed.; Mc Graw-Hill, USA.

Train, D., 1957: "Transmission of forces through a powder mass during the process of pelleting"; *Trans. I.Chem.E.*, **35**, pp. 258-266.

Tüzün, U., 1987: "Effects of consolidation and yield history on the measured angles of friction of articulated solids" in "Tribology in Particulate Technology", Ch.1.3; Briscoe, B.J and Adams, M.J. Eds.; Adam Hilger, UK.

Tüzün, U.; Adams M.J. and Briscoe, B.J., 1988: "An interface dilation model for the prediction of wall friction in a particulate bed"; *Chem. Eng. Sci.*, **43** (5), pp. 1083-1098.

Van Den Bergh, W.J.B. and Scarlett, B., 1987: "Influence of particle breakage on the wall friction of brittle particulate solids"; *Powder Tech.*, **49**, pp. 277-288.

Van Der Zwan, J. and Siskens, C.A.M., 1982: "The compaction and mechanical properties of agglomerated materials"; *Powder Tech.*, **33**, pp. 43-54.

Van Groenu, A.B. and Lissenburg, R.C.D., 1983: "Inhomogeneous density in die compaction: Experiments and finite-element calculations"; *Comm. Am. Ceram. Soc.*, C156-C158.

Veale, C.R., 1972: "Fine Powders-Preparation, Properties and Uses" Applied Science Publishers, UK.

Walker, D.M., 1966: "An approximate theory for pressures and arching in hoppers"; *Chem. Eng. Sci.*, **21**, pp. 975-997.

Walker, E.E.; 1923a: "The properties of powders. Part VI. The compressibility of powders"; *Trans. Faraday Soc.*, **19**, pp. 73-82.

Walker, E.E.; 1923b: "The properties of powders. Part VII. The distribution of density in columns of compressed powders"; *Trans. Faraday Soc.*, **19**, pp. 83-89.

Walker, E.E.; 1923c: "The properties of powders. Part VIII. The influence of the velocity of compression on the apparent compressibility of powders"; *Trans. Faraday Soc.*, **19**, pp. 614-622.

Waye, B.E., 1967: "Introduction to Technical Ceramics"; MaClaren & Sons; UK.

Wendlandt, W.W.M., 1986: "Thermal Analysis", 3rd. ed.; Chemical Analysis, Vol.19; Elving P.J. and Winefordner, J.D. Eds.; John Wiley and Sons, USA.

Wischnitzer, S., 1981: "Introduction to Electron Microscopy"; 3rd. ed.; Pergamon Press, USA.

Yashima, S.; Kanda, Y. and Sano, S., 1987: "Relationships between particle size and fracture energy or impact velocity required to fracture as estimated from single particle crushing"; *Powder Tech.*, **51**, pp. 277-282.

Youshaw, R.A. and Halloran, J.W., 1982: "Compaction of spray-dried powders"; *Am. Ceram. Soc. Bull.*, **61** (2), pp. 227-230.